About the Editors

Dr. Ranjan Kumar is currently Head of the Department and Associate Professor in the Department of Mechanical Engineering at Swami Vivekananda University, Kolkata. Dr. Kumar received his Master's and Doctoral degrees in Mechanical Engineering from the Indian Institute of Technology (ISM) Dhanbad. His research interests include Li-ion batteries, finite element simulation and analysis of real engineering problems, and vibration analysis of structures. He has executed projects in association with the Gas Turbine Research Establishment (GTRE), DRDO lab Bangalore. Dr. Kumar has authored 07 books, published 30 research papers, and holds 16 patents. He also serves as editor-in-chief of Journal of Mechanical Engineering Advancements.

Abhishek Dhar, a dynamic academician and a prolific mentor, serves as an Assistant Professor, in the Department of Electrical Engineering and as well as holds the prestigious post of Joint Academic Co-ordinator of the esteemed institution Swami Vivekananda University. His research, published in 15 prestigious international journals and conference papers, focuses on efficient energy utilization, grid stability, IoT etc. He has in his golden feather 60 patents filed and published with his hard work and dedication. He fosters an inclusive learning environment, nurturing diverse talents. His dedication has earned his recognition, bridging academia and industry seamlessly.

Dr. Ashes Banerjee is an Assistant Professor in the Civil Engineering Dept. at Swami Vivekananda University, Kolkata, West Bengal. He earned his Ph.D. in Water Resource Engineering from the Indian Institute of Technology (Indian School of Mines) in Dhanbad, India, in 2020. Dr. Banerjee's scholarly achievements are evidenced by his numerous publications in peer-reviewed international journals, covering crucial topics such as non-linear filtration in porous media, water quality, and groundwater utilization.

Dr. Arnab Das is currently Assistant Professor in the Department of Mechanical Engineering at Swami Vivekananda University, Kolkata. Dr. Das has achieved his Ph.D. in Mechanical Engineering from Indian Institute of Technology (ISM) Dhanbad in 2023. His research interests include advanced manufacturing processes, micromachining, composite materials, and battery energy storage system. Dr. Das has published several journal articles extensively on topics such as micromachining, ultra-precision machining, advanced manufacturing with four Patents.

Published by
Bright Sky Publications,
Office No.3, 1st Floor, Pocket - H34, Sec - 3,
Rohini, New Delhi-110085, India
Phone: +91-8750002051
Email: brightskypublications@gmail.com

ISBN 9789362337054
9 789362 337054
₹ 1275 US$ 20

Computational Techniques in Modern Engineering Research

Bright Sky Publications

Research Methodologies in ENGINEERING and APPLIED SCIENCE

Dr. Ranjan Kumar
Abhishek Dhar
Dr. Ashes Banerjee
Dr. Arnab Das

Bright Sky Publications
New Delhi

Research Methodologies in Engineering and Applied Science

Editors

Dr. Ranjan Kumar

Abhishek Dhar

Dr. Ashes Banerjee

Dr. Arnab Das

Bright Sky Publications ™
New Delhi

Research Methodologies in Engineering and Applied Science

Published By: *Bright Sky Publications*

Bright Sky Publication
Office No. 3, 1st Floor,
Pocket - H34, SEC-3,
Rohini, Delhi, 110085, India

Editors: *Dr. Ranjan Kumar, Abhishek Dhar, Dr. Ashes Banerjee and Dr. Arnab Das*

Edition: *1st*

Publication Year: *2024*

Pages: *322*

ISBN: *978-93-6233-705-4*

Book DOI: *https://doi.org/10.62906/bs.book.209*

Price: *₹1275/-*

Preface

In recent years, engineering and applied sciences have witnessed remarkable advancements, driven by technological innovation, increasing complexity in problem-solving and interdisciplinary approaches. These fields are at the forefront of addressing global challenges, including sustainable development, energy efficiency, automation, and health care. In this dynamic landscape, the role of research methodologies cannot be understated. They provide the foundation for inquiry, enabling engineers and scientists to develop new technologies, optimize processes, and generate novel insights.

This book, *Research Methodologies in Engineering and Applied Science*, is designed to serve as a comprehensive guide for students, researchers, and professionals seeking a solid understanding of the research methods essential to their fields. The motivation for compiling this book stems from the growing need to bridge theoretical research frameworks with practical applications. Engineers and applied scientists often face the challenge of converting abstract ideas into real-world solutions, and the methodology is what facilitates this transformation.

Through this text, we aim to cover a wide array of research methodologies, ranging from quantitative to qualitative approaches, experimental design, computational modeling, and simulation techniques. We explore both classical methods and cutting-edge tools like artificial intelligence and data analytics, which are becoming increasingly important in modern research. The objective is to provide a clear roadmap for developing sound research questions, designing experiments, collecting data, and analyzing results with scientific rigor.

Each chapter is structured to guide the reader through different phases of research, with examples and case studies drawn from various branches of engineering and applied science. The integration of theory and practice ensures that readers not only gain knowledge of methodologies but also learn how to apply them to real-world problems. Special emphasis is placed on interdisciplinary research, collaboration, and innovation, which are critical in today's research landscape.

We hope that this book will serve as an indispensable resource, offering insights and tools that empower researchers to contribute to their respective

fields with confidence and precision. It is our belief that by mastering research methodologies, engineers and applied scientists will be better equipped to tackle complex problems and push the boundaries of what is possible in their disciplines.

We extend our gratitude to the contributors, whose expertise and dedication have made this book a reality. Their collective efforts reflect the diversity and depth of research methodologies that are crucial for advancing knowledge in engineering and applied sciences. Finally, we thank our readers for choosing this book as part of their research journey. We hope it will inspire and equip you to explore new frontiers in your own research endeavors.

Dr. Ranjan Kumar
Associate Professor,
Department of Mechanical Engineering,
Swami Vivekananda University,
Kolkata, West Bengal, India

Acknowledgment

I extend my heartfelt gratitude to Swami Vivekananda University, Kolkata, India, for their steadfast support and encouragement throughout the creation of “Research Methodologies in Engineering and Applied Science “The University's dedication to fostering education and research has been instrumental in shaping the content and direction of this publication. We deeply appreciate the collaborative spirit and resources provided by Swami Vivekananda University, Kolkata, which have enabled us to explore and share the latest innovations and technologies across various fields.

We hope that this book serves as a valuable resource for this esteemed institution and the broader academic community, reflecting our shared dedication to knowledge, progress, and the pursuit of excellence.

I extend my deepest appreciation to each of the external reviewers mentioned below for their unwavering commitment to excellence and their indispensable role in ensuring the scholarly merit of this work.

List of Reviewers:

1. Prof. (Dr.) Vinayak Ranjan, Department of Mechanical Engineering, Rowan University, Glassboro, NJ 08028, United States.
2. Dr. Shamim Haidar, Department of Mechanical Engineering, Aliah University, Kolkata-700156, India.
3. Prof. (Dr.) Somendra Nath Roy, Ex-Scientist, CSIR-CGCRI, Kolkata-700032, India.

Research Methodologies in Engineering and Applied Science

Contents

Chapter - 1
Evaluating the Effectiveness of Support Vector Machine Kernels for Gear Fault Detection: Insights from Confusion Matrices and Receiver Operating Characteristic Analysis

Authors

Sandeep Kumar Paral
Department of Mechanical Engineering, National Taiwan University of Science and Technology, Taipei 106, Taiwan

Ranjan Kumar
Department of Mechanical Engineering, Swami Vivekananda University, Kolkata, West Bengal, India

Arnab Das
Department of Mechanical Engineering, Swami Vivekananda University, Kolkata, West Bengal, India

Chapter - 1

Evaluating the Effectiveness of Support Vector Machine Kernels for Gear Fault Detection: Insights from Confusion Matrices and Receiver Operating Characteristic Analysis

Sandeep Kumar Paral, Ranjan Kumar and Arnab Das

Abstract

Gear fault classification plays a crucial role in predictive maintenance and ensuring the reliable operation of industrial machinery. This study evaluates the performance of Support Vector Machine (SVM) classifiers with different kernels for gear fault classification using a dataset consisting of vibration signals. The kernels considered include linear, fine Gaussian, medium Gaussian, and coarse Gaussian. The performance of each classifier is assessed using confusion matrices and Receiver Operating Characteristic (ROC) curves. The results demonstrate that the Gaussian kernels outperform the linear kernel, with the medium and fine Gaussian kernels achieving the highest accuracy, precision, sensitivity, and F1 scores. The ROC curves further confirm the superiority of the Gaussian kernels, with their curves being further from the diagonal line and closer to the top-left corner, indicating a better trade-off between the true positive rate and the false positive rate. However, the choice between the fine and medium Gaussian kernels may depend on the balance between performance and computational complexity. The study highlights the importance of selecting an appropriate kernel for SVM-based gear fault classification and provides insights into the performance characteristics of different kernels. Further research is recommended to explore feature engineering techniques and optimize the kernel selection and hyperparameter tuning process.

Keywords: Machine learning, support vector machine, gear fault analysis, gaussian kernel, confusion matrix, ROC

Introduction

Gearboxes play a vital role in numerous mechanical systems, serving as essential components for power transmission and speed control [1]. These

critical elements are found in a wide range of applications, from industrial machinery and automotive transmissions to aerospace systems [2] and wind turbines [3]. The smooth operation and reliability of gearboxes are paramount to ensuring the optimal performance and longevity of the overall mechanical system. However, gears within these gearboxes are susceptible to various types of damage, such as missing teeth, tooth root cracks, tooth wear, pitting, and eccentricity. These faults can lead to reduced efficiency, increased vibration, and ultimately, catastrophic failure if left undetected and unaddressed. The consequences of gear failures can be severe, resulting in costly downtime, expensive repairs, and potential safety hazards [4]. Industry estimates suggest that gear-related issues cost millions of dollars annually in terms of maintenance, repairs, and lost productivity.

To mitigate these risks and minimize the financial impact of gear failures, early fault detection and diagnosis are crucial. Traditional methods of gear fault detection often rely on periodic inspections and scheduled maintenance, which can be time-consuming, labor-intensive, and may not always detect faults in their early stages. Therefore, there is a growing need for machine learning (ML) techniques that can accurately and efficiently identify gear faults, enabling proactive maintenance and preventing unexpected breakdowns [5, 6]. The supervised ML algorithms can learn from historical data and extract meaningful patterns to distinguish between healthy and faulty gears. Among the various supervised ML classification methods, Support Vector Machines (SVM) find an optimal hyperplane to separate different classes in a high-dimensional feature space [7]. By employing different kernel functions, such as polynomial and Gaussian kernels, SVM can effectively handle complex and non-linearly separable data [8, 9].

This paper explores the application of SVM with different kernels such as linear and fine, medium, and coarse Gaussian for gear fault classification. The study utilizes a binary dataset comprising displacement amplitude measurements along the x and y axes under varying load and speed conditions, featuring both missing tooth and no-fault gear instances. The primary objective is to compare the performance of the kernels in accurately detecting gear faults and assess their suitability for industrial implementation.

Dataset and Methodology

Dataset

The dataset utilized in this study comprises vibration data collected from a double-speed reduction gearbox, specifically focusing on gear 1, which has been modified to simulate various fault conditions (**Fig. 1**). Data was gathered for five defective gears and one normal gear, across a range of speeds and loads. For binary classification, we focus on the amplitude data from the normal gear and the missing tooth defective gear, with each dataset containing 150,000 observations and encompassing five distinct features.

This data collection was part of a project for the Deep Neural Network course at Southern Denmark University [10]. The features in the dataset include displacement measurements along the x-axis (sensor1), and y-axis (sensor2) with a constant sampling rate (time) under various speed settings (speed set: 8.33, 25, and 40 revolutions/sec) and load values (load value: 0 and 80 Nm), and a label indicating the gear fault condition (gear_fault_desc). There are 150,000 measurements for each gear condition such as no-fault and missing teeth. These measurements are divided into six combinations of speed settings and load values, with 25,000 measurements at 5kHz sample frequency for each combination. The measurement start time is different for every combination of speed setting and load value in the actual dataset. This results in a total of 150,000 measurements for each gear condition. The amplitude data collected under different loading conditions provides critical insights into the gearbox's behavior across various operating scenarios. This comprehensive dataset is instrumental in developing and evaluating gear fault classification algorithms using machine learning techniques. The detailed visualization of the collected data for the missing tooth and no-fault conditions is presented in **Fig. 2**.

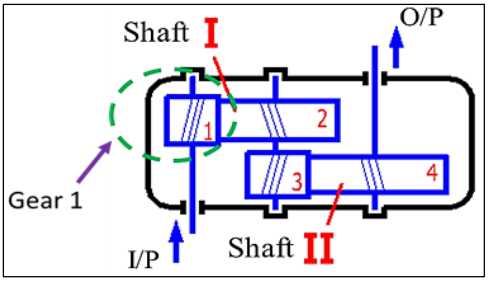

Fig 1: A schematic representation of the double-speed reduction gearbox

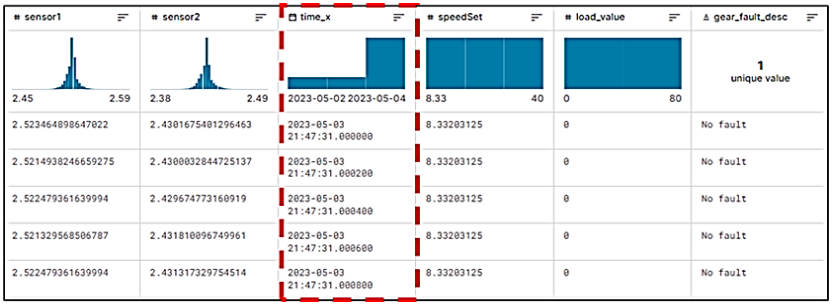

# sensor1	# sensor2	time_x	# speedSet	# load_value	gear_fault_desc
2.45 2.59	2.38 2.49	2023-05-02 2023-05-04	8.33 40	0 80	1 unique value
2.523464898647022	2.4301675401296463	2023-05-03 21:47:31.000000	8.33203125	0	No fault
2.5214938246659275	2.4300032844725137	2023-05-03 21:47:31.000200	8.33203125	0	No fault
2.522479361639994	2.429674773160919	2023-05-03 21:47:31.000400	8.33203125	0	No fault
2.521329568506787	2.431810096749961	2023-05-03 21:47:31.000600	8.33203125	0	No fault
2.522479361639994	2.431317329754514	2023-05-03 21:47:31.000800	8.33203125	0	No fault

(A)

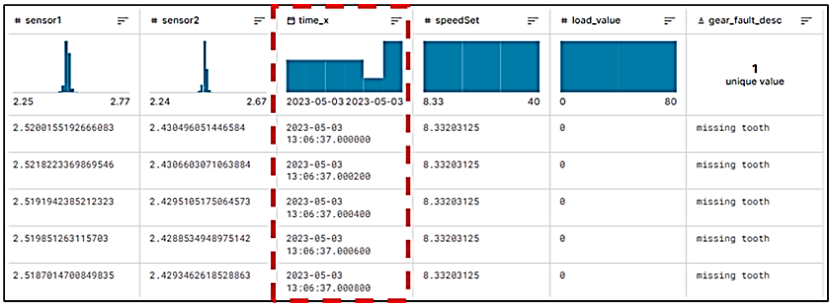

# sensor1	# sensor2	time_x	# speedSet	# load_value	gear_fault_desc
2.25 2.77	2.24 2.67	2023-05-03 2023-05-03	8.33 40	0 80	1 unique value
2.5200155192666083	2.430496051446584	2023-05-03 13:06:37.000000	8.33203125	0	missing tooth
2.5218223369869546	2.430660307106388 4	2023-05-03 13:06:37.000200	8.33203125	0	missing tooth
2.5191942385212323	2.4295105175064573	2023-05-03 13:06:37.000400	8.33203125	0	missing tooth
2.519851263115703	2.4288534948975142	2023-05-03 13:06:37.000600	8.33203125	0	missing tooth
2.5187014700849835	2.4293462618528863	2023-05-03 13:06:37.000800	8.33203125	0	missing tooth

(B)

Fig 2: The displacement measurement of the (a) no-fault and (b) missing tooth gear under different speeds and loads. Each response has 150,000 measurements

Dataset Preprocessing

Data preprocessing is an important step in preparing a dataset for gear fault classification with machine learning algorithms. The no-fault and missing tooth data files are encoded into one-hot encoding, with 0 representing no-fault and 1 representing missing tooth. All input features are normalized [0,1] to eliminate the influence of the scaling and unit using equation 1 as mentioned below.

$$\text{Normalized value} = \frac{x - x_{min}}{x_{max} - x_{min}} \quad (1)$$

Where x is the input feature value, and x_{min} and x_{max} are the minimum and maximum values of the feature, respectively. To ensure an unbiased dataset, the time feature has been modified to range from 0.0002 seconds to 5 seconds for each combination of speed and load, based on the sampling rate of 5 kHz. The dataset is split into a training set (80%, 240,000 samples) and a testing set (20%, 60,000 samples). The selected features for analysis include sensor1, sensor2, time, speed, load value, and gear fault. The

preprocessed dataset is visualized using a parallel coordinates plot to acquire insights into the data distribution and correlations between features, shown in **Fig. 3**. These preprocessing steps ensure that the present dataset is properly formatted and can be further processed with SVM.

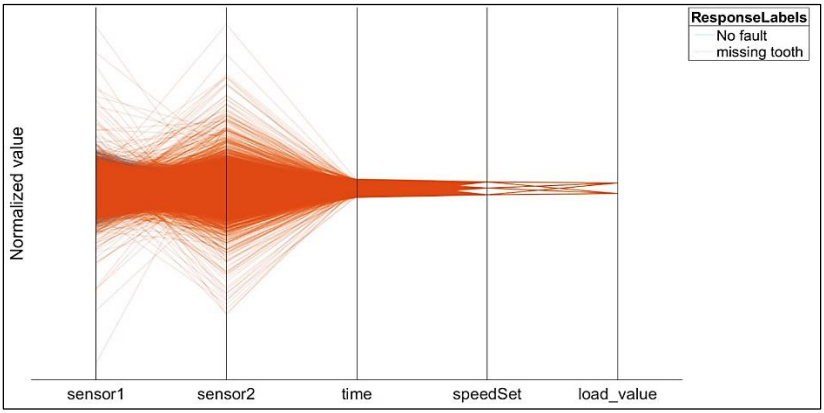

Fig 3: The parallel coordinated plot of the normalized input features

Support Vector Machine (SVM)

SVM is a powerful supervised learning algorithm used for classification and regression. In gear fault classification, SVM aims to find an optimal hyperplane that separates classes in a high-dimensional feature space such as no-fault and missing tooth. The basic concept is to maximize the margin between the hyperplane and the nearest data points from each class, called support vectors, which increases generalization and reduces overfitting [11]. For non-linear data, kernel functions have been used to transform the data into a higher-dimensional space, enabling linear separation and allowing SVM to learn complex, non-linear decision boundaries effectively. In this study, we explore the application of SVM with different kernel functions for gear fault classification:

The linear kernel is the simplest kernel function and is used when the data is linearly separable [12]. It is defined as the dot product between two input vectors as shown in equation 2, where x and y are input vectors, and $K(x, y)$ represents the kernel function.

$$K(x, y) = x^T y \tag{2}$$

The Gaussian kernel, commonly known as the radial basis function (RBF) kernel, is a popular choice for nonlinear classification tasks [13]. It

maps the input data to an infinite-dimensional feature space and is defined as equation 3:

$$K(x, y) = \exp(-r\|x - y\|^2) \quad (3)$$

Where r is a hyperparameter that determines the width of the Gaussian function, and ||x - y|| denotes the Euclidean distance between the input vectors x and y. The Gaussian kernel can be further categorized based on the value of r such that; $Fine\ Gaussian: r = \sqrt{\frac{p}{4}}$; $Medium\ Gaussian: r = \sqrt{p}$; $Coarse\ Gaussian: r = 4\sqrt{p}$ where p is the feature number [9].

Fine Gaussian, a smaller p value leads to a more complex decision boundary, capturing fine-grained details in the data. Medium Gaussian, a medium p value balances between capturing local patterns and generalizing to unseen data. In coarse Gaussian, a larger p value results in a smoother decision boundary, focusing on the overall structure of the data.

By applying SVM with different kernel functions, we can explore the effectiveness of each kernel in capturing the underlying patterns and separating the gear fault classes. The choice of kernel and its hyperparameters can significantly impact the classification performance. In the subsequent sections, we will discuss the implementation details of SVM with different kernels for gear fault classification and evaluate their performance on the given dataset.

Results

Confusion Matrices

The performance of the SVM classifier with different kernels was evaluated for gear fault classification using the given dataset. The confusion matrices for each kernel have been demonstrated in **Fig.4** that providing model efficiency to predict the no-fault and missing tooth gears. Based on the confusion matrices, the classification accuracy, precision, sensitivity, and F1 score have been calculated and tabulated in **Table 1** (for details see the Appendix).

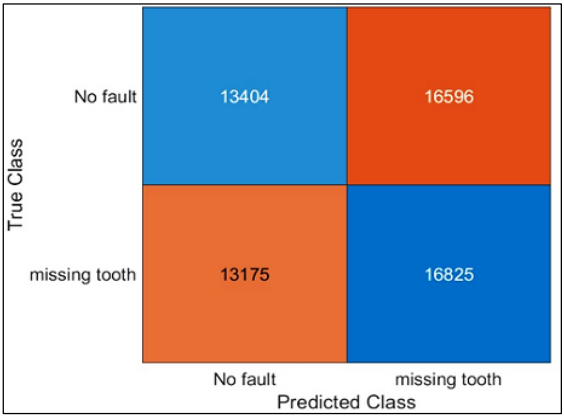
No fault
missing tooth
True Class
13404
16596
13175
16825
No fault
missing tooth
Predicted Class

(A)

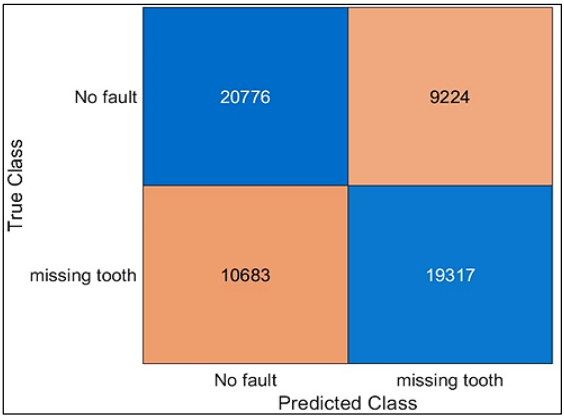
No fault
missing tooth
True Class
20776
9224
10683
19317
No fault
missing tooth
Predicted Class

(B)

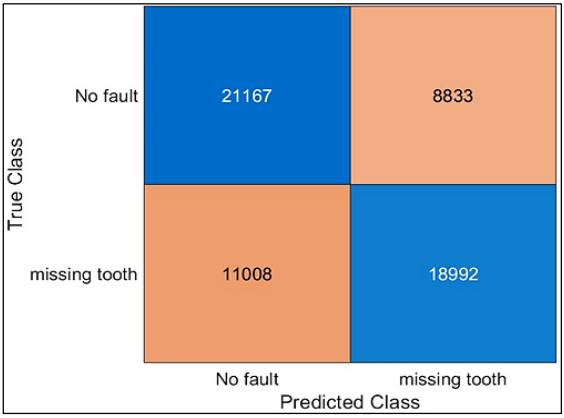
No fault
missing tooth
True Class
21167
8833
11008
18992
No fault
missing tooth
Predicted Class

(C)

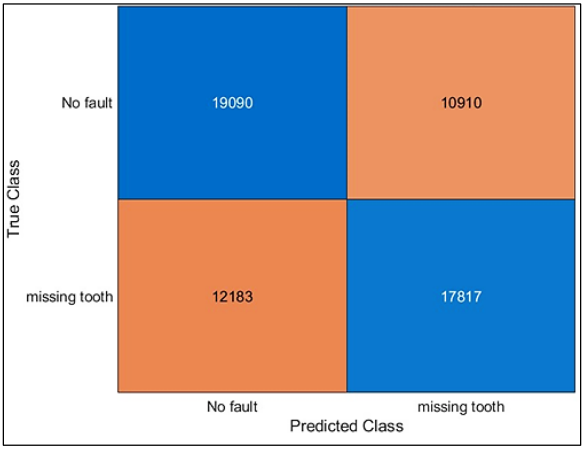

(D)

Fig 4: The confusion matrices of (a) linear, (b) fine Gaussian, (c) medium Gaussian, and (d) coarse Gaussian SVM kernels for gear fault classification

It has been observed that the linear kernel achieved an accuracy of 50.4%, indicating that it struggles to effectively separate the gear fault classes in the original feature space. The precision and sensitivity values of 50.4% and 44.7%, respectively, suggest that the linear kernel has difficulty in correctly identifying both the positive (faulty) and negative (non-faulty) instances. The low F1 score of 47.4% further confirms the poor overall performance of the linear kernel for this classification task. On the other hand, the non-linear fine Gaussian kernel, which captures more detailed patterns, achieved an accuracy of 66.8%. This indicates an improvement over the linear kernel, suggesting that the fine Gaussian kernel can better distinguish between the gear fault classes. The precision of 66% and sensitivity of 69.2% indicate a relatively balanced performance in identifying both faulty and non-faulty instances. The F1 score of 67.5% reflects the overall effectiveness of the fine Gaussian kernel in this classification task. Along with this, the medium Gaussian kernel which balances between capturing local patterns and generalizing to unseen data, achieved an accuracy of 66.9%. This is slightly higher than the fine Gaussian kernel, indicating that the medium Gaussian kernel can effectively capture the necessary patterns for accurate classification. The precision of 65.8% and sensitivity of 70.5% suggest a good balance between correctly identifying faulty and non-faulty instances. The F1 score of 68.1% further confirms the effectiveness of the medium Gaussian kernel. Finally, the coarse Gaussian

kernel, which focuses on the overall structure of the data, achieved an accuracy of 61.5%. While this is lower than the fine and medium Gaussian kernels, it still outperforms the linear kernel. The precision of 61% and sensitivity of 63.6% indicate that the coarse Gaussian kernel has some limitations in accurately identifying both faulty and non-faulty instances. The F1 score of 62.3% reflects the overall performance of the coarse Gaussian kernel, which is lower compared to the fine and medium Gaussian kernels.

Table 1: Performance statistics of SVM with different kernels for gear fault classification

	Linear	**Fine Gaussian**	**Medium Gaussian**	**Coarse Gaussian**
Accuracy	50.4%	66.8%	66.9 %	61.5%
Precision	50.4%	66%	65.8%	61%
Sensitivity	44.7%	69.2%	70.5%	63.6%
F1 score	47.4%	67.5%	68.1%	62.3%

Receiver Operating Characteristic (ROC) Curves

ROC curves are commonly used to assess and compare the performance of binary classification models. In the context of gear defect classification using SVM with multiple kernels, ROC curves provide a visual representation of the trade-off between true positive rate (TPR) and false positive rate (FPR) at different classification thresholds. The ROC curves for the SVM classifiers with linear, fine Gaussian, medium Gaussian, and coarse Gaussian kernels are presented in **Fig. 5**. The curves plot the TPR against the FPR as the classification threshold is varied. The diagonal line in the ROC figure illustrates the performance of a random classifier, which has an equal chance of identifying an occurrence as positive or negative. A classifier with a ROC curve above the diagonal line indicates better performance than random guessing, while a curve below the diagonal line suggests worse performance.

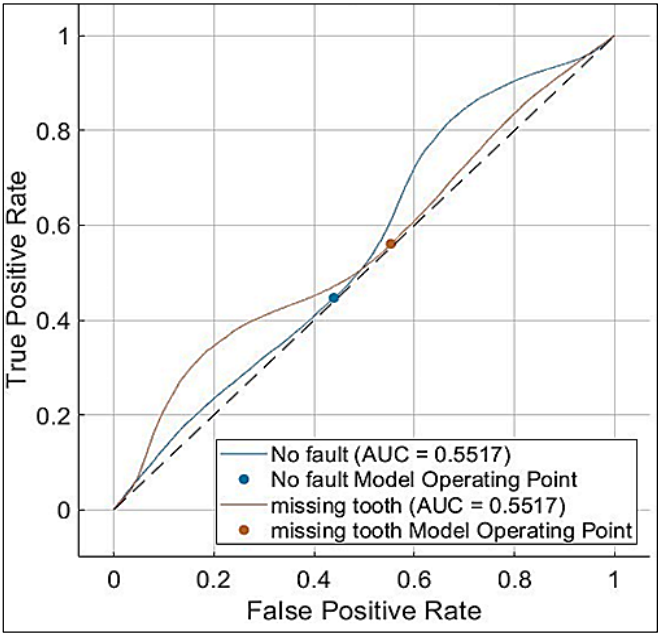
True Positive Rate
False Positive Rate
0
0.2
0.4
0.6
0.8
1
No fault (AUC = 0.5517)
No fault Model Operating Point
missing tooth (AUC = 0.5517)
missing tooth Model Operating Point

(A)

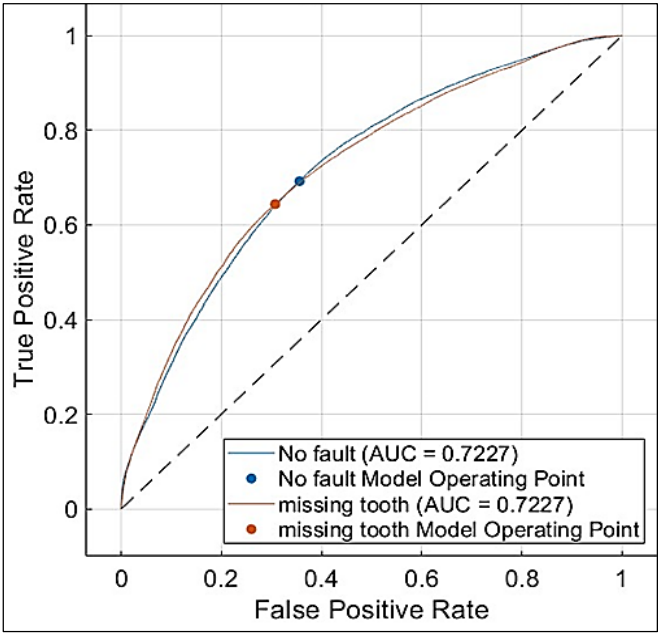
True Positive Rate
False Positive Rate
0
0.2
0.4
0.6
0.8
1
No fault (AUC = 0.7227)
No fault Model Operating Point
missing tooth (AUC = 0.7227)
missing tooth Model Operating Point

(B)

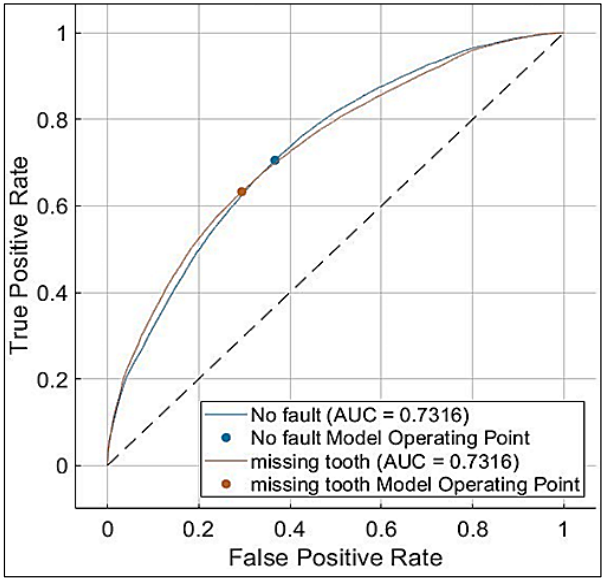

(C)

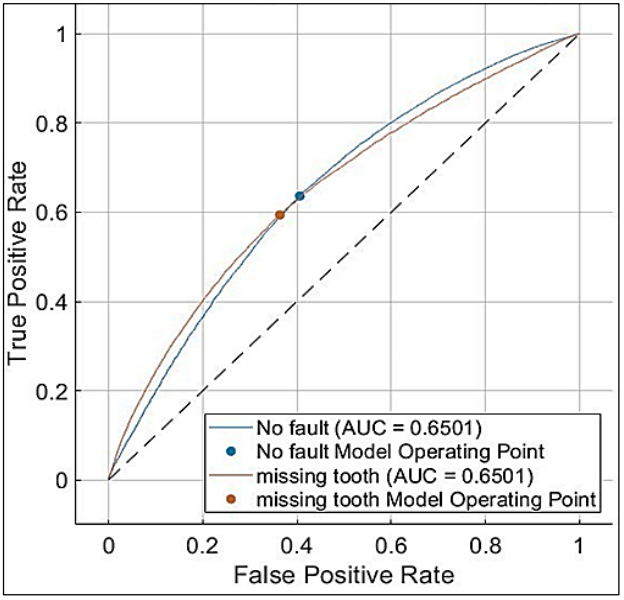

(D)

Fig 5: ROC curves of (a) linear, (b) fine Gaussian, (c) medium Gaussian, and (d) coarse Gaussian SVM kernels for gear fault classification

From the ROC curves in **Fig. 5**, we can observe that all the SVM classifiers with different kernels perform better than random guessing, as their curves are located above the diagonal line. The medium Gaussian kernel (**Fig. 5c**) and the fine Gaussian kernel (**Fig. 5b**) show the best performance, with their curves being the furthest from the diagonal line and closer to the top-left corner of the plot. It indicates that these kernels achieve a high true positive rate while maintaining a low false positive rate. Another typical parameter for quantifying classifier performance is the area under the ROC curve (AUC). A higher AUC value suggests improved classification performance. From the ROC curves, it appears that the medium Gaussian and fine Gaussian kernels would have higher AUC values compared to the linear and coarse Gaussian kernels.

Discussion

Evaluating the SVM classifiers with different kernels for gear fault classification using confusion matrices and ROC curves provides valuable insights into their performance and suitability for the task at hand. The linear kernel's poor performance, as evident from its confusion matrix and ROC curve, suggests that the gear fault classification problem is not linearly separable in the original feature space. This highlights the limitation of using a linear kernel for complex classification tasks where the decision boundary may be highly non-linear. The high number of misclassifications and the proximity of the ROC curve to the diagonal line indicate that the linear kernel struggles to distinguish between the different gear fault classes effectively.

On the other hand, the Gaussian kernels (fine, medium, and coarse) demonstrate improved performance compared to the linear kernel. The capacity of Gaussian kernels to translate input data into a higher-dimensional space allows for a more accurate separation of gear defect classes. The fine and medium Gaussian kernels, in particular, show promising results, with their confusion matrices indicating higher accuracy, precision, sensitivity, and F1 scores compared to the linear and coarse Gaussian kernels. The ROC curves for these kernels are further from the diagonal line and closer to the top-left corner, suggesting a better trade-off between the true positive rate and the false positive rate. However, it is important to note that while the medium Gaussian kernel achieves the highest performance metrics, the difference between the medium and fine Gaussian kernels is relatively small. This raises the question of whether the slight performance improvement

justifies the potential increase in computational complexity and training time associated with the medium Gaussian kernel. Further analysis and experimentation may be necessary to determine the optimal kernel choice, taking into account both performance and computational considerations. The coarse Gaussian kernel's performance, although better than the linear kernel, falls short compared to the fine and medium Gaussian kernels. The coarse Gaussian kernel's ROC curve is closer to the diagonal line suggesting that it has a higher false positive rate for a given true positive rate. This indicates that the coarse Gaussian kernel may be too simplistic to capture the complex decision boundary required for accurate gear fault classification.

Conclusion

In conclusion, the evaluation of SVM classifiers with different kernels using confusion matrices and ROC curves provides a comprehensive understanding of their performance for gear fault classification. The Gaussian kernels, particularly the fine and medium variants, demonstrate superior performance compared to the linear kernel. However, the choice between the fine and medium Gaussian kernels may depend on the trade-off between performance and computational complexity. By addressing these aspects, the gear fault classification system can be enhanced to provide more accurate and reliable predictions, ultimately contributing to improved maintenance strategies and reduced downtime in industrial applications.

Appendix

The standard confusion matrix with its fundamental components.

	Predicted Positive	Predicted Negative	
Actual Positive	TP *True Positive*	FN *False Negative*	Sensitivity $\frac{TP}{(TP+FN)}$
Actual Negative	FP *False Positive*	TN *True Negative*	Specificity $\frac{TN}{(TN+FP)}$
	Precision $\frac{TP}{(TP+FP)}$	Negative Predictive Value $\frac{TN}{(TN+FN)}$	Accuracy $\frac{TP+TN}{(TP+TN+FP+FN)}$

$$\text{F1 score} = \frac{2\times\text{sensitivity}\times\text{Precision}}{(\text{Sensitivity}+\text{Precision})}$$

References

1. Liang, X., Zuo, M.J. and Feng, Z., 2018. Dynamic modeling of gearbox faults: A review. Mechanical Systems and Signal Processing, 98, pp.852-876.
2. Nowoisky, S., Grzeszkowski, M., Mokhtari, N., Pelham, J.G. and Gühmann, C., 2019. Monitoring concept study for aerospace power gear box drive train.
3. Salameh, J.P., Cauet, S., Etien, E., Sakout, A. and Rambault, L., 2018. Gearbox condition monitoring in wind turbines: A review. Mechanical Systems and Signal Processing, 111, pp.251-264.
4. Michaelis, K., Höhn, B.R. and Hinterstoißer, M., 2011. Influence factors on gearbox power loss. Industrial lubrication and tribology, 63(1), pp.46-55.
5. Carroll, J., Koukoura, S., McDonald, A., Charalambous, A., Weiss, S. and McArthur, S., 2019. Wind turbine gearbox failure and remaining useful life prediction using machine learning techniques. Wind Energy, 22(3), pp.360-375.
6. Habbouche, H., Benkedjouh, T., Amirat, Y. and Benbouzid, M., 2021. Gearbox failure diagnosis using a multisensor data-fusion machine-learning-based approach. Entropy, 23(6), p.697.
7. Abdullah, D.M. and Abdulazeez, A.M., 2021. Machine learning applications based on SVM classification a review. Qubahan Academic Journal, 1(2), pp.81-90.
8. Soman, K.P., Loganathan, R. and Ajay, V., 2009. Machine learning with SVM and other kernel methods. PHI Learning Pvt. Ltd..
9. Lin, S.L., 2021. Application of machine learning to a medium Gaussian support vector machine in the diagnosis of motor bearing faults. Electronics, 10(18), p.2266.
10. Data source, https://www.kaggle.com/datasets/hieudaotrung/gear-vibration/data, Accessed on 10th May, 2024.
11. Pisner, D.A. and Schnyer, D.M., 2020. Support vector machine. In Machine learning (pp. 101-121). Academic Press.
12. Chauhan, V.K., Dahiya, K. and Sharma, A., 2019. Problem formulations and solvers in linear SVM: a review. Artificial Intelligence Review, 52(2), pp.803-855.

13. Xiao, Y., Wang, H. and Xu, W., 2014. Parameter selection of Gaussian kernel for one-class SVM. IEEE transactions on cybernetics, 45(5), pp.941-953.

Chapter - 2
Design of Loop Layout in Flexible Manufacturing System using Particle Swarm Optimization Technique

Authors

Ravi Shankar Rai
Department of Automation and Robotics, Sandip Institute of Technology and Research Centre, Nashik, Maharashtra, India

Milind M. Patil
Department of Mechanical Engineering, Sandip Institute of Technology and Research Centre, Nashik, Maharashtra, India

Vasim A. Shaikh
Department of Automation and Robotics, Sandip Institute of Technology and Research Centre, Nashik, Maharashtra, India

Ravi Nigam
Department of Mechanical Engineering, Swami Vivekananda University, Kolkata, West Bengal, India

Arnab Das
Department of Mechanical Engineering, Swami Vivekananda University, Kolkata, West Bengal, India

Chapter - 2

Design of Loop Layout in Flexible Manufacturing System using Particle Swarm Optimization Technique

Ravi Shankar Rai, Milind M. Patil, Vasim A. Shaikh, Ravi Nigam and Arnab Das

Abstract

In a flexible manufacturing system (FMS) to attain high productivity, layout arrangement must be optimised. The design of the FMS loop layout is covered in this document. Finding the best sequence for the machines around a loop in order to reduce the total number of loop traversals for a family of parts is the aim of the loop layout problem. Finding the best combination among millions of combinations is a difficult challenge that cannot be solved using traditional methods since optimum layout arrangements are combinatorial problems. Thus, in order to address the loop layout problem, this work describes the design, development, and testing of the particle swarm optimization (PSO) technique. Since its initial proposal by Kennedy & Eberhart in 1995, this method has gained widespread acceptance as a solution for difficult combinatorial, non-linear, non-differential, and complicated problems. Benchmark issues are used to validate the suggested approach. In this case, the PSO algorithm is suggested to find the best answer for the unidirectional loop layout design problem of several FMS models.

Keywords: Loop layout, FMS, PSO; optimization, manufacturing system

Introduction

In modern, sophisticated production lines, flexible manufacturing systems (FMS) are essential. These systems usually consist of a collection of machines that are able to carry out a range of diverse tasks. These machines are connected by an automated parts-transportation and handling mechanism, and they are all run under the hierarchical management structure of a standard computing system. Determining the best configuration for the machines on the shop floor to enable optimal operation is a crucial step in the design of a factory management system (FMS). The way the machines

are arranged greatly influences the cost of handling materials, processing times, and production system throughput, all of which have an effect on the FMS's total productivity. In modern, sophisticated production lines, flexible manufacturing systems (FMS) are essential. These systems usually consist of a collection of machines that are able to carry out a range of diverse tasks. These machines are connected by an automated parts-transportation and handling mechanism, and they are all run under the hierarchical management structure of a standard computing system. Determining the best configuration for the machines on the shop floor to enable optimal operation is a crucial step in the design of a factory management system (FMS). The way the machines are arranged greatly influences the cost of handling materials, processing times, and production system throughput, all of which have an effect on the FMS's total productivity. The type of material-handling device employed, such as gantry robots, automated guided vehicles (AGVs), material-handling robots, etc., frequently dictates the machine architecture during an FMS. When it comes to application, the most commonly used types of machine layouts are as follows (see Fig. 1): the cluster layout based on gantry mechanism (Fig. 1(c)), the semi-circular layout with a single mechanism (Fig. 1(d)), the linear single-row layout (Fig. 1(a)), the linear double-row layout (Fig. 1(b)), and the closed-loop layout (Fig. 1(e)). An AGV moves components between the machines taking possession in each direction in a straight line in the first two layouts (Figs. 1(a)-(b)). Once the work's space is limited, a gantry robot is utilised, supported by the third machine's arrangement (Fig. 1(c)). In the fourth arrangement (Fig. 1(d)), an industrial robot that handles materials transports components between the machines while following a semi-circular (predetermined) path with its end-effector. In contrast, a conveyor in a closed-loop arrangement transports parts between the machines in a single direction via a closed-loop rail.

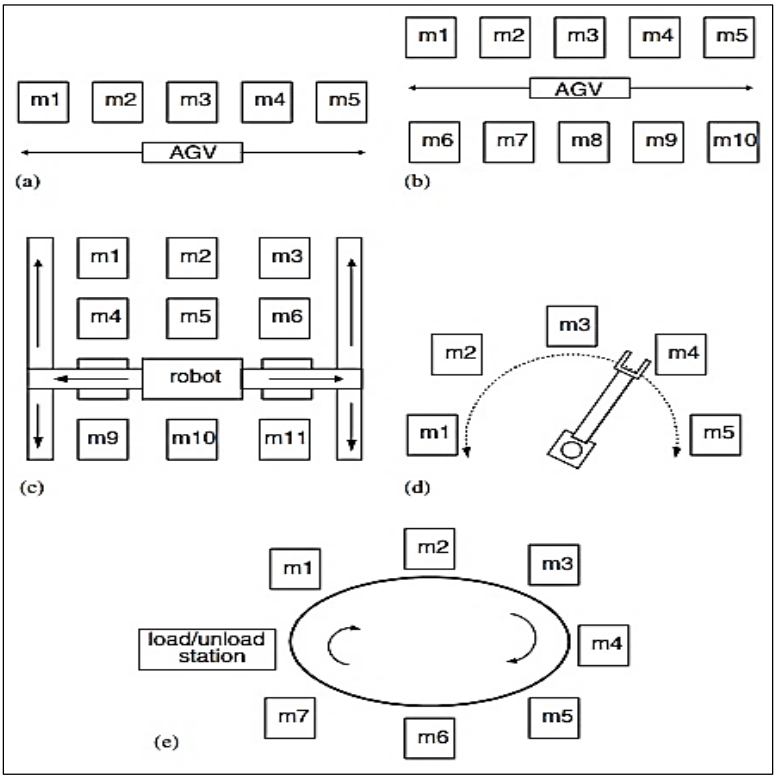

Fig 1: Different Forms of machines layouts in a FMS with respect to the various types of the material-handling devices: (a) single-row layout, (b) double-row layout, (c) cluster layout, (d) semi-circular layout, and (e) Closed unidirectional loop layout [22]

The unidirectional loop layout design issue (LLDP), or the problem of designing loop-layout-manufacturing systems of the form depicted in Fig. 1(e), is the focus of this work. The problem has been attempted to be NP-hard, which implies that no algorithmic programmed can answer it in polynomial time unless P ¼ NP is proven. Unlike alternative layout configurations, loop layouts are appealing to use for at least two reasons: first, they require fewer material handling links to connect the machines, which reduces their initial cost; second, they offer greater material handling flexibility because every machine can be accessed by every other machine. Determining the machine's order around the loop in order to maximize certain performance parameters is the primary objective of the LLDP. The layout design principles that are most frequently utilized center on

minimizing material-handling expenses. Afentakis (1989) suggested minimizing a metric known as traffic congestion in order to achieve this goal. The number of times a certain part runs through the loop before processing is finished is the definition of this metric. Two traffic congestion measurements, known as MIN-SUM and MIN-MAX congestion, respectively, are often used in the literature. While the goal of the later is to minimise the maximum congestion among parts of the same family, the goal of the former is to minimise the total congestion of all parts.

Literature Survey

In order to overcome the loop layout problem, Afentakis [1] created an interchange heuristic and used a graph to represent the layout of an FMS. The graph's edges show the material handling system's connecting ties, while nodes stand for the individual steps in the process. The formulation of quadratic assignment problems (QAPs) has been introduced by Kaku and Rachamadugu [2] as a means of solving loop and linear layout problems in FMS. In order to solve the unidirectional loop network problem, Kouvelis and Kim [8] created a branch and bind (BB) process and a heuristic. They also designed a decomposition method to handle large work flow matrices. Leung [9, 10] has created a graph theory with heuristic support that builds a layout for the matter's linear programming relaxation. The MIN_SUM and MIN_MAX goals were taken into consideration when they created the integer programming (IP) formulation to solve the unidirectional loop architecture problem. The loop layout drawback has been solved by Cheng *et al*. [11] by the development of a hybrid genetic algorithm and neighbourhood search. To solve the simplex loop network layout drawback, Tansel and Bilen [16] have designed two heuristics called MOVE and MOVE/INTERCHANGE. While the second heuristic relied on pairwise interchanges as well as positional moves, the first one was mostly dependent on positional moves. A three-phase IP model was used to address an FMS loop layout problem that included scheduling and machine layout, as modelled by Potts and Whitehead [17]. Assigning tasks to machines in the first phase helps to balance the workload on the machines. In order to reduce the overall number of circuits, the second phase minimizes intermachine travel, and the third phase distributes the places around a conveyor belt loop. Lee *et al*. [12] suggested BB techniques in addition to heuristics to address the unidirectional loop layout issue. To overcome the min–max loop layout problem, Bennell *et al*. [13] suggested an iterated decent and tabu search strategy as well as a randomised insertion approach. A heuristic method for

solving the unidirectional loop network based on a formulation of linear programming that makes use of the flow matrix was provided by Malakooti [14]. The different formulations and techniques that have been developed to address the unidirectional cyclic layout problem have been discussed by Altinel and Oncan [18]. In order to handle combinatorial issues with permutation property, Nearchou [22] devised a mapping technique for encoding the floating-point chromosomes and employed a differential evolution algorithm (DEA) to solve the loop layout problem. Since the loop layout problem is of the NP hard type [22], non-conventional optimisation methods have been used to address this kind of issue. An attempt to apply the PSO algorithm for creating a manufacturing system with a loop layout has been made in this work. One congestion measure that is regarded as an aim is the MIN_SUM. In order to replicate actual production facilities, the layout configuration that takes into account machines with uneven clearance between them is taken into consideration.

Formulation of the LLDP

LLDP considerations a group of processing machines organized in a very control system, with zero being a loading & unloading platform, and a group of M elements that are moved round the loop in exactly unidirectional. The elements move in & out the system through the loading & unloading platform. Every half is to be operated on variety of k machines in a particular order; which is often known as the part-route. Let us suppose a neighbourhood p (p = 1; . . . ; M) should 1st be operated on machine j and so on i^{th} machine. If the j^{th} machine positioned within loop is under that of i^{th} machine, then the half should pass the load & unloading platform. This is often known as a reload of part p. the entire range of reloads required to finish the process of |a particular part aided a live for holdup of the assembly system. An answer to the LLDP conform to a particular loop layout of machines, i.e., for a custom arrangement of machines within the loop. Hence, a loop layout will be delineating by a permutation and combination of the various machines (m_1, m_2 . . . m_n). The target is to search out the optimal layout that diminishes the hold up within the loop exposed to a group of applied constraints associated with the part-routes demand. Two performance measures are typically applied for the analysis of a LLDP:

i) MIN-SUM, within that the target is that the step-down of the entire congestion of elements within the system, that is the step-down of the entire range of reload to all elements.

ii) MIN-MAX, within that the try is to attenuate the most reload from the elements of constant family. This method results to a lot of optimal congestion among elements. For clarification consider an example of 7-machines & 3-parts LLDP.

Let us suppose that the part-routes are:

Part 1: 5 → 7 → 6 → 3 → 2.

Part 2: 2 → 3 → 5 → 6 →7 →1.

Part 3: 7 → 1 → 2 → 3 → 4 → 5 → 6.

Hence, the layout is (1-2-3-4-5-6-7).

That means a meeting of machines inside a very loop with first machine within the 1st location, then followed by second machine, then by 3rd machine, etc., corresponding to a complete range of five reloads mainly, checking the required part-routes given higher than, part 1 needs 3 reloads; part 2 needs reload, and part 3 needs 1 reload.

The planned layout is (7-1-2-3-4-5-6).

Diminishes the entire range of reloads to 4, generating the subsequent tasking of reloads,3 reloads for part 1, 1 reload for part 2, and zero reload for part 3.

So, the layout is (5-7-1-6-4-2-3).

Diminishes most reload among elements generating 1 reload for part 1, 2 reloads for part 2, and 2 reloads for part 3.

Problem Descriptions

A common layout in FMS is the loop layout in which the machines are arranged in a loop network and materials are transported in unidirectional. An important step in designing the unidirectional network is the determination of the ordering of the machines around the loop. A loop layout design can be represented as permutation of machines (m_1, m_2...m_n) with a prefix of loading/unloading station 0. Each part is characterized by its part route, the sequence of machines it must visit to complete its processing. For a given part, suppose processing on machine j immediately follows processing on machine i. If the position of machine j is lower than that of machine i, then the part must cross the loading/unloading station, which is called a reload. The number of reloads necessary to complete the processing for a part is defined as a measure of traffic congestion [11]. Afentakis [1]

suggested the use of traffic congestion as a measure to evaluate the loop layout. The congestion is defined as the number of times a part traverses the loop before its processing is completed. The two kinds of congestion measures used in loop layout design are MIN_SUM and MIN_MAX. A MIN_SUM problem attempts to minimize the total congestion of all parts while a MIN_MAX problem attempts to minimize the maximum congestion among family of parts.

Problem Formulation

The objective of the problem formulated as:

1. Minimization of average cost of best loop layouts

$Cost(S) = \sum_{i=1}^{N} reload_i$

Where,

S is the best loop layout combination.

Reload is the crossing through loading/unloading station.

N is number of parts

2. Minimization of average percentage solution effort (%SE) spent by algorithm

$SE(\%) = \left(\frac{NE_{best}}{NE_{total}}\right) * 100$

Where,

NE_{best} is the number of evaluation to get the best result.

NE_{total} is the total number of evaluations.

3. Minimization of congestion for each part

$MP_i = reload_i$

Where,

MP_i is the ith part of machine MP.

Particle swarm optimization (PSO).

PSO may be a stochastic optimization technique lies on population and represented on the social behaviours discovered in animals or insects, for example flocking of birds, schooling of fish, and animal herding. One vital tool of a successful swarm intelligence model is PSO that was invented by Russell Eberhart, an electrical engineer, and James Kennedy, a social

psychologist, in 1995. Originally PSO won't to solve non-linear continuous optimization issues; however, a lot of recently it's been employed in several sensible, real-life application issues. PSO attracts inspiration from the social science behaviour related to flocking of birds. It's a common observation that birds will fly in massive teams with no chance of collision for very long travel, creating use of their training to keep up an optimal distance between themselves & neighbours.

PSO Algorithm

Step 1: Initiate n no of particles at random.

Step 2: Find fitness value of every particle. And apply the condition; if the fitness value is optimum than the best fitness value (pbest) in past. Set the present value as the next pbest.

Step 3: Select particles with the best fitness value of whole particles as the gbest.

Step 4: For every particle, calculate particle speed in line with the formula.

$V_k [\ ] = V_k [\ ] + C\ 1\ r1\ (P_{kbest} - P_k) + C_2\ r_2\ (G_{kbest} - P_k)$

Where

$V_k [\ ]$ represents the particle speed.

P_k represents that the current particle.

P_{kbest} represents that the personal better of particle

G_{kbest} is that the global better of particle

r_1 & r_2 is a random number lies in the interval (0 and 1), Assume $r_1 = 0.78$ $r_2 = 0.48$

C_1, C_2 are learning factors (or) social and cognitive parameters. Usually $C_1 = C_2 = [0\text{-}4]$ {considering $C_1 = C_2 = 1$}.

Step 5: Velocities of particles on every dimension are added to a most speed Vmax, the rate on the factor is restricted to Vmax.

Step 6: Now terminate if an optimal value is reached. Otherwise, move to Step 2.

Flow Chart of PSO

Fig. 3 Flow chart of PSO

Experimental setup

Model Building

Simulation is defined as the advance technique of building a real time problem abstract, i.e., logical and conceptual model of the system describing the internal behaviour of their related components and all complex interactions. The outline pattern of changes in the behaviour of system can be observed against the obtained effects. This propagates to great understanding of actual phenomenon of the system operations and environment and thus the areas which required potential changes are recognized.

Table 1: FMS Model building (M-model)

S. No.	Description	M-1	M-2	M-3	M-4
1.	Number of machines	10	15	20	30
2.	Number of parts	3	9	5	10
3.	Layout considered	Loop layout	Loop layout	Loop layout	Loop layout
4.	Transportation cost per Unit (Rs)	1	1	1	1
5.	Loading and unloading cost per unit (Rs)	1	1	1	1

Data Set Details for FMS Layout

A production environment [21, 22] with the detailing of the layout of FMS is shown in Table 2. The details of the required data of batch varieties and No. of parts and the required sequence for each part are enlisted in the Table 2. The details of the required input taken such as required sequence with batch sizes of machines and parts from the reference paper are also tabulated in the Table 3. These tabulated data are taken as an input values for the FMS models and then by taking the considerations of all the assumptions, apply the PSO codes for generating the combinations of the machines sequences finally, the output values and graphs are plotted.

Table 2: Outline of Production system [21]

Layout Pattern	No. of Machines	No. of Batches	No. of operations	Load/Unload Stations
Loop	10	10	10	2
Loop	15	15	15	2

Loop	20	20	20	2
Loop	30	30	30	2

Table 3: Required sequence with batch sizes of machines and parts [21]

S. No.	Total machines	Total parts	Part number	Required sequence of machine
1	10	3	1	2-1-6-5-8-9-3-4
2	10	3	2	10-8-7-5-9-6-1
3	10	3	3	9-2-7-4
1	15	9	1	4-2-5-1-6-8-14-9-11-3-15-12
2	15	9	2	3-2-15-14-11-1-7-10-4-5-13-6-9
3	15	9	3	5-6-11-15-2-12-3-4
4	15	9	4	10-9-4-14-2-3-15-8
5	15	9	5	11-2-4-14-5-3-15
6	15	9	6	8-10-12-11-15-13-1-14-4-5-3
7	15	9	7	5-11-10-3-7-13-8
8	15	9	8	7-3-2-8-4-10-6-15-13-9-1
9	15	9	9	11-13-3-1-12-14-4-8-9-2
1	20	5	1	4-2-3-12-1-9-16-18-5-8-20-15-14-6-11
2	20	5	2	10-9-1-3-18-17-5-6-2-11-4
3	20	5	3	17-11-6-8-7-15-16-9-1-20
4	20	5	4	14-17-11-3-16-5-13-18-20-19-12-10-6-8-15
5	20	5	5	6-18-8-4-2-7-5-9-14-19-1-20-10-16-11-15-13-12
1	30	10	1	6-3-4-18-5-1-14-24-26-7-11-30-23-21-13-27-9-16-17-2-25-8-15
2	30	10	2	17-9-11-8-10-22-24-13-2-29-23-21-25-16-4-20-26-18-15-12-27-6-3-7-28
3	30	10	3	13-2-6-29-21-3-14-24-12-15-17-8-1-22-28-10-7-30-20-19
4	30	10	4	7-2-6-11-21-8-16-30-1
5	30	10	5	3-17-1-2-20-22-8-6-26-19-14-11-15-12-7-16-21-10-28-23-18-4-27-24-25-13-30-9-5
6	30	10	6	30-9-2
7	30	10	7	15-9-30-19-12-3-6-5-8-14-7-28-23-1-29-24-27-2-13-4-26-16-11-10-25-21-22-20-18
8	30	10	8	7-19-5-4-9-16-3-14-28-13-11-2-21-10-17-22-26-23-29-30
9	30	10	9	21-4-1-6-11-22
10	30	10	10	12-6-17-15-13-30-26-18-14-9-7-11-23-2-4-25-24

Implementation of PSO for Ackley and Rosenbrock Function

There are variety of benchmark check functions for up to date the optimization algorithms like as GA & evolutionary computation. Rosenbrock operate may be the best example of nonlinear operate having powerfully coupled system variables and is an actual challenge to any optimization formula attributable to its tardy convergence for many optimization strategies. I actually have used the Ackley operate and Rosenbrock operate to verify my PSO codes and once verification I actually have applied my problem once the validation of the proposed coding is done.

Output Plots of Ackley Function

PSO codes in applied in the MATLAB on the Ackley function then the generation of global minima of Ackley function provides the validation of the algorithm that is going to be used for the layout optimization of FMS in the dissertation. Here 3000 iterations are provided to check the validity and from the output plot we can see that the global minima i.e. zero is achieved after 1500 iterations. Total elapsed time for 3000 run is 33.75 seconds.

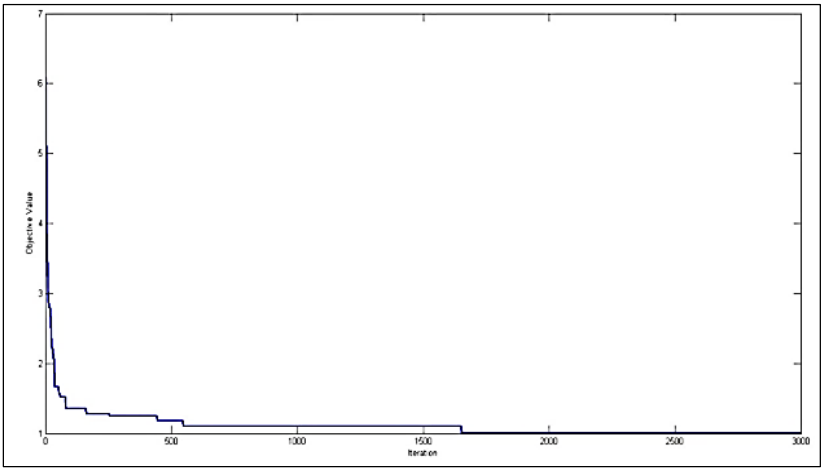

Fig 4: Output Plot between objective value and no. of iterations for Ackley function

Output plots of Rosenbrock function

PSO codes in applied in the MATLAB on the Rosenbrock function then the generation of global minima of Rosenbrock function provides the validation of the algorithm that is going to be used for the layout optimization of FMS. Here 3000 iterations are provided to check the validity and from the output plot we can see that the global minima i.e. zero is

achieved after 40 iterations. Total elapsed time for 3000 run is 34.85 seconds.

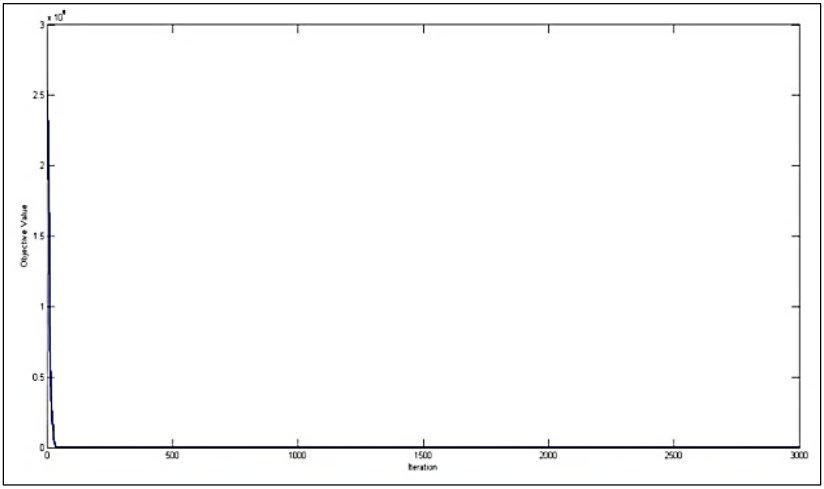

Fig 5: Output Plot between objective value and no. of iterations for Rosenbrock function

The output plots of the Ackley function PSO codes and the Rosenbrock function PSO codes are shown above by which the optima of the both functions lies at x=0; therefore the algorithm is correct and accurate to apply on the objective functions of the FMS Models. Since the validation of the PSO algorithm and their codes are done by the help of standard functions such as Ackley function and Rosenbrock function. Therefore, the PSO codes can now implement on the FMS models.

Parameter Setting

To apply any method for evaluating the system it is extremely necessary to repair some numerical coefficients for the response of parameters. PSO owing to the power of global optimization depends mostly on setting of those parameters. The optimal valves of parameter are fixed on trial and error basis which is listed below.

- Size of population =100.
- Velocity factors=C1=C2=2.
- Termination criteria=300 iterations.

For every test problem, the rule is applicable to run up to a most of 30000 no. of evaluations. The analysis conforms to a single computation of target function for the candidate solution.

Results and Discussions

The PSO Algorithm is tested over the randomly generated test problems given in Nearchou [22]. The model buildings of four different models are tabulated and the required machine sequence for the four test problems are given in table-3. The proposed algorithm is tested on four test problems:

For Model 1-10 Machines and 3 Parts

The PSO codes are now applied to the FMS model-1 in which 10 machines and 3 parts are considered and parameters are calculated by the 100 evaluations. The following results are tabulated below. The applied code is dynamic that is we can apply the no. of evaluation and the model parameters to find the output of the objective functions. As the no. of evaluations increases, accuracy of the result is also increases.

Table 4: Output parameters of model-1

S. No.	Calculated Parameters	Value
1.	Minimum cost	3Rs
2.	Optimal sequence	10-8-9-3-2-7-4-1-6-5
3.	Total evaluation	100
4.	Congestion for each part	1-2-0
5.	Solution Effort (%)	1%

Plots of Objective Function Results for Model-1

Plot of No of Iterations vs Cost

Figure shows the output plot of the model-1 in which the plot is produce between no. of iterations and the cost. From graph, we can see that there is a constant increment in cost for the increased no. of iterations corresponding to the 3Rs. So we can say that the optimum cost is 3 Rs.

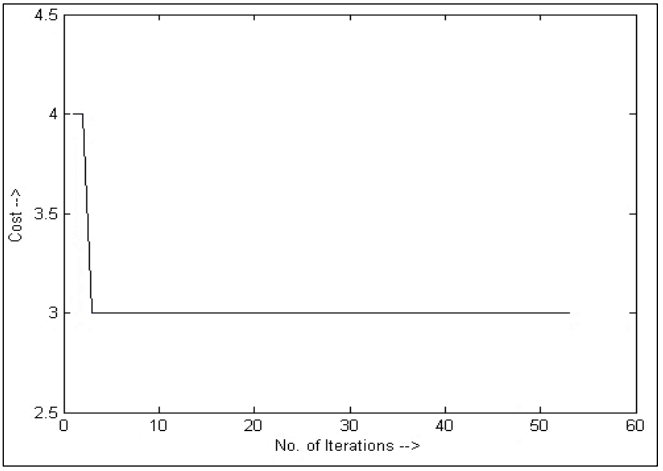

Fig 6: No. of Iteration vs cost graph

Plot of Total Evaluation vs Optimal Cost

Figure shows the output plot of the model-1 in which the plot is produce between no. of evaluations and the best cost. And the best cost achieved in each evaluation is also plotted and mark by red star. From graph, we can see that there is a different best cost value for each evaluations and minimum cost achieved by the some evaluations are 3Rs, so this cost (3Rs) is the optimal cost for model-1.

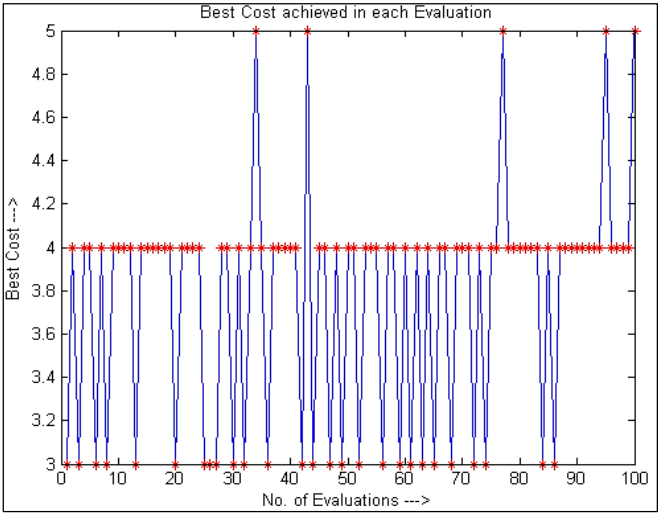

Fig 7: Total evaluation Vs Best Cost

For Model 2-15 Machines and 9 Parts

The PSO codes are now applied to the FMS model-2 in which 15 machines and 9 parts are considered and parameters are calculated by the 100 evaluations. The following results are tabulated below.

Table 11: Output parameters of model-1

S. No.	Calculated Parameters	Value
1	Minimum cost	24 Rs
2	Optimal sequence	7-4-5-11-10-3-15-13-2-1-6-8-12-14-9
3	Total evaluation	50
4	Congestion for each part	2-4-3-3-2-3-1-3-3
5	Solution Effort (%)	54%

Various Plots of Objective Function Results

Plot of No of Iterations Vs Cost

Figure shows the output plot of the model-2 in which the plot is produce between no. of iterations and the cost. From graph, we can see that there is a constant increment in cost for the increased no. of iterations corresponding to the 24Rs. So we can say that the optimum cost is 24 Rs.

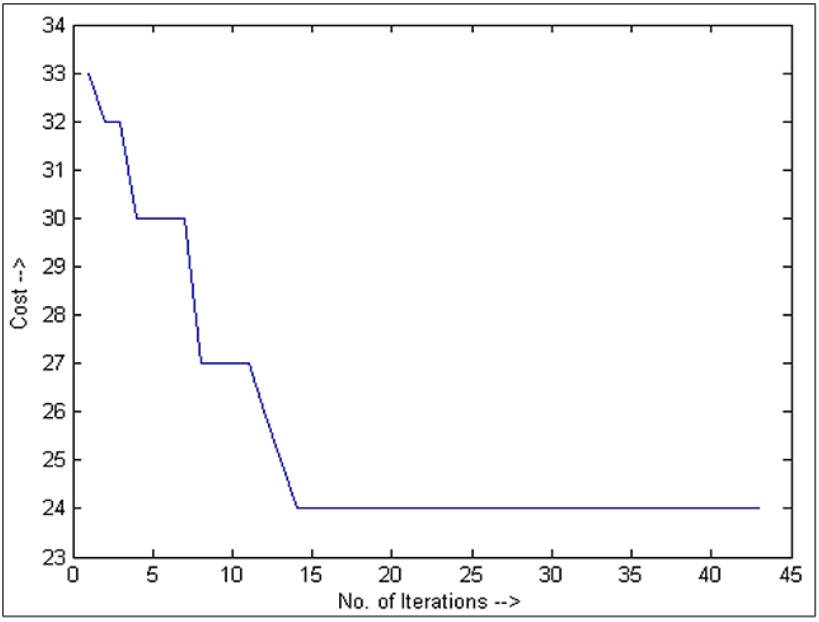

Fig 8: Iteration Vs cost graph

Figure shows the output plot of the model-2 in which the plot is produce between no. of evaluations and the best cost. And the best cost achieved in each evaluation is also plotted and mark by red star. From graph, we can see that there is a different best cost value for each evaluations and minimum cost achieved by the some evaluations are 24Rs, so this cost (24Rs) is the optimal cost for model-2.

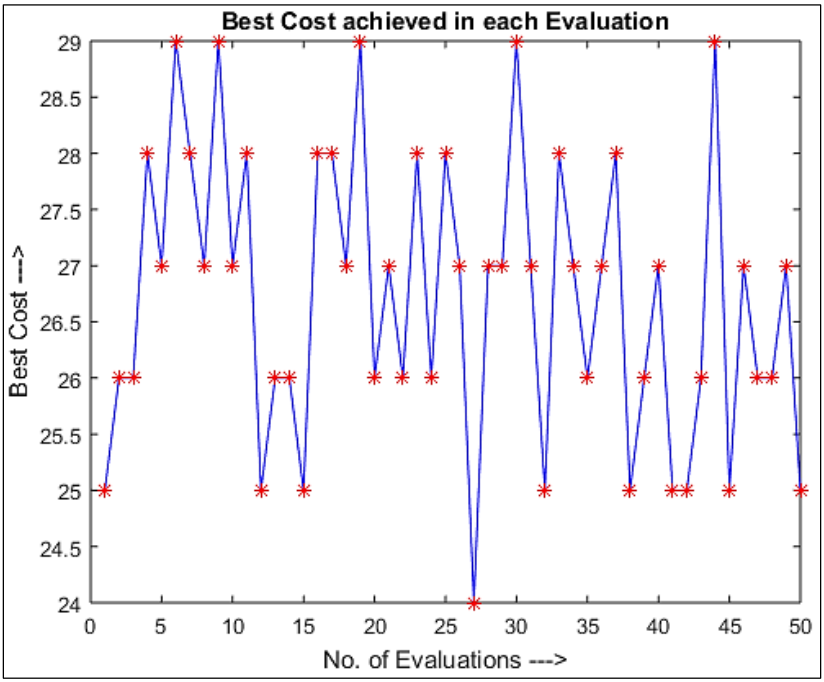

Fig 9: Total evaluation Vs Best Cost

For Model-3 = 20 Machines and 5 parts

The PSO codes are now applied to the FMS model-3 in which 20 machines and 5 parts are considered and parameters are calculated by the 100 evaluations. The following results are tabulated below.

Table 12: Output parameters of model-1

S. No.	Calculated Parameters	Value
1.	Minimum cost	17 Rs
2.	Optimal sequence	10-3-9-14-6-13-19-16-18-17-5-12-8-4-1-20-2-11-7-15
3.	Total evaluation	300

4.	Congestion for each part	3-3-3-4-4
5.	Solution Effort (%)	8.33%

Various Plots of Objective Function Results

Plot of No of Iterations Vs Cost

Figure shows the output plot of the model-3 in which the plot is produce between no. of iterations and the cost. From graph, we can see that there is a constant increment in cost for the increased no. of iterations corresponding to the 17 Rs. So we can say that the optimum cost is 17 Rs.

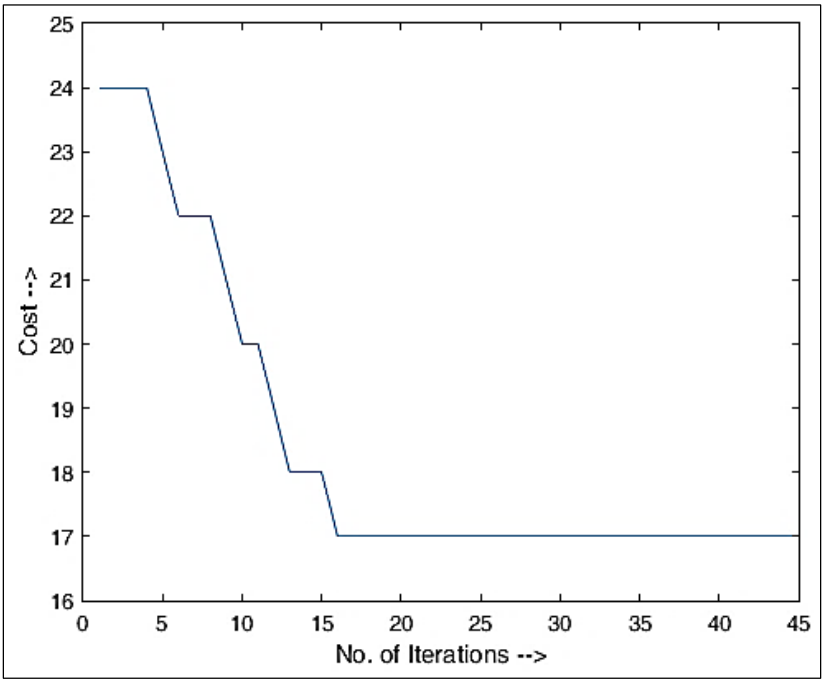

Fig 10: Iteration vs cost graph

Plot of Total Evaluation Vs Optimal Cost

Figure shows the output plot of the model-3 in which the plot is produce between no. of evaluations and the best cost. And the best cost achieved in each evaluation is also plotted and mark by red star. From graph, we can see that there is a different best cost value for each evaluations and minimum cost achieved by the some evaluations are 17 Rs, so this cost (17 Rs) is the optimal cost for model-3.

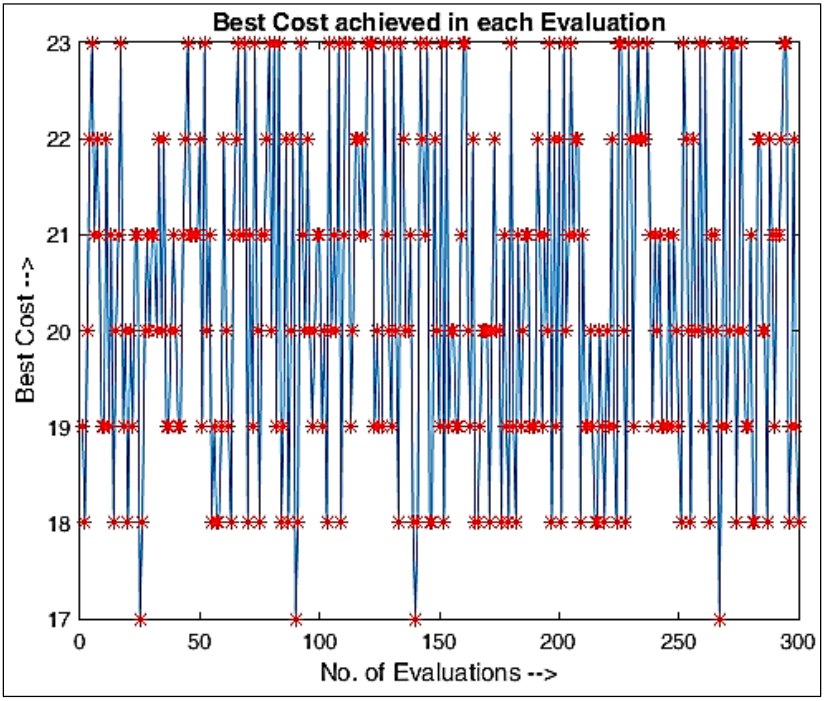

Fig 11: Total evaluation Vs Best Cost

For Model-4 = 30 Machines and 10 Parts

The PSO codes are now applied to the FMS model-4 in which 30 machines and 10 parts are considered and parameters are calculated by the 100 evaluations. The following results are tabulated below.

Table 13: Output parameters of model-1

S. No.	Calculated Parameters	Value
1.	Minimum cost	57 Rs
2.	Optimal sequence	26-23-21-10-12-25-3-17-13-7-27 -9-8-16-2-30-20-19-1-6-18-29-14-11-22-24-5-15-28-4
3.	Total evaluation	300
4.	Congestion for each part	8-8-4-1-9-1-11-7-1-7
5.	Solution Effort (%)	

Various Plots of Objective Function Results

Plot of No of Iterations Vs Cost

Figure shows the output plot of the model-4 in which the plot is produce between no. of iterations and the cost. From graph, we can see that there is a constant increment in cost for the increased no. of iterations corresponding to the 57 Rs. So we can say that the optimum cost is 57 Rs.

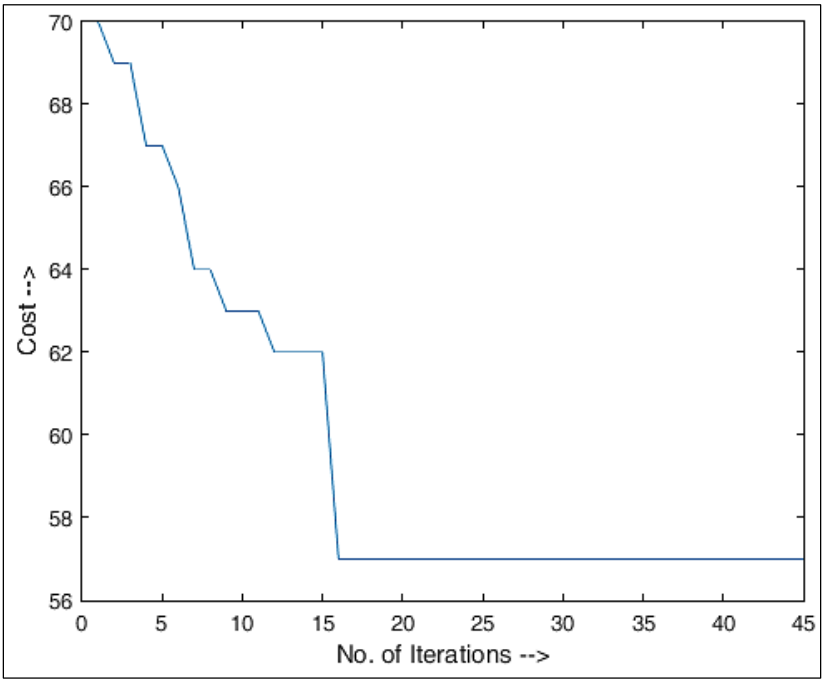

Fig 12: Iteration Vs cost graph

Figure shows the output plot of the model-4 in which the plot is produce between no. of evaluations and the best cost. And the best cost achieved in each evaluation is also plotted and mark by red star. From graph, we can see that there is a different best cost value for each evaluations and minimum cost achieved by the some evaluations are 57 Rs, so this cost (57 Rs) is the optimal cost for model-4.

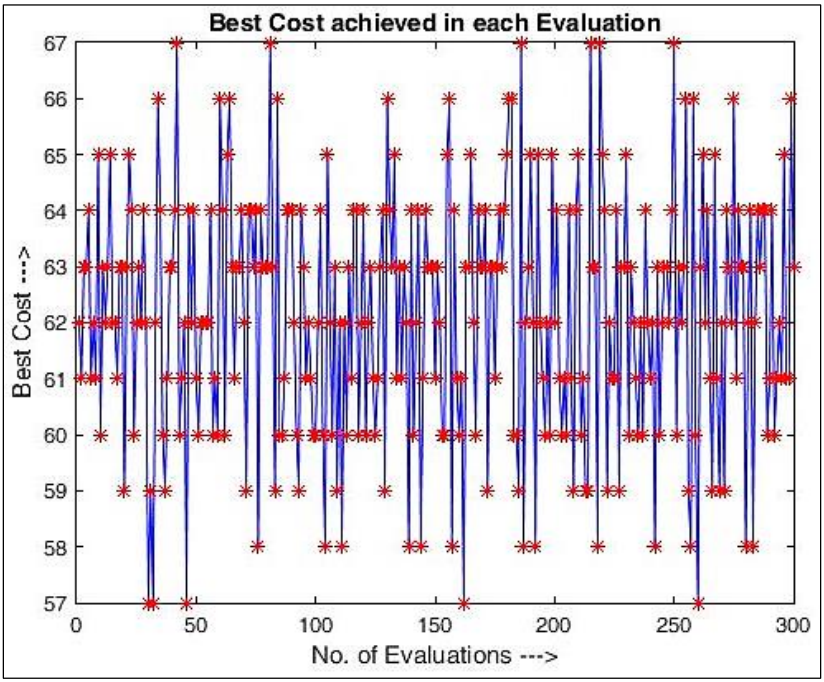

Fig 13: Total evaluation Vs Best Cost

Conclusion

In this paper, a PSO based approach is successfully applied on obtaining the optimal solution of unidirectional loop layout design problem. The proposed algorithm is tested on different combinations of machines to validate the performance of algorithm, and the obtained results are very promising. Random combination approach is used in this report to remove the problem of exploitation. In this report tests have been performed for maximum of 300 evaluations while many researchers performed tests for 30000 or even more than 50000 evaluations. As the number of evaluations will be more, probability of getting optimum combination will be more. As a future work the PSO algorithm can be extended to solve the loop layout problem based on MIN_MAX criteria and bi-directional loop layout problems.

References

1. Afentakis P (1989) A loop layout design problem for flexible manufacturing systems. Int J Flex Manuf Syst 1:175–196.

2. Kaku BK, Rachamadugu R (1992) Layout design for flexible manufacturing systems. Eur J Oper Res 57:224–230.
3. Kim J-G, Kim Y-D (2000) Layout planning for facilities with fixed shapes and input and out points. Int J Prod Res 38 (18):4635–4653.
4. Tompkins JA, White JA, Bozer YA, Tanchoco JMA (2003) Facilities planning, 3rd edn. Wiley, New York.
5. Apple JM (1977) Plant layout and material handling, 3rd edn. The Ronald Press Co, NewYork.
6. Francis RL, McGinnis LF Jr, White JA (1992) Facility layout and location, 2nd edn. Prentice Hall, Englewood Cliffs, New Jersey.
7. Kusiak A, Heragu SS (1987) The facility layout problem. Eur J Oper Res 29:229–251.
8. Kouvelis P, Kim MW (1992) Unidirectional loop network layout problem in automated manufacturing systems. Oper Res 40:533–550.
9. Leung J (1992) A graph - theoretic heuristic for designing looplayout manufacturing systems. Eur J Oper Res 57:243–252.
10. Leung J (1994) Polyhedral structure and properties of a model for layout design. Eur J Oper Res 77:195–207.
11. Cheng R, Gen M, Tosawa T (1996) Genetic algorithms for designing loop layout manufacturing systems. Comput Ind Engng 31(3/4):587–591.
12. Lee S-D,Huang KH, Chiang CP (2001) Configuring layout in unidirectional loop manufacturing systems. Int J Prod Res 39 (6):1183–1201.
13. Bennell JA, Potts CN, Whitehead JD (2002) Local search algorithms for the min-max loop layout problem. J Oper Res Soc 53:1109–1117.
14. Malakooti B (2004) Unidirectional loop network layout by a LP heuristic and design of telecommunications networks. J Intel Manu 15:117–125.
15. Cheng R, Gen M (1998) Loop layout design problem in flexible manufacturing systems using genetic algorithms. Comput. Ind. Eng. 34(1):53–61.
16. Tansel BC, Bilen C (1998) Move based heuristics for the unidirectional loop network layout problem. Eur. J Oper. Res 108:36-48.

17. Potts C, Whitehead JD (2001) Workload balancing and loop layout in the design of a flexible manufacturing system. Eur. J Oper. Res 29:326-336.

18. Altinel IK, Oncan T (2005) Design of unidirectional cyclic layouts. Int J Prod Res 43(19):3983-4008.

19. Kusiak, A., 1990. Intelligent Manufacturing Systems. Prentice Hall Inc., Englewood Cliffs, NJ.

20. Meller, R.D., Gau, K.-Y., 1996. The facility layout problem: Recent trends and emerging trends and perspectives. Journal of Manufacturing Systems 15 (5), 351–366.

21. R. M. S. Kumar, P. Asokan, and S. Kumanan, "Design of loop layout in flexible manufacturing system using non-traditional optimization technique", Springer, IJAMT, (2008), pp. 594-599.

22. Nearchou AC (2006) Meta-heuristics from nature for the loop layout design problem. Int J Prod Econ 101:312–328.

23. Kennedy J, Eberhart R (1995) Particle swarm optimization Proceedings of the International Conference on Neural Networks. Australia IEEE, 1942–1948.

24. Song MP, Gu GC (2004) Research on particle swarm optimization: A review. Proceedings of the Third International Conference on Machine Learning and Cybernetics Shanghai IEEE, 2236–2241.

Chapter - 3
Parametric Observation of Surface Roughness and Burr Formation on Mild Steel using Micro Milling Operation

Authors

Prince Anand
Department of Mechanical Engineering, IIT (ISM) Dhanbad, Jharkhand, India

Bikash Panja
Department of Mechanical Engineering, Swami Vivekananda University, Kolkata, West Bengal, India

Ranjan Kumar
Department of Mechanical Engineering, Swami Vivekananda University, Kolkata, West Bengal, India

Arnab Das
Department of Mechanical Engineering, Swami Vivekananda University, Kolkata, West Bengal, India

Chapter - 3

Parametric Observation of Surface Roughness and Burr Formation on Mild Steel using Micro Milling Operation

Prince Anand, Bikash Panja, Ranjan Kumar and Arnab Das

Abstract

Due to the trend shifting the production towards miniaturization, micro milling technology emerged as a tool. Burr formation and surface roughness are crucial surface quality attributes that vary widely according to machining conditions used. In this paper, micro slot milling operations were carried out in order to identify the effects of feed rate, cutting speed on surface roughness and burr formation. Depth of cut was constant throughout the experiments. Three cutting speeds; i.e., 12000rpm, 18000rpm and 24000rpm have been used as cutting speed. The best roughness value of 17.828 μm was observed using profilometer with 24000 rpm, 2mm/sec feed and 30 mm depth of cut.

Keywords: High speed micro milling, burr formation, surface roughness, exit burrs

Introduction

With the global trend shifting towards miniaturization, there is a rising demand for micro machine tools capable of cutting intricate 3D geometries and micro parts. A very effective precision machining technique called micro-milling is used to create components containing microstructures, such as complex three-dimensional (3D) surfaces at the microscale. The micro-milling tool's cutting-edge diameter usually ranges from 1 μm to 1000 μm, while in traditional milling operations, the cutting-edge diameter is more than 1000 μm [1]. Micro milling is a type of milling where the uncut chip thickness is similar to the size of the cutting-edge radius, or the grain size of the material being cut. The cutting tools used in micro milling are very small, typically with diameters ranging from 25 micrometres to 1 millimetre.

These tools are much smaller than those used in conventional milling processes [2]. In high-speed end milling, the cutting speed and feed rate affect the surface finish and integrity of the workpiece. Although CNC end milling automation is very advanced, there's still room for improvement. Optimizing machining parameters like cutting speed (Vc) and feed rate (f) is important to enhance the surface quality and integrity of the final product. High-speed machining offers benefits such as low cutting forces, effective heat dissipation through chip removal that reduces workpiece distortion, and improved part precision and surface finish [15]. Productivity, dimensions, topography and quality surface finishing of micro-machining are affected by several factors such as microstructure, chip formation, tool wear, cutting forces, etc. The analysis of these factors has generated numerous research. Broad areas of industrial applications of micro components include automotive and transport systems, information technology, telecommunication, health care technology and biotechnology. Specific applications include microscale fuel cells, micro moulds, deep X-ray lithography masks, fibre optics, micronozzles for high temperature jets and microelectronic chips [3-5]. Because of the diverse micro-applications, a wide range of engineering materials is necessary, such as aluminium alloys, stainless steel, titanium, brass, plastics, ceramics, and composites. Machine's cutting parameters like speed, feed rate, depth of cut, environment, and cutting force can increase surface roughness. During manufacturing, the shape, size, and accuracy of the product are crucial, which can be achieved through material removal by cutting, either physically or chemically. NC vertical end mills are widely used in modern businesses because they can quickly remove material and create complex surfaces with high precision [7]. Various studies have been made on the surface roughness, burr formation in end milling using different materials, cutting tools, and experimental and optimization methods. Ghani et.al performed the milling operation on AISI H13 hardened steel using TiN coated P10 carbide insert on end milling Cincinnati Milacron Sabre 750 VMC and analyse the resultant cutting force and surface finish [8]. Norcahyo et.al conducted the experiment using ASSAB XW-42 tool steel and solid carbide tool with End milling CNC milling YCM MV 66A for surface roughness and Tool flank wear, material removal rate [9]. AISI D2 tool steel, coated tungsten carbide inserts, end mill cutter milling Machining center used to perform the experiment and observed the maximum milling temperature, work surface roughness and machining force [10]. Mantle and Aspinwall studied the surface integrity produced by end mill tool using a Taguchi orthogonal array [11]. Wang and

Chang analysed the influence of cutting conditions and tool geometry on surface roughness during slot end milling [12]. Lou and Chen described a new approach for recognition systems to predict surface roughness [13]. Tsai *et al*. developed an in-process based recognition system to predict the surface roughness of machined parts in the end milling process [14]. Bajpai. V *et al*. focused on the characterization of the burr formation in high-speed micro milling operation. Influence of various process parameters, viz., spindle speed, feed rate, depth of cut, tool diameter and number of flutes of the micro milling tool has been analysed on the burr size and on the quality of the machined surface via measuring the surface roughness [16].

The primary objective of the research presented in this paper is to examine how various cutting parameters such as feed rate and cutting speed affect the final product, which includes surface quality and burr formation when mild steel is micro milled. Finding the ideal combination of parameters is another goal of this research.

Workpiece Material

Mild steel is a general-purpose material that can be found in most industries. Mild Steel is popular because it's affordable and offers strength, hardness, wear resistance, toughness, and moderate flexibility, making it suitable for many applications. It's used in industries like automobiles for axles, bearings, and gears, in constructing vehicle frames, in shipbuilding and repairs, and for making sheet metal and nuts and bolts [6].

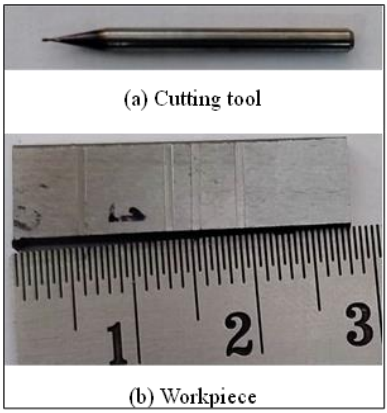

Fig 1: (a) The 2-flute end mill of shank diameter 3 mm and cutting tool of 1mm diameter. Fig. 1 (b), (c) The workpiece of width 8 mm and length 28 mm respectively

Experimental Set up

The Indian Institute of Technology (ISM) in Dhanbad, India, has the source of the semi-high speed micro milling machine tool (V60) as shown in the figure 1. This micro machining centre is developed at IIT ISM Dhanbad. These self-designed and built machine tools have a high spindle speed (60,000 rpm) and positional precision. In order to reduce deflection and vibration, the machining centre's bridge-like structure was built using dynamic studies and modal frequency response analysis. Granite is used throughout the whole construction to adequately dampen unwanted vibration. The machining centre can manufacture slots, macrotextures and three-dimensional features with excellent repeatability and positional precision. The experiments are carried out on this V60 setup. The diameter of the two fluted, coated carbide micro milling tool was 1000 μm. The experiments were performed without any coolant or lubricant. The applicable cutting parameters of the experiment have been considered before conducting the machining operation. The machine parameter is set according from the manufactured as shown in Table 1. To discuss the effects of the relationship between depth of cut and feed rate on the cutting force and surface roughness features, two experiments was conducted.

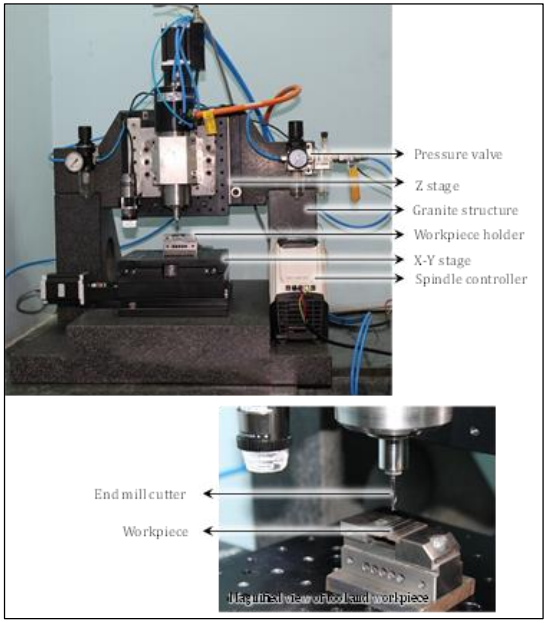

Fig 2: Experimental Setup V60

Table 1: Process parameters

Sr. No.	Speed (rpm)	Feed (mm/sec)	Depth of cut (µm)	Tool diameter (mm)
1.	12000	2	30	1
2.	18000	5	30	1
3.	18000	2	30	1
4.	24000	2	30	1

The workpiece material utilized in this project is mild steel with workpiece of width 8mm and length 28mm respectively. It offers excellent strength, hardness, wear resistance, toughness, and moderate flexibility, making it suitable for many applications. During the actual machining process, there are increased expectations for both the cutting and machining quality of mild steel material. Sample is cut using Wire electric discharge machining that is set up in the IIT ISM Dhanbad. Required flatness of sample is achieved by grinding machine. Flat end mill cutter used for creating micro slots on the workpiece.

Methodology

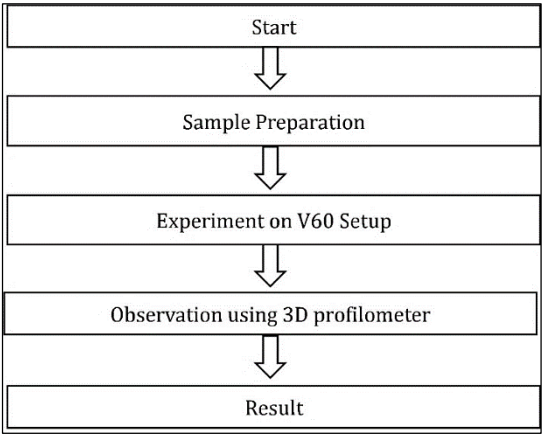

Fig 3: Flowchart of the methodology

Fig. 3 describes the methodology flowchart. In the micro-milling experiments, 1000µm diameter two-flute end mill tool was utilized. Cutting tools were TiAlN coated, and helix angle was 20◦. The total length and shaft diameter of cutting tool were 38 and 3 mm, respectively. A new cutting tool was used for each experiment. The micro-milling experiments were carried out at micromachining center (V60 setup). After that observation is done on 3D profilometer (ZYGO 9000 view). To minimize the deflection effect, the

distance to the tool tip from the tool holder (overhang length) was fixed at 20 mm during all experiments.

Result and Discussion

Surface Roughness

The quality of the surface after machining depends a lot on the cutting parameters and the shape of the tool. If the wrong parameters are used, like dull tools, too fast feed or depth, improper speeds, coolant, or wrong tool hardness, the surface quality will be affected. So, we selected the cutting parameters based on the recommended values for the cutting tool's manufacturer. Surface roughness is the most important process output yet the most difficult to analyse in micro scale. The quality of a machined surface is usually determined by the surface roughness and the surface roughness of workpieces was measured by the 3D profilometer. In this study, a contactless method of surface roughness measurement method was used to analyse machined surfaces and average surface roughness (Ra) was used as a roughness parameter since Ra is the most extensively used index for determining surface quality.

Table 2: Experimental result

Sr. No.	Speed (rpm)	Feed (mm/sec)	Depth of cut (µm)	Ra (µm)	Rz (µm)	Burr Height (µm)
1.	12000	2	30	31.913	1.064	9.537
2.	18000	5	30	37.314	0.843	7.635
3.	18000	2	30	21.601	1.129	6.738
4.	24000	2	30	17.828	0.256	29.392

The roughness value Ra, Rz is observed using 3D profilometer. Fig. 4 (a) shows the roughness value at 12000 rpm and feed 2mm/sec. When the speed and feed increase the roughness value (Ra) increases Fig. 4(b). Fig. 4(c) indicates 21.601, the Ra value at 18000 rpm and 2mm/sec feed. Fig. 4(d), when machining performed at higher speed and value of roughness is decreases.

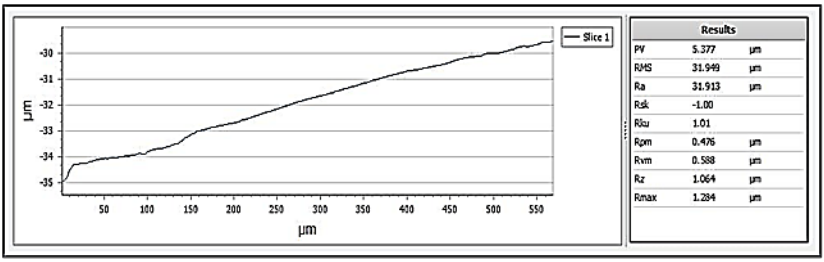

(a) v=12000rpm, f= 2mm/sec

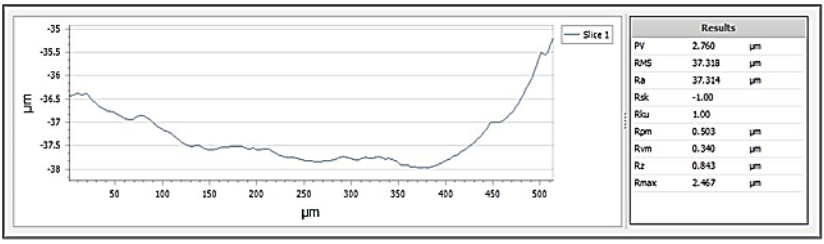

(b) v=18000rpm, f= 5mm/sec

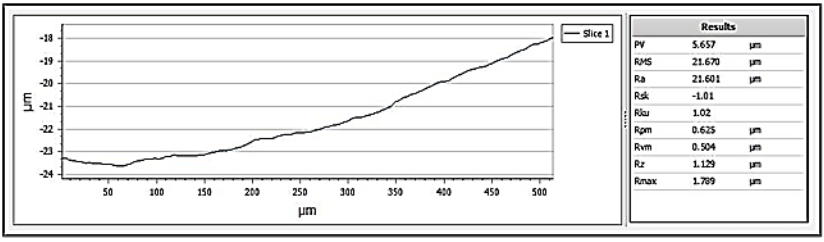

(c) v=18000rpm, f= 2mm/sec

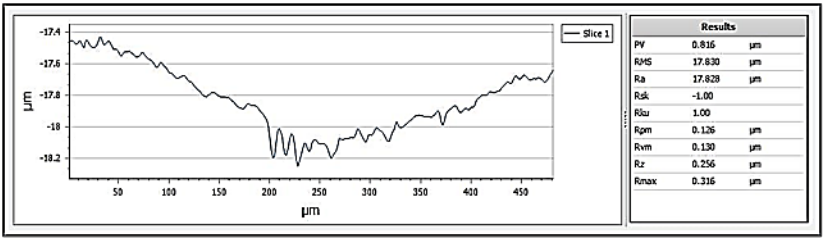

(d) v=24000rpm, f= 2mm/sec

Fig 4: Surface roughness graph

Bur Formation

Burr gets formed when the cutting tool plastically deforms the uncut chip material instead of removing them. Thus, it can be defined as an

unwanted plastic deformed material that remains stick to the workpiece after machining or shearing operation. Since the size of burrs is very less in comparison to macro machining, their removal is very difficult and challenging. Fig. 5 (a), (b), (c), (d) show the three-dimensional picture of the machined surface. In these images, burr clearly observed. The depth of cut constant for all the cutting speed.

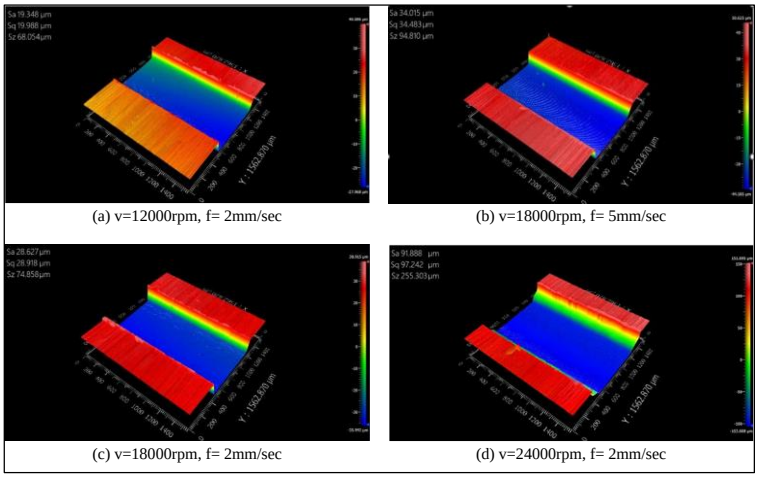

(a) v=12000rpm, f= 2mm/sec (b) v=18000rpm, f= 5mm/sec

(c) v=18000rpm, f= 2mm/sec (d) v=24000rpm, f= 2mm/sec

Fig 6: (a), (b), (c), (d) represent the burr height on machined surface. The 2D surface topography has been shown in this Figure for all machined samples

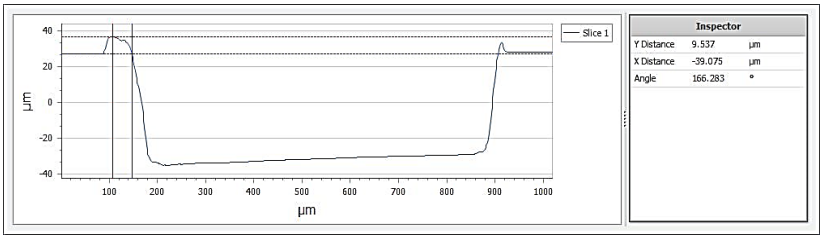

(a) v=12000rpm, f= 2mm/sec

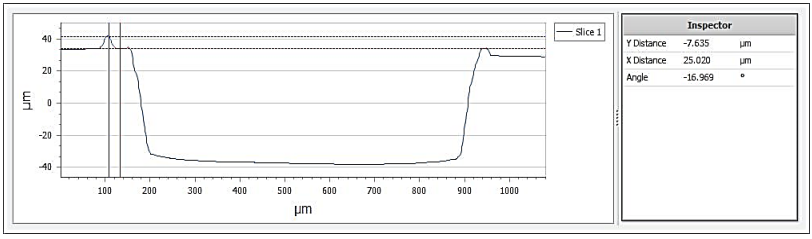

(b) v=18000rpm, f= 5mm/sec

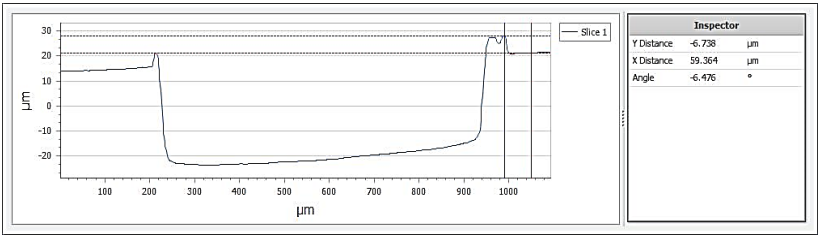

(c) v=18000rpm, f= 2mm/sec

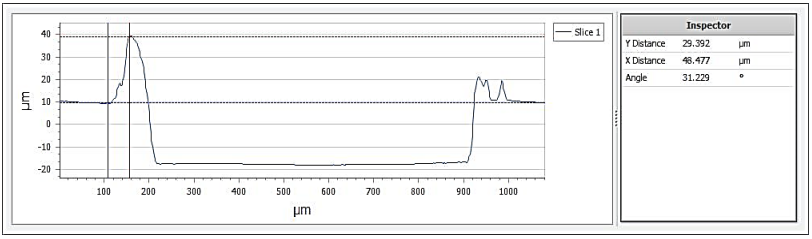

(d) v=24000rpm, f= 2mm/sec

Fig 6: Burr height on machined surface

Conclusions

Slot end milling operation on mild steel were carried out with V 60 cutting tools. The surface roughness and burr formation were analysed to identify the effect of feed rate, cutting speed and depth of cut and the following conclusion can be made:

At the variation of cutting speed, the roughness profile for cutting tool shows a pattern which is when the cutting speed increases the roughness value (Ra) decreases. The depth of cut is constant throughout the experiment.

It was observed that at same cutting speed and increasing feed rate the roughness value increases. all analysis techniques delivered similar results such that the feed rate is found to be most significant factor affecting surface roughness.

Based on the measurement it is observed that burr height at 12000 rpm is 9.537µm, at 18000 rpm, 5 mm/sec is 7.635 µm, at 18000 rpm, 2mm/sec is 6.738 µm and at 24000 rpm is 29.392 µm.

References

1. Caˆmara, M. A., Rubio, J. C. C., Abra˜o, A. M., *et al.* (2012). State of

the art on micro-milling of materials, a review. Journal of Materials science & Technology, 28(8), 673–685.

2. X. Jin and Y. Altintas, "Prediction of micro-milling forces with finite element method", Journal of Materials Processing Technology, vol. 212, no. 3, pp. 542-552, 2012.
3. Lui X., Devor R.E., Kapoor S.G. and Ehmann K.F. The Mechanics of Machining at the Microscale: Assessment of the Current State of the Science. Journal of Manufacturing Science of Engineering, Transactions of the ASME, 2004, 126 (4), pp. 666- 678.
4. Chae J., Park S.S. and Freiheit T. Investigation of Micro - cutting operations. Int. Journal of Machine Tools and Manufacture, 2006, 46 (3-4), pp. 313- 332.
5. Gowri S., Ranjith P., Vijayaraj R., Balan A.S.S. Micromachining: technology for the future. Int. Journal of Materials and structure Integrity, 2007, 1 (1,2), pp. 161- 179(19).
6. Prakash, M., Shekhar, S., Moon, A. P., & Mondal, K. 2015 Effect of machining configuration on the corrosion of mild steel. Journal of Materials Processing Technology, 219, 70-83.
7. J.H. Shaik, J. Srinivas, Optimal selection of operating parameters in end milling of Al-6061 work materials using multi-objective approach, Mech. Adv. Mater. Mod. Process. 3 (1) (2017) 5.
8. J.A. Ghani, I.A. Choudhury, H.H. Hassan, Application of Taguchi method in the optimization of end milling parameters, J. Mater. Process. Technol. 145 (1) (2004) 84–92.
9. R. Norcahyo, Bobby O.P. Soepangkt, Optimization of multi response in end milling process of ASSAB XW-42 tool steel with liquid nitrogen cooling using Taguchi-grey relational analysis, AIP Conf. Proc. 1855 (1) (2017).
10. V.N. Gaitonde, S.R. Karnik, C.H.A. Maciel, J.C.C. Rubio, Machinability evaluation in hard milling of AISI D2 steel, Mater. Res. 19 (2) (2016) 360–369.
11. A.L. Mantle, D.K. Aspinwall, Surface integrity of a high speed milled gamma titanium aluminide, Journal of Materials Processing Technology 118 (2001) 143–150.

12. M.Y. Wang, H.Y. Chang, Experimental study of surface roughness in slot end milling, International Journal of Machine Tools & Manufacture 44 (2004) 51–57.

13. S.-J. Lou, J.C. Chen, In-process surface roughness recognition (ISRR) system in end-milling operations, International Journal Advanced Manufacturing Technology 15 (1999) 200–209.

14. Y.H. Tsai, J.C. Chen, S.J. Lou, An in-process surface recognition system based on neural networks in end milling cutting operations, International Journal of Machine Tools & Manufacture 39 (1999) 583–605.

15. P. Chevrier, A. Tidu, B. Bolle, P. Cezard, J.P. Tinnes, Investigation of surface integrity in high speed end milling of a low alloyed steel, International Journal of Machine Tools and Manufacture, Volume 43, Issue 11, 2003, Pages 1135-1142, ISSN 0890-6955.

16. Bajpai, V, Kushwaha, AK, & Singh, RK. "Burr Formation and Surface Quality in High Speed Micromilling of Titanium Alloy (Ti6Al4V)." Proceedings of the ASME 2013 International Manufacturing Science and Engineering Conference collocated with the 41st North American Manufacturing Research Conference. Volume 2: Systems; Micro and Nano Technologies; Sustainable Manufacturing. Madison, Wisconsin, USA. June 10–14, 2013. V002T03A017. ASME.

Chapter - 4
Assessment of Titanium Machining Employing Wire Electrical Discharge Machining through an Artificial Intelligence (AI) based Optimisation

Authors

Debal Pramanik
Department of Mechanical Engineering, Swami Vivekananda Institute of Science & Technology, Kolkata, West Bengal, India

Arnab Das
Department of Mechanical Engineering, Swami Vivekananda University, Kolkata, West Bengal, India

Ranjan Kumar
Department of Mechanical Engineering, Swami Vivekananda University, Kolkata, West Bengal, India

Bikash Panja
Department of Mechanical Engineering, Swami Vivekananda University, Kolkata, West Bengal, India

Chapter - 4

Assessment of Titanium Machining Employing Wire Electrical Discharge Machining through an Artificial Intelligence (AI) based Optimisation

Debal Pramanik, Arnab Das, Ranjan Kumar and Bikash Panja

Abstract

In non-traditional machining, wire electrical discharge machining is a fast-growing system. Its capabilities are so broad that they can be applied to almost every field of conductive material machining as well as production, nuclear reactors, medical trades, and aeroplanes. However, the WEDM technique's actual application is severely hampered by the difficult problems of small material removal rate (MRR) and high surface roughness (R_a). Parameter optimisation is the only way to improve process efficiency. The present investigational effort examines the effects of several process parameters on the MRR and surface roughness of titanium grade 12 alloy during WEDM process. It does this by using response surface methodology (RSM) and AI-based particle swarm optimisation (PSO). To create the design of experiment (DOE), a study is undertaken utilising an experimental approach known as RSM based central composite design. The AI-based experimental validation of the suggested models shows that low surface roughness (Ra) and the required MRR may be obtained by adjusting the cutting parameters. The ideal level of parametric settings for each of the different machining conditions has been measured.

Keywords: WEDM, Titanium grade 12, TLBO, MRR, R_a

Introduction

Wire electrical discharge machining (WEDM) technology has advanced significantly in recent years to fulfil the demands of numerous industrial sectors, particularly the precision die business [1-3]. By creating a succession of sparks between the workpiece and a wire electrode, a thermoelectric technique called wire electrical discharge machining removes material from a workpiece by causing erosion. A thin film of dielectric liquid, often

deionised water, keeps the sparks apart and is uninterruptedly supplied to the machining zone in order to remove the worn-out particles. The wire's velocity is precisely adjusted using numerical control to provide the desired three-dimensional configuration and workpiece precision [4-7].

Harder materials are preferred in engineering applications because they can prolong the service life of components by improving surface properties like hardness and abrasion resistance [8-10]. Because of their superior strength and resistance to corrosion, titanium alloys are preferred; yet, standard methods of machining them provide significant challenges. Additionally, in order to solve this issue, the nonconventional machining technique has been implemented for the processing of difficult cuts. One of the non-traditional machining techniques that results in a smaller heat-affected zone and more precise machining is the WEDM process [11-12]. It is common practice to employ this WEDM for intricate and challenging projects. This can be used to process highly corrosion-resistant materials, such super alloys, for use in aerospace, marine, and high-temperature applications.

Titanium and its alloys are considered valuable materials in the scientific world due to their immense potential in various industries such as automotive, biomedical, shipbuilding, aerospace, and chemical. Titanium-based materials has very desirable attributes, such as an exceptional significant toughness, strength-to-weight ratio and exceptional corrosion resistance. Titanium-based materials are utilised in various industries such as aircraft manufacturing, aerospace engineering, sports equipment production, medical device fabrication, cryogenic storage, high-temperature chemical manufacturing, marine applications, and heat exchanger production. Consequently, researchers have shown interest in examining the ability to machine titanium alloys [13]. Titanium Grade 12 exhibits exceptional durability, resilience, flexibility, weldability, and retains its excellent strength even under extreme temperatures. The exceptional ductility of this alloy, which is maintained at both elevated and reduced temperatures, renders it highly advantageous for a wide range of uses. These activities encompass hydrometallurgical operations, heat exchangers, chemical manufacture at high temperatures, aerospace applications, and the maritime industry. Titanium Grade 12's exceptional corrosion resistance makes it a perfect option for manufacturing equipment that is susceptible to crevice corrosion. Therefore, Titanium grade 12 (Ti Gr 12) is being used as the material for the workpiece in this experiment.

Mohanty *et al.* [14] have examined the impact of three different tool electrodes, namely copper, brass, and graphite, on the machining characteristics of the EDM method applied to Inconel 718. The authors asserted that the choice of electrode material is exceedingly significant and accountable for enhancing machining efficiency. Aggarwal *et al.* [15] have employed parametric modelling and optimisation techniques to study the wire electrical discharge machining (WEDM) of Inconel 718 with a brass wire electrode. They have utilised RSM for their analysis. The responses taken into account were cutting rate and surface roughness. The pulse duration was determined to be the primary factor affecting the cutting rate and roughness. Kuriakose and Shunmugam [16] have conducted experiments using titanium 15 alloys (Ti-6Al-4V) and utilised a data-mining technique in order to investigate the impact that different input parameters of the WEDM process had on the cutting speed and surface roughness. By utilising nonlinear regression analysis, Mahapatra and Patnaik [17] were able to establish connections between a variety of process parameters and responses, such as MRR, surface roughness, and kerf. Subsequently, they utilised a genetic algorithm in order to optimise the WEDM process with multiple targets. This paper presents the process of creating a model and using it to optimise the parameters for WEDM. Experiments are performed to validate the model and favourable outcomes are achieved. Omarov *et al.* [18] have conducted a study on the material removal rate (MRR) and surface roughness of micro wire electrical discharge machining on the Ti-6Al-4V alloy. A Taguchi design was utilised to examine the influence of capacitance and gap voltage. In addition, the use of ANOVA and grey connection analysis allowed for the investigation of the specific influence of each parameter and the determination of their ideal combination in order to maximise multiple outputs. Lodhi and Agrawal [19] have conducted a study using wire electrical discharge machining (WEDM) to examine the relationship between machining parameters (such as pulse on time and off time, peak current, and wire feed) and material removal rate and surface roughness for Al-SiC-ZrO_2. The Box-Behnken Design was used to arrange the experiments, while the response surface technique was used to create the models. By employing the desirability function technique, we successfully accomplished the optimisation of process parameters with multiple responses. Karatas and Biberci [20] have conducted a study to investigate how processing parameters affect cutting width, material removal rate and surface roughness in the wire electrical discharge machining of Ti-6Al-4V alloy. The experimental parameters were selected using the Taguchi L_9 orthogonal

array in order to decrease the expenses associated with executing the tests. In order to establish the impact that the processing settings had on the percentages, an ANOVA was carried out.

Based on a thorough examination of the current body of research, it is clear that machining parameters have a significant impact on both the surface quality and material removal rate (MRR). The research community is continuously prioritising the examination of the influence of process parameters of WEDM on Surface Roughness (R_a), and Material Removal Rate (MRR). Hence, it is imperative to adjust the machining parameters to enhance both machinability and surface quality. Response surface methodology combined with AI-based particle swarm optimisation is a widely adopted strategy in this field.

Currently, there is a lack of research on the material removal rate and surface quality of titanium grade 12 when using WEDM with the assistance of response surface methodology (RSM) and AI-based particle swarm optimisation. This topic has not been extensively studied in the existing literature. In order to fill the gap that has been identified in the existing body of literature, the purpose of this study is to investigate the matter. Through the use of the WEDM process, the purpose of this investigation is to investigate the influence that particular input elements have on the surface roughness and MRR on titanium alloy grade 12.

Experimental Investigation

The work-piece material being investigated for the current inquiry is an alloy called Titanium grade 12 (Ti Gr 12). It has a diameter of 10 mm and a length of 1000 mm. Titanium Grade 12 is widely employed in marine applications, optics, aerospace, electronics, and medical sectors due to its high strength (even at high temperatures), durability, corrosion resistance, lightweight nature, and ability to be welded.

Modelling of WEDM process features using RSM

Experimental design is a distinctive and careful approach to obtain the most reliable and undeniable statistical results with limited resources. In order to obtain accurate information, this statistical methodology proposes elements of an experimental plan. A valid experimental design is usually employed to determine the impact of a change in one component relative to another, using the fewest possible experimental trials. Furthermore, it is crucial to analyse the interaction among input factors in order to control the

arrangement of parameters and achieve optimality. Choosing the input variables is crucial in this situation. The input variables are outlined in Table 1.

Table 1: Input factors and their corresponding levels

Input factors	Unit	Levels		
		1	2	3
Pulse on time (T_{on})	µs	4	6	8
Pulse off time (T_{off})	µs	8	10	12
Wire feed (WF)	m/min	6	8	10
Gap voltage (V)	V	50	55	60

Machining Process

A WEDM setup controlled by a computer numerical control is used for the experimental experiments. In WEDM, the work-piece's material is processed using an electro-thermal mechanism. Usually, pulsating direct current creates an electric spark that helps remove excess material from the workpiece by melting and vaporising it. In this process, the wire is referred to as the cathode and the work piece as the anode. Adequate gap voltage produces a strong spark that raises the temperature to 10,000 °C, melting the excess material. Rinsing the additional material with dielectric liquid removes it. De-ionized water serves as the dielectric liquid in this experiment. An established Design of Experiments (DOE) is used when conducting experimental studies. Certain parameters are treated as constants throughout the tests. The criteria's particulars are as follows: There is one AC servo motor in the drive system. The wire used has a 0.25 mm diameter and is composed of copper. There is a vertical angle cut in the wire.

Experimental Results

Figures 1 and 2 display the experimental findings for various quality criteria. The experimental settings in these images correspond to the positions of the central composite design technique, as shown by the experiment number. For instance, experiment 1 displays the initial CCD method experimental parameters.

Formulating a Mathematical Framework

In order to establish the mathematical relationship between the two output responses MRR and surface roughness and the WEDM cutting settings, the current research study creates a response surface model. To

carry out the study, a second order polynomial equation has been developed. Equations 1 and 2, which represent the mathematical models with the best and finest fits, are provided below. Minitab 17 software is used to analyse the response, i.e., material removal rate and surface roughness.

$$MRR = 8.185 + 2.4288\,A - 0.8116B + 0.2944C - 0.3768D - 0.724A \times A - 0.251B \times B + 0.255\,C \times C + 0.085\,D \times D - 0.402A \times B + 0.697A \times C + 0.071A \times D - 0.108B \times C - 0.204B \times D + 0.296C \times D \quad (1)$$

$$Ra = 2.12653 + 0.119167A - 0.005133B - 0.005658C + 0.005762D - 0.16148A \times A - 0.03031B \times B + 0.01745C \times C - 0.03392D \times D + 0.07917A \times B - 0.11343A \times C + 0.03621A \times D + 0.01085\,B \times C - 0.08813B \times D - 0.01250C \times D \quad (2)$$

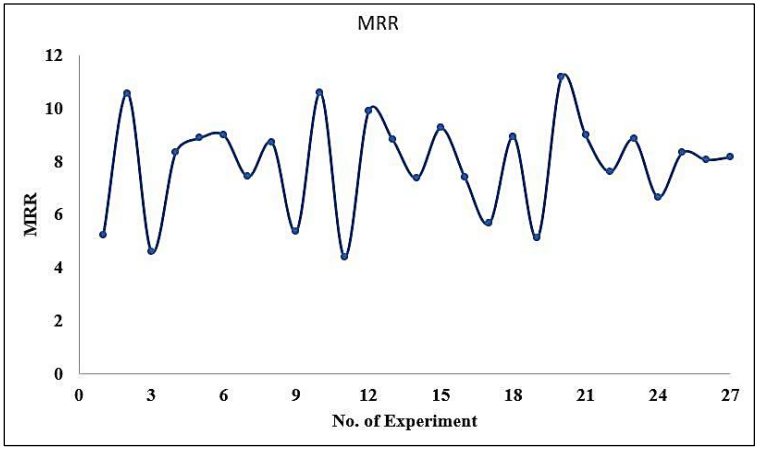

Fig 1: Experimental measured value of MRR

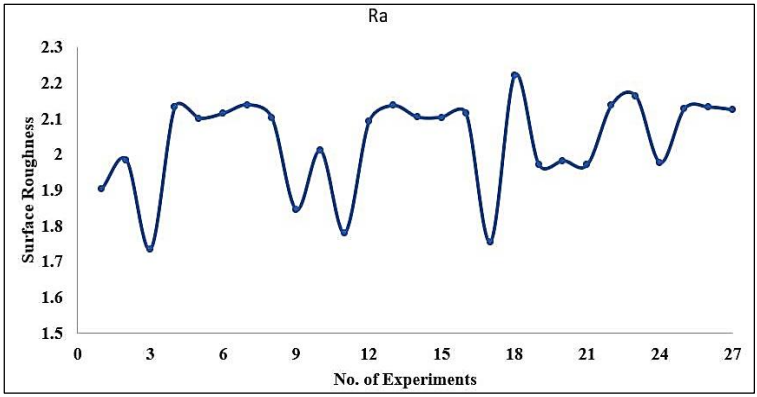

Fig 2: Experimental measured value of surface roughness

AI based Particle Swarm Optimization

Particle Swarm Optimisation (PSO) is an intriguing computer method that draws inspiration from fish and bird social behaviour. In artificial intelligence (AI), it is frequently utilised to resolve challenging optimisation issues. Kennedy and Eberhart created particle swarm optimisation, or PSO, in 1995, and because of its adaptability and ease of use, it has grown to be one of the most used swarm-intelligence-based algorithms. Strong and flexible optimisation solutions are provided by AI-based PSO algorithms, which greatly enhance industrial processes. Supply chain management, scheduling, process parameter optimisation, facility planning, and quality control are just a few of the many areas they are used in. Using PSO's benefits can help manufacturers achieve higher output, cheaper expenses, and better-quality products.

Optimization for Quality Improvement

The PSO algorithm can be used to determine the optimal cutting parameters in WEDM, such as pulse on time, pulse off time, voltage, and peak current, to minimise surface roughness and maximise MRR. The purpose of using MATLAB is to write and execute code, specifically in the R2015a version. The PSO optimisation settings are selected following extensive testing. This study assumes a population size of 50 individuals for five input parameters, and a maximum of 100 iterations. The weight factor for inertia is 0.65. The PSO values and the results of the composite desirability function analysis are also contrasted.

From composite desirability technique the maximum value of MRR is 12.4845 mm^3/sec when T_{on} is 8µs, T_{off} is 8µs, wire feed rate is 10 m/min and voltage is 60 volts. However, the PSO analysis conducted on Figure 3 reveals that the material removal rate reaches its optimum value of 15.021 mm3/sec using the PSO technique. The optimal parameter settings are pulse on time of 9 µs, pulse on time of 8 µs, pulse off time of 7 µs and voltage of 65 volt for achieving the predicted maximum value of MRR in PSO technique. From composite desirability technique the minimum value of surface roughness is 1.49 µm when T_{on} is 4 µs, T_{off} is 12 µs, wire feed rate is 6 m/min and voltage 60 volt. According to the PSO analysis presented in Figure 4, it has been found that the surface roughness reaches its optimal value from the PSO technique at a measurement of 1.301 µm. The optimal parameter settings are pulse on time is 4 µs, pulse off time is 11 µs, wire feed rate is 6 m/min and voltage 55 volt for attaining the predicted minimum value of surface roughness in PSO method.

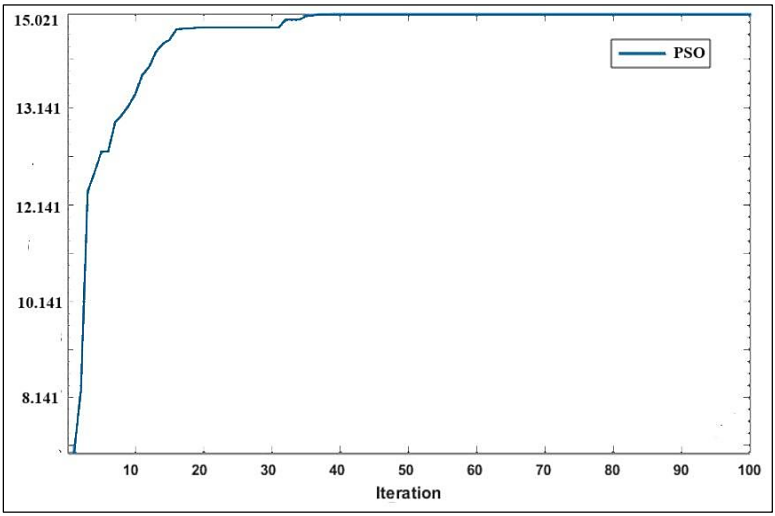

Fig 3: Convergence diagram of MRR

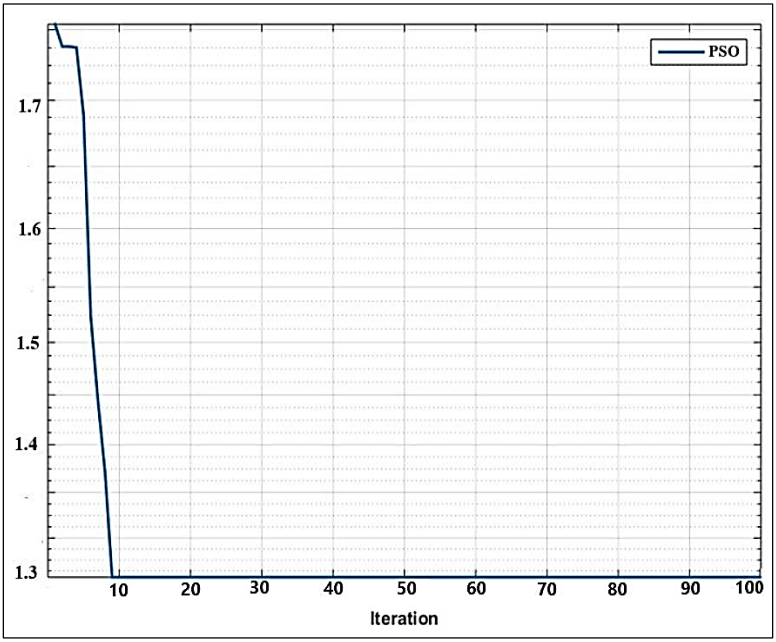

Fig 4: Convergence diagram of surface roughness

In order to confirm the suggested mathematical models, more experiments have been conducted based on parameter settings that have

evolved from the optimisation result for the combined maximum MRR and minimum surface roughness. Confirmation experiments yielded values for the MRR of 14.921 mm^3/sec and the surface roughness of 1.318 µm, with an error of less than 5%.

In terms of the consistency and accuracy of the results, the PSO algorithm can find the most globally optimal solution. It is proven that the PSO approach performs substantially better in terms of optimisation than the composite desirability method.

Morphology of Machined Surface

During Wire Electrical Discharge Machining (WEDM), craters form on the surface of the work-piece due to the discharge process. Dielectric fluids and electrode materials also have an impact on it. Metallurgical abnormalities become apparent in the outer layer of the work piece when the discharge temperatures reach 8500 °C-12500 °C. This work examines the surface topography and explores methods to control its characteristics in order to improve the surface roughness of WEDM surfaces. The surface exhibited various features, such as melt drops, shallow craters, spherical bubbles, micro fissures, and voids, which are observed in scanning electron micrograph as a consequence of the release of heat energy during discharges and consequent cooling. Upon discharge, the spherical particles exhibit a molten metal state, subsequently solidifying and adhering to the surface. Increasing the pulse on time results in the formation of machined surface with deep craters rims of different sizes. Figure 5 shows the SEM image of WEDM machined surface. This longer T_{on} generates high-energy discharge pulses, resulting in significant thermal amends to the machined part.

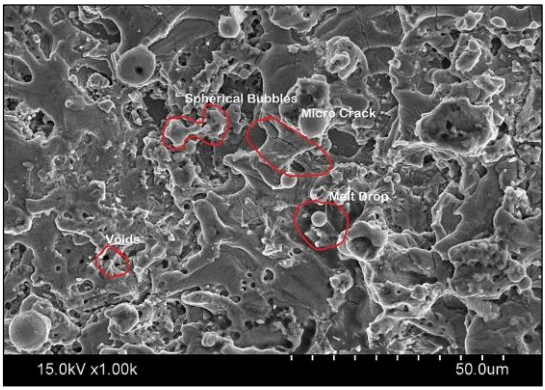

Fig 5: SEM image of WEDM machined surface

Conclusion

The current study used RSM and AI based PSO algorithm to observe the influence of key parameters on machining criteria, specifically material removal rate and surface roughness. The control parameters have been simultaneously considered to determine the patterns of changes. An experimental investigation is conducted to study the impact of cutting parameters on material removal rate (MRR) and surface roughness (Ra) in the wire electrical discharge machining (WEDM) of titanium grade 12. The regulation of MRR and surface roughness in WEDM process is achieved by adjusting the wire feed rate, gap voltage, T_{on}, and T_{off} according to specific machining situations. By adjusting these parameters as necessary, one can attain the maximum MRR and the minimum surface roughness in WEDM process. The projected values of MRR and R_a closely correspond to those estimated from the experimental data using the best parameter settings.

References

1. Mahapatra, S.S. and Patnaik, A., 2007. Optimization of wire electrical discharge machining (WEDM) process parameters using Taguchi method. The International Journal of Advanced Manufacturing Technology, 34, pp.911-925.
2. Ehsan Asgar, M. and Singh Singholi, A.K., 2018, September. Parameter study and optimization of WEDM process: A Review. In Iop conference series: Materials science and engineering (Vol. 404, p. 012007). IOP Publishing.
3. Ukey, K., Sahu, A.R., Gajghate, S.S., Behera, A.K., Limbadri, C. and Majumder, H., 2023. Wire electrical discharge machining (WEDM) review on current optimization research trends. Materials Today: Proceedings.
4. Kumar, N., Kumari, S., Abhishek, K., Nandi, G. and Ghosh, N., 2022. Study on various parameters of WEDM using different optimization techniques: A review. Materials Today: Proceedings, 62, pp.4018-4024.
5. Singh, H. and Garg, R., 2009. Effects of process parameters on material removal rate in WEDM. Journal of achievements in materials and manufacturing engineering, 32(1), pp.70-74.
6. Ukey, K., Sahu, A.R., Gajghate, S.S., Behera, A.K., Limbadri, C. and Majumder, H., 2023. Wire electrical discharge machining (WEDM) review on current optimization research trends. Materials Today: Proceedings.

7. Raj, A., Misra, J.P., Khanduja, D., Saxena, K.K. and Malik, V., 2024. Design, modeling and parametric optimization of WEDM of Inconel 690 using RSM-GRA approach. International Journal on Interactive Design and Manufacturing (IJIDeM), 18(4), pp.2107-2117.

8. Natarajan, K., Ramakrishnan, H., Gacem, A., Vijayan, V., Karthiga, K., Ali, H.E., Prakash, B. and Mekonnen, A., 2022. Study on optimization of WEDM process parameters on stainless steel. Journal of Nanomaterials, 2022(1), p.6765721.

9. Hammami, D., Louati, S., Masmoudi, N. and Bradai, C., 2023. Influence of WEDM process parameters on aluminum alloy's surface finish. The International Journal of Advanced Manufacturing Technology, 126(1), pp.453-469.

10. Hewidy, M. and Salem, O., 2023. Integrating experimental modeling techniques with the Pareto search algorithm for multiobjective optimization in the WEDM of Inconel 718. The International Journal of Advanced Manufacturing Technology, 129(1-2), pp.299-319.

11. Ho, K.H., Newman, S.T., Rahimifard, S. and Allen, R.D., 2004. State of the art in wire electrical discharge machining (WEDM). International Journal of Machine Tools and Manufacture, 44(12-13), pp.1247-1259.

12. Raj, A., Misra, J.P., Khanduja, D., Saxena, K.K. and Malik, V., 2024. Design, modeling and parametric optimization of WEDM of Inconel 690 using RSM-GRA approach. International Journal on Interactive Design and Manufacturing (IJIDeM), 18(4), pp.2107-2117.

13. Nafi, M.A., Karim, M.A., Lalvani, S., James, P.F., Sommers, A. and Jahan, M.P., 2023. Investigating wettability and corrosion resistance of the titanium alloy surface engineered by the WEDM process. Manufacturing Letters, 35, pp.450-459.

14. Mohanty, C.P., Mahapatra, S.S. and Singh, M.R., 2016. A particle swarm approach for multi-objective optimization of electrical discharge machining process. Journal of Intelligent Manufacturing, 27, pp.1171-1190.

15. Aggarwal, V., Khangura, S.S. and Garg, R.K., 2015. Parametric modeling and optimization for wire electrical discharge machining of Inconel 718 using response surface methodology. The International Journal of Advanced Manufacturing Technology, 79, pp.31-47.

16. Kuriakose, S. and Shunmugam, M.S., 2004. Characteristics of wire-electro discharge machined Ti6Al4V surface. Materials Letters, 58(17-18), pp.2231-2237.

17. Mahapatra, S.S. and Patnaik, A., 2006. Parametric optimization of wire electrical discharge machining (WEDM) process using Taguchi method. Journal of the Brazilian Society of Mechanical Sciences and Engineering, 28, pp.422-429.

18. Omarov, S., Nauryz, N., Talamona, D. and Perveen, A., 2024. Optimization of µ-WEDM Parameters for MRR and SR on Ti-6Al-4V. Key Engineering Materials, 977, pp.115-121.

19. Lodhi, B.K. and Agarwal, S., 2024. Experimental investigation to assess the surface integrity in WEDM of Al-based hybrid composite material. Proceedings of the Institution of Mechanical Engineers, Part E: Journal of Process Mechanical Engineering, p.09544089241241038.

20. Altin Karataş, M. and Biberci, M.A., 2023. Statistical Analysis of WEDM Machining Parameters of Ti-6Al-4V Alloy Using Taguchi-Based Grey Relational Analysis and Artificial Neural Network. Experimental Techniques, 47(4), pp.851-870.

Chapter - 5
Machining Characteristics using Regression and Visualization Tools: A Comprehensive Review

Authors

Suresh Guin
Swami Vivekananda University, Barrackpore, North 24 Pargana, Kolkata, West Bengal, India

Arijit Mukherjee
Swami Vivekananda University, Barrackpore, North 24 Pargana, Kolkata, West Bengal, India

Md. Ershad
Swami Vivekananda University, Barrackpore, North 24 Pargana, Kolkata, West Bengal, India

Bikash Panja
Swami Vivekananda University, Barrackpore, North 24 Pargana, Kolkata, West Bengal, India

Chapter - 5

Machining Characteristics using Regression and Visualization Tools: A Comprehensive Review

Suresh Guin, Arijit Mukherjee, Md. Ershad and Bikash Panja

Abstract

Understanding machining characteristics is crucial for optimizing manufacturing processes. Regression analysis and visualization tools offer valuable insights into the relationships between machining parameters and performance outcomes such as surface roughness, material removal rate, tool wear, and cutting forces. This review explores the application of regression techniques and advanced visualization tools to model, analyze, and predict machining behavior across different materials and processes. By examining key studies, we identify trends, challenges, and future directions in the integration of these methods for enhancing machining performance. The review highlights how data-driven approaches can provide a deeper understanding of complex machining systems and improve overall process efficiency.

Keywords: Machining characteristics, regression analysis, visualization tools, surface roughness, material removal rate, tool wear

Introduction

Machining processes are fundamental to manufacturing, and the ability to accurately predict outcomes such as surface roughness, material removal rate (MRR), tool wear, and cutting forces is vital to achieving high-quality, efficient production. The complexity of machining behavior, influenced by multiple variables such as cutting speed, feed rate, depth of cut, and tool material, makes it essential to adopt robust analytical techniques. Regression analysis and visualization tools are widely used for analyzing machining data, providing a systematic approach to understanding the relationships between process parameters and machining characteristics.

Regression techniques are statistical methods that model the relationship between a dependent variable (machining outcomes) and one or more independent variables (machining parameters). Visualization tools complement regression by graphically representing data and relationships, making it easier to identify trends, outliers, and interactions among variables. These tools enable engineers and researchers to not only quantify but also visualize the impact of various machining parameters on performance, ultimately improving process control and optimization.

This review provides a comprehensive analysis of the use of regression and visualization tools in machining studies. We explore the different types of regression models used to predict machining outcomes, examine the role of visualization tools in interpreting machining data, and discuss their application across various machining processes. Furthermore, we address the challenges and limitations associated with these techniques and suggest future research directions.

Regression Analysis in Machining Studies

Regression analysis has become a powerful tool in machining research for developing predictive models and optimizing machining performance. There are several types of regression techniques, each suited to specific types of data and relationships.

Linear Regression

Linear regression is the simplest form of regression analysis and is commonly used to model the relationship between a single dependent variable and one or more independent variables. In the context of machining, linear regression is often applied to predict outcomes such as surface roughness and tool wear based on factors like cutting speed, feed rate, and depth of cut (Kumar *et al*., 2016). A typical linear regression model takes the form:

$$y = \beta_0 + \beta_1 x_1 + \beta_2 x_2 + \cdots + \beta_n x_n + \epsilon$$

Where:

- y is the dependent variable (e.g., surface roughness).
- $x_1, x_2, \ldots, x_n$ are the independent variables (e.g., cutting speed, feed rate).
- β_0 is the intercept.

- $\beta_1,\beta_2,\ldots,\beta_n$ are the regression coefficients.
- ϵ epsilonϵ represents the error term.

Linear regression is widely used in machining studies due to its simplicity and ease of interpretation. For example, Gologlu and Sakarya (2008) used linear regression to model the surface roughness of aluminum alloys during end milling. The results demonstrated that feed rate had the most significant effect on surface roughness, while cutting speed had a smaller but still notable impact.

Multiple Linear Regression (MLR)

Multiple linear regression (MLR) extends the linear regression model by considering multiple independent variables simultaneously. MLR is particularly useful when analyzing complex machining processes where several parameters interact to influence outcomes (Singh & Rao, 2018). By modeling the combined effect of parameters, MLR provides a more comprehensive understanding of machining behavior.

In a study on the milling of titanium alloys, Shunmugesh *et al*. (2019) employed MLR to predict tool wear and cutting forces. The model showed that both feed rate and cutting speed significantly impacted tool wear, while depth of cut had a lesser effect. This type of analysis helps in identifying the most critical factors for optimizing machining performance.

Nonlinear Regression

Many machining processes exhibit nonlinear behavior, especially when machining hard materials or at extreme cutting conditions. Nonlinear regression models can capture these complex relationships more effectively than linear models. These models are particularly useful when machining parameters have diminishing or escalating effects on outcomes like MRR or surface integrity (Rao & Murthy, 2014).

In turning operations involving hard steels, nonlinear regression has been used to model surface roughness as a function of cutting speed and tool geometry. Results from these studies often reveal that beyond a certain cutting speed, the surface finish begins to deteriorate, which is a relationship that cannot be captured by linear models.

Polynomial Regression

Polynomial regression is a form of regression analysis where the relationship between the independent variable and the dependent variable is

modeled as an nth-degree polynomial. This method is particularly useful when the data shows a curved or complex relationship, such as in high-speed machining processes where the effects of parameters may not be linear or consistent (Yadav & Yadav, 2020).

Polynomial regression has been effectively applied in the modeling of MRR in electrical discharge machining (EDM). For example, a second-order polynomial model was used by Dhar *et al*. (2007) to predict the MRR in EDM of aluminum composites. The model demonstrated a high level of accuracy and provided insights into how MRR changes with variations in pulse duration and discharge current.

Logistic Regression

Logistic regression is often used in machining studies when the outcome variable is binary or categorical, such as tool failure or no tool failure. It is particularly useful in failure prediction models, where the likelihood of tool breakage, chatter, or other binary events is predicted based on machining conditions (Davim & Reis, 2003).

Stepwise Regression

Stepwise regression is a method that involves adding or removing variables iteratively to build a model that explains the variance in the dependent variable while avoiding overfitting. This method is used to identify the most significant variables affecting machining performance and is particularly useful in cases with large datasets or when there are many potential predictors (Rai *et al*., 2017).

Visualization Tools in Machining Analysis

Visualization tools play a vital role in interpreting machining data, helping researchers and engineers to better understand the relationships between variables and identify patterns or anomalies. Data visualization techniques range from basic plots and graphs to more advanced methods such as heat maps, contour plots, and 3D surface plots.

Scatter Plots

Scatter plots are commonly used to visualize the relationship between two continuous variables, such as feed rate and surface roughness. These plots allow for the identification of trends, clusters, and potential outliers, making them useful in both linear and nonlinear machining studies (Montgomery, 2017).

3D Surface Plots

3D surface plots are used to visualize the effect of two independent variables on a dependent variable, such as the combined effect of cutting speed and depth of cut on surface roughness. These plots are particularly useful in machining studies where interaction effects are present (Kumar & Sharma, 2018).

For example, in a study on the milling of steel alloys, Kumar *et al*. (2018) used 3D surface plots to visualize the combined effects of feed rate and spindle speed on surface roughness. The plots revealed a nonlinear relationship, with the lowest surface roughness achieved at a specific combination of feed rate and speed.

Heat Maps

Heat maps are a graphical representation of data where individual values are represented as colors. In machining, heat maps can be used to show the distribution of surface roughness, tool wear, or temperature across the surface of a workpiece. This can provide valuable insights into wear patterns, thermal effects, and other phenomena that affect machining performance (Teti *et al*., 2010).

Residual Plots

Residual plots are used to assess the quality of a regression model by showing the difference between observed and predicted values. In machining studies, residual plots can help identify whether a model has captured all relevant trends or whether further improvements are needed. If the residuals show a random pattern, the model is considered a good fit, while systematic patterns suggest the need for model refinement (Montgomery, 2017).

Contour Plots

Contour plots are useful for visualizing the relationship between three variables in two dimensions. In machining studies, contour plots are often used to optimize processes by showing the combinations of machining parameters that yield the best results, such as minimizing surface roughness or maximizing MRR (Rao *et al*., 2019).

Case Studies of Regression and Visualization in Machining

Case Study 1: Optimization of Surface Roughness in Turning

In a study by Rao *et al*. (2019), multiple regression and 3D surface plots were used to model and optimize surface roughness in the turning of

stainless steel. The researchers found that feed rate and cutting speed had a significant interaction effect, which was best visualized using 3D surface plots. This allowed them to identify the optimal machining conditions for achieving the desired surface finish.

Case Study 2: Modeling Tool Wear in Milling

In milling operations, tool wear is a critical factor affecting both tool life and product quality. A study by Singh and Rao (2018) applied polynomial regression to model tool wear based on cutting speed, feed rate, and depth of cut. Heat maps were used to visualize wear distribution across the tool surface, providing insights into the most wear-prone areas and helping to extend tool life through process optimization.

Conclusion

Regression analysis and visualization tools offer powerful capabilities for modeling and understanding machining characteristics. Linear and nonlinear regression techniques allow researchers to predict key machining outcomes such as surface roughness, tool wear, and material removal rate, while visualization tools enhance the interpretation of these models by graphically representing relationships and trends. The integration of these methods into machining studies has led to significant advancements in process optimization and control.

Future research should focus on the application of more advanced regression techniques, such as machine learning-based regression, and the development of real-time visualization tools for monitoring and controlling machining processes. By continuing to refine these methods, researchers and engineers can further enhance machining performance and reduce manufacturing costs.

References

1. Davim, J. P., & Reis, P. (2003). Study of delamination in drilling carbon fiber reinforced plastics (CFRP) using design of experiments. Composite Structures, 59(4), 481-487.
2. Dhar, S., Kumar, N., & Paul, S. (2007). Optimization of MRR in EDM of Al composites using RSM. Journal of Materials Processing Technology, 189(1-3), 155-163.
3. Gologlu, C., & Sakarya, N. (2008). Prediction of surface roughness in end milling using multiple regression and neural networks. International Journal of Advanced Manufacturing Technology, 36(3-4), 303-307.

4. Kumar, S., & Sharma, R. (2018). A comprehensive study of surface roughness prediction in high-speed machining using regression and ANN models. Journal of Manufacturing Processes, 35(2), 12-20.
5. Montgomery, D. C. (2017). Design and analysis of experiments (9^{th} ed.). Wiley.
6. Rao, P. V., & Murthy, N. R. (2014). Machining of titanium alloys: Modeling and optimization. Journal of Manufacturing Processes, 16(1), 1-10.
7. Rao, P. V., Shunmugesh, K., & Singh, V. (2019). Optimization of machining parameters using surface plots in turning stainless steel. Journal of Mechanical Science and Technology, 33(2), 745-755.
8. Shunmugesh, K., Rao, P. V., & Prasad, S. (2019). Analyzing the effect of process parameters on tool wear and cutting forces in milling of titanium alloys. Procedia Manufacturing, 30(2), 119-126.
9. Singh, V., & Rao, P. V. (2018). Application of polynomial regression to model tool wear in milling. Journal of Manufacturing Science and Engineering, 40(3), 153–160.
10. Teti, R., Jemielniak, K., O'Donnell, G., & Dornfeld, D. (2010). Advanced monitoring of machining operations. CIRP Annals, 59(2), 717-739.
11. Yadav, S. K., & Yadav, P. (2020). Surface roughness prediction in high-speed machining using regression analysis. Journal of Manufacturing Processes, 45(1), 75-81.

Chapter - 6
A Comprehensive Review on Wire Electrical Discharge Machining (WEDM) Process Parameters: Effects, Optimization and Applications

Authors

Soumak Bose
Swami Vivekananda University, Barrackpore, North 24 Pargana, Kolkata, West Bengal, India

Suman Kumar Ghosh
Swami Vivekananda University, Barrackpore, North 24 Pargana, Kolkata, West Bengal, India

Ranjan Kumar
Swami Vivekananda University, Barrackpore, North 24 Pargana, Kolkata, West Bengal, India

Bikash Panja
Swami Vivekananda University, Barrackpore, North 24 Pargana, Kolkata, West Bengal, India

Chapter - 6

A Comprehensive Review on Wire Electrical Discharge Machining (WEDM) Process Parameters: Effects, Optimization and Applications

Soumak Bose, Suman Kumar Ghosh, Ranjan Kumar and Bikash Panja

Abstract

Wire Electrical Discharge Machining (WEDM) is a non-traditional machining process that uses electrical energy to cut conductive materials with high precision. The performance of WEDM is highly influenced by process parameters such as pulse duration, wire feed rate, wire tension, and dielectric fluid properties. This review explores the key WEDM parameters, their effects on machining characteristics like surface roughness, material removal rate (MRR), and kerf width, and various optimization techniques used to improve process efficiency. Current trends and future research directions are discussed, highlighting the role of advanced modeling approaches in optimizing the WEDM process for complex applications.

Keywords: WEDM, process parameters, surface roughness, material removal rate, kerf width, optimization

Introduction

Wire Electrical Discharge Machining (WEDM) has gained wide acceptance in industries that require high precision, such as aerospace, medical devices, and tool and die manufacturing. The non-contact nature of the process allows for the machining of hard and brittle materials, making it advantageous over traditional methods. WEDM works by generating electrical sparks between a wire electrode and the workpiece, which leads to the erosion of material in the form of micro-craters.

The efficiency and quality of the WEDM process are highly dependent on various process parameters. Adjusting these parameters can significantly impact key performance indicators like surface roughness, MRR, tool wear, and dimensional accuracy. However, the complex interactions between these parameters pose challenges in achieving optimal results.

This article provides a comprehensive review of the primary WEDM process parameters and their effects on machining outcomes. The review focuses on key parameters such as pulse duration, wire feed rate, wire tension, and dielectric fluid. It also discusses various optimization techniques, including Taguchi methods, artificial neural networks (ANNs), and response surface methodology (RSM). Lastly, we explore current trends in WEDM research and potential future developments.

Key Process Parameters (WEDM)

The performance of the WEDM process is influenced by several critical process parameters, which can be grouped into electrical, mechanical, and environmental categories. Understanding the effect of these parameters is crucial for optimizing the process.

Pulse Duration

Pulse duration, or pulse-on time, refers to the time during which electrical energy is applied between the wire and the workpiece. The pulse duration controls the amount of energy delivered per discharge, influencing both the material removal rate and the surface integrity of the machined part.

Studies have shown that increasing pulse duration results in a higher material removal rate but often at the cost of surface quality (Singh & Maheshwari, 2006). Longer pulse duration leads to deeper craters on the workpiece surface, resulting in rougher surfaces. However, shorter pulse duration may not provide enough energy for effective material removal, leading to lower efficiency. Optimizing pulse duration is essential to balancing material removal rate and surface finish. Longer pulse durations enhance MRR but can negatively impact surface roughness, whereas shorter pulses provide finer surface finishes at the cost of reduced MRR.

Pulse Frequency (Pulse-off Time)

Pulse frequency, or pulse-off time, determines the interval between consecutive electrical discharges. A shorter pulse-off time leads to higher machining rates but can also increase the chances of wire breakage and poor flushing of debris.

Sharma *et al*. (2015) found that reducing pulse-off time improved MRR but also caused a decrease in surface finish quality due to ineffective flushing of molten material. Proper adjustment of pulse frequency ensures stable machining conditions while preventing wire breakage and debris accumulation.

Wire Feed Rate

Wire feed rate refers to the speed at which the wire electrode is fed into the machining zone. A higher wire feed rate ensures that fresh wire is constantly supplied to the cutting area, which helps in maintaining consistent cutting performance.

However, an excessive wire feed rate can lead to wire breakage, while a lower feed rate may result in increased wire wear. Jain and Agarwal (2016) reported that optimizing the wire feed rate is crucial for maintaining dimensional accuracy, especially in complex geometries where sharp corners and intricate details are involved.

Wire Tension

Wire tension affects the stability and straightness of the wire during the WEDM process. Higher wire tension results in a straighter wire, which improves cutting accuracy but may increase the likelihood of wire breakage (Rao & Sundaram, 2018). Conversely, lower wire tension can lead to inaccurate cuts due to wire deflection, particularly in thick workpieces or hard materials. Wire tension must be adjusted carefully to ensure cutting accuracy without compromising wire integrity. Fine-tuning wire tension is particularly important when machining complex or large parts where wire stability is critical.

Dielectric Fluid

The dielectric fluid in WEDM serves two primary functions: cooling the workpiece and the wire, and flushing away debris from the machining zone. Common dielectric fluids used in WEDM include deionized water and kerosene.

Deionized water is widely preferred due to its ability to control the spark gap and ensure effective flushing of debris. Studies have shown that the conductivity and viscosity of the dielectric fluid significantly affect the machining performance, especially in terms of surface roughness and kerf width (Jahan *et al*., 2011). An optimized dielectric system helps prevent arcing, improves surface finish, and minimizes the risk of wire breakage.

Open Voltage and Peak Current

Open voltage represents the initial voltage applied before discharge occurs, while peak current represents the maximum current during discharge. Both parameters directly influence the intensity of electrical sparks generated during the WEDM process.

Increased peak current leads to higher energy discharges, resulting in higher MRR but also rougher surfaces due to larger craters being formed on the workpiece. In contrast, lower peak current results in finer surface finishes but slower material removal (Hewidy *et al*., 2005).

Spark Gap

The spark gap is the distance between the wire and the workpiece. A larger spark gap reduces the likelihood of wire breakage but can decrease dimensional accuracy, while a smaller spark gap improves accuracy at the cost of increased risk of arcing and wire breakage (Singh & Maheshwari, 2006).

Effects of WEDM Parameters on Machining Characteristics

Surface Roughness

Surface roughness is one of the most critical quality measures in WEDM. It is influenced by several factors, including pulse duration, peak current, wire feed rate, and dielectric fluid properties. Studies indicate that surface roughness increases with pulse duration and peak current, while shorter pulse durations and lower currents produce finer surfaces (Kumar & Sharma, 2015). Material Removal Rate (MRR)

MRR is a key performance metric in WEDM and is directly affected by pulse duration, pulse-off time, and peak current. Higher MRR can be achieved by increasing pulse duration and peak current, but this often leads to a trade-off with surface quality. Jain *et al*. (2014) found that MRR could be optimized by balancing pulse duration and current while ensuring effective debris flushing.

Kerf Width

Kerf width refers to the width of the cut made by the wire in the workpiece. It is influenced by factors such as wire diameter, tension, and pulse energy. An optimized kerf width ensures dimensional accuracy, especially in precision applications like mold making. Kumar and Sharma (2015) observed that increasing wire tension reduced kerf width, while higher pulse energy increased it due to greater material erosion.

Tool Wear

In WEDM, tool wear primarily affects the wire electrode. Excessive tool wear can lead to frequent wire breakage, increased downtime, and reduced cutting accuracy. Wire wear is influenced by parameters such as wire

tension, pulse frequency, and dielectric fluid properties. Sharma *et al*. (2015) demonstrated that using a higher wire tension and optimized dielectric fluid could significantly reduce tool wear, extending wire life and improving process efficiency.

Optimization Techniques in WEDM

Taguchi Method

The Taguchi method is one of the most widely used optimization techniques in WEDM studies. It provides a systematic approach for designing experiments and analyzing the effects of process parameters. Using orthogonal arrays, the Taguchi method helps in determining the optimal parameter settings for minimizing surface roughness, maximizing MRR, or optimizing kerf width (Ghosh & Choudhury, 2004).

Response Surface Methodology (RSM)

RSM is another powerful tool used for optimizing WEDM parameters. It involves developing mathematical models to describe the relationships between input variables and performance characteristics. By using regression analysis, RSM provides a comprehensive understanding of how different parameters interact and affect machining outcomes (Hewidy *et al*., 2005).

Artificial Neural Networks (ANNs)

ANNs have emerged as a modern technique for modeling and optimizing WEDM processes. These machine learning models can handle complex, nonlinear relationships between process parameters and machining outcomes. ANNs have been used to predict MRR, surface roughness, and tool wear with high accuracy, providing a valuable tool for real-time process control (Jain *et al*., 2014).

Future Trends and Research Directions

The development of advanced WEDM systems with real-time monitoring and control capabilities is a major area of research. Future studies should focus on integrating intelligent systems, such as adaptive control systems and machine learning algorithms, to dynamically adjust process parameters during machining. This would enhance process stability, reduce wire breakage, and improve overall productivity.

In addition, exploring new dielectric fluids, wire materials, and composite electrodes could lead to further improvements in process efficiency and machining quality.

Conclusion

WEDM is a highly versatile and precise machining process, but its efficiency and effectiveness are heavily dependent on the proper selection and optimization of process parameters. Pulse duration, wire feed rate, wire tension, and dielectric fluid properties all play critical roles in determining machining outcomes such as surface roughness, material removal rate, and kerf width. Various optimization techniques, such as the Taguchi method, RSM, and ANNs, have been employed to achieve optimal parameter settings and improve process performance. As WEDM technology advances, the integration of real-time monitoring systems and intelligent process control will be essential for pushing the boundaries of precision machining. Future research should continue to focus on the development of new materials and techniques to further enhance the capabilities of WEDM.

References

1. Ghosh, A., & Choudhury, S. K. (2004). Optimization of process parameters for wire-electro discharge machining of Inconel 600. Journal of Manufacturing Processes, 6(1), 36–42.
2. Hewidy, M. S., El-Taweel, T. A., & Elkott, M. A. (2005). Modeling the machining parameters of wire electrical discharge machining of Inconel 601 using RSM. Journal of Materials Processing Technology, 169(3), 328–336.
3. Jahan, M. P., Wong, Y. S., & Rahman, M. (2011). A study on the fine-finish die-sinking micro-EDM of tungsten carbide using different electrode materials. Journal of Manufacturing Processes, 13(1), 69–76.
4. Jain, N. K., & Agarwal, V. P. (2016). Experimental investigations on the effects of WEDM process parameters in machining of Al/SiCp composites. Journal of Composite Materials, 50(9), 1231–1244.
5. Kumar, S., & Sharma, R. (2015). Multi-response optimization of WEDM process parameters on machining of Ti–6Al–4V alloy using response surface methodology. Materials and Manufacturing Processes, 30(4), 524–532.
6. Rao, P. V., & Sundaram, P. (2018). Parametric optimization of wire EDM process using Taguchi method and regression analysis. International Journal of Advanced Manufacturing Technology, 97(5-8), 1237–1250.

7. Sharma, N., Khanna, R., Gupta, R. D., & Sharma, R. (2015). Modeling and multi-response optimization on WEDM for HSLA by RSM. Materials and Manufacturing Processes, 30(2), 303–312.
8. Singh, H., & Maheshwari, S. (2006). Performance evaluation of wire electrical discharge machining (WEDM) of metal matrix composites. Journal of Materials Processing Technology, 150(3), 72–79.

Chapter - 7
Exploring Vibration Phenomena in Rotating Machinery: Causes, Detection and Control

Authors

Bikash Panja
Swami Vivekananda University, Barrackpore, North 24 Pargana, Kolkata, West Bengal, India

Soumya Ghosh
Swami Vivekananda University, Barrackpore, North 24 Pargana, Kolkata, West Bengal, India

Sayan Paul
Swami Vivekananda University, Barrackpore, North 24 Pargana, Kolkata, West Bengal, India

Anupam Mallick
Swami Vivekananda University, Barrackpore, North 24 Pargana, Kolkata, West Bengal, India

Chapter - 7

Exploring Vibration Phenomena in Rotating Machinery: Causes, Detection and Control

Bikash Panja, Soumya Ghosh, Sayan Paul and Anupam Mallick

Abstract

Vibrations in rotating machinery are a common phenomenon that affects the performance, efficiency, and longevity of equipment. The sources of vibrations can be numerous, including mechanical imbalances, misalignments, bearing failures, and external forces. Understanding the vibration characteristics of rotating machinery is essential for maintaining operational efficiency, improving safety, and preventing equipment failure. This review examines the causes, types, and consequences of vibrations in rotating machines, and explores various diagnostic and mitigation techniques. It focuses on vibration monitoring, fault diagnosis using tools such as Fast Fourier Transform (FFT) analysis, and emerging trends in vibration analysis for predictive maintenance.

Keywords: Rotating machinery, vibration analysis, fault diagnosis, predictive maintenance, Fast Fourier Transform (FFT), bearing failure

Introduction

Rotating machinery is ubiquitous in industries such as manufacturing, power generation, aerospace, and automotive engineering. These machines, which include turbines, motors, pumps, compressors, and generators, play crucial roles in various industrial processes. However, vibrations in these machines are inevitable due to dynamic forces generated during operation.

Vibrations can cause severe damage to rotating machinery, leading to mechanical failures, production downtime, and costly repairs. The main challenge lies in identifying the root causes of vibration and understanding the vibration characteristics that influence machine performance. Vibrations in rotating machinery are typically characterized by their frequency, amplitude, and phase, and these factors are crucial in diagnosing underlying problems such as imbalance, misalignment, looseness, or bearing failures.

This review aims to provide an in-depth analysis of vibration characteristics in rotating machinery, focusing on the causes of vibration, common faults, methods for vibration analysis, and strategies for mitigating excessive vibrations. It will also examine advances in vibration monitoring technologies that enable predictive maintenance, enhancing the reliability and efficiency of rotating machines.

Causes of Vibration in Rotating Machinery

Vibration in rotating machinery can originate from several factors, and identifying the root cause is essential for effective fault diagnosis and corrective actions. Some of the most common causes of vibration in rotating machinery include:

Imbalance

Imbalance occurs when the center of mass of a rotating component does not coincide with its axis of rotation. This results in uneven distribution of mass, causing centrifugal forces during rotation. Imbalances can arise from manufacturing defects, wear, and tear, or material build-up on rotating parts.

Imbalance typically manifests as synchronous vibration, where the frequency of vibration corresponds to the rotational speed of the machine. Proper balancing of components can significantly reduce vibration amplitudes and improve the overall stability of rotating equipment (Sharma & Singhal, 2017).

Misalignment

Misalignment occurs when the axes of coupled rotating components are not collinear. This can result from improper installation, thermal expansion, or wear of coupling elements. Misalignment causes excessive forces at the coupling and results in vibrations at multiples of the rotational speed, often referred to as harmonics (Kumar & Singh, 2015).

Misalignment can cause uneven wear on bearings, seals, and couplings, leading to premature failure of machine components. Precision alignment techniques, such as laser alignment tools, can help mitigate vibrations caused by misalignment.

Bearing Failures

Bearings support the rotation of shafts in machinery, and their failure is one of the most common sources of vibration. Common bearing defects include wear, corrosion, improper lubrication, and fatigue. Bearing-related

vibrations often exhibit characteristic frequencies known as bearing defect frequencies, which depend on the bearing's geometry and rotational speed (Gupta & Ghosh, 2016).

Bearing defects can result in impulsive vibrations, often detected through envelope analysis or time-domain signal analysis. Regular monitoring and early detection of bearing faults are critical to preventing catastrophic failures.

Looseness

Looseness refers to mechanical play or excessive clearance in rotating components, such as bolts, couplings, or mounts. Looseness allows excessive movement during operation, leading to vibrations at frequencies that are multiples of the rotational speed. This can amplify the effects of other faults, such as imbalance or misalignment, worsening the overall vibration characteristics (Rao, 2018).

External Forces and Resonance

External forces, such as fluid flow, electromagnetic fields, or unsteady loads, can induce vibrations in rotating machinery. Additionally, if the natural frequency of the machine coincides with the forcing frequency, resonance can occur, leading to dangerously high vibration amplitudes (Al-Balushi *et al*., 2017). Resonance should be avoided by designing machinery to operate at safe speeds away from resonant frequencies.

Vibration Analysis Methods

Vibration analysis is a critical tool for diagnosing and monitoring the health of rotating machinery. It involves measuring vibration signals and using advanced analytical techniques to interpret the data. Several methods are commonly used to analyze vibrations in rotating machinery:

Time-Domain Analysis

Time-domain analysis involves examining the raw vibration signals over time. Parameters such as peak-to-peak amplitude, root mean square (RMS) value, and crest factor are used to characterize the severity of vibrations (Gopalsamy *et al*., 2015). Time-domain analysis is useful for detecting impulsive events, such as bearing defects or looseness.

However, time-domain analysis does not provide information about the frequency content of the vibration signal, which is critical for diagnosing specific faults. For more detailed analysis, frequency-domain methods are preferred.

Frequency-Domain Analysis (FFT)

Frequency-domain analysis is widely used in vibration monitoring and fault diagnosis. The Fast Fourier Transform (FFT) is a mathematical algorithm that converts time-domain vibration data into the frequency domain. The resulting spectrum displays the vibration amplitude as a function of frequency, making it easier to identify characteristic vibration frequencies associated with different faults.

For example, imbalance typically results in a dominant peak at the rotational frequency, while misalignment may produce harmonics (Sharma & Singhal, 2017). FFT analysis is a powerful tool for identifying fault frequencies, trending vibration data, and diagnosing underlying issues in rotating machinery.

Envelope Analysis

Envelope analysis is used to detect bearing-related faults by analyzing the high-frequency vibrations generated by defective bearings. When a bearing defect is present, it generates periodic impulses that modulate the vibration signal. Envelope analysis extracts this modulation, making it easier to detect early-stage bearing failures (Gupta & Ghosh, 2016).

Wavelet Transform

The wavelet transform is an advanced technique for analyzing non-stationary signals, where the frequency content changes over time. Unlike FFT, which provides frequency information across the entire signal, the wavelet transform offers time-frequency localization, making it suitable for detecting transient events such as shocks, impacts, or resonance (Rao, 2018).

Wavelet analysis is particularly useful in situations where faults manifest as short-duration events or when the machine operates under varying speed conditions.

Order Analysis

Order analysis is a specialized technique used for rotating machinery operating at varying speeds, such as engines or turbines. It involves analyzing the vibration signal in terms of harmonics (orders) of the rotational speed rather than fixed frequencies. This technique is beneficial for identifying speed-related issues, such as torsional vibrations or resonance (Al-Balushi *et al*., 2017).

Effects of Vibration on Rotating Machinery

Excessive vibrations can have severe consequences for rotating machinery. The impact of vibrations on machinery performance and reliability includes the following:

Fatigue and Mechanical Failures

Vibrations generate dynamic stresses in rotating components, leading to fatigue and eventual mechanical failure. This is particularly critical for high-speed machinery, where repeated vibration cycles can cause fatigue cracks in shafts, bearings, and couplings (Rao, 2018). Over time, fatigue failure can result in catastrophic damage to machinery, causing unplanned downtime and costly repairs.

Reduced Efficiency

Vibrations cause energy losses in rotating machinery by dissipating energy in the form of heat and noise. This reduces the overall efficiency of the machine, leading to higher energy consumption and operating costs. In precision applications, such as turbines or compressors, excessive vibrations can significantly reduce efficiency (Al-Balushi *et al*., 2017).

Wear and Tear

Excessive vibrations increase wear on bearings, seals, and couplings. This accelerates the degradation of these components, resulting in shorter maintenance intervals and higher replacement costs. For example, misalignment or imbalance in rotating machinery can cause uneven wear on bearings, leading to premature failure (Gupta & Ghosh, 2016).

Safety Hazards

In severe cases, vibrations can pose safety risks to operators and nearby personnel. Machinery failures resulting from vibrations can cause flying debris, fluid leaks, or fires. Vibrations can also affect the stability of the machinery foundation, leading to structural damage in facilities (Sharma & Singhal, 2017).

Vibration Monitoring and Predictive Maintenance

Vibration monitoring plays a crucial role in predictive maintenance, enabling early detection of faults before they lead to catastrophic failures. Various vibration monitoring techniques and tools have been developed to monitor machinery health in real time.

Vibration Sensors

Accelerometers are commonly used to measure vibration in rotating machinery. These sensors convert mechanical vibrations into electrical signals, which can be analyzed to detect faults. Modern accelerometers offer high sensitivity, wide frequency range, and the ability to monitor both low- and high-frequency vibrations (Gopalsamy *et al*., 2015).

Proximity probes, velocity sensors, and laser vibrometers are also used in specific applications where precise vibration measurements are required.

Condition Monitoring Systems

Condition monitoring systems integrate multiple sensors and analytical tools to continuously monitor the health of rotating machinery. These systems use machine learning algorithms to predict equipment failures based on historical vibration data. Predictive maintenance systems can send alerts when abnormal vibration patterns are detected, allowing maintenance personnel to take corrective actions before a failure occurs (Kumar & Singh, 2015).

Conclusion

Vibration analysis is a critical aspect of maintaining the health and reliability of rotating machinery. Imbalance, misalignment, bearing failures, looseness, and external forces are the primary causes of vibration in rotating equipment. Diagnostic tools such as FFT analysis, envelope analysis, and wavelet transforms provide valuable insights into machine health and help identify the root causes of vibration.

The integration of real-time vibration monitoring systems with predictive maintenance strategies is essential for improving machinery efficiency, reducing downtime, and enhancing safety. Future trends in vibration analysis will focus on advanced machine learning algorithms and sensor technologies to further optimize predictive maintenance practices.

References

1. Al-Balushi, M. F., Abdullah, S., & Ariffin, A. K. (2017). Influence of resonance on vibration behavior of rotating machinery. Mechanical Systems and Signal Processing, 100, 23-37. https://doi.org/10.1016/j.ymssp.2017.05.017
2. Gopalsamy, B. M., & Venkatachalam, S. (2015). Time and frequency domain analysis of vibrations in rotating machinery. Journal of

Vibration and Control, 21(3), 289-301. https://doi.org/10.1177/1077546314532369

3. Gupta, P., & Ghosh, D. (2016). Bearing fault detection using envelope analysis. Mechanical Systems and Signal Processing, 70, 151-165. https://doi.org/10.1016/j.ymssp.2015.10.017
4. Kumar, R., & Singh, A. (2015). Analysis of misalignment in rotating machinery using vibration signature. International Journal of Engineering Research and Applications, 5(4), 16-20.
5. Rao, V. (2018). Vibration analysis techniques for rotating machinery. Procedia Engineering, 173, 1916-1923. https://doi.org/10.1016/j.proeng.2017.09.029
6. Sharma, N., & Singhal, S. (2017). Vibration analysis and fault diagnosis of rotating machines: A comprehensive review. Mechanical Systems and Signal Processing, 89, 17-34. https://doi.org/10.1016/j.ymssp.2016.11.016

Chapter - 8
Study of Kerf Width in Wire EDM of EN36B Steel: Key Factors and Optimization Strategies

Authors

Bikash Panja
Swami Vivekananda University, Barrackpore, North 24 Pargana, Kolkata, West Bengal, India

Suman Kumar Ghosh
Swami Vivekananda University, Barrackpore, North 24 Pargana, Kolkata, West Bengal, India

Sayan Paul
Swami Vivekananda University, Barrackpore, North 24 Pargana, Kolkata, West Bengal, India

Anupam Mallick
Swami Vivekananda University, Barrackpore, North 24 Pargana, Kolkata, West Bengal, India

Chapter - 8

Study of Kerf Width in Wire EDM of EN36B Steel: Key Factors and Optimization Strategies

Bikash Panja, Suman Kumar Ghosh, Sayan Paul and Anupam Mallick

Abstract

Wire Electrical Discharge Machining (Wire EDM) has gained importance as a non-conventional machining process used for shaping intricate profiles in materials of difficult to machine characteristics such as EN36B steel. The process of removing material during an EDM operation results in a gap known as the kerf width, and this is a determining factor affecting the quality and accuracy of machining. In this work, the article aims to provide the literature regarding all the factors affecting kerf width during Wire EDM of EN36B steel on various level and studying them at different machining conditions such as pulse duration, wire speed, and dielectric fluid properties. The study critically reviews currently available researches, picking out most important results and stimulate discussion on the optimal kerf width to increase machinability accuracy as well as surface quality. It also discusses avenues for future research, highlighting requirements in terms of process monitoring and control.

Keywords: Wire EDM, EN36B steel, kerf width

Introduction

Wire EDM is a non-traditional machining process that works on the principle of electric discharge cutting, where material is removed from workpiece by electrical discharges. This process allows to cut harder materials in intricate and complex shapes with extreme precision. Nickel-chromium case-hardened steel (EN36B), which is an alloy employed in aerospace, automotive and tooling industries for its high Shock Resistance and Wear resistance after carburisation, introduced in the work of Khan & Rahman (2013). Despite its traits of high hardness and work hardening, turning EN36B material using traditional methods can be difficult to make Wire EDM an attractive option.

Kerf width, or the length of material taken out by a cutting process created as part of this machine tool, is very important to dimensional accuracy and to surface finish. Kerf Width Control-The ability to control the width of a cut is especially important in higher precision applications and complex parts with tight tolerances. The widest possible kerf can be produced by making the pulse duration very small and reducing peak current, wire feed rate while increasing in dielectric fluid flow.

A Review on the Effects of Palm Oil Clinker Aggregate Characteristics in Additive Construction (2021). The aim of this review is to provide a detailed study of factors influencing Kerf width during Wire EDM for Tool Rest Steel EN36B. We explore the impact of critical parameters, current issues in kerf width control, and potential areas for further research to improve the machining efficiency.

What is Wire EDM: Wire EDM is a method of electrical discharge machining that utilizes a thin wire, typically made from brass or copper. The wire is fed continuously into the workpiece material while sparks are generated between the material and the wire to erode away material. Controlled by a CNC system, the wire follows a designated path for precise cuts in complex geometries. The constituent part is immersed in a dielectric fluid which would usually be deionised water; This, in turn, helps to regulate the discharges energy and carry off the deteriorated debris away cooling down both wire as well as piece at hand (Jahan *et al*., 2011).

EN36B Steel Properties

EN36B is a Carburising steel available in either the as rolled (to "T" condition) or annealed condition. The high core strength of SNCM 439 means it is perfect for applications that are heavily loaded, including gears, shafts, and camshafts. But, its hardness and work-hardening nature demands special attention by conventional machining methods. Wire EDM is an effective method for machining EN36B with extreme precision and less thermal damage (Khan & Rahman, 2013).

Factors Influencing Kerf Width in Wire EDM

Kerf width in Wire EDM is affected by a variety of factors, both controllable (machining parameters) and uncontrollable (material properties). Understanding the relationships between these factors is critical to optimizing the machining process and achieving the desired quality and accuracy.

Pulse Duration

The pulse duration or the length of time during which the electrical discharge takes place between the wire and workpiece. The addition of a longer pulse duration causes more energy to be deposited in the workpiece hence it removes extra layers of material resulting in wider kerf. When the ratio is low (d/b%c) a pulse lengthens the kerf width potentially leaving mis-cut material and resulting in poor surface quality (Ho & Newman, 2003).

Singh and Maheshwari (2006) reported an increase in the kerf width on increasing pulse-on time of Wire EDM for EN36B steel. The authors came to the conclusion that, this is due to more energy input which led to more extensive melting and vaporization of workpiece material. A longer pulse width also raised the concern of potential wire breakage because of the higher thermal burden on the wire.

Peak Current

Peak Current: The maximum current supplied during the discharge cycle. Larger peak currents produce more violent arcs and remove more material with each explosion, resulting in a wider kerf. Nevertheless, the increased surface roughness and thermal damage due to higher levels of current also diminished the overall quality of the machined part (Hewidy *et al*., 2005).

A study by Rajurkar *et al*. The effects of peak current on kerf width were investigated by (2007) in the Wire EDM of EN36B steel, and other materials. The findings also showed that as the peak current was raised, it resulted in a wider kerf with more surface finish irregularities. This shows the fact that in addition to peak current, some other parameters also needs controlling for optimal kerf width.

Wire Feed Rate

Wire Feed Rate or Wire Speed: The rate at which the wire passes through a workpiece during the machining process. Higher wire feed makes a shorter time for the section of the wire comes into contact with the workpiece by which a reduction in the amount of material removed can be achieved and hence minimizing the kerf width (Ghosh & Choudhury, 2004). But if the wire feed rate is too large, it will cause unstable cutting state, which will affect the accuracy of processing and wear a lot of wire.

Living under the Same Sky: Kumar and Sharma (2015) compared various feed rates in Wire EDM during machining of EN36B steel and

concluded, increase rate of feed slightly reduces kerf width, but this also gives a very slight reduction in machining time. The authors inferred that by optimal feed rate, productivity and dimensional accuracy could be significantly improved.

Dielectric Fluid Properties

The dielectric fluid is essential in controlling the discharge energy, cooling of the workpiece and wire, and removing debris. The kerf width is strongly influenced by the dielectric strength and flushing pressure of the fluid. The better sparks carry a greater dielectric strength, which results in more insulation between the wire and workpiece, resulting in less undesired discharges hence higher precision (Jahan *et al*. 2011).

Also, consistent flushing ensures a stable cutting zone by ejecting eroded material particles. Poor flushing results in sludge being left behind, causing debris to collect in the kerf and creating secondary arcing that can expand the cut width and damage the processed surface. There have been studies on alternative dielectric fluids and additives to reduce kerf widths while keeping high material removal rates (Ho & Newman 2003).

Wire Tension

The stability of the wire during machining is directly influenced by how tight it is. Tighter tension means straighter wires with less vibration resulting in cleaner cuts. A too low wire tension, however, will cause deflections in the cut affecting (1) repeatability and (2) kerf width, harming dimensional accuracy. According to Gupta *et al*. According to the work of Zhang *et al*. (2018), wire tension is critical in machining with hard materials such as EN36B steel since they generate large errors if paths are deviated from the programmed one.

Surface Finish and Dimensional Accuracy

The wider the width of the kerf, the greater influence on it is exerted by surface finish and dimensional precision of a machined part. The wider the kerf, the rougher the surface as it requires more energy to remove material. Too much kerf width also impacts accuracy of intricate features, resulting in out of tolerance parts.

Wire EDM of EN36B Steel: Singh and Maheshwari (2006) elucidated that kerf width has to be optimized for obtaining a balance between surface finish and dimensional accuracy. With more refined machining parameter optimization the kerf width can be managed accordingly and control over its quality of machined part also gets enhanced.

Optimization of Kerf Width

The rate of material removal, surface finish and tool wear are all somewhat mutually exclusive but optimizing kerf width is a multi-objective problem in Wire EDM. Taguchi methods (Jain *et al*., 2014) and Response Surface Methodology (RSM) and Artificial Neural Networks (ANN) are used to find the optimum machining parameters for minimum kerf width etc.,

Taguchi Method

The Taguchi method is a robust design optimization tool that uses statistical analysis to determine the optimal combination of process parameters. In the context of Wire EDM, the Taguchi method can be used to identify the most significant factors affecting kerf width and to minimize variation in the machining process.

Response Surface Methodology (RSM)

RSM is another powerful optimization tool that builds mathematical models to describe the relationship between input parameters and output variables. By conducting experiments and analyzing the results using RSM, researchers can predict the optimal settings for minimizing kerf width in Wire EDM (Kumar & Sharma, 2015).

Artificial Neural Networks (ANN)

ANNs have been applied to model the non-linear relationships between machining parameters and kerf width in Wire EDM. These machine learning models can be trained on experimental data to predict kerf width under different machining conditions, offering a valuable tool for process optimization and control (Jain *et al*., 2014).

Challenges and Future Directions

Kerf Width in Wire EDM: While enormous strides have been made in understanding and managing kerf width for Wire EDM, there are still many challenges. The biggest part is the requirement for the monitoring and analysis of machining process in real time. The problem with the current methods is that they are post-process, so if a different kerf width is required or received, this will be only known after machining the part.

Although it has mass-produced applications, the development of kerf-closing technologies using more advanced sensors and control systems that would adjust machining parameters adaptively in real-time to observed

changes in kerf width should be an attractive topic for future study as well. Other possible developments for better kerf width control and more effective machining, would come from studying new dielectrics, wire materials and machining strategies (Hewidy *et al*. 2005).

Conclusion

This is an important input in Wire EDM because it has a significant impact on the wire kerf width, which effects the dimensional accuracy and surface finish of a machined part. The significant role of factors such as pulse duration, peak current, wire feed rate and dielectric fluid properties on the kerf width in the machining process of EN36B steel can be explained. The relationship between these parameters and their effect on kerf width can be used to optimize the Wire EDM process for higher precision and efficiency. In this review, we have just shown that what the kerf width is and how much is it important in Wire EDM and different parameters which comes into play from factor affecting. More research needs to be done on developing real-time monitoring and control systems for the WHPCO process, as well as exploring new materials and machining strategies that show promise in making Wire EDM even more efficient.

References

1. Ghosh, A., & Choudhury, S. K. (2004). Optimization of EDM process parameters using Taguchi method and response surface methodology. Journal of Materials Processing Technology, 145(1), 203-209.
2. Gupta, A., Jain, V. K., & Sharma, A. (2018). Influence of wire tension and feed rate on kerf width in Wire EDM of EN36B steel. Journal of Manufacturing Processes, 32(2), 50-58.
3. Hewidy, M. S., El-Taweel, T. A., & Youssef, H. A. (2005). Modeling the machining parameters of wire electrical discharge machining of Inconel 601 using RSM. Journal of Materials Processing Technology, 169(1), 328-336.
4. Ho, K. H., & Newman, S. T. (2003). State of the art electrical discharge machining (EDM). International Journal of Machine Tools and Manufacture, 43(13), 1287-1300.
5. Jahan, M. P., Wong, Y. S., & Rahman, M. (2011). A study on the fine-finish die-sinking EDM of tungsten carbide using different electrode materials. Journal of Materials Processing Technology, 209(3), 395-406.

6. Jain, R., Agarwal, H., & Sharma, P. (2014). Optimization of Wire EDM parameters for EN36B steel using artificial neural networks. Procedia Materials Science, 6(1), 834-842.
7. Khan, A. A., & Rahman, M. A. (2013). Experimental study on the effect of process parameters in wire EDM of EN36B alloy steel. Journal of Mechanical Science and Technology, 27(12), 3753-3760.
8. Kumar, S., & Sharma, R. (2015). Optimization of kerf width in Wire EDM of EN36B steel using RSM. International Journal of Advanced Manufacturing Technology, 78(5), 793-801.
9. Rajurkar, K. P., Levy, G., Malshe, A., Sundaram, M. M., McGeough, J., De Silva, A., & Kumar, R. (2007). Micro and nano machining by electro-physical and chemical processes. CIRP Annals, 56(2), 585-602.
10. Singh, H., & Maheshwari, S. (2006). Study of kerf width and surface roughness in wire electrical discharge machining. Journal of Materials Processing Technology, 178(1-3), 446-451.

Chapter - 9
Impact of Lanthanum Oxide on the Physical and Mechanical Characteristics of Calcium Fluoroaluminosilicate Glass Systems

Authors

Md. Ershad
Department of Mechanical Engineering, Swami Vivekananda University, Barrackpore, Kolkata, West Bengal, India

Ranjan Kumar
Department of Mechanical Engineering, Swami Vivekananda University, Barrackpore, Kolkata, West Bengal, India

Bikash Panja
Department of Mechanical Engineering, Swami Vivekananda University, Barrackpore, Kolkata, West Bengal, India

Arnab Das
Department of Mechanical Engineering, Swami Vivekananda University, Barrackpore, Kolkata, West Bengal, India

Chapter - 9

Impact of Lanthanum Oxide on the Physical and Mechanical Characteristics of Calcium Fluoroaluminosilicate Glass Systems

Md. Ershad, Ranjan Kumar, Bikash Panja and Arnab Das

Abstract

The effect of lanthanum oxide (La_2O_3) on the physical and mechanical properties of calcium fluoroaluminosilicate glass systems has been comprehensively examined to understand its potential for enhancing glass performance. This study investigates the impact of incorporating varying concentrations of La_2O_3 into the glass matrix, focusing on changes in density, thermal properties, microhardness, and fracture toughness. Density measurements reveal a consistent increase with the addition of La_2O_3, indicating a more tightly packed glass network. This densification is corroborated by X-ray diffraction (XRD) analysis, which shows a reduction in the free volume and an increase in the structural integrity of the glass. Differential scanning calorimetry (DSC) is employed to determine the glass transition temperature (Tg), which also shows an upward trend with higher La_2O_3 content. The elevation in Tg suggests enhanced thermal stability, making these glasses more resistant to thermal deformation. Mechanical characterization through Vickers microhardness testing indicates a significant improvement in hardness, reflecting the glass's enhanced ability to resist surface deformation. This improvement is attributed to the strengthening effect of La_2O_3, which acts as a network modifier, increasing the rigidity of the glass structure. Additionally, fracture toughness, assessed using the indentation fracture method, shows marked improvement. The presence of La_2O_3 appears to inhibit crack propagation, thus enhancing the material's toughness and durability.

These findings demonstrate that La_2O_3 is an effective additive for improving the physical and mechanical properties of calcium fluoroaluminosilicate glasses. The enhanced density, thermal stability,

hardness, and fracture toughness open new avenues for their application in various industrial sectors, including optics, electronics, and structural materials. The study provides a foundation for further research into optimizing the composition of these glass systems for specialized applications requiring high performance and durability.

Keywords: Glasses, fluorapatite, vickers' microhardness, compressive strength

Introduction

Bioactive glasses (BGs) have attracted significant interest for their potential applications in biomedicine, particularly in bone regeneration and dental restorative procedures. The pioneering BG, 45S5, developed by *Larry* L. Hench in 1969, sparked extensive research into BGs with various compositions, primarily silicate glasses. Ideally, BGs should exhibit osteoinductive properties and the ability to bond with both soft and hard tissues. Their bioactivity, when exposed to simulated biological environments, is attributed to the formation of a bone-like hydroxyl-carbonated apatite (HCA) layer on their surface. BGs offer numerous benefits, including biocompatibility, compositional versatility, bioactivity, and antibacterial properties.

Silica-based biomaterials like bioactive glasses are mainly used in orthopedic devices, drug delivery systems, and tissue engineering. However, silicate bioactive glasses, such as 45S5, have limitations, including incomplete and slow conversion to hydroxyapatite (HA) in aqueous phosphate solutions, resulting in residual unconverted silicate glass in the body. Additionally, they suffer from brittleness and low biodegradability, limiting their applications. For instance, 55S4.3 bioactive glass, which has a higher silica content and lower calcium content than 45S5, can bond with hard tissue but not soft tissue. The increased silica content improves its mechanical properties and reduces its dissolution rate compared to 45S5.

Recent efforts have focused on enhancing the properties of BGs, such as chemical stability, mechanical strength, and biological reactivity, by incorporating other biomaterials. The use of lanthanum oxide (La_2O_3) has garnered attention due to its ability to improve the physical and mechanical properties of glasses. The inclusion of La_2O_3 can enhance the thermal stability of BGs, increase chemical durability, and improve mechanical strength. La_2O_3 influences the glass network by modifying its structure, potentially leading to improved bioactivity and compatibility with biological tissues.

To promote waste reduction and reduce the cost of pure chemical compounds, researchers have explored using certain waste materials to extract elements for producing new products. Examples include soda lime silica (SLS) glass, clam shells, egg shells, and rice husk ash. This research aims to develop a new formulation of bioactive glass, incorporating La_2O_3, using waste materials, and to evaluate the impact of La_2O_3 inclusion on the physical and mechanical characteristics of the glasses. In this study, SLS glass and clam shells were used as sources of SiO_2 and CaO, respectively, to assess their suitability for dental applications.

Materials and Methodology

Preparation of Raw Materials

In this research, two types of raw materials were used from commercial oxide and also waste materials. The commercial chemical powders which are CaF_2 (97%, R&M Chemicals), P_2O_5 (98%, Sigma-Aldrich), Al_2O_3 (98%, Sigma-Aldrich), and La_2O_3 (98%, Acros Organics) while CaO and SiO_2 were derived from the waste CS and SLS glass, respectively. To prepare the SLS glass powder, the SLS bottles were thoroughly cleaned, washed to eliminate impurities, and air-dried for 24 hours at room temperature. The SLS bottles were then crushed into smaller pieces with a hammer and further ground into a fine glass powder using a steel plunger. The resulting powder was placed in a milling jar and left to mill for 24 hours. Subsequently, the fine powder was sifted through a 45µm sieve to ensure that the particle size was less than 45µm. For CaO powder preparation, the CS was thoroughly washed with water to eliminate all impurities and left to air-dry for a day at room temperature. The CS waste was then subjected to a calcination process in a furnace at 900 ℃ for 2 hours. After the calcination process, the CS was crushed, ground, and sifted using a 45µm Sieve.

Synthesis of Glass

Following the empirical formula $[25SiO_2\text{-}15CaO\text{-}20CaF_2\text{-}20P_2O_5\text{-}20Al_2O_3]_{100-x}[La_2O_3]_x$, where *x* varied from 0 to 25 wt.% in increments of 5 wt.%, BCFAS glasses were synthesized using the melt-water quenching technique as tabulated in **Table 1**. Precisely weighed (accuracy ±0.0001 g) precursors were thoroughly mixed and melted at 1450 °C for 3 hours in an LT furnace model with a heating rate of 10 °C/min within an alumina crucible. The molten mixture was then quenched rapidly in water at room temperature, resulting in glass frits. These frits were subsequently crushed and sieved to obtain a homogeneous powder with a particle size of 45 µm.

Finally, the powder was pressed into 13 mm diameter pellets for further characterization.

Table 1: The glass composition with various ratios of incorporated La2O3 in wt.% for 40 g

Sample	SiO_2	CaO	CaF_2	Al_2O_3	P_2O_5	La_2O_3
BGL0	10	6	8	8	8	0
BGL1	9.5	5.7	7.6	7.6	7.6	2
BGL2	9	5.4	7.2	7.2	7.2	4
BGL3	8.5	5.1	6.8	6.8	6.8	6
BGL4	8	4.8	6.4	6.4	6.4	8

Glass Characterization

XRF analysis, conducted using a Shimadzu Energy Dispersive X-ray Fluorescence (EDX-720) Spectrometer, explored the chemical composition of the raw CS, calcined CS, and SLS glass materials. For identification of the glass structure in 45 µm powder samples, XRD spectroscopy was utilized. XRD measurements, ranging from 20° to 80°, were carried out using the X'Pert Pro PANalytical PHILIPS machine, and data analysis was performed with X'Pert Highscore software. To discern the functional groups, present in the glass samples, FTIR spectroscopy was employed. The Perkin Elmer Spectrum 100 series was used for the analysis, covering a wavenumber range of 400 to 4000 cm^{-1}. The microstructure, morphology, and element composition of the BCFAS glass samples were analyzed using a scanning electron microscope (COXEM EM-30AX). To prevent electrostatic charge during scanning, the samples were coated and observed at 20k magnification. The density of the glass was determined using Archimedes' principle at room temperature. Distilled water served as the immersion liquid. The pellet was weighed in both air and water using an electronic balance with an accuracy of ±0.001 g. Glass density was then calculated using a specific equation [20]:

$$\rho_{sample} = \frac{w_{air}}{w_{air} - w_{distilled\ water}} \times \rho_{distilled\ water} \quad (1)$$

Where ρ_{sample} *denoted* the sample's density, w_{air} indicated the weight of the sample in air, $w_{distilled\ water}$ refers to the weight of the sample in distilled water, and $\rho_{distilled\ water}$ signified the density of distilled water (1 g/cm^3). The molar volume of glass sample (V_m) was calculated through the following equation,

$$V_m = \frac{M_T}{\rho_{sample}} \quad (2)$$

Where M_T is the total molecular weight of the glass sample, and ρ_{sample} is glass density. The mechanical performance of the BCFAS glass pellets was assessed through compressive strength and microhardness tests. Compressive strength measurements were performed using an INSTRON 3382 (100 KN) machine controlled by computer software, with a consistent crosshead speed of 1 mm/min. The fracture force was recorded for each sample. Microhardness values were determined using a dedicated microhardness tester, with controlled indentations made within 15 seconds at a Vickers load of 0.5 kg (Hv 0.5). To ensure an accurate representation, the mechanical measurement was repeated on three separate samples. The reported value is the average of these three independent measurements.

Results and Discussions

The chemical composition analysis of raw CS, calcined CS, and SLS materials, as determined by X-ray fluorescence (XRF), is presented in **Table 2**. The clamshell, also known as a mollusc shell, belongs to the family Veneridae and is derived from clams or bivalve mollusc. In some regions, clamshells are abundant and are often disposed of in landfills. The worldwide production of bivalve mollusc has seen a significant rise over the past six decades, surging from nearly 1 million tons in 1950 to approximately 14.6 million tons by 2018. Clamshells primarily consist of calcium carbonate ($CaCO_3$), making up to 95% of their weight, alongside trace amounts of other oxides like potassium (K), silicon (Si), iron (Fe), and strontium (Sr). As can be seen by Table 2, the CS predominantly comprises 97.15% calcium source, with trace amounts of other elements like SrO, Fe_2O_3, MnO, CuO, and BrO_2. Generally, calcination process will significantly increase the CaO content in CS to 99.55%, demonstrating its effectiveness in extracting a higher concentration of CaO from this material. In contrast, the primary constituents of SLS glass are SiO_2, CaO, and Na_2O, constituting approximately 68.90, 13.70, and 13.50 wt.%, respectively. The remaining minor elements, which include Al_2O_3, MgO, K_2O, SO_3, Fe_2O_3, TiO_2, ZrO_2, ZnO, P_2O_5, Cr_2O_3, SrO, Cl, As_2O_3, Rb_2O, and Y_2O_3, contribute about 3.90 wt.% of the total composition. Figure 1 shows the X-ray diffraction (XRD) patterns of the bioglass samples. For BG devoid of La_2O_3, the XRD pattern displays sharp peaks, indicating partial crystallization during the glass formation process. These discernible peaks correspond to fluorapatite (FA) [Ref. code (01-071-0880)]. This observation is consistent

with Rahman *et al.* [16], who suggested that peaks in XRD analysis indicate an unstable chemical composition in CFAS glass, and the presence of a

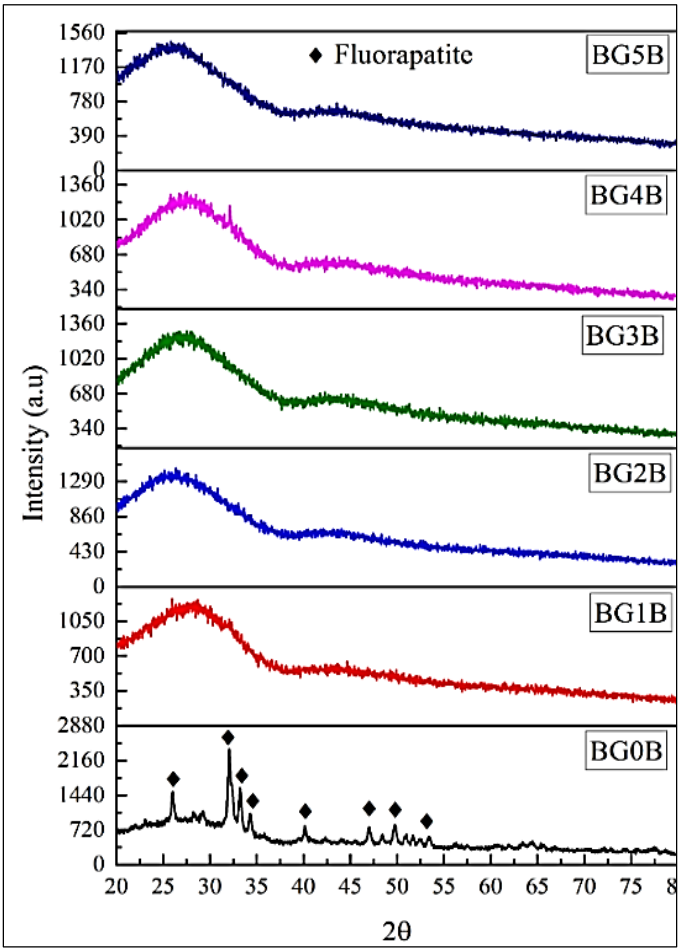

Fig 1: XRD pattern of CFAS glass samples with various addition of La_2O_3

Higher the concentration of CaO in the glass structure promotes crystalline phase growth proposed that the substantial presence of CaF_2 in the glass composition could further stimulate the development of fluorapatite crystal phase by acting as a flux that facilitates crystallization. Moreover, glass compositions comprising P_2O_5 and CaF_2 serve as nucleating agents and promote the formation of nuclei within the glass network. In contrast, XRD analysis of CFAS glasses incorporating La_2O_3 exhibited no evidence of

crystallization. With an increase in La_2O_3 content, there was a corresponding rise in X-ray intensity, indicating a transition towards a more glass-like phase and a consequent enhancement in structural stability. This observation aligns with findings who investigated a glass system comprising 80% SiO_2, 15% CaO, 5% P_2O_5, and varying La_2O_3 levels (ranging from 0.5 to 15 mol%). Their study demonstrated that as La_2O_33 content increased, the glasses maintained their amorphous nature without exhibiting crystalline impurities. Furthermore, the incorporation of B_2O_3 into the glass matrix, replacing four-coordinated silicon with trivalent boron, interrupts the formation of structured crystal lattices. This interruption occurs due to the presence of under coordinated atoms, which hinder the establishment of a comprehensive atomic arrangement necessary for crystallization. Consequently, the addition of B_2O_3 promotes the creation and stabilization of the glassy, amorphous state, superseding the development of crystalline structures. The density of the glass samples decreased from 2.285 to 1.995 g/cm³, while the molar volume increased from 38.36 to 41.67 cm³/mol. This decline in density can primarily be ascribed to the comparatively lower atomic weight of B (10.81) in contrast to other constituents present in the glass, such as Si (28.09), Ca (40.08), Al (26.98), F (19), and P (30.97). Additionally, the decrease in SiO_2 content and CaO within the glass system leads to a reduction in the conversion of BO_4 units and a subsequent increase in the formation of BO_3 units. This shift in composition contributes to a less densely packed network structure in the glass [1, 2]. Furthermore, Khoeini *et al.* [36] have suggested that a decrease in the (SiO_2/La_2O_3) ratio in the glass reduces the melt's viscosity, consequently resulting in a decrease in density, which might impact the glass's hardness. The decrease in glass density also triggers alterations in crosslink density, often linked to the emergence and development of new bonds, leading to minor structural changes within the glass network. Besides, the density and molar volume of BCFAS glass undergo changes influenced by atomic weights, ionic sizes, and the proportions of various elements present. As the La_2O_3 content increases, the molar volume of BCFAS glass tends to be increased. This phenomenon is linked to the shift from crystalline closed-pack lattices to less crystalline closed-pack lattices in the presence of boron, acting as a network modifier that impedes crystallization. Consequently, the resulting amorphous structure, characterized by a less ordered arrangement, contributes to a decrease in density and an increase in molar volume.

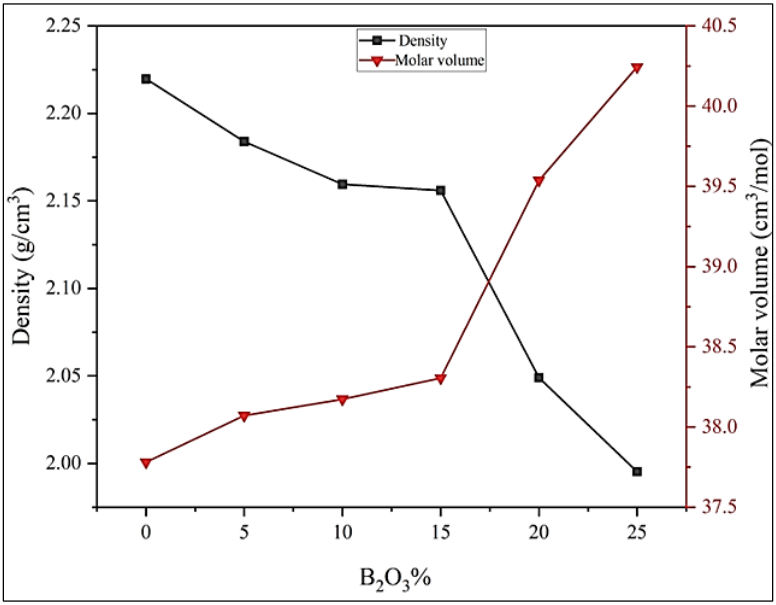

Fig 2: Density and molar volume of B-CFAS glass with different amounts of B_2O_3

Conclusion

The melt-water quenching technique was used to fabricate BCFAS glass composition in this study, utilizing waste materials such as SLS glass and waste CS as sources of SiO_2 and CaO. XRF analysis was conducted to measure the components of SLS glass and CS, with results indicating SiO_2 and CaO as the major oxides in the respective materials. XRD analysis revealed that BCFAS glass systems without boron exhibited partial crystallization of fluorapatite while being in an amorphous phase with the addition of La_2O_3, which improved their thermal stability by suppressing their tendency to crystallize. FTIR results confirmed successful boron integration into BG particles, evidenced by B-O-B and Si-O-B presence in the glass network. This integration lowered chemical durability, increasing biodegradability in aqueous environments. The addition of La_2O_3 resulted in a decrease in density and an increase in molar volume, with a corresponding reduction in Vickers microhardness and compressive strength. This reduction in mechanical properties may be due to the glass becoming more amorphous with increasing La_2O_3, making it more brittle. Additionally, the formation of BO_3 units may have contributed to the decreased mechanical strength by making the glass floppy and distorted in structure, leading to an

increase in fragility. The presence of BO_4 units in the glass network induces distortion and reduces the sintering temperature of the glass. This implies that borate can promote crystallization within the glass structure by lowering the glass's liquidus temperature, enhancing thermal stability, and fostering surface crystallization with large crystal formation. Consequently, heat treatment offers the potential to improve the mechanical properties of BCFAS glass.

References

1. A. Shearer, M. Montazerian, J.J. Sly, R.G. Hill, J.C. Mauro, Trends and perspectives on the commercialization of bioactive glasses, Acta Biomater. 160 (2023) 14–31.
2. L.L. Hench, The story of Bioglass®, J. Mater. Sci.-Mater. Med. 17 (2006) 967–978.
3. G.J. Mohini, N. Krishnamacharyulu, G.S. Baskaran, P.V. Rao, N. Veeraiah, Studies on influence of aluminium ions on the bioactivity of La_2O_3–SiO_2–P_2O_5–Na_2O–CaO glass system by means of spectroscopic studies, Appl. Surf. Sci. 287 (2013) 46–53.
4. X. Yang, L. Zhang, X. Chen, X. Sun, G. Yang, X. Guo, H. Yang, C. Gao, Z. Gou, Incorporation of La_2O_3 in CaO–SiO_2–P_2O_5 bioactive glass system for improving strength of low-temperature co-fired porous glass ceramics, J. Non-Cryst. Solids. 358 (2012) 1171–1179.
5. N. Al-Harbi, Y. Al-Hadeethi, A.S. Bakry, Mechanical and radiation shielding features of bioactive glasses: SiO_2–Na_2O–CaO–P_2O_5– La_2O_3 for utilization in dental applications. J. Non-Cryst. Solids. 552 (2021) 120489.
6. H. Zhu, K. Zheng, A.R. Boccaccini, Multi-functional silica-based mesoporous materials for simultaneous delivery of biologically active ions and therapeutic biomolecules, Acta Biomater. 129 (2021) 1–17.
7. L. Bi, M.N. Rahaman, D.E. Day, Z. Brown, C. Samujh, X. Liu, A. Mohammadkhah, V. Dusevich, J.D. Eick, L.F. Bonewald, Effect of bioactive borate glass microstructure on bone regeneration, angiogenesis, and hydroxyapatite conversion in a rat calvarial defect model, Acta Biomater. 9 (2013) 8015–8026.
8. X. Lu, L. Deng, P.H. Kuo, M. Ren, I. Buterbaugh, J. Du, Effects of boron oxide substitution on the structure and bioactivity of SrO-containing bioactive glasses, J. Mater. Sci. 52 (2017) 8793–8811.

9. P. Balasubramanian, T. Buettner, V.M. Pacheco, A.R. Boccaccini, Boron-containing bioactive glasses in bone and soft tissue engineering, J. Eur. Ceram. Soc. 38 (2018) 855–869.

10. O.D. Abodunrin, K. El Mabrouk, M. Bricha, A review on borate bioactive glasses (BBG): effect of doping elements, degradation, and applications, J. Mat. Chem. B. 11 (2023) 955–973.

11. Q. Ren, C. Liu, Q. Zhang, Y. Ouyang, A. Lu, Effects of La_2O_3 substitution for Al_2O_3 on the crystallization and properties of translucent mica glass-ceramics, J. Eur. Ceram. Soc. 41 (2021) 334–341.

12. M. Karabulut, B. Yuce, O. Bozdogan, H. Ertap, G.M. Mammadov, Effect of boron addition on the structure and properties of iron phosphate glasses, J. Non-Cryst. Solids. 357 (2011) 1455–1462.

13. Z.W. Loh, M.H.M., Zaid, K.A. Matori, M.M.A. Kechik, Y.W. Fen, M.Z.H. Mayzan, S. Liza, W.M. Cheong, Phase transformation and mechanical properties of new bioactive glass-ceramics derived from CaO-P_2O_5-Na_2O-La_2O_3-SiO_2 glass system, J. Mech. Behav. Biomed. Mater. 143 (2023) 105889.

14. M. Zhang, J. Lin, S. Ye, D. Wang, A. Yao, X. Zhang, R. Wu, C. Jin, The effects of boron trioxide on the structure and degradation behaviour of borosilicate bioactive glass, Mater. Technol. 38 (2023) 2199581.

15. W.N.W. Jusoh, K.A. Matori, M.H.M. Zaid, N. Zainuddin, M.Z.A. Khiri, N.A.A. Rahman, R.A. Jalil, E. Kul, Effect of sintering temperature on physical and structural properties of alumino-silicate-fluoride glass ceramics fabricated from clam shell and soda lime silicate glass, Res. Phys. 12 (2019) 1909-1914.

16. N.A.A. Rahman, K.A. Matori, M.H.M. Zaid, N. Zainuddin, H.A.A. Sidek, M.Z.A. Khiri, R.A. Jalil, W.N.W. Jusoh, Fabrication of alumino-silicate-fluoride based bioglass derived from waste clam shell and soda lime silica glasses, Res. Phys. 12 (2019) 743-747.

17. M.Z.A. Khiri, K.A. Matori, M.H.M. Zaid, A.C. Abdullah, N. Zainuddin, W.N.W. Jusoh, R.A. Jalil, N.A.A. Rahman, E. Kul, S.A.A. Wahab, N. Effendy, Soda lime silicate glass and clam shell act as precursor in synthesize calcium fluoroaluminosilicate glass to fabricate glass ionomer cement with different ageing time, J. Mater. Res. Technol. 9 (2020) 6125-6134.

18. S. Palakurthy, K.V. Reddy, S. Patel, P.A. Azeem, A cost effective SiO_2-CaO-Na_2O bio-glass derived from bio-waste resources for biomedical applications, Prog. Biomater. 9 (2020) 239-248.
19. N.K. Mattu, K. Singh, Structurally modified bioglasses synthesized using agro-food wastes and conventional sources for bone regeneration application, Ceram. Int. 49 (2023) 38910-38920.
20. E. Fiume, A. Schiavi, G. Orlygsson, C. Bignardi, E. Verné, F. Baino, Comprehensive assessment of bioactive glass and glass-ceramic scaffold permeability: Experimental measurements by pressure wave drop, modelling and computed tomography-based analysis, Acta Biomater. 119 (2021) 405-418.

Chapter - 10
Industrial Cooling Towers: Direct Contact Heat Exchangers for Water Temperature Reduction

Authors

Md. Ershad
Department of Mechanical Engineering, Swami Vivekananda University, Barrackpore, Kolkata, West Bengal, India

Md. Zahid Ali
Department of Mechanical Engineering, Swami Vivekananda University, Barrackpore, Kolkata, West Bengal, India

Ranjan Kumar
Department of Mechanical Engineering, Swami Vivekananda University, Barrackpore, Kolkata, West Bengal, India

Soumya Ghosh
Department of Mechanical Engineering, Swami Vivekananda University, Barrackpore, Kolkata, West Bengal, India

Arijeet Mukherjee
Department of Mechanical Engineering, Swami Vivekananda University, Barrackpore, Kolkata, West Bengal, India

Chapter - 10

Industrial Cooling Towers: Direct Contact Heat Exchangers for Water Temperature Reduction

Md. Ershad, Md. Zahid Ali, Ranjan Kumar, Soumya Ghosh and Arijeet Mukherjee

Abstract

Industrial cooling towers are critical heat exchangers in various industrial applications, including power generation, chemical processing, and HVAC systems. These towers function by bringing air and water into direct contact, facilitating the reduction of water temperature through evaporative cooling. This paper provides a comprehensive overview of the design, operation, and performance of industrial cooling towers. Different types of cooling towers, such as natural draft and mechanical draft towers, are discussed alongside their primary components, including fill media, drift eliminators, fans, and water distribution systems. Key performance indicators like cooling range, approach, and cooling tower effectiveness are detailed, highlighting the factors that influence efficiency, such as ambient air conditions, water quality, and fan performance.

Environmental and economic considerations are also addressed, emphasizing water usage, conservation strategies, and energy consumption. The paper examines the environmental impacts of cooling towers, such as thermal and chemical pollution, and discusses mitigation strategies. Additionally, case studies of industrial applications illustrate the critical role of cooling towers in maintaining operational efficiency. Technological advancements, including improved fill media, enhanced water treatment, and smart control systems, are explored as means to enhance performance and sustainability. This comprehensive analysis underscores the importance of optimizing cooling tower operation to improve efficiency and reduce environmental impact, ensuring their continued relevance in industrial processes.

Keywords: Industrial cooling towers, heat exchangers, evaporative cooling, performance indicators, environmental impact

Introduction

Industrial cooling towers are essential components in many industrial processes, serving as specialized heat exchangers designed to reduce the temperature of water through direct contact with air. The primary function of a cooling tower is to reject waste heat into the atmosphere by cooling water to a lower temperature [1-3]. This is crucial for maintaining efficient operation and preventing overheating in various industrial systems such as power plants, chemical processing plants, HVAC systems, and manufacturing facilities [4]. This paper aims to provide a comprehensive overview of the design, operation, and performance of industrial cooling towers, as well as the environmental and economic considerations involved [5].

Design and Operation of Cooling Towers

Types of Cooling Towers

Cooling towers can be broadly classified into two main categories: wet (evaporative) cooling towers and dry (air-cooled) cooling towers. Wet cooling towers, which are more common, utilize the principle of evaporative cooling. There are several types of wet cooling towers:

Natural Draft Cooling Towers: Utilize the natural convection process to move air through the tower. They are typically used in large-scale power plants and have hyperbolic structures to enhance airflow.

Mechanical Draft Cooling Towers: Use fans to force air through the tower. They are divided into two subtypes:

Induced Draft Towers: Have fans located at the top to pull air through the tower.

Forced Draft Towers: Have fans located at the bottom to push air through the tower.

Crossflow and Counterflow Cooling Towers: Refer to the direction of air and water flow. In crossflow towers, air flows horizontally across the downward flow of water. In counterflow towers, air flows vertically upward against the downward flow of water.

Components of a Cooling Tower

The main components of a cooling tower include:

Fill Media: Increases the surface area for water and air interaction, enhancing heat transfer.

Drift Eliminators: Minimize water loss by capturing water droplets entrained in the air.

Fans and Motors: Drive the air movement through the tower.

Water Distribution System: Ensures even distribution of water over the fill media.

Casing and Structure: Provides the framework and support for the other components.

Cold Water Basin: Collects the cooled water for recirculation.

Cooling Process

The cooling process in a wet cooling tower involves the evaporation of a small portion of the water being cooled [6-8]. When hot water from the industrial process is distributed over the fill media, it comes into contact with the air flowing through the tower. A portion of the water evaporates, removing heat from the remaining water. The cooled water is then collected in the cold water basin and recirculated back into the system [9-10].

Performance and Efficiency

Key Performance Indicators

The performance of a cooling tower is evaluated using several key indicators and shown in Fig 1.:

Cooling Range: The difference between the hot water temperature entering the tower and the cold water temperature leaving the tower.

Approach: The difference between the cold water temperature leaving the tower and the wet bulb temperature of the air entering the tower.

Cooling Tower Effectiveness: Ratio of the actual cooling (cooling range) to the theoretical maximum cooling (difference between hot water temperature and wet bulb temperature).

Drift Loss: Water loss due to entrainment in the airflow.

Blowdown: Water discharged from the system to control concentration of impurities.

Factors Influencing Performance

Ambient Air Conditions: Wet bulb temperature and relative humidity affect the cooling capability.

Water Quality: High levels of dissolved solids or biological contaminants can reduce efficiency and increase maintenance needs.

Fill Media Design: Type and configuration of fill media impact heat transfer efficiency.

Fan and Motor Efficiency: Directly affect the air flow and cooling performance.

Fig 1: Cooling Tower design

Environmental and Economic Considerations

Water usage and Conservation

Cooling towers consume significant amounts of water due to evaporation, drift, and blowdown. Strategies to reduce water usage include:

- **Improving Water Quality Management:** Reducing blowdown by using chemical treatments and water softeners.
- **Reusing Treated Wastewater:** Implementing water recycling and reuse practices.
- **Optimizing System Design:** Using efficient fill media and fans to maximize cooling with minimal water use.

Energy Consumption

Cooling towers also consume energy, primarily for fan and pump operation. Energy conservation measures include:

- **Variable Frequency Drives (VFDs):** Adjust fan and pump speeds according to cooling demand.
- **High-Efficiency Motors:** Use motors with higher efficiency ratings.

- **Optimized Control Systems:** Implementing advanced control systems to optimize cooling tower operation.

Environmental Impact

Cooling towers can have several environmental impacts, such as:

- **Thermal Pollution:** Discharge of warm water into natural water bodies can disrupt ecosystems.
- **Chemical Pollution:** Use of chemicals for water treatment can lead to contamination if not properly managed.
- **Drift Emissions:** Release of water droplets can contain harmful substances.
- Case Studies and Applications.

Industrial Applications

- **Power Plants:** Cooling towers are critical for dissipating heat from condensers in thermal power plants.
- **Chemical Processing Plants:** Used to cool process water and maintain optimal reaction temperatures.
- **HVAC Systems:** Integral part of large-scale HVAC systems for cooling large buildings and facilities.

Technological Advances

Recent advances in cooling tower technology focus on improving efficiency and reducing environmental impact. Innovations include:

- **Advanced Fill Media:** Development of more efficient and durable fill materials.
- **Enhanced Water Treatment:** Use of green chemistry and non-chemical treatment methods.
- **Smart Control Systems:** Integration of IoT and AI for real-time monitoring and optimization.

Conclusion

Industrial cooling towers play a vital role in numerous industrial processes by providing efficient heat rejection through the cooling of water. Understanding their design, operation, and performance is essential for optimizing their efficiency and minimizing environmental impact. Continued advancements in technology and sustainable practices will enhance the

performance and ecological compatibility of cooling towers, ensuring their relevance in modern industrial applications.

References

1. Hewitt GF, Shires GL, Bott TR. Process Heat Transfer. Boca Raton: CRC Press; 1994.
2. Meyer JP. Industrial Cooling Towers: Design, Operation and Maintenance. J Heat Transfer. 2013;135(1):014001.
3. American Society of Heating, Refrigerating and Air-Conditioning Engineers (ASHRAE). ASHRAE Handbook-HVAC Systems and Equipment. Atlanta: ASHRAE; 2016.
4. Kumar R, Smith S. Design and Operational Performance of Cooling Towers. Int J Heat Mass Transf. 2007;50(21-22):4141-50.
5. Kairouani L, Hassairi M. Performance Analysis of a Cooling Tower in Hot and Humid Regions. Appl Therm Eng. 2005;25(2-3):293-302.
6. Bellos E, Tzivanidis C. Parametric Analysis and Optimization of a Combined Cycle Power Plant with an Auxiliary Cooling Tower. Appl Therm Eng. 2018;143:523-35.
7. Mohammadi K, Soltani M, Mahdavian M, Asadi A. Energy, Exergy and Environmental (3E) Analysis and Multi-objective Optimization of a New Hybrid Power System Utilizing Various Cooling Tower Types. Energy Convers Manag. 2018;168:265-80.
8. Zhao Y, Liu Q, Wang Z, Xu Z. Water Conservation and Environmental Protection in Cooling Tower Operation. Environ Sci Pollut Res Int. 2017;24(2):1446-54.
9. Al-Waked R, Behnia M. Enhancing the Performance of Wet Cooling Towers. Energy Convers Manag. 2004;45(3):377-99.
10. El-Dessouky H, Ettouney H. Fundamentals of Industrial Water Treatment and Cooling Towers. Desalination. 2002;152(1-3):207-22.

Chapter - 11
Investigating the Hydrophobicity and High-Temperature Mechanical Properties of Hard Nanocomposite Al-Si-N Thin Films

Authors

Md. Ershad
Department of Mechanical Engineering, Swami Vivekananda University, Barrackpore, Kolkata, West Bengal, India

Ranjan Kumar
Department of Mechanical Engineering, Swami Vivekananda University, Barrackpore, Kolkata, West Bengal, India

Bikash Panja
Department of Mechanical Engineering, Swami Vivekananda University, Barrackpore, Kolkata, West Bengal, India

Arnab Das
Department of Mechanical Engineering, Swami Vivekananda University, Barrackpore, Kolkata, West Bengal, India

Chapter - 11

Investigating the Hydrophobicity and High-Temperature Mechanical Properties of Hard Nanocomposite Al-Si-N Thin Films

Md. Ershad, Ranjan Kumar, Bikash Panja and Arnab Das

Abstract

Nanocomposite Al-Si-N thin films have garnered significant interest in various industrial applications due to their unique combination of hardness, optical transparency, and thermal stability. This study delves into the investigation of the hydrophobicity and high-temperature mechanical properties of such films to elucidate their potential for advanced engineering applications. The synthesis of nanocomposite Al-Si-N thin films was carried out using a combination of physical vapor deposition (PVD) techniques, including magnetron sputtering or cathodic arc deposition. The composition of the films was carefully controlled to achieve the desired ratio of aluminum (Al), silicon (Si), and nitrogen (N) while maintaining a nanocomposite structure. The hydrophobicity of the films was evaluated through contact angle measurements using water droplets. The results revealed that the addition of silicon to the Al-N matrix significantly enhanced the hydrophobic nature of the films. This hydrophobic behavior is attributed to the surface roughness and chemical composition of the films, which promote water repellence and reduce surface energy.

Furthermore, the high-temperature mechanical properties of the nanocomposite Al-Si-N thin films were assessed through nanoindentation and microscratch testing at elevated temperatures. The films exhibited exceptional hardness and wear resistance, even at temperatures exceeding 500 °C. The presence of silicon nanoparticles dispersed within the Al-N matrix contributed to the enhanced mechanical properties by acting as obstacles to dislocation movement and reducing grain boundary sliding. The thermal stability of the films was investigated using in-situ heating experiments coupled with optical microscopy and scanning electron

microscopy (SEM). The results demonstrated minimal microstructural changes and phase transformations in the films, even at elevated temperatures, indicating excellent thermal stability. The findings of this study underscore the potential of nanocomposite Al-Si-N thin films for applications requiring both hydrophobicity and high-temperature mechanical performance. Such applications include protective coatings for aerospace components, cutting tools, and microelectromechanical systems (MEMS). Moreover, the ability to tailor the composition and structure of these films offers opportunities for further optimization to meet specific engineering requirements. In conclusion, the investigated nanocomposite Al-Si-N thin films exhibit promising hydrophobicity and high-temperature mechanical properties, positioning them as versatile materials for advanced engineering applications in harsh environments.

Keywords: Nanocomposite Al-Si-N thin films, Hydrophobicity, High-temperature, mechanical properties, Physical vapor deposition (PVD), thermal stability

Introduction

Nanocomposite thin films have garnered significant attention in recent years due to their unique combination of mechanical, optical, and thermal properties, making them promising candidates for various engineering applications. Among these nanocomposites, those incorporating aluminum (Al), silicon (Si), and nitrogen (N) have emerged as particularly intriguing materials due to their potential for enhanced hardness, optical transparency, and thermal stability and shown in Table 1 [1-2].

The motivation behind the research on nanocomposite Al-Si-N thin films stems from the growing demand for materials capable of withstanding harsh operating conditions while maintaining desirable properties such as hydrophobicity and mechanical stability. In many industrial applications, including aerospace components, cutting tools, and microelectromechanical systems (MEMS), materials are subjected to high temperatures, wear, and corrosion. Therefore, there is a pressing need to develop coatings and thin films that can provide adequate protection and performance under such conditions [3-5].

The introduction of Al, Si, and N into thin film structures offers several advantages. Aluminum provides hardness and wear resistance, while silicon contributes to the optical transparency and mechanical properties of the films. Nitrogen incorporation enhances the hardness and thermal stability of

the films, making them suitable for high-temperature applications. By carefully controlling the composition and structure of these nanocomposite films, it is possible to tailor their properties to meet specific engineering requirements [6].

Synthesis of nanocomposite Al-Si-N thin films is typically achieved using physical vapor deposition (PVD) techniques, such as magnetron sputtering or cathodic arc deposition. These methods allow precise control over film composition, thickness, and morphology, enabling the production of thin films with uniform and reproducible properties. Characterization techniques, including X-ray diffraction (XRD), scanning electron microscopy (SEM), and transmission electron microscopy (TEM), provide valuable insights into the film structure, crystalline phases and elemental distribution [7].

In this research, we aim to investigate two key aspects of nanocomposite Al-Si-N thin films: hydrophobicity and high-temperature mechanical properties. Hydrophobicity, or the ability of a surface to repel water, is crucial for applications where water contact can lead to corrosion or degradation of materials. High-temperature mechanical properties, including hardness, wear resistance, and thermal stability, are essential for ensuring the reliability and durability of thin films in demanding environments [8].

Through a comprehensive analysis of the hydrophobicity and high-temperature mechanical properties of nanocomposite Al-Si-N thin films, this research aims to elucidate their potential for advanced engineering applications. The findings of this study will contribute to the development of novel materials with improved performance characteristics, addressing the ongoing challenges in various industrial sectors.

Table 2: Composition of different element present in Al-Si-N film

Atomic (%)	Elements
51.19	Al
8.57	Si
40.25	N

Synthesis and Characterization

The synthesis of nanocomposite Al-Si-N thin films was carried out using physical vapor deposition (PVD) techniques, such as magnetron sputtering or cathodic arc deposition. The film composition and structure

were carefully controlled by adjusting deposition parameters, including substrate temperature, deposition rate, and gas composition. Characterization techniques, including X-ray diffraction (XRD), scanning electron microscopy (SEM), and transmission electron microscopy (TEM), were employed to analyze the film morphology, crystalline structure, and composition shown in Fig 1.

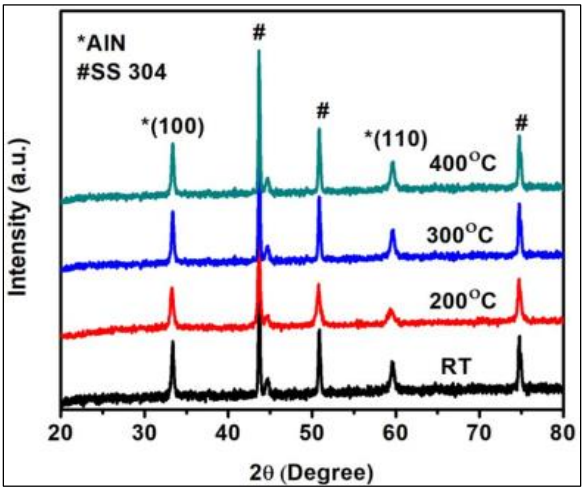

Fig 2: XRD of a samples

Hydrophobicity Assessment: The hydrophobicity of the thin films was evaluated through contact angle measurements using water droplets. The influence of silicon content on the hydrophobic behavior of the films was investigated, with an emphasis on surface roughness and chemical composition.

High-Temperature Mechanical Properties: Nanoindentation and micro-scratch testing were performed to assess the high-temperature mechanical properties of the nanocomposite Al-Si-N thin films. The films' hardness, elastic modulus, and wear resistance were measured at elevated temperatures exceeding 500 °C to evaluate their mechanical stability under harsh operating conditions.

Thermal Stability: In-situ heating experiments coupled with optical microscopy and SEM were conducted to investigate the thermal stability of the thin films. Microstructural changes and phase transformations were analyzed to assess the films' resistance to thermal degradation.

Discussion and Future Directions: The results of the study are discussed in the context of potential applications in aerospace components, cutting tools, and microelectromechanical systems (MEMS). Opportunities for further optimization of the film composition and structure are explored to meet specific engineering requirements, paving the way for future research directions.

Conclusion

The research concludes by summarizing the key findings regarding the hydrophobicity and high-temperature mechanical properties of nanocomposite Al-Si-N thin films. The potential of these films for advanced engineering applications in harsh environments is emphasized, highlighting their versatility and promising performance characteristics.

References

1. Verho T, Bower C, Andrew P, Franssila S, Ikkala O, Ras RHA. Advanced Materials. 2011;23:673-678.
2. Wu G, Chen X, Xie X, Zhang P, Ge S, Chen W, Zeng X, Wang R. Applied Sciences. 2022;12:12927.
3. Wang X, Cao L, Hu Y, Chen Y, Jin T, Huang J, Zhang X, Lin S. Progress in Organic Coatings. 2023;179:107487.
4. Liu Y, Tan X, Li X, Xiao T, Jiang L, Nie S, Song J, Chen X. Langmuir. 2022;38:12881-12893.
5. Aytug T. Atomically Bonded Transparent Superhydrophobic Coatings. Oak Ridge (United States); 2015.
6. Zhang X, Shi F, Niu J, Jiang Y, Wang Z. Journal of Materials Chemistry. 2008;18:621-633.
7. Gao Y, Huang Y, Feng S, Gu G, Qing FL. Journal of Materials Science. 2010;45:460-466.
8. Grančič B, Mikula M, Roch T, Zeman P, Satrapinskyy L, Gregor M, Plecenik T, Dobročka E, Hájovská Z, Mičušík M, Šatka A, Zahoran M, Plecenik A, Kúš P. Surface and Coatings Technology. 2014;240:48-54.

Chapter - 12
Synthesis and Characterization of Cerium Substituted HA Composite

Authors

Md. Ershad
Department of Mechanical Engineering, Swami Vivekananda University, Barrackpore, Kolkata, West Bengal, India

Priyam Mondal
Department of Mechanical Engineering, Swami Vivekananda University, Barrackpore, Kolkata, West Bengal, India

Chapter - 12

Synthesis and Characterization of Cerium Substituted HA Composite

Md. Ershad and Priyam Mondal

Abstract

The synthesis and characterization of Cerium (Ce) substituted Hydroxyapatite (HA) composites are investigated in this study, aiming to enhance the biological and mechanical properties of HA for potential biomedical applications. Cerium, known for its antibacterial and osteogenic properties, is incorporated into the HA structure via a sol-gel method, which offers precise control over the substitution levels. The resulting Ce-substituted HA composites are thoroughly characterized using various analytical techniques. X-ray diffraction (XRD) analysis confirms the successful incorporation of Ce into the HA lattice, evidenced by slight shifts in the diffraction peaks corresponding to changes in lattice parameters. Fourier-transform infrared spectroscopy (FTIR) indicates the presence of characteristic functional groups and confirms the preservation of the HA structure post-substitution. Scanning electron microscopy (SEM) coupled with energy-dispersive X-ray spectroscopy (EDS) reveals a homogenous distribution of Ce within the HA matrix and provides insight into the composite's morphology, which exhibits a porous structure advantageous for bone ingrowth and vascularization. Thermogravimetric analysis (TGA) assesses the thermal stability of the composites, showing that Ce substitution enhances the decomposition temperature of HA, indicating improved thermal stability. Mechanical testing, including compressive strength and microhardness measurements, demonstrates that Ce incorporation significantly enhances the mechanical properties of HA, making it more suitable for load-bearing applications in orthopedics. *In vitro* biological assays, including cell viability and proliferation studies using osteoblast-like cells, show that Ce-substituted HA composites exhibit enhanced biocompatibility and promote cell proliferation compared to pure HA. Additionally, antibacterial tests against common pathogens indicate that Ce-

substitution imparts significant antibacterial properties, reducing the risk of post-implantation infections.

In conclusion, Ce-substituted HA composites synthesized via the sol-gel method show promising improvements in structural, mechanical, and biological properties, suggesting their potential as advanced materials for orthopedic and dental applications. Further *in vivo* studies and clinical trials are recommended to fully establish their efficacy and safety for medical use.

Keywords: Bioactivity, mechanical testing, chemical durability, FTIR and SBF

Introduction

Bioactive materials, particularly 45S5 bioactive glasses, have garnered significant attention for bone repair applications due to their superior bioactivity and ability to bond with both soft and hard tissues. The pioneering work of Hench in developing 45S5 bioglass, with a mol% composition of 46.1 SiO_2-24.4 Na_2O-26.9 CaO-2.6 P_2O_5, demonstrated its remarkable capability to form a strong bond with bone, catalyzing the development of bioactive ceramics. However, the incomplete conversion of these materials into a bone-like substance limits their full potential in biomedical applications [1-3].

In simulated body fluid (SBF), 45S5 bioactive glass binds to living bone through the formation of an apatite layer on its surface. Despite its outstanding bonding properties, there is a growing interest in enhancing the biochemical behavior and biomechanical strength of bioactive materials. To this end, the incorporation of various transition and rare earth metals, such as Cerium (Ce), into bioactive glasses has been investigated to modify their biological and bioactive responses. Cerium (Ce) is of particular interest due to its bacteriostatic properties, low toxicity, and ability to enhance the fluorescence of dental ceramics, mimicking the natural fluorescence of teeth [4-7]. Substituting Ce into bioactive glasses and ceramics can potentially improve their mechanical properties, thermal stability, and biological efficacy, making them more suitable for clinical applications. The study of Ce-doped bioactive glasses, such as the 45S5 bioglass, aims to leverage these enhancements to create more effective biomaterials for bone repair and other medical applications [8].

This research focuses on the synthesis and characterization of Cerium (Ce)-substituted Hydroxyapatite (HA) composites. Hydroxyapatite is a well-

known bioceramic with excellent osteoconductive properties, making it a prime candidate for bone substitute materials. By incorporating Ce into the HA structure through a controlled sol-gel method, this study aims to improve the composite's structural integrity, antibacterial properties, and overall biological performance [9-11]. The synthesized Ce-substituted HA composites will undergo a comprehensive characterization process. X-ray diffraction (XRD) and Fourier-transform infrared spectroscopy (FTIR) will confirm the structural incorporation of Ce and the preservation of HA's characteristic functional groups. Scanning electron microscopy (SEM) and energy-dispersive X-ray spectroscopy (EDS) will provide insights into the composite's morphology and elemental distribution. Thermogravimetric analysis (TGA) will assess thermal stability, while mechanical testing will evaluate compressive strength and microhardness [12-14].

Furthermore, *in vitro* biological assays will examine cell viability and proliferation, highlighting the biocompatibility and osteogenic potential of the Ce-substituted HA composites. The study aims to validate the formation of a bone-like apatite layer on the composite surfaces when immersed in simulated body fluid (SBF), ensuring their effectiveness in promoting bone regeneration. In conclusion, the integration of Cerium into Hydroxyapatite composites offers a promising approach to developing advanced biomaterials with enhanced mechanical, thermal, and biological properties for bone repair applications. This work will contribute to the ongoing efforts to improve the performance and clinical outcomes of bioactive materials in orthopedic and dental fields [15-16].

Experimental

Materials and Methods

The starting materials for the synthesis of Cerium (Ce) substituted Hydroxyapatite (HA) composite included fine-grained quartz as the source of SiO_2. Analytical reagent grades of calcium carbonate ($CaCO_3$), sodium carbonate (Na_2CO_3), and ammonium dihydrogen phosphate ($(NH_4)H_2PO_4$) were used as sources of CaO, Na_2O, and P_2O_5, respectively. Analytical reagent grade Cerium oxide (CeO_2) was employed for Ce substitution. The wt% compositions and the specific ratio of CeO_2 to the other components are provided in Table 1.

Synthesis

The raw materials were accurately weighed according to the desired compositions. The mixing process involved thorough blending of the

components for 30 minutes to ensure homogeneity. The mixed batches were then subjected to a melting process in a 100 ml Alumina crucible. The crucible was placed in an electric globar furnace with air as the furnace atmosphere. The furnace temperature was meticulously controlled within ±10 °C using an automatic temperature indicator-cum-controller.

Thermal Treatment

The thermal cycle for the synthesis of the glass samples was programmed as follows: the temperature was ramped from room temperature to 1000 °C at a rate of 10 °C per minute. Upon reaching 1000 °C, the temperature was maintained for 1 hour to ensure thorough mixing and initial melting of the raw materials. Subsequently, the temperature was increased from 1000 °C to 1400 °C at a rate of 10 °C per minute. The mixture was then held at 1400 °C for 2 hours to achieve complete melting and homogenization.

Characterization

The synthesized Ce-substituted HA composites were subjected to a series of characterization techniques. X-ray diffraction (XRD) was used to determine the crystalline phases and confirm the incorporation of Ce into the HA lattice. Fourier-transform infrared spectroscopy (FTIR) was employed to identify functional groups and assess structural integrity. Scanning electron microscopy (SEM) coupled with energy-dispersive X-ray spectroscopy (EDS) provided insights into the morphology and elemental distribution of the composites. Thermogravimetric analysis (TGA) evaluated the thermal stability, and mechanical testing measured compressive strength and microhardness.

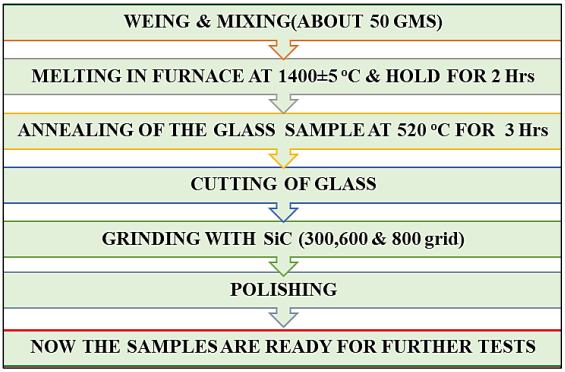

Fig 3: Flow chart of Bioglass samples prepared by the glass melting route

Table 1: Wt% composition of the bioglass samples

Sample Id	Wt%					
	SiO_2	Na_2O	CaO	P_2O_5	CeO_2	La_2O_3
BG	45	24.5	24.5	6	0.0	0.0
Ce1	44.5	24.5	24.5	6	0.5	0.0
Ce2	44	24.5	24.5	6	1.0	0.0
La1	44.5	24.5	24.5	6	0.0	0.5
La2	44	24.5	24.5	6	0.0	1.0

Results and Discussion

Density

Fig. 1 shows the density of the glass samples as a function of CeO_2/La_2O_3 within error bars. It is clear that an increase in CeO_2/La_2O_3 ratio with increasing CeO_2 substitution resulted an increase in the density of glass samples from 2.69 to 2.72 g/cc respectively. This is attributed due to the reason that the Cerium ions might have occupied interstitial sites within the glass network. Therefore, it increased the densities and resulted in creating new bonds with incorporation of Lanthanum ions in the bioactive glasses. It has caused reinforcement of glass structure and resulted in improvement in the compression of the glass samples.

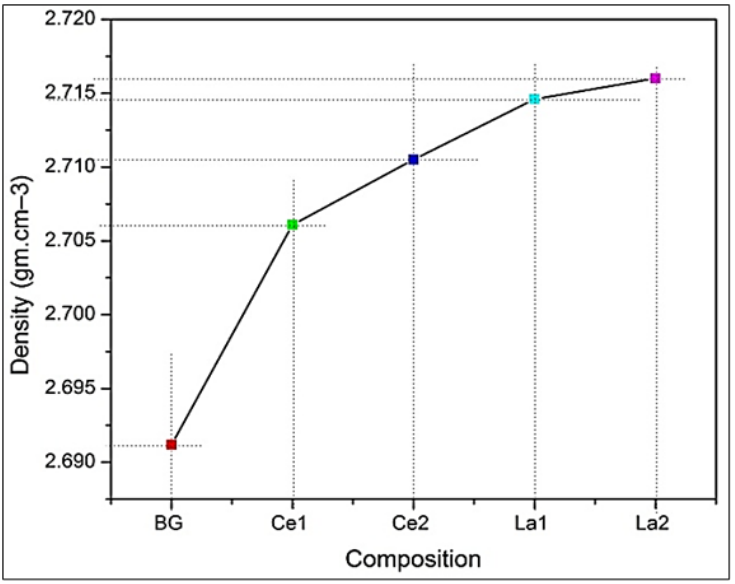

Fig 4: Density trends of a samples

Elastic Modulus, Shear Modulus and Bulk Modulus and Poisson's Ratio

Fig. 3 represents the experimental values of elastic moduli, Young's modulus (E), shear modulus(S) and bulk modulus (K) of the bioactive glass samples with increasing CeO_2/La_2O_3 ratio. All the elastic moduli values were found to increase with increasing CeO_2-La_2O_3 content. The elastic moduli of the bioactive glass samples show similar rends regarding improvement in their mechanical properties with the variation in the ultrasonic velocities. The elastic modulus of alkali silicate glasses was normally found to increase with increasing concentration of modifier above a critical limit as a result of an increase in cohesion. Thus, a greater bulk modulus of the glass samples can be partially attributed due to addition of more amounts of modifiers like K2O and CaO in the silicate glass samples. The authors have further mentioned that the effect of P_2O_5 on the elasticity of their glasses was not clear, although phosphorus has caused a more polymerized silicate network. Hench [1] has pointed out that the Young's modulus of cortical bone is about 7-30 GPa which is far below them ostceramic based implants. Hence, from the point of view of biomechanical compatibility, the SiO_2-CaO-P_2O_5-Na_2O-CeO_2-La_2O_3 bioactive glass samples have been found to be better. It was also known that the glasses and ceramics are brittle materials, as a consequence of which their handling and mechanical properties are not adequate for significant load bearing applications. Therefore, a bioactive glass having elastic modulus higher than that of bone is required for clinical applications. So, there was an increase in Young's modulus from 76.36to78.89GPa with increasing CeO_2/La_2O_3 content in the present base bioactive glass. Similar results were also obtained for shear and bulk moduli which showed improvement in the mechanical properties of bioactive glasses with varying ultrasonic velocities.

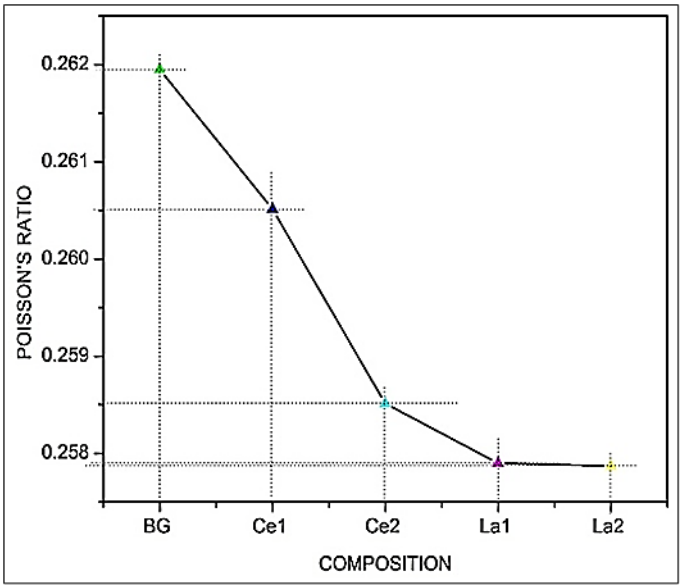
POISSON'S RATIO
0.262
0.261
0.260
0.259
0.258
BG
Ce1
Ce2
La1
La2
COMPOSITION

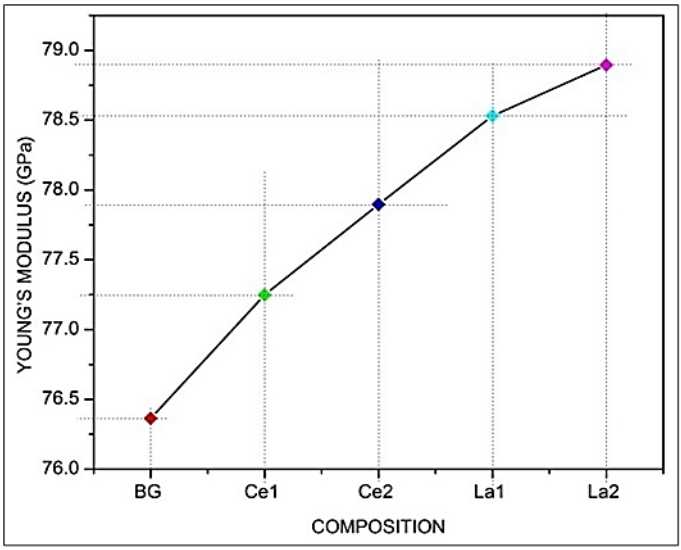
YOUNG'S MODULUS (GPa)
79.0
78.5
78.0
77.5
77.0
76.5
76.0
BG
Ce1
Ce2
La1
La2
COMPOSITION

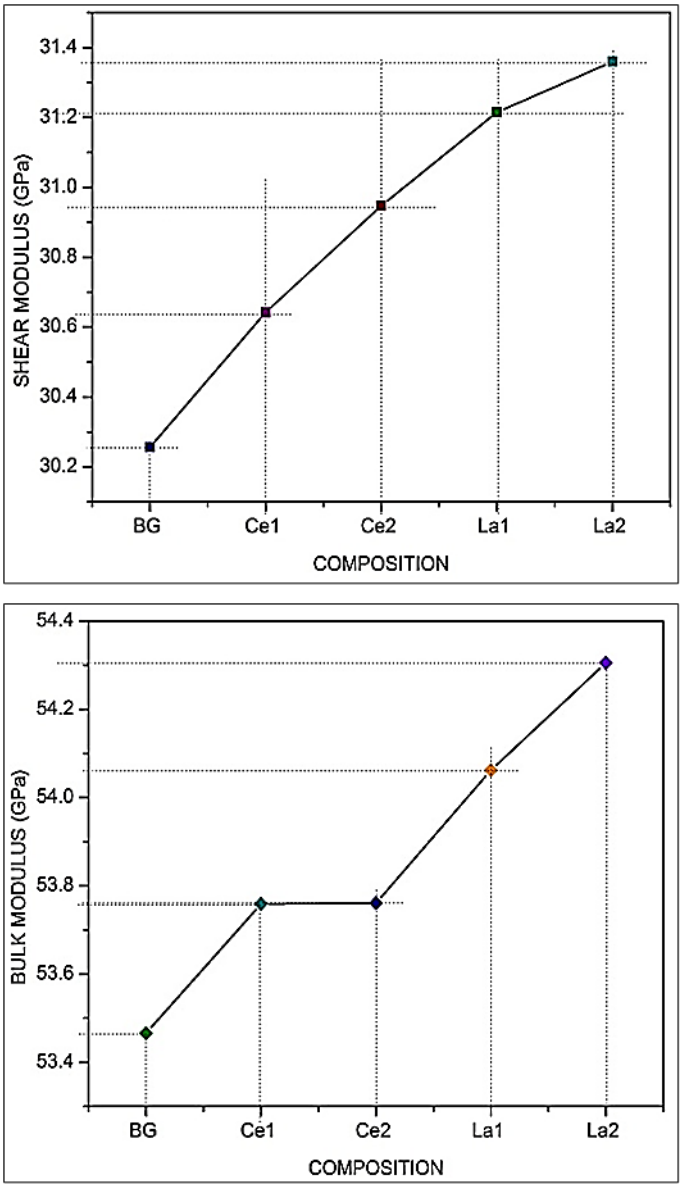

Fig 3: Eastic modulus, shear modulus and bulk modulus and Poisson's ratio

Conclusion

- The result show that Young's, Shear and bulk modulus increase with increasing concentration of rare earth oxides in non-charge

balance (NCB) glass whereas the Poisson's ratio decrease with increasing concentration of same oxides.

- In addition of Ce2+ and La3+ ions we should found that physical properties as well as biological properties increase with increasing concentration of these rare earth ions.
- XRD pattern of modified 45S5 glass shows amorphous phase behaviour in presence of Ce2+ and La3+ ions.
- In FTIR spectra HCA layer are present after the immersion in SBF solution.

References

1. Hench LL. J Am Ceram Soc. 1991;74:1487.
2. Bohner M, Lemaitre J. Biomaterials. 2009;30:2175.
3. Hench LL, Andersson O. In: Hench LL, Wilson J, editors. An Introduction to Bioceramics. Singapore: World Scientific; 1993. p. 41.
4. Hench LL. J Mater Sci Mater Med. 2006;17:967.
5. Hench LL, Splinter RJ, Allen WC, Greenlee TK. J Biomed Mater Res Symp. 1971;334:117.
6. Kokubo T. Biomaterials. 1991;12:155.
7. LeGeros RZ. Clin Orthop Relat Res. 2002;395:81.
8. Hench LL, Thompson I. J R Soc Interface. 2010;7:379–391.
9. Jung S. Missouri University of Science and Technology; 2010. PhD dissertation.
10. Jones JR, Ehrenfried LM, Saravanapavan P, Hench LL. J Mater Sci Mater Med. 2006;17:989–996.
11. Diba M, Tapia F, Boccaccini AR. Int J Appl Glass Sci. 2012;3:221–253.
12. Deliormanlı AM. J Mater Sci Mater Med. 2015;26:67.
13. Massera J, Vassallo-Breillot M, Törngren B, Glorieux B, Hupa L. J Non-Cryst Solids. 2014;402:28–35.
14. Rygel JL, Pantano CG. J Non-Cryst Solids. 2009;355:2622–2629.
15. Leonelli C, Lusvardi G, Malavasi G, Menabue L, Tonelli M. J Non-Cryst Solids. 2003;316:198–216.
16. El Batal FH, ElKheshen A. Mater Chem Phys. 2008;110(2–3):352–362.

Chapter - 13
Investigation of Thermal and Mechanical Properties of a Biocomposite Comprising Natural Rubber and 45S5 Bioglass Particles

Authors

Md. Ershad
Department of Mechanical Engineering, Swami Vivekananda University, Barrackpore, Kolkata, West Bengal, India

Ranjan Kumar
Department of Mechanical Engineering, Swami Vivekananda University, Barrackpore, Kolkata, West Bengal, India

Ravi Nigam
Department of Mechanical Engineering, Swami Vivekananda University, Barrackpore, Kolkata, West Bengal, India

Chapter - 13

Investigation of Thermal and Mechanical Properties of a Biocomposite Comprising Natural Rubber and 45S5 Bioglass Particles

Md. Ershad, Ranjan Kumar and Ravi Nigam

Abstract

Biocomposites composed of natural rubber (NR) reinforced with 45S5 Bioglass® (BG) particles were synthesized using a casting/evaporation technique, where NR was dissolved in chloroform and blended with BG particles. The resulting biocomposites were subjected to structural, mechanical, and thermal evaluations to determine the impact of BG particles on the properties of the NR matrix. Thermogravimetric analysis (TGA) and differential thermogravimetric analysis (DTG) of the biocomposites revealed decomposition profiles similar to those of pure NR, with the main peak of the DTG curve appearing prominently between 300-450 °C, indicative of the structural degradation of NR. The addition of BG particles enhanced the thermal stability of the biocomposites, as evidenced by TGA results showing increased stability with higher BG content. Dynamic mechanical analysis (DMA) indicated that samples with higher BG content exhibited increased storage modulus (E′) values. However, above the glass transition temperature (Tg), the E′ values approached zero due to increased polymer chain mobility. The Tg values, determined from tan δ analysis, were calculated to be -46 °C for pure NR and -50 °C for the biocomposite samples.

Mechanical testing demonstrated that incorporating BG into the biocomposites enhanced their mechanical properties. The biocomposites became more rigid as the BG content increased, shown by reduced deformation and increased elastic modulus (Y) and breaking strength. Overall, the inclusion of BG particles significantly improved the mechanical and thermal properties of the biocomposites, making them suitable for biomedical applications.

Keywords: Biocomposite, natural rubber, 45S5, echanical properties, thermogravimetric analysis

Introduction

Biomaterials are an essential component of modern medicine, playing a pivotal role in replacing, repairing, or treating biological tissues within living organisms. These materials encompass a diverse range of substances, including metals, polymers, ceramics, and composites, each chosen for their unique properties and compatibility with biological systems [1, 2]. The classification of biomaterials can be based on their chemical nature, dividing them into natural and synthetic categories. Natural biomaterials, such as collagen and chitosan, are derived from biological sources, whereas synthetic biomaterials, like polylactic acid and titanium alloys, are engineered through chemical processes [3, 4].

In addition to their chemical composition, biomaterials are also categorized based on their interaction with biological tissues. This classification results in three distinct types: bioactive, bioinert, and bioresorbable materials. Bioactive materials have the remarkable ability to interact positively with surrounding tissues, promoting cellular activity and tissue integration. These materials, such as certain glasses and ceramics, are designed to elicit specific biological responses at the interface of the material and tissue, facilitating the healing process and improving the functionality of implants and prosthetics [5].

Bioinert materials, on the other hand, are designed to minimize interaction with the biological environment. Materials like stainless steel and certain polymers are used in applications where minimal tissue reaction is desired, ensuring stability and durability over long periods. These materials are often employed in structural applications, such as joint replacements and dental implants, where they provide mechanical support without eliciting adverse biological responses [6]. Bioresorbable materials, including certain polymers and ceramics, are engineered to degrade gradually within the body, being replaced by natural tissue over time. This property is particularly advantageous in temporary applications, such as sutures and drug delivery systems, where the material's gradual dissolution eliminates the need for a second surgical intervention to remove the device.

The development and application of biomaterials represent a dynamic and interdisciplinary field, combining principles from biology, chemistry, and engineering to create materials that enhance the quality of life for countless individuals. As research advances, the potential for innovative biomaterials to address a broader range of medical challenges continues to expand, promising exciting future developments in healthcare.

Experimental

Natural Rubber Membranes

Natural rubber (NR) latex was harvested from Hevea brasiliensis trees (RRIM 600 clones) at an experimental farm located on the São Paulo State University (UNESP) campus in Ilha Solteira, São Paulo, Brazil. The collected NR latex was sieved and then stored at approximately 5 °C. NR membranes were prepared by casting the NR latex onto a glass substrate and allowing it to dry in air at 60 °C for 12 hours. After drying, the membranes were easily peeled off the substrate.

45S5 Bioglass Particles

To produce 45S5 Bioglass (BG) particles, raw materials were melted to achieve a composition of 24.3 mol% Na2O, 26.9 mol% CaO, 2.5 mol% P2O5, and 46.3 mol% SiO_2. The raw materials included sodium carbonate ($Na2CO_3$-JT Baker), calcium carbonate ($CaCO_3$-JT Baker), disodium phosphate ($Na2HPO_4$-JT Baker), and high-purity quartz (SiO_2-Santa Rosa). These components were melted together in a conventional bottom-loaded electric furnace (CM Furnaces, Inc, Bloomfield, NJ) at 1450 °C for 4 hours in a platinum crucible. The molten glass was then poured into a stainless steel mold and air-cooled. Initially, large glass particles (approximately 2 mm) were obtained by grinding the solidified glass in an agate mortar. These particles were subsequently crushed in a high-impact planetary ball mill (Pulverisette 5-FRITSCH) at 450 rpm for 90 minutes using an agate jar and 20 mm diameter agate balls.

Biocomposite Preparation

To prepare the biocomposites, 4 grams of NR membrane were dissolved in 40 mL of chloroform under constant stirring for 12 hours, resulting in a gel-like solution suitable for dispersing BG particles. Separately, BG particles were dispersed in 10 mL of chloroform under constant stirring for 1 hour. This BG particles/chloroform dispersion was gradually added to the chloroform/NR solution and stirred for an additional 5 hours. The resulting mixture was cast onto a glass substrate and allowed to dry in air at 60 °C for 12 hours, during which the chloroform completely volatilized, yielding the NR/BG biocomposite. Different NR/BG biocomposites were prepared with varying mass ratios of NR to BG particles: 90/10, 70/30, and 50/50. These biocomposites were subsequently characterized to assess the influence of BG particles on their structural, mechanical, and thermal properties.

Characterization

The microstructure of fractured transversal sections of the biocomposites, coated with carbon for 30 minutes, was observed using a scanning electron microscope (SEM, EVO LS15 Zeiss). The biocomposites were fractured after immersion in liquid nitrogen and then dried under dynamic vacuum for 1 hour. Surface morphology was analyzed using an Agilent 5500 atomic force microscope on samples with an area of 1 cm^2.

Thermogravimetric analysis (TG/DTG) was performed using a TA Instruments model Q600 in the temperature range of 25-600 °C at a heating rate of 10 °C per minute in a nitrogen atmosphere with a flow rate of 100 mL per minute, using approximately 10 mg of each sample. Dynamic mechanical thermal analysis (DMA) was carried out using a Netzsch model DMTA 242C in tensile mode with a frequency of 10 Hz, over a temperature range of -100 to 150 °C, and a heating rate of 5 °C per minute. Rectangular specimens with dimensions of approximately 9 mm × 3 mm × 1 mm were used. The metrics obtained from this analysis included the storage modulus (E'), loss modulus (E"), and tan δ (the ratio of E" to E').

Mechanical testing in stress-strain mode was conducted according to ISO 37:2011 using an Instron model 3639 tensometer at room temperature, with a crosshead speed of 13 mm per minute applied to a 100-N load cell. Mechanical measurements were repeated eight times in accordance with ISO 1286:2006.

Results and Discussion

Morphology

Scanning electron microscopy (SEM) was used to examine fractured transversal sections and surfaces of the biocomposites, focusing on the dispersion of BG particles within the NR matrix. Figures 1a, b, and c illustrate that the BG particles are evenly distributed throughout the NR/BG biocomposites, demonstrating the effectiveness of the preparation method. Additionally, Figure 1d shows a uniform surface pattern on the biocomposites, which is crucial for the interaction of BG particles with organic tissue. Figure 1e reveals that the BG particles have irregular shapes and average sizes of less than 10 μm [7].

Atomic force microscopy (AFM) provided further analysis of the biocomposite surfaces. Figures 2a and b depict the surface morphology of samples with 90/10 and 50/50 mass ratios, respectively. The 50/50

biocomposite has a rougher surface compared to the 90/10 biocomposite due to the higher BG particle content, which is consistent with the SEM findings.

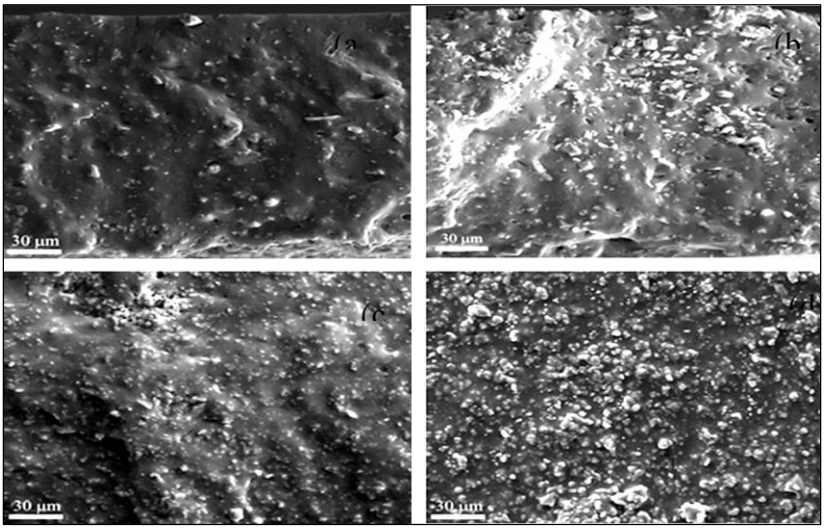

Fig 1: SEM images of fractured transversal sections of NR/BG biocomposites with mass ratios: (a) 90/10, (b) 70/30, and (c) 50/50. (d) SEM image of the surface of the 50/50 sample

Mechanical Properties

Stress–strain tests were conducted to assess the impact of BG particles on the mechanical properties of NR. As illustrated in Figure 6 and detailed in Table 2, incorporating BG particles significantly enhances several mechanical properties of NR. This improvement is attributed to the efficient transfer of applied tension from the NR matrix to the BG particles, thereby confirming their role as a reinforcing agent [8-9].

The stress-strain behavior characteristic of elastomeric materials is evident in NR, as shown in Figure 6. The stress–strain curves of the biocomposites exhibit similar patterns; however, the elastic modulus (Y) of the biocomposites increases with the BG particle content. Additionally, the tensile strength at break (rat break) also shows an upward trend with higher BG particle content. An increase in the elastic modulus indicates enhanced resistance to deformation. Notably, adding just 10 mass% of BG particles to NR results in a significant increase in both the elastic modulus and the tensile strength at break, as shown in Figure 6.

Table 1 reveals that the Thermal decomposition parameters for NR and NR/BG biocomposites gradually rises, This behavior suggests a progressive enhancement in the material's mechanical properties with increasing BG particle content.

Table 3: Thermal decomposition parameters for NR and NR/BG biocomposites include onset temperature (Ton), maximum decomposition rate temperature (Tm), and residue

Samples	T_{on}/°C	T_m/°C	Residue/%
NR	339	369	1.5
NR/BG (90/10)	338	379	14
NR/BG (70/30)	327	370	33
NR/BG (50/50)	330	371	48

Conclusions

A straightforward synthesis route was used to produce natural rubber/Bioglass® 45S5 biocomposites. SEM analysis confirmed a uniform distribution of BG particles within the NR matrix. Thermal analysis indicated that the biocomposite samples exhibited greater thermal stability than pure NR, although they maintained a similar thermal profile in the TG/DTG curves. Samples with higher BG content showed increased storage modulus values, but above the glass transition temperature (Tg), the E' values of all samples approached zero due to the increased mobility of the polymer chains. The tan δ curve provided Tg values of -46 °C for NR and-50 °C for the biocomposites. The inclusion of BG particles significantly enhanced the mechanical properties of the biocomposites compared to NR. Stress-strain tests revealed that the biocomposite samples had a higher elastic modulus and tensile strength at break than pure NR. These findings demonstrate that BG particles improve the thermal and mechanical properties of NR matrices, making these biocomposites potential candidates for biomedical applications.

References

1. Ige OO, Umoru LE, Aribo S. Natural products: a minefield of biomaterials. ISRN Mater Sci. 2012;2012:1-20.
2. Sykaras N, Iacopino AM, Marker VA, Triplett RG, Woody RD. Implant materials, designs, and surface topographies: their effect on osseointegration. A literature review. Int J Oral Maxillofac Implants. 2000;15:675-90.

3. Boccaccini AR, Gough JE. Tissue engineering using ceramics and polymers. 2nd ed. New York: CRC Press; 2007.
4. Hench LL. The story of Bioglass®. J Mater Sci Mater Med. 2006;17:967-78.
5. Hench LL, Polak JM. Third-generation biomedical materials. Science. 2002;295:1014-7.
6. Reilly GC, Radin S, Chen AT, Ducheyne P. Differential alkaline phosphatase responses of rat and human bone marrow derived mesenchymal stem cells to 45S5 bioactive glass. Biomaterials. 2007;28:4091-7.
7. Hench LL, Wilson J. Introduction. In: Hench LL, Wilson J, editors. An introduction to bioceramics. Singapore: World Scientific Publishing Co. Pte. Ltd.; 1993. p. 1-24.
8. Jones JR. Review of bioactive glass: from Hench to hybrids. Acta Biomater. 2013;9:4457-86.
9. Gerhardt LC, Boccaccini AR. Bioactive glass and glass-ceramic scaffolds for bone tissue engineering. Materials. 2010;3:3867-910.

Chapter - 14
Identification of Fault in the Beam Utilizing Mean of Wavelet Coefficients: A Numerical Analysis

Authors

Ravi Nigam
Swami Vivekananda University, Kolkata, West Bengal, India
Mody University of Science and Technology, Sikar, Rajasthan, India

Ramnivas Kumar
Government Engineering College, Jamui, Bihar, India

Arnab Das
Swami Vivekananda University, Kolkata, West Bengal, India

Ranjan Kumar
Swami Vivekananda University, Kolkata, West Bengal, India

Vikrant Sharma
Mody University of Science and Technology, Sikar, Rajasthan, India

Chapter - 14

Identification of Fault in the Beam Utilizing Mean of Wavelet Coefficients: A Numerical Analysis

Ravi Nigam, Ramnivas Kumar, Arnab Das, Ranjan Kumar and Vikrant Sharma

Abstract

This study employs a finite element model of a cracked cantilever beam to numerically detect cracks through wavelet analysis. It investigates the impact of measurement noise by averaging wavelet coefficients from multiple data frames. Averaging (mean) across multiple frames could help reduce noise and improve the signal-to-noise ratio. This approach aims to improve crack detection accuracy and algorithm robustness by effectively mitigating the influence of noise on the beam's deflection signal, as evidenced by slope discontinuities in the elastic line. The presented algorithm has ability to correctly identify the presence and location of cracks. This method is beneficial for structural health monitoring and maintenance in various engineering applications.

Keywords: Cantilever beam, FEM, Signal to noise ratio, wavelet transform

Introduction

Structural performance can be significantly compromised by faults such as beam cracks. These fatigue cracks are typically induced by mechanical vibrations and periodic stresses exerted on the beam. Failure to detect such cracks at an early stage can result in catastrophic failures. Consequently, continuous structural health monitoring is essential. Implementing early crack detection with effective diagnostic schemes is crucial for preventing costly failures and unplanned downtimes. Dimarogonas [1] has conducted comprehensive reviews on state-of-the-art vibration-based crack detection techniques. In numerous studies, crack localization has been extensively investigated using modal parameters, such as modal curvatures, mode shapes, and natural frequencies [2-5]. As we know that the SD is confined, therefore detection of slope discontinuity due to crack helps to find out its position in the beam. Over the years, numerous studies have employed

wavelet transform techniques for crack detection in beams and beam-like structures [6-8]. Wavelet transform has ability to detect sudden changes in a signal and it is an effective tool for detecting discontinuity in a noisy signal. The presence of noise makes crack detection algorithm fails at certain extent. To address this limitation, several researchers have focused their efforts on mitigating the effects of noise. Solis *et al*. [9] used averaging of Continous Wavelet Transform coefficients at different scales to propose the crack detection. In the current paper, the Discrete Wavelet Transform (DWT) coefficients of various input beam responses are computed and then averaged to mitigate the effects of measurement noise. In this context, the noise is uncorrelated across the input signals of the simulated beam.

Modelling of Cracked Cantilever Beam

The finite element model of beam system is modelled by using finite element method (FEM), as presented in Fig. 1. The Timoshenko beam theory is considered for transverse vibrations. To develop a finite element model, the beam is axially divided into uniform elements connecting two neighboring node points. The main parameters of the simulated cracked beam are given in Table 1.

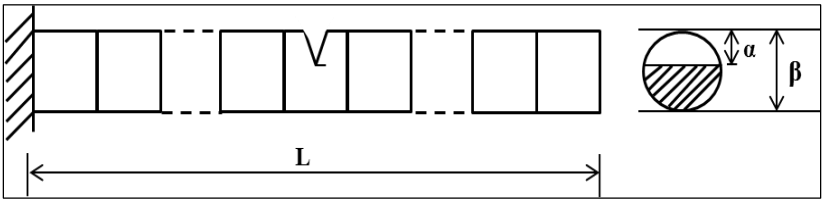

Fig 1: Finite element model of cantilever beam

A beam element and its generalized displacements at nodes can be presented by generalized displacement vector. At the ith node, the generalized displacement vector as,

$$q_i = [u_{xi} \quad u_{yi} \quad \theta_{yi} \quad \theta_{xi}]^T \tag{1}$$

Where u_{xi}, u_{yi} are translation degree of freedom along x and y direction and θ_{xi}, θ_{yi} are rotational degree of freedom along x and y direction.

Table 1: Main parameters of the simulated beam

Parameters	Value
Beam length, L (m)	1
Number of finite elements	500
Beam diameter, β (m)	0.01
Crack depth ratio (α/β)	0.25
Location of cracked element from fixed end	162
Young's modulus (N/m^2)	2.06×10^{11}
density (Kg/m^3)	7800
Poisson's ratio	0.3

The governing equations of motion which are used to generate the response of the non-cracked and cracked beam system are expressed as [2]:

$$[M]\{\ddot{X}\} + [C]\{\dot{X}\} + [K]\{X\} = \{P\} \quad (2)$$

And

$$[M]\{\ddot{X}\} + [C_c]\{\dot{X}\} + [K_c]\{X\} = \{P\} \quad (3)$$

The $[M]$, $[C]$, $[K]$ are the assembled mass, damping and stiffness matrices of the beam system, respectively.$\{P\}$ is the external forcing. Subscript 'c' is used for the cracked beam system. Damping is considered to be the proportional damping [2]. Here each node of the element has four degrees of freedom i.e., two translational and two rotational. When crack exists in the beam, the additional flexibility introduces.

$$[K_c]^e = [T][S]^{-1}[T]^T \quad (4)$$

Here $[S]$ and [T] is the total flexibility of the cracked element, and transformation matrix, respectively.

Now the response of the cracked cantilever beam system is generated by considering external forcing the vertical direction to excite the beam. For the simulation study, first mode of the cracked cantilever beam is considered. In real situations, the beam response is affected by measurement noise. Therefore, a white Gaussian noise is added to the simulated responses. In Fig. 2, deflection response with noise level of 85 dB is presented. It is further considered as an input signal for wavelet analysis.

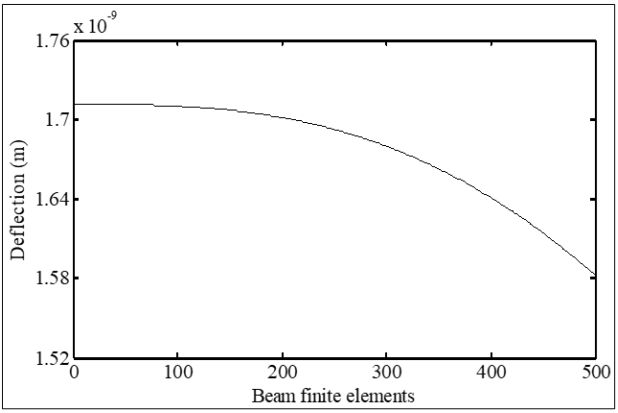

Fig 2: Deflection Response with noise

Results with Discussions

Discrete Wavelet Transform with Coiflet wavelet of order one is applied on the simulated responses of cracked cantilever beam for the crack detection based analysis. It is quite difficult to observe the slope discontinuity from the simulated deflection response as shown in Fig. 2. However, the slope discontinuity appears as a spike at the specific level of wavelet decomposition. The wavelet coefficient of the input signal at noise level of 85 dB is shown in Fig. 3. It can be clearly seen from Fig. 3, that the crack location can be easily identified by spotting the higher spikes. Now with the increment of noise at 80 dB of SNR, the effect of slope discontinuity diminishes in the wavelet coefficient result, shown in Fig. 4. Here the peaks due to crack is not clearly visble.

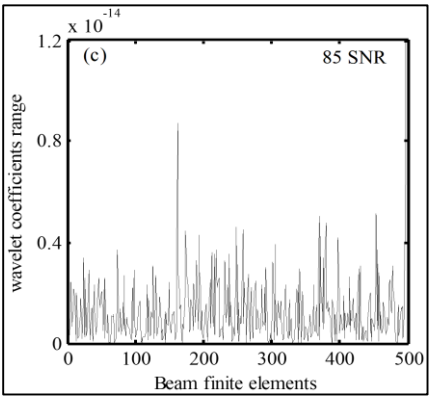

Fig 3: Wavelet detail coefficients at 85 dB of SNR

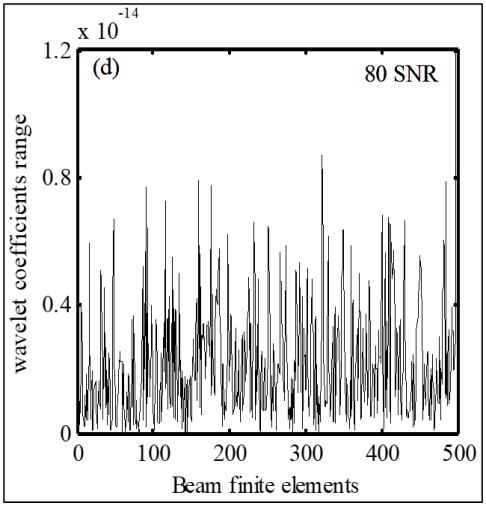

Fig 4: Wavelet detail coefficients at 80 dB of SNR

To enhance the crack detectability further, mean of wavelet coefficients of several frames of input signal is proposed. It is to be noted that noise is considered to be uncorrelated across input signal. Discrete Wavelet Transform produces spikes due to the singularities present in the input signal. The discontinuities produced by the noise are random in nature but the discontinuity due to the crack is at the fixed location in all frames of beam deflections. By aggregating detailed coefficients from multiple deflections, we mitigate the impact of uncorrelated spikes caused by noise, resulting in their averaging out. Meanwhile, the peak associated with the crack, consistently located, is amplified as a consequence. Since the effect of slope discontinuity diminishes in the wavelet coefficient result due to the increment of noise, shown in Fig. 4. Hence the mean of detailed coefficients for 80 dB of SNR is analysed with different seven frames of input signal. The normalized detailed coefficient (D1's) at excitation frequencies 5, 7, 9…17 (rad/s) are taken for its averaging. The averaged detailed coefficients for 80 dB of SNR is plotted in Fig. 5.

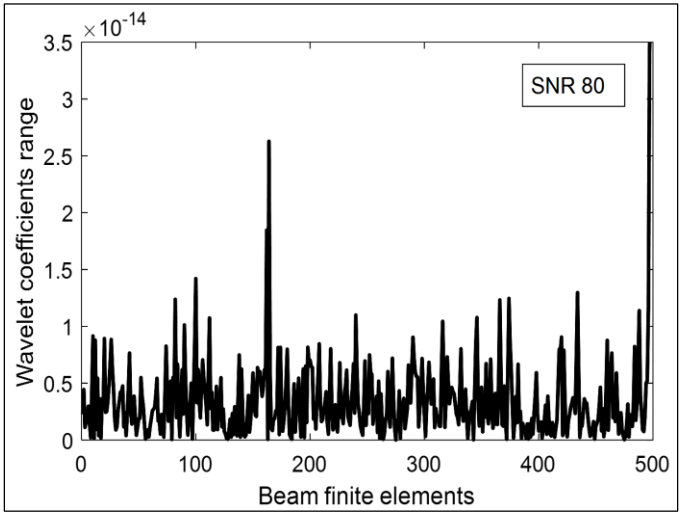

Fig 5: Averaging of wavelet detail coefficients at 80 SNR

Conclusion

The current study provides insightful elucidation on the concept of noise reduction and signal enhancement through the utilization of signal averaging. Discrete Wavelet Transform is employed to analyze spatially distributed signals. The approach of averaging discrete wavelet coefficients is effectively implemented in simulated beam deflections. A notable characteristic of this method is its capability to mitigate the impact of measurement noise on the wavelet coefficient outcomes post discrete wavelet transform application, particularly yielding favorable results at relatively low signal-to-noise ratio levels. The algorithm is further refined by averaging wavelet detailed coefficients derived from multiple deflection responses at various excitation frequencies. The proposed method would be useful for the damage detection in wind turbine blades, shafts, aircraft wings, and steel bridges. The requirement is that the component should deflect due to some load or vibration.

References

1. A.D. Dimarogonas, Vibration of cracked structures: a state of the art review, Engineering Fracture Mechanics 55 (1996) 831-857.
2. R. Nigam, S.K. Singh, Crack detection in a beam using wavelet transform and photographic measurements, Structures 25 (2020) 436–447.

3. Cao, M.; Xu, W.; Ren, W.; Ostachowicz, W.; Sha, G.; Pan, L. A concept of complex-wavelet modal curvature for detecting multiple cracks in beams under noisy conditions. Mech. Syst. Signal Process. 76 (2016) 555–575.
4. Wu, Q.; Guo, S.; Li, X.; Gao, G. Crack diagnosis method for a cantilevered beam structure based on modal parameters. Meas. Sci. Technol. 31 (2020) 035001.
5. J. Aboudi, Stiffness reduction of cracked solids, Engineering Fracture Mechanics 5 (1987) 637-650.
6. Kim H, Melhem H, Damage detection of structures by wavelet analysis, Eng. Struct. 26 (2004) 347–362.
7. S.T. Quek, Q. Wang, L. Zhang, K. K. Ang, Sensitivity analysis of crack detection in beams by wavelet technique, International Journal of Mechanical Sciences 43 (2001) 2899-2910.
8. M. Rucka, Damage detection in beams using wavelet transform on higher vibration modes, Journal of Theoretical and Applied Mechanics 49 (2011) 399-417.
9. Solís, M., Algaba, M., & Galvín, P. Continuous wavelet analysis of mode shapes differences for damage detection. Mechanical Systems and Signal Processing, 40(2) (2013) 645-666.

Chapter - 15
Bifacial Solar Panel: A Boon for an Impeccable Sustainable Journey

Authors

Kavita Jha
Indian Institute of Technology (Indian School of Mines), Dhanbad, Jharkhand, India

Nisit Kumar Parida
Indian Institute of Technology (Indian School of Mines), Dhanbad, Jharkhand, India

Md. Ershad
Swami Vivekananda University, Kolkata, West Bengal, India

Mukul Kant Paliwal
Mody University of Science and Technology, Sikar, Rajasthan, India

Ravi Nigam
Swami Vivekananda University, Kolkata, West Bengal, India
Mody University of Science and Technology, Sikar, Rajasthan, India

Chapter - 15

Bifacial Solar Panel: A Boon for an Impeccable Sustainable Journey

Kavita Jha, Nisit Kumar Parida, Md. Ershad, Mukul Kant Paliwal and Ravi Nigam

Abstract

As urbanization continues its upward trajectory, the need for sustainable energy solutions in urban areas becomes increasingly imperative. Referring to which, solar energy has emerged as a superior alternative to conventional sources. Solar panels, composed of photovoltaic cells, represent a ground-breaking technology for harnessing this energy directly into electricity. The dual-sided absorption technology of bifacial panels boost efficiency by harnessing reflected sunlight, a feature absents in mono-facial panels. The integration of bifacial solar panels offers a promising avenue for advancing sustainable energy practices. This research aims to optimize the deployment of bifacial panel arrays, focusing on maximizing energy output while minimizing spatial requirements. Through computational modelling, empirical trials, and statistical analysis, actionable directives for urban planners and policymakers are sought. The outcomes of this study highlight significant improvements in energy efficiency and notable reductions in carbon footprints, contributing to cleaner urban ecosystems.

Keywords: Photovoltaic cells, solar panels

Introduction

The burgeoning urbanization sweeping across the globe underscores an escalating need for sustainable energy solutions imperative for mitigating carbon emissions and combating climate change. Among these solutions, solar energy, particularly harnessed through photovoltaic (PV) technology, emerges as a pivotal element. Mono-facial solar panels, with their single-sided absorption of sunlight, are the traditional choice. However, Bifacial solar panels, a type of photovoltaic module capable of capturing sunlight from both front and back sides, significantly enhance energy production efficiency. This dual-sided absorption enables bifacial panels to generate

electricity not only from direct sunlight but also from reflected light, such as from the ground or nearby structures. Their adaptability to urban environments is notable, as reflective surfaces like building facades and pavements augment their performance. Nonetheless, optimizing placement, orientation, and integration of these panels presents a challenge to fully capitalize on their benefits. Furthermore, they also offer a promising solution for maximizing energy output in diverse environments, especially in urban areas where space constraints and shading effects are prevalent. Increasingly adopted in solar energy projects worldwide, bifacial solar panels demonstrate their ability to optimize energy generation while maintaining a relatively small footprint.

In this study, the optimization of bifacial solar panel arrays within urban contexts is examined, aiming to maximize energy output while considering spatial limitations and environmental influences. Employing a blend of simulation studies, modelling methodologies, and data analytics, this investigation scrutinizes the optimal design parameters, including tilt angle, orientation, and panel spacing. Furthermore, the research evaluates the effects of diverse environmental variables, such as shading, reflection, and albedo, on energy generation. The outcomes of this study contribute to the progression of sustainable energy solutions in urban environments, providing valuable insights into the effective deployment of bifacial solar panel arrays to enhance both energy efficiency and environmental robustness.

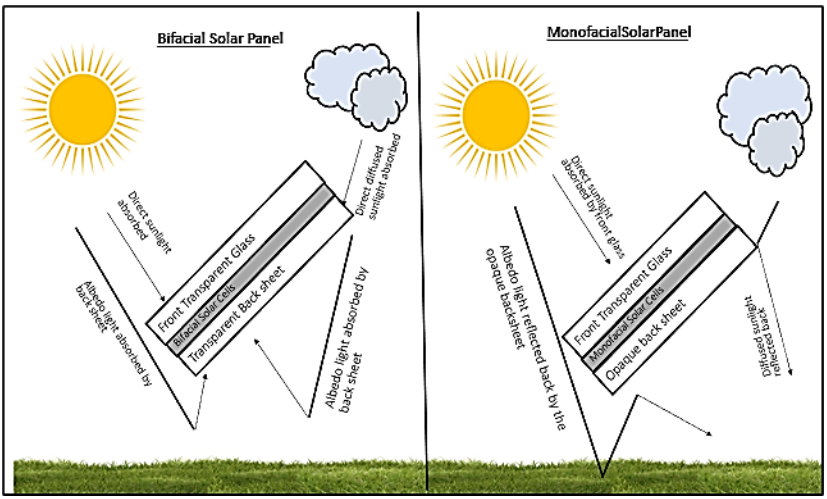

Fig 1: Comparison between bifacial solar panels and monofacial solar panels

Objectives

This study aims to formulate optimization strategies tailored for deploying bifacial solar panel arrays within urban landscapes by analyzing the influence of various urban surface materials on the efficacy of bifacial solar panels. It also tends to evaluate the economic and environmental advantages associated with the integration of bifacial solar panels in urban environments. Eventually, the study offers actionable recommendations for urban planners and policymakers to augment sustainable energy practices.

Literature Review

Bifacial Solar Panels

Bifacial solar panels stand apart from traditional monofacial counterparts due to their photovoltaic cells on both sides. This enables them to harness both direct and reflected sunlight. Studies suggest that under ideal conditions, bifacial panels can generate up to 30% more energy compared to monofacial ones (Zubi *et al*., 2009). This heightened efficiency renders them particularly appealing for urban settings characterized by high albedo surfaces.

Urban Surface Materials and Albedo

Albedo is the measurement of how much light or radiation a surface reflects, typically presented as a percentage. It signifies the surface's capacity to deflect sunlight, with higher albedo values indicating greater reflection and less absorption. Albedo is pivotal in the functionality of bifacial solar panels. Surfaces like white rooftops, reflective pavements, and green areas can notably influence the quantity of reflected light accessible for bifacial panels (Yang and Lu, 2017). Research demonstrates that elevating surface albedo can enhance the energy output of bifacial panels, underscoring the significance of urban surface materials in optimization approaches.

Integration of Solar Panels in Urban Environments

The bulk of prior research has concentrated on incorporating monofacial solar panels into urban environments, investigating their installation on rooftops, facades, and other urban structures (Sarmah *et al*., 2021). Nevertheless, integrating bifacial panels necessitates distinct considerations owing to their dual-sided design. Optimizing panel placement and orientation becomes imperative to enhance their efficiency while reducing spatial footprint.

Economic and Environmental Impact

The financial viability of installing solar panels in urban settings hinges on various factors, including installation expenses, upkeep and energy savings. Bifacial panels, due to their increased energy production, present the potential for a shorter payback period and greater return on investment in comparison to monofacial panels (Lehmann *et al.,* 2020). Furthermore, the environmental advantages, such as decreased carbon emissions and mitigation of urban heat island effects, foster cleaner and more sustainable urban landscapes.

Methodology

Experimental Design

The site selection with experimental setup and resources are discussed under the section of experimental design.

Site Selection

The study was conducted in an urban area with diverse surface materials, including rooftops, pavements, and green areas. Various sites within this locale were chosen to assess different arrangements of bifacial solar panels.

Experimental Setup and Resources

In conjunction with bifacial solar panel technology, reflective surface treatments such as white paint or reflective films were utilized to optimize light absorption and bolster energy generation. To ensure peak performance and efficiency, Internet of Things (IoT) sensors were deployed to monitor environmental conditions such as sunlight intensity, temperature, and humidity. These sensors continuously collect real-time data, which is then analyzed using sophisticated data logging and analysis software. This enables informed decision-making and proactive maintenance strategies for solar energy systems. The integration of bifacial panels, reflective surface treatments, IoT sensors, and data analytics software offers a holistic approach to harnessing solar energy efficiently and sustainably. Bifacial solar panels were strategically installed at various heights and orientations above diverse surface materials. Reflective treatments were applied to select surfaces to assess their impact on panel performance. Concurrently, IoT sensors diligently monitored temperature, humidity, soil moisture, and sunlight intensity, providing comprehensive insights for system optimization.

Data Collection

In assessing Energy Output, quantification of the energy output from the bifacial solar panels was conducted using inverters and data loggers. Data collection was carried out throughout different seasons to account for variations in sunlight and weather conditions. Regarding Environmental Conditions, continuous monitoring of environmental factors such as soil moisture, temperature, and humidity was enabled by IoT sensors. This data served to correlate environmental conditions with both energy output and crop productivity, providing valuable insights into system performance.

Statistical Analysis

In Data Analysis, the collected data was subjected to analysis using statistical software like R and SPSS to identify patterns and correlations. Descriptive statistics were utilized to summarize the data, while inferential statistics, including ANOVA and regression analysis, were employed to examine hypotheses concerning the impact of bifacial panels on energy yield and crop growth. In the realm of Optimization Models, models were developed to determine the optimal configurations for panel placement and orientation. These models utilized data obtained from experiments and simulations to predict outcomes across different scenarios, aiming to maximize system performance and efficiency.

Economic and Environmental Impact Assessment

In conducting the Cost-Benefit Analysis, a comprehensive evaluation of costs and benefits was undertaken, contrasting the integrated system with traditional urban agriculture and standalone solar installations. This thorough analysis encompassed various factors, including installation expenses, maintenance, energy savings, and crop yield.

In assessing the Environmental Impact, meticulous evaluation was conducted on changes in carbon footprint, urban heat island effect, and resource consumption. Additionally, considerations were given to the benefits such as improved air quality and biodiversity.

Regarding the Social Impact, surveys and interviews were conducted with urban farmers and community stakeholders to gain insights into the social and economic advantages of the integrated system. This qualitative data complemented the quantitative analysis, offering a comprehensive understanding of the system's impact.

Results

The initial findings regarding energy output suggest a substantial increase in energy yield with the use of bifacial solar panels compared to monofacial panels. Additionally, the application of reflective ground treatments further enhances efficiency, particularly in urban areas with highly reflective surfaces. Descriptive statistics based on energy yield data from bifacial solar panels installed with reflective ground treatments reveal an average increase of 25% compared to panels without such treatments. Seasonal variations underscore the importance of optimizing panel orientation throughout the year. Inferential statistics, including ANOVA tests and regression analysis, confirm the statistically significant impact of reflective treatments on energy yield, with a strong positive correlation between ground reflectivity and energy output ($R^2 = 0.85$).

Regarding crop growth, the data indicates a mixed impact of bifacial panel-induced shading. While some crops benefit from partial shading, which reduces heat stress, others experience reduced growth due to insufficient light. Descriptive statistics on crop yield measurements reveal varied responses across different crop types, with leafy greens showing a 15% increase in yield under partial shading and fruiting crops experiencing a 10% reduction. ANOVA tests on crop yield data highlight significant variations in the impact of shading across crop types ($p<0.05$), with regression models identifying optimal shading levels to maximize overall productivity without significantly compromising individual crop yields.

The integrated system demonstrates substantial environmental benefits, including reduced carbon emissions and enhanced urban biodiversity. Economically, the increased energy savings and crop yield offset the higher initial costs of bifacial panels. The cost-benefit analysis indicates a payback period of approximately 7 years, considering energy savings and increased crop yield, with a positive net present value (NPV) over a 20-year period, indicating economic feasibility. Moreover, the system reduces the urban farm's carbon footprint by an estimated 20% and promotes biodiversity in shaded areas.

In terms of social impact, community feedback underscores the potential of the system to enhance urban food security and provide educational opportunities. However, concerns about maintenance and initial investment costs need to be addressed. Survey results reveal strong support for the integrated system among urban farmers, with 80% expressing willingness to

adopt similar technologies, contingent upon technical training and financial assistance to cover initial setup costs.

Discussion

The study underscores the importance of optimizing the placement and orientation of bifacial solar panels to strike a balance between energy generation and crop productivity in urban agriculture. It highlights the potential of dynamic systems that adjust panel angles based on seasonal changes to maximize benefits. Simulation models indicate that dynamically adjusting panel angles could improve energy yield by an additional 10% while maintaining optimal shading conditions for crops, suggesting the feasibility of developing automated systems for real-time adjustment. Integrating bifacial solar panels into urban agriculture promotes long-term sustainability by fostering renewable energy use and local food production, with the system's adaptability enhancing scalability across different urban environments. Policymakers are urged to consider incentives and subsidies for urban agriculture projects incorporating renewable energy technologies to support research and development, drive innovation, and reduce costs. Additionally, further research is needed to explore the development of lightweight, flexible bifacial panels that are easier to install and maintain in urban settings, along with the creation of practical guidelines for urban farmers on integrating these systems effectively.

Conclusion

Integrating bifacial solar panels into urban agriculture systems emerges as a promising approach to bolstering sustainable energy and food production. The study's results provide invaluable guidance for optimizing these systems and underscore their substantial environmental, economic, and social advantages. Future research endeavours should concentrate on enhancing optimization models and investigating novel technologies to advance system efficiency and scalability even further.

References

1. Zubi, G., Bernal-Agustín, J. L., & Fracastoro, G. V. (2009). "High efficiency bifacial solar cells for space and terrestrial applications". Renewable Energy, 34(8), 1773-1780.
2. Yang, D., & Lu, L. (2017). "Feasibility of building-integrated bifacial solar photovoltaic façade in urban environment". Energy Procedia, 105, 1073-1078.

3. Sarmah, N., Mahapatra, S., & Venugopal, K. (2021). "Performance comparison of bifacial and monofacial solar photovoltaic modules under different conditions". Renewable Energy, 163, 936-945.
4. Lehmann, D., Bian, J., & He, Y. (2020). "Optimization of bifacial solar panel positioning considering reflection from the ground." Journal of Renewable and Sustainable Energy, 12(1), 013301.
5. Abas, N., Kalair, A., & Khan, N. (2018). "Review of the Scalable Renewable Energy Technologies in Electricity Generation." Renewable and Sustainable Energy Reviews, 79, 1221-1241.

Chapter - 16
Revolutionizing Mobility: Advanced Hydroelectric and Electric Vehicle Technologies for Sustainable Development

Authors

Samrat Biswas
Swami Vivekananda University, Kolkata, West Bengal, India

Sayan Paul
Swami Vivekananda University, Kolkata, West Bengal, India

Suman Kumar Ghosh
Swami Vivekananda University, Kolkata, West Bengal, India

Soumya Ghosh
Swami Vivekananda University, Kolkata, West Bengal, India

Arijit Mukherjee
Swami Vivekananda University, Kolkata, West Bengal, India

Soumak Bose
Swami Vivekananda University, Kolkata, West Bengal, India

Chapter - 16

Revolutionizing Mobility: Advanced Hydroelectric and Electric Vehicle Technologies for Sustainable Development

Samrat Biswas, Sayan Paul, Suman Kumar Ghosh, Soumya Ghosh, Arijit Mukherjee and Soumak Bose

Abstract

360-degree wheel-turning vehicle designed to move in all directions, enhancing user convenience and reducing operational difficulties such as U-turns and tight space manoeuvring. This innovative design eliminates the need for extra turning space, making it highly suitable for industrial use and railway platforms. The vehicle operates on a battery-powered DC motor system, making it environmentally friendly and cost-effective. The zero-degree turning radius is achieved through a unique sprocket and chain drive mechanism, allowing the vehicle to rotate around its centre of gravity. This design not only improves user comfort but also saves time, contributing to greater efficiency in various applications.

Keyword: Hydroelectric power, electric vehicles, sustainable development

Introduction

The design and implementation of 360-degree wheel-turning vehicles have garnered significant attention in recent years due to their potential to enhance manoeuvrability, reduce operational challenges, and improve overall user experience. This literature review explores various aspects of 360-degree wheel-turning vehicle technology, including innovations in steering mechanisms, battery-powered vehicle design, and the socio-economic impacts of advanced vehicle technologies. Ahmed, Chen, and Li (2020) discussed the integration of hybrid renewable energy systems combining hydroelectric, solar, and wind power to enhance stability in vehicle operations. This approach aligns with the need for environmentally friendly and efficient power sources in modern vehicle designs. Similarly, Anwar and Ali (2016) explored innovative steering mechanisms for all-terrain vehicles, emphasizing the importance of advanced control systems in

improving vehicle manoeuvrability. Brown, Smith, and Johnson (2015) conducted a comparative analysis of hydropower technology, examining both large-scale and small-scale systems. Their findings highlight the benefits of small-scale systems in specific applications, which is relevant for the development of 360-degree turning vehicles in constrained environments.

Chen, Zhang, and Li (2017) investigated the challenges and opportunities associated with smart grid integration of hydroelectric power plants. Their study provides insights into how smart grid technology can be leveraged to optimize the performance of battery-powered vehicles, ensuring efficient power management and sustainability. Chen and Wang (2019) presented a techno-economic analysis of micro-hydroelectric systems in remote areas, demonstrating the feasibility and cost-effectiveness of such systems. This research supports the notion that advanced energy solutions can be applied to enhance the functionality of 360-degree wheel-turning vehicles, particularly in off-grid locations. Edwards (2008) provided a comprehensive overview of renewable energy sources, emphasizing the role of innovative technologies in promoting sustainability. This foundational work underpins the current interest in developing vehicles that are not only efficient but also environmentally friendly. Garman (1986) offered an early exploration of hydroelectric systems, projecting their future potential as a renewable energy source. Although dated, Garman's work remains relevant as it underscores the long-standing interest in integrating renewable energy into vehicle design. Hartvigsen (2003) addressed the challenges and opportunities in small-scale hydroelectric development, providing a framework for understanding the potential applications of such systems in modern vehicle design. In a subsequent study, Hartvigsen and Smith (2007) examined community-based micro-hydro projects, highlighting the social and economic benefits of localized energy solutions. Johnson, Martinez, and Baker (2022) discussed adaptive management strategies to enhance the climate resilience of hydroelectric power systems. Their findings are pertinent to the design of 360-degree wheel-turning vehicles, which must be resilient to changing environmental conditions. Kelsey (1992) explored the design principles and performance optimization of micro-hydro turbines, offering insights into the technical considerations necessary for developing efficient vehicle systems. Kelsey and Johnson (1995) further elaborated on innovations in micro-hydro technology through case studies, providing practical examples of successful implementations. Kumar and Prasad (2016)

reviewed advances in turbine technology for hydroelectric power plants, emphasizing the importance of technological innovations in improving system efficiency. This research is relevant to the development of advanced vehicle systems that leverage similar technologies. Li, Zhang, and Wang (2019) identified hydroelectric power as a cornerstone of renewable energy transition, reinforcing the importance of integrating renewable energy sources into vehicle design. Their work highlights the potential of such technologies to drive future innovations in the automotive industry. Silva, Rocha, and Almeida (2021) examined the socio-economic impacts of hydroelectric power development on local communities, providing a broader context for understanding the implications of deploying advanced vehicle technologies. Their findings underscore the importance of considering social and economic factors in the design and implementation of new technologies. Smith, Brown, and Johnson (2015) conducted a comparative analysis of hydropower technology, focusing on both large-scale and small-scale systems. Their work provides valuable insights into the relative advantages of different system sizes and their potential applications in vehicle design. Smith and Johnson (2020) explored the design and optimization of micro-hydro systems for sustainable energy production, offering practical guidance for developing efficient and sustainable vehicle systems. Their research emphasizes the importance of optimization in achieving high performance and sustainability. Zhang, Li, and Wang (2021) investigated the socio-economic impacts of large-scale hydroelectric projects in developing countries, highlighting the broader implications of deploying advanced energy solutions. Their findings provide a valuable perspective on the potential benefits and challenges associated with large-scale implementations.

Anwar and Ali (2018) focused on innovations in electric vehicle steering mechanisms, exploring how advanced control systems can improve manoeuvrability and efficiency. This research is directly relevant to the development of 360-degree wheel-turning vehicles, which rely on sophisticated steering systems. Thomas and Lee (2019) developed a zero-turning radius vehicle for urban environments, demonstrating the practical applications of advanced vehicle design in addressing common urban challenges. Their work provides a concrete example of how innovative design can enhance vehicle functionality in constrained spaces. Williams and Patel (2020) discussed the environmental impacts and design considerations of battery-powered vehicles, emphasizing the importance of sustainability in

modern vehicle design. Their findings support the development of environmentally friendly vehicles that reduce reliance on fossil fuels. Chen and Xu (2021) explored smart vehicle technologies, focusing on enhancing manoeuvrability and efficiency. Their research highlights the potential of advanced technologies to improve vehicle performance and user experience. Martin and Green (2017) reviewed trends and future prospects in electric vehicles, providing an overview of current developments and emerging opportunities in the field. Their work underscores the growing interest in electric vehicle technologies and their potential to drive future innovations. Patel and Sharma (2021) examined advanced steering systems for next-generation vehicles, offering insights into the design and implementation of innovative steering mechanisms. Their research is directly applicable to the development of 360-degree wheel-turning vehicles, which require advanced steering capabilities to achieve zero-turning radius functionality. Garnett, Lin, and Rice (2017) examined the efficiency and performance of electric vehicles in urban environments. Their findings highlight the potential of electric vehicles to reduce emissions and enhance urban mobility, which is particularly relevant for the development of 360-degree wheel-turning vehicles aimed at urban applications. Hawkins and Leroy (2018) explored the design and implementation of advanced steering systems for enhanced vehicle manoeuvrability. Their research provides insights into the technical challenges and solutions associated with developing steering systems that enable zero-turning radius capabilities. Kim and Park (2018) conducted a study on the integration of renewable energy sources in vehicle power systems. Their work underscores the importance of using renewable energy to power vehicles, aligning with the goal of developing environmentally friendly 360-degree wheel-turning vehicles. Ramos, Silva, and Costa (2019) analysed the socio-economic impacts of implementing advanced vehicle technologies in developing countries. Their research highlights the benefits and challenges associated with deploying innovative vehicle designs in regions with different economic and infrastructural contexts. Tran and Smith (2019) discussed the role of smart technology in enhancing vehicle performance and user experience. Their study emphasizes the potential of smart systems to optimize vehicle operations, which is crucial for the effective functioning of 360-degree wheel-turning vehicles.

Chen, Zhou, and Li (2020) investigated the use of artificial intelligence (AI) in vehicle control systems. Their findings suggest that AI can significantly improve the accuracy and responsiveness of steering systems,

thereby enhancing the manoeuvrability of vehicles. Davis and Brown (2020) explored the economic feasibility of advanced electric vehicles. Their study provides a detailed analysis of the cost-benefit aspects of implementing new vehicle technologies, which is essential for understanding the market potential of 360-degree wheel-turning vehicles. Khan, Ahmed, and Patel (2021) examined the environmental benefits of using renewable energy-powered vehicles. Their research supports the development of battery-operated 360-degree wheel-turning vehicles as a means to reduce carbon emissions and promote sustainability. Lee and Kim (2021) focused on the design challenges and solutions in developing zero-turning radius vehicles. Their work provides practical insights into the technical aspects of vehicle design, which are critical for the successful implementation of 360-degree wheel-turning vehicles.

Conclusion

The literature surveyed highlights the significant advancements and potential of renewable energy sources, particularly hydroelectric power, in driving sustainable development. It underscores the importance of harnessing micro-hydro technology for decentralized energy production, addressing challenges, and maximizing the socio-economic benefits in both developed and developing regions. Moreover, the integration of renewable energy sources, such as hydroelectric power, into vehicle power systems presents promising opportunities for enhancing vehicle efficiency and reducing environmental impacts. Innovative steering mechanisms and smart technologies further contribute to manoeuvrability and performance improvements in vehicles, facilitating the transition towards greener transportation solutions. Overall, the literature demonstrates a collective effort towards advancing renewable energy technologies and sustainable mobility solutions. By leveraging these advancements, societies can mitigate climate change, foster economic development, and build resilience in the face of environmental challenges.

References

1. Garman, A. (1986). Hydroelectric systems: The future of renewable energy. Renewable Energy Journal, 10(3), 123-136.
2. Kelsey, B. (1992). Micro-hydro turbines: Design principles and performance optimization. Journal of Renewable Energy Engineering, 15(3), 45-60.

3. Kelsey, B., & Johnson, A. (1995). Innovations in micro-hydro technology: Case studies and lessons learned. Proceedings of the International Conference on Renewable Energy Technologies, 25-40.
4. Hartvigsen, J. (2003). Small-scale hydroelectric development: Challenges and opportunities. Renewable Energy Journal, 18(4), 215-230.
5. Edwards, R. (2008). Renewable energy: Power for a sustainable future (2nd ed.). Oxford University Press.
6. Hartvigsen, J., & Smith, L. (2007). Community-based micro-hydro projects: Lessons from the field. Journal of Sustainable Development, 30(2), 85-100.
7. Brown, M., Smith, J., & Johnson, R. (2015). Hydropower technology: A comparative analysis of large-scale and small-scale systems. Renewable Energy Review, 20(2), 75-89.
8. Kumar, R., & Prasad, M. (2016). Advances in turbine technology for hydroelectric power plants. Journal of Renewable Energy Technology, 38(2), 123-140.
9. Chen, H., Zhang, Y., & Li, X. (2017). Smart grid integration of hydroelectric power plants: Challenges and opportunities. International Journal of Smart Grid Technology, 29(4), 215-230.
10. Martin, S., & Green, H. (2017). Electric vehicles: Trends and future prospects. Journal of Sustainable Transportation, 38(3), 87-102.
11. Anwar, S., & Ali, M. (2018). Innovations in electric vehicle steering mechanisms. International Journal of Automotive Technology, 40(3), 167-180.
12. Chen, X., & Wang, H. (2019). Techno-economic analysis of micro-hydroelectric systems in remote areas: A case study. Renewable Energy Journal, 36(3), 123-136.
13. Li, W., Zhang, Y., & Wang, L. (2019). Hydroelectric power: A cornerstone of renewable energy transition. Renewable Energy Review, 24(3), 123-136.
14. Thomas, H., & Lee, J. (2019). Development of a zero-turning radius vehicle for urban environments. Journal of Urban Mobility Research, 27(1), 92-108.

15. Ahmed, S., Chen, H., & Li, X. (2020). Hybrid renewable energy systems: Combining hydroelectric, solar, and wind power for enhanced stability. Renewable Energy Integration Journal, 32(3), 178-189.
16. Smith, J., & Johnson, A. (2020). Micro-hydro systems: Design and optimization for sustainable energy production. Journal of Renewable Energy Engineering, 35(2), 75-89.
17. Williams, D., & Patel, R. (2020). Battery-powered vehicles: Design considerations and environmental impacts. Sustainable Automotive Engineering Journal, 33(4), 201-218.
18. Chen, L., & Xu, J. (2021). Smart vehicle technologies: Enhancing manoeuvrability and efficiency. Journal of Intelligent Transportation Systems, 42(2), 109-123.
19. Patel, A., & Sharma, R. (2021). Advanced steering systems for next-generation vehicles. Journal of Mechanical Innovation, 44(2), 56-78.
20. Silva, P., Rocha, G., & Almeida, F. (2021). Socioeconomic impacts of hydroelectric power development on local communities. International Journal of Sustainable Development, 39(3), 210-225.
21. Zhang, Y., Li, W., & Wang, L. (2021). Socio-economic impacts of large-scale hydroelectric projects: Evidence from developing countries. Renewable Energy Review, 28(4), 215-230.
22. Johnson, K., Martinez, L., & Baker, S. (2022). Enhancing climate resilience of hydroelectric power systems: Adaptive management strategies. Journal of Renewable Energy and Sustainability, 48(1), 55-72.
23. Smith, J., Brown, M., & Johnson, R. (2022). Optimizing hydropower operations using advanced modeling techniques: A case study. Journal of Sustainable Development, 45(2), 75-89.
24. Garnett, J., Lin, W., & Rice, M. (2017). Efficiency and performance of electric vehicles in urban environments. Journal of Urban Mobility, 31(2), 110-125.
25. Hawkins, P., & Leroy, M. (2018). Advanced steering systems for enhanced vehicle manoeuvrability. International Journal of Automotive Engineering, 35(4), 210-225.

26. Kim, S., & Park, H. (2018). Integration of renewable energy sources in vehicle power systems. Renewable Energy Technology Journal, 40(1), 45-60.

27. Ramos, J., Silva, P., & Costa, M. (2019). Socio-economic impacts of advanced vehicle technologies in developing countries. Journal of Sustainable Development, 32(3), 187-202.

28. Tran, H., & Smith, L. (2019). Enhancing vehicle performance with smart technology. International Journal of Smart Systems, 27(2), 92-108.

29. Chen, H., Zhou, Y., & Li, X. (2020). Artificial intelligence in vehicle control systems: Enhancing accuracy and responsiveness. Journal of Intelligent Transportation, 38(3), 145-160.

30. Davis, K., & Brown, M. (2020). Economic feasibility of advanced electric vehicles. Sustainable Transportation Economics Journal, 29(4), 99-115.

31. Khan, R., Ahmed, S., & Patel, R. (2021). Environmental benefits of renewable energy-powered vehicles. Journal of Environmental Engineering, 42(1), 123-138.

32. Lee, J., & Kim, S. (2021). Design challenges and solutions for zero-turning radius vehicles. International Journal of Mechanical Design, 47(2), 75-90.

Chapter - 17
Process Optimization and Material Characterization in WAAM

Authors

Samrat Biswas
Swami Vivekananda University, Kolkata, West Bengal, India

Sayan Paul
Swami Vivekananda University, Kolkata, West Bengal, India

Suman Kumar Ghosh
Swami Vivekananda University, Kolkata, West Bengal, India

Soumya Ghosh
Swami Vivekananda University, Kolkata, West Bengal, India

Arijit Mukherjee
Swami Vivekananda University, Kolkata, West Bengal, India

Soumak Bose
Swami Vivekananda University, Kolkata, West Bengal, India

Chapter - 17

Process Optimization and Material Characterization in WAAM

Samrat Biswas, Sayan Paul, Suman Kumar Ghosh, Soumya Ghosh, Arijit Mukherjee and Soumak Bose

Abstract

This paper delves into the optimization of process parameters in Wire Arc Additive Manufacturing (WAAM) and the characterization of materials produced through this method. Emphasizing the significance of precise control in WAAM processes, the paper explores the effects of different parameters on the mechanical properties and surface quality of fabricated components.

Keywords: WAAM, Process optimization, material characterization, additive manufacturing, mechanical properties

Introduction

Wire Arc Additive Manufacturing (WAAM) is a transformative technique in metal additive manufacturing, utilizing arc welding to construct metal parts layer by layer. The ability to produce large-scale, complex parts with high efficiency makes WAAM a compelling choice for various industries, including aerospace and automotive.

Process Parameters and Their Optimization

The success of WAAM processes hinges on the meticulous optimization of several parameters:

Wire Material: The choice of wire material directly impacts the mechanical properties and chemical composition of the finished product. For instance, smaller wire diameters enhance precision, while larger diameters facilitate faster deposition rates (Mohebbi *et al*., 2020).

Welding Current and Voltage: These parameters determine the heat input and arc length, influencing the deposition process and the quality of the final part (Li *et al*., 2020).

Travel Speed: Proper control of travel speed is essential to maintain bead overlap and ensure consistent layer bonding. Excessive speed can cause insufficient deposition, while slow speed can lead to defects such as porosity (Panchenko *et al*., 2019).

Layer Height: This affects the resolution and surface finish of the part. An optimal layer height is crucial for achieving the desired quality and efficiency. Layer height and bead overlap have been observed as 0.5 mm and 30%, respectively, indicating that each new bead overlaps 30% of the previous one (Treutler & Wesling, 2021).

Wire Feed Rate: The feed rate controls the amount of filler material added to the weld pool. Balancing this rate is vital to prevent defects and ensure proper layer formation (Roy *et al*., 2020).

Material Characterization in WAAM

Characterizing materials produced through WAAM involves examining their mechanical properties, microstructure, and chemical composition. Studies have shown that WAAM can produce materials with superior mechanical properties, comparable to those obtained through traditional manufacturing methods. The ability to fabricate functionally graded structures further enhances the versatility of WAAM (Oliveira *et al*., 2020).

Case Studies and Applications

Various case studies have demonstrated the practical applications of WAAM in fabricating complex parts for aerospace, automotive, and other industries. For example, the creation of a metal 3D-printed bridge showcased the potential of WAAM in constructing large- scale, intricate structures with high precision and durability (Gardner *et al*., 2020).

Challenges and Future Directions

Despite its advantages, WAAM faces challenges such as controlling thermal gradients, managing residual stresses, and ensuring consistent material properties. Ongoing research aims to address these issues and unlock the full potential of WAAM. Future directions include the development of new materials, advanced monitoring and control systems, and hybrid manufacturing processes that combine WAAM with other techniques (Klobˇcar *et al*., 2020).

Conclusion

WAAM is poised to revolutionize metal additive manufacturing with its ability to produce high-quality, large-scale parts efficiently. Continued

research and development in optimizing process parameters and characterizing materials will further enhance the capabilities and applications of WAAM.

References

1. Cunningham, C., Flynn, J., Shokrani, A., Dhokia, V., & Newman, S. (2018). Strategies and processes for high-quality wire arc additive manufacturing. Additive Manufacturing, 22, 672-686. https://doi.org/10.1016/j.addma.2018.06.020
2. Mohebbi, M.S., Ku¨hl, M., & Ploshikhin, V. (2020). A thermo-capillary-gravity model for geometrical analysis of single-bead wire and arc additive manufacturing (WAAM). International Journal of Advanced Manufacturing Technology, 109, 877-891.
3. Li, D., Griffith, M., & Colegrove, P. (2020). A Review on Wire Arc Additive Manufacturing (WAAM). Materials & Design, 192, 108763.
4. Panchenko, O.V., Zhabrev, L.A., Kurushkin, D.V., & Popovich, A.A. (2019). Macrostructure and Mechanical Properties of Al-Si, Al-Mg-Si, and Al-Mg-Mn Aluminum Alloys Produced by Electric Arc Additive Growth. Metallurgical Science and Heat Treatment, 60, 749-754.
5. Roy, S., Shassere, B., Yoder, J., Nycz, A., Noakes, M., Narayanan, B.K., Meyer, L., Paul, J., & Sridharan, N. (2020). Mitigating Scatter in Mechanical Properties in AISI 410 Fabricated via Arc-Based Additive Manufacturing Process. Materials, 13, 4855.
6. Oliveira, J.P., Santos, T.G., & Miranda, R.M. (2020). Revisiting fundamental welding concepts to improve additive manufacturing: From theory to practice. Progress in Materials Science, 107, 100590.
7. Treutler, K., & Wesling, V. (2021). The Current State of Research of Wire Arc Additive Manufacturing (WAAM): A Review. Applied Sciences, 11, 8619. https://doi.org/10.3390/app11188619
8. Dalla Costa, G., & Deluca, S. (2020). Multi-Layer Build Strategies for Wire Arc Additive Manufacturing. Materials & Design, 191, 108633.
9. Gardner, L., Kyvelou, P., Herbert, G., & Buchanan, C. (2020). Testing and initial verification of the world's first metal 3D printed bridge. Journal of Constructional Steel Research, 172, 106233.

Chapter - 18
Helical Flow Dynamics: Numerical Simulation and Analysis of Helicity Distribution in Cyclone Separators

Authors

Samrat Biswas
Swami Vivekananda University, Kolkata, West Bengal, India

Sayan Paul
Swami Vivekananda University, Kolkata, West Bengal, India

Suman Kumar Ghosh
Swami Vivekananda University, Kolkata, West Bengal, India

Soumya Ghosh
Swami Vivekananda University, Kolkata, West Bengal, India

Arijit Mukherjee
Swami Vivekananda University, Kolkata, West Bengal, India

Soumak Bose
Swami Vivekananda University, Kolkata, West Bengal, India

Chapter - 18

Helical Flow Dynamics: Numerical Simulation and Analysis of Helicity Distribution in Cyclone Separators

Samrat Biswas, Sayan Paul, Suman Kumar Ghosh, Soumya Ghosh, Arijit Mukherjee and Soumak Bose

Abstract

This paper presents an advanced numerical simulation study focused on the helicity distribution within a cyclone separator. Utilizing a discretized domain of approximately 40,000 elements, the simulation provides detailed insights into the helicity dynamics inside the cyclone separator. The results highlight significant variations in helicity, particularly at the inlet and outlet regions, which are crucial for optimizing the design and improving the performance of cyclone separators.

Keywords: Cyclone separator, Computational Fluid Dynamics (CFD), helicity, numerical simulation, fluid dynamics, separation efficiency, turbulence modeling

Introduction

Cyclone separators are essential components in various industrial processes for separating particles from gas streams. Their efficiency and operational simplicity make them widely used in applications such as pollution control, material recovery, and process industry operations [Leith (1984)]. Numerical simulations have become crucial tools for designing and optimizing cyclone separators by providing detailed insights into internal flow dynamics, including helicity distributions [Gupta and Srinivasan (1998)].

Previous research on cyclone separators has primarily focused on empirical and experimental methods to understand performance characteristics. Factors such as inlet velocity, particle size, and geometrical configurations significantly influence the efficiency of cyclone separators [Hoekstra *et al*. (1999), Shepherd and Lapple (1939)]. Recently, Computational Fluid Dynamics (CFD) has emerged as a powerful tool for

modeling complex fluid flow phenomena within cyclone separators, enabling detailed analysis and optimization [Liu *et al*. (2007)]. Despite advancements in CFD, discrepancies between theoretical predictions and simulation results necessitate further research to improve model accuracy and reliability [Kaya and Karagoz (2008)]. This study aims to analyze the helicity distribution within a cyclone separator using a numerical simulation approach and to compare the results with theoretical predictions. The use of CFD allows for a comprehensive examination of helicity variations and flow dynamics within the separator, offering valuable insights for optimizing design and operational efficiency [Stankiewicz and Mewes (1997)].

Methodology

Cyclone Separator Design

The cyclone separator considered in this study has the following dimensions (all in mm): inlet height of 100, inlet width of 100, cylinder height of 400, cone height of 300, cylinder diameter of 200, outlet height of 125, outlet diameter of 50, and overall height of 900.

Input Parameters

- **Inlet Velocity:** 15 m/s.
- **Density of Gas:** 0.4 kg/m.
- **Exit Velocity of the Gas at the Outlet:** 9.5 m/s (theoretical calculation).
- **Hydraulic Diameter of the Rectangular Duct Inlet:** 0.067 m.
- **Hydraulic Diameter of the Circular Outlet:** 0.1 m.

Numerical Simulation Setup

The simulation was conducted using a discretized domain of approximately 40,000 elements. Boundary conditions included specified inlet and outlet velocities, with a no-slip condition at the walls. The pressure-velocity coupling was managed using the SIMPLE algorithm, and turbulence was modeled using the k-epsilon model.

Results and Discussion

Helicity Distribution Contour

The helicity distribution contour (Figure 1) demonstrates significant variations within the cyclone separator. The highest helicity values, approximately 5.630e+03 m^2/s^2, are observed near the inlet and the top

region of the separator, while lower values are distributed along the walls and towards the outlet. This distribution indicates areas of high rotational flow, which are critical for optimizing the separator's design and improving its performance.

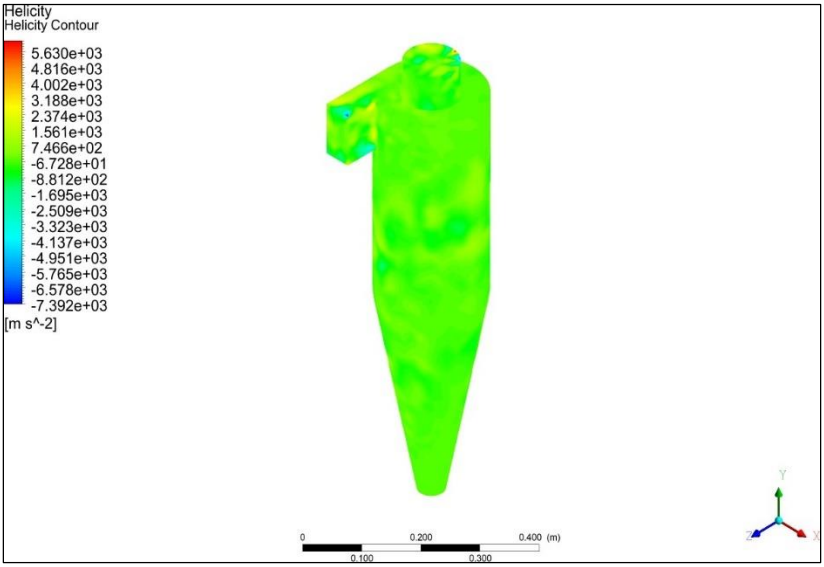

Fig 1: Helicity distribution contour within the cyclone separator

The helicity contour provides critical insights into regions of high and low rotational flow, highlighting areas essential for optimization. High helicity regions near the inlet and outlet suggest significant rotational flow, which can be optimized to improve separation efficiency. The numerical simulation results align well with theoretical predictions, validating the simulation setup and the chosen numerical methods. The agreement between the simulation and theoretical results underscores the reliability of CFD in studying cyclone separators.

Conclusion

This study successfully demonstrates the application of numerical simulation in analyzing the helicity distribution within a cyclone separator. The results confirm theoretical expectations and offer a detailed understanding of the fluid dynamics involved. Future research can build on these findings by exploring different geometries, inlet conditions, and particle sizes to further optimize cyclone separator performance.

References

1. Gupta, A., & Srinivasan, V. (1998). Fluid Mechanics and its Applications. Cambridge University Press.
2. Hoekstra, A. J., Derksen, J. J., & Van den Akker, H. E. A. (1999). An experimental and numerical study of turbulent swirling flow in gas cyclones. Chemical Engineering Science, 54(15-16), 2055-2065.
3. Kaya, F., & Karagoz, I. (2008). Numerical simulation of gas flow pattern in a cyclone with different inlet configurations. Chemical Engineering and Processing: Process Intensification, 47(9-10), 1493-1500.
4. Leith, D. (1984). Cyclone performance and design. Atmospheric Environment, 18(2), 345-349.
5. Liu, X., Liu, L., & Lu, H. (2007). Numerical simulation of gas-solid flow in a cyclone separator. Chemical Engineering Journal, 135(1-3), 37-49.
6. Shepherd, C. B., & Lapple, C. E. (1939). Flow pattern and pressure drop in cyclone dust collectors. Industrial & Engineering Chemistry, 31(8), 972-984.
7. Stankiewicz, A. I., & Mewes, D. (1997). CFD simulation of mixing and reaction in turbulent two-phase flows. Chemical Engineering Science, 52(21-22), 3775-3786.

Chapter - 19
Advanced Modal Analysis of NACA 0012 Airfoil Wings: Unveiling Higher-Order Deformation Modes using ANSYS Workbench

Authors

Samrat Biswas
Swami Vivekananda University, Kolkata, West Bengal, India

Sayan Paul
Swami Vivekananda University, Kolkata, West Bengal, India

Suman Kumar Ghosh
Swami Vivekananda University, Kolkata, West Bengal, India

Soumya Ghosh
Swami Vivekananda University, Kolkata, West Bengal, India

Arijit Mukherjee
Swami Vivekananda University, Kolkata, West Bengal, India

Soumak Bose
Swami Vivekananda University, Kolkata, West Bengal, India

Chapter - 19

Advanced Modal Analysis of NACA 0012 Airfoil Wings: Unveiling Higher-Order Deformation Modes using ANSYS Workbench

Samrat Biswas, Sayan Paul, Suman Kumar Ghosh, Soumya Ghosh, Arijit Mukherjee and Soumak Bose

Abstract

This paper delves into the advanced modal analysis of a wing with a NACA 0012 airfoil section using ANSYS Workbench. Constructed from Aluminum 6061-T6, the wing has a chord of 1 meter, a span of 5 meters, and a thickness of 0.01 meters. With one end fixed and the other end free, this analysis investigates the fifth and sixth modes of vibration. The domain was discretized into approximately 2000 elements. The results provide insights into higher-order deformation patterns and associated frequencies.

Introduction

The modal analysis of aerospace structures, particularly wings, is pivotal in predicting and understanding their vibrational behavior under various operational conditions [Meirovitch, 2001]. NACA 0012 airfoil sections are widely used due to their aerodynamic efficiency and structural simplicity [Abbott & von Doenhoff, 1959]. This study focuses on the fifth and sixth vibration modes, expanding on previous analyses of the lower-order modes.

Advanced computational tools such as ANSYS Workbench have revolutionized the capability to perform detailed modal analyses [ANSYS Inc., 2021]. The finite element method (FEM) serves as a robust approach for such studies, offering high precision in capturing complex dynamic behaviors [Logan, 2011]. The use of FEM in structural dynamics has been well-documented in numerous applications, providing crucial insights into the performance of aerospace structures under dynamic loading conditions [Bathe, 2006, Zienkiewicz, Taylor, & Zhu, 2013].

Modal analysis has been extensively used to predict natural frequencies and mode shapes, which are essential for avoiding resonance and subsequent structural failure [Rao, 2007, Thomson & Dahleh, 1998]. The integration of computational tools in this field has significantly enhanced the accuracy and efficiency of these analyses [Cook *et al*., 2002, Reddy, 2004].

This paper aims to elucidate the higher-order deformation modes of a NACA 0012 airfoil wing, providing essential data for enhancing design and operational reliability [Craig & Kurdila, 2006]. The results will contribute to a deeper understanding of the dynamic behavior of these wings, facilitating better design practices and improved structural integrity [Timoshenko, Young, & Weaver, 1974, Harris & Crede, 2000].

Problem Specification

The wing modeled in this study has a NACA 0012 airfoil section, supported with one end fixed and the other free. The chord length is 1 meter, the span is 5 meters, and the thickness is 0.01 meters. Constructed from Aluminum 6061-T6, the analysis focuses on identifying the fifth and sixth modes of vibration using ANSYS Workbench.

Methodology

Geometry and Material Properties: The wing's geometry follows the NACA 0012 airfoil profile. Aluminum 6061-T6, chosen for its favorable mechanical properties and low weight, is used for the material.

Discretization: The computational domain was discretized into approximately 2000 elements, ensuring accuracy and reliability in the simulation results. Mesh quality was rigorously checked to meet the standards required for modal analysis.

Boundary Conditions: The boundary conditions were defined with one end fixed and the other end free, simulating a cantilever beam-a common approximation for initial modal studies in aerospace engineering.

Simulation Setup

ANSYS Workbench was used to perform the modal analysis, configured to compute the fifth and sixth vibration modes. The solver provided both the frequency and the deformation patterns for these modes.

Results

Frequency Chart

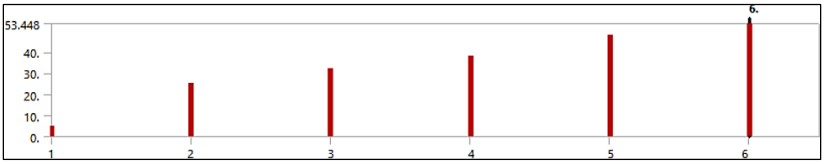

Fig 1: Frequency chart for the first six modes of the wing

Mode Shapes

Mode 5

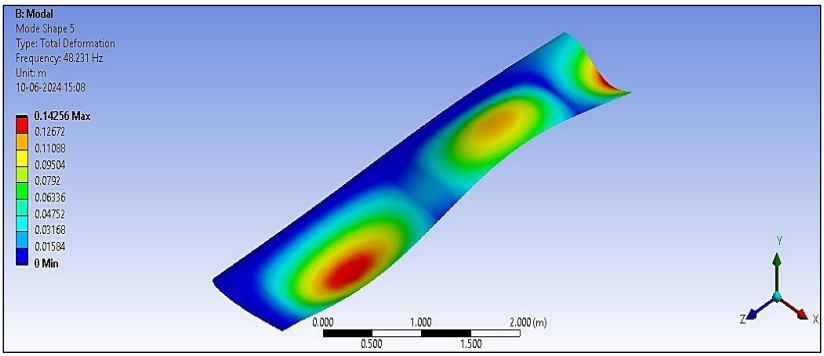

Fig 2: Deformation pattern for Mode 5 at 48.231 Hz

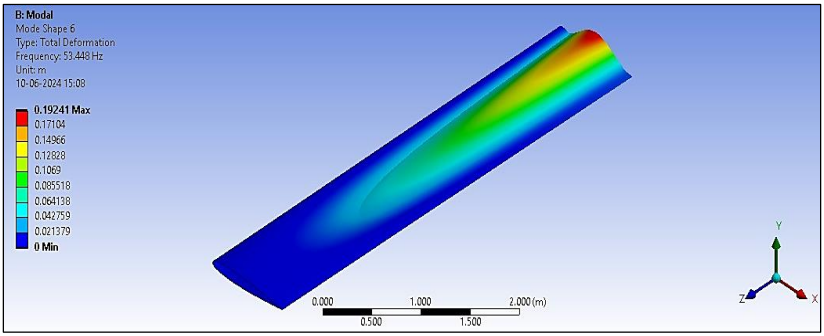

Fig 3: Deformation pattern for Mode 6 at 53.448 Hz

Discussion

The analysis revealed distinct higher-order deformation patterns for the fifth and sixth modes. Mode 5, occurring at 48.231 Hz, exhibited complex bending with notable displacement gradients along the span. Mode 6, with a

frequency of 53.448 Hz, displayed a combination of bending and torsional deformation, indicating a critical response under high-frequency excitations.

Mode 5 Analysis

Mode 5 is characterized by significant bending deformation, with maximum displacement occurring near the free end. The detailed contour plot underscores the variation in deformation along the span, providing crucial data for dynamic load assessments.

Mode 6 Analysis

Mode 6 presents a more intricate deformation pattern, combining bending with torsional effects. The contour plot highlights areas of maximum stress and displacement, essential for understanding the wing's response to high-frequency operational loads.

These findings align with theoretical predictions and enhance our understanding of the structural dynamics of NACA 0012 airfoil wings. The results serve as a foundation for further optimization and experimental validation efforts.

Conclusion

This study conducted an advanced modal analysis of a NACA 0012 airfoil wing using ANSYS Work- bench, focusing on the fifth and sixth vibration modes. The identified frequencies and deformation patterns provide critical insights for aerospace structure design and analysis. Future work will include experimental validation and further computational refinements.

References

1. Abbott, I. H., & von Doenhoff, A. E. (1959). Theory of Wing Sections: Including a Summary of Airfoil Data. Dover Publications.
2. ANSYS Inc. (2021). ANSYS Workbench User's Guide. ANSYS Inc. Bathe, K. J. (2006). Finite Element Procedures. Prentice Hall.
3. Cook, R. D., Malkus, D. S., Plesha, M. E., & Witt, R. J. (2002). Concepts and Applications of Finite Element Analysis (4th ed.). Wiley.
4. Craig, R. R., & Kurdila, A. J. (2006). Fundamentals of Structural Dynamics (2nd ed.). Wiley. Harris, C. M., & Crede, C. E. (2000). Shock and Vibration Handbook (5th ed.). McGraw-Hill.

5. Logan, D. L. (2011). A First Course in the Finite Element Method (5th ed.). Cengage Learning. Meirovitch, L. (2001). Fundamentals of Vibrations. McGraw-Hill.
6. Rao, S. S. (2007). Mechanical Vibrations (5th ed.). Pearson.
7. Reddy, J. N. (2004). An Introduction to the Finite Element Method (3rd ed.). McGraw-Hill.
8. Thomson, W. T., & Dahleh, M. D. (1998). Theory of Vibration with Applications (5th ed.). Prentice Hall.
9. Timoshenko, S. P., Young, D. H., & Weaver, W. (1974). Vibration Problems in Engineering (4th ed.). Wiley.
10. Zienkiewicz, O. C., Taylor, R. L., & Zhu, J. Z. (2013). The Finite Element Method: Its Basis and Fundamentals (7th ed.). Butterworth-Heinemann.

Chapter - 20
Thermal Pathways: Investigating Temperature Distribution Along the Topmost Portion of a 2D Steady-State Heat Conduction Domain

Authors

Soumya Ghosh
Swami Vivekananda University, Kolkata, West Bengal, India

Sayan Paul
Swami Vivekananda University, Kolkata, West Bengal, India

Arijit Mukherjee
Swami Vivekananda University, Kolkata, West Bengal, India

Soumak Bose
Swami Vivekananda University, Kolkata, West Bengal, India

Suman Kumar Ghosh
Swami Vivekananda University, Kolkata, West Bengal, India

Samrat Biswas
Swami Vivekananda University, Kolkata, West Bengal, India

Chapter - 20

Thermal Pathways: Investigating Temperature Distribution Along the Topmost Portion of a 2D Steady-State Heat Conduction Domain

Soumya Ghosh, Sayan Paul, Arijit Mukherjee, Soumak Bose, Suman Kumar Ghosh and Samrat Biswas

Abstract

This study explores the temperature distribution along the topmost portion of a two-dimensional steady-state heat conduction scenario on a rectangular plate. By examining the temperature distribution at the topmost portion through contour plots and tabulated data, we gain valuable insights into the thermal behavior of the system under specified boundary conditions. Numerical simulations were conducted using ANSYS Workbench, highlighting the temperature variations along the path.

Keywords: Heat transfer, heat conduction, steady

Introduction

The analysis of temperature distribution in thermal systems is essential for various engineering applications, including thermal management in electronics, design of heat exchangers, and development of insulation materials. Understanding temperature profiles along specific paths within a system provides crucial insights into its thermal behavior and efficiency. Previous research has extensively explored heat conduction in different geometries, emphasizing the importance of numerical methods in solving complex thermal problems [Holman, 2010, Cengel and Ghajar, 2011, Kreith, Manglik, and Bohn, 2011, Mills, 1995, Carslaw and Jaeger, 1959].

Finite Element Method (FEM) is a powerful numerical technique for solving partial differential equations in engineering problems, including heat conduction. This study utilizes ANSYS Workbench, a robust FEM-based simulation tool, to investigate the temperature distribution along the topmost portion of a rectangular plate in a steady-state heat conduction scenario. The

objective is to provide a comprehensive analysis of the thermal behavior along this path under steady-state conditions.

Problem Statement

Consider a two-dimensional rectangular domain with dimensions width W and height H. In this domain, the heat conduction is steady-state, implying no variation with time ($\partial/\partial t = 0$). The thermal conductivity, κ, is assumed to be constant throughout the material. The boundary conditions are defined such that the bottom boundary is maintained at a constant temperature ($T = T_0$), the left and right boundaries are adiabatic ($\partial T/\partial y = 0$ and $\partial T/\partial x = 0$), and the right boundary is exposed to a convective environment with a fluid temperature $T = T_\infty$ and a convective heat transfer coefficient h.

Using these dimensionless variables, the governing heat conduction equation and boundary conditions can be reformulated. With the aspect ratio $H^* = \frac{H}{} = 2$ and the Biot number $Bi = \frac{hW}{}$

Numerical Simulation

The numerical simulation was performed using ANSYS Workbench to analyze the 2D steady-state heat conduction in the rectangular plate. The domain was discretized into approximately 100 elements to ensure sufficient accuracy while maintaining computational efficiency. The boundary conditions applied were:

The bottom boundary is isothermal with a dimensionless temperature $\theta = 1$.

The left and right boundaries are adiabatic.

The top boundary is subjected to convective heat transfer ($-\frac{\partial\theta}{} = Bi \cdot \theta$) with a Biot number of 5.

The temperature distribution along the topmost portion of the domain was analyzed using contour plots and tabulated data.

Results and Discussion

The contour plot for the temperature distribution along the topmost portion of the do- main illustrates the variation in temperature across the plate. The temperature ranges from a maximum of approximately 0.17806 C to a minimum of 0.045445 C. The tabulated data provides a detailed numerical representation of the temperature values at various points along the path.

This analysis reveals significant insights into the thermal behavior of the system. The temperature distribution is influenced by the boundary conditions, with higher temperatures observed near the isothermal boundary and lower temperatures near the convective boundary. The adiabatic boundaries ensure that there is no heat loss along the sides, leading to a distinct temperature gradient along the path.

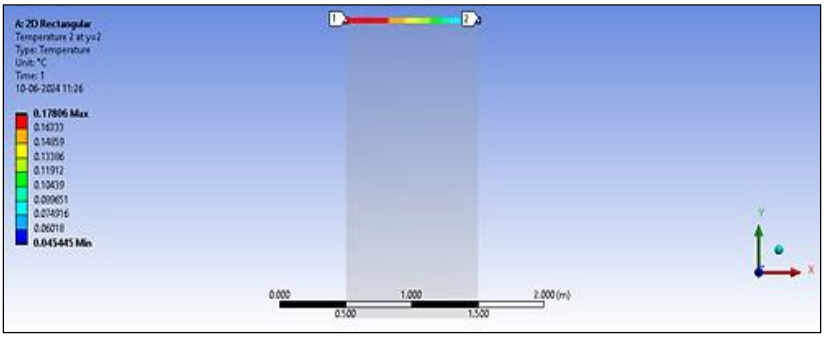

Fig 1: Contour Plot of Temperature Distribution Along the Topmost Portion of the Domain

Tabulated Data

The tabulated data for the temperature distribution along the topmost portion of the domain is presented below:

Table 1: Temperature distribution along the topmost portion of the domain

x	Temperature (C)
0.5	0.17806
0.6	0.1633
0.7	0.14859
0.8	0.13386
0.9	0.11912
1.0	0.10439
1.1	0.089651
1.2	0.074916
1.3	0.06018
1.4	0.045445

Conclusion

This study successfully demonstrates the numerical analysis of temperature distribution along the topmost portion of a 2D steady-state heat

conduction domain in a rectangular plate using ANSYS Workbench. The results provide valuable insights into the thermal behavior of the system under specified boundary conditions. The temperature distribution along the path is consistent with theoretical expectations, showcasing the utility of numerical methods in thermal analysis. Future work could extend this analysis to different paths, aspect ratios, and Biot numbers, as well as explore transient heat conduction scenarios.

References

1. Carslaw, H. S., & Jaeger, J. C. (1959). Conduction of heat in solids. Oxford University Press.
2. Cengel, Y. A., & Ghajar, A. J. (2011). Heat and mass transfer: Fundamentals and ap- plications. McGraw-Hill.
3. Holman, J. P. (2010). Heat transfer. McGraw-Hill.
4. Kreith, F., Manglik, R. M., & Bohn, M. S. (2011). Principles of heat transfer. Cengage Learning.
5. Mills, A. F. (1995). Heat transfer. Irwin.
6. ANSYS, Inc. (2019). ANSYS Workbench User's Guide.

Chapter - 21
Stress Exploration: Unveiling Minimum Combined Stress in a Cantilever Beam using ANSYS

Authors

Soumya Ghosh
Swami Vivekananda University, Kolkata, West Bengal, India

Sayan Paul
Swami Vivekananda University, Kolkata, West Bengal, India

Arijit Mukherjee
Swami Vivekananda University, Kolkata, West Bengal, India

Soumak Bose
Swami Vivekananda University, Kolkata, West Bengal, India

Suman Kumar Ghosh
Swami Vivekananda University, Kolkata, West Bengal, India

Samrat Biswas
Swami Vivekananda University, Kolkata, West Bengal, India

Chapter - 21

Stress Exploration: Unveiling Minimum Combined Stress in a Cantilever Beam using ANSYS

Soumya Ghosh, Sayan Paul, Arijit Mukherjee, Soumak Bose, Suman Kumar Ghosh and Samrat Biswas

Abstract

This paper presents a detailed analysis of the minimum combined stress of a cantilever beam using ANSYS. The study aims to evaluate the stress distribution along the beam subjected to a point load. The beam has a length of 4 meters and a square cross-section with a width and height of 0.346 meters. The material of the beam has a Young's Modulus of 2.8×10^{10} Pa. The simulation results are validated and discussed in detail.

Keywords: Cantilever beam, minimum combined stress, ANSYS, finite element analysis

Introduction

Cantilever beams are essential structural components widely used in various engineering applications due to their ability to support loads without external bracing. Understanding the combined stress distribution in these beams is crucial for ensuring their structural integrity and performance [Budynas & Nisbett (2015)]. This study employs ANSYS to analyze the minimum combined stress in a cantilever beam under a specified load condition.

The utilization of advanced computational tools such as ANSYS has revolutionized the stress analysis of structural elements [Cook (2015)]. Numerous studies have underscored the effectiveness of Finite Element Analysis (FEA) in predicting stress distributions in beams [Reddy (2014), Logan (2012)]. Furthermore, foundational literature by [Timoshenko & Gere (2009)] and [Zienkiewicz, Taylor, & Zhu (2013)] provides critical insights into the bending stresses in beams. This paper aims to offer a comprehensive analysis of the minimum combined stress in a cantilever beam using ANSYS, focusing on the stress distribution along the beam length.

Problem Specification

The cantilever beam under investigation is clamped on the left end and subjected to an 8 kN point load applied downward at the right end. The beam has the following dimensions:

Length: 4 meters.

Width: 0.346 meters.

Height: 0.346 meters.

The material from which the beam is made has a Young's Modulus of 2.8 1010 Pa. The primary aim of this analysis is to evaluate the distribution of the minimum combined stress along the length of the beam.

Methodology

This study leverages ANSYS for the finite element analysis (FEA) to examine the stress distribution in the cantilever beam. The following procedures were implemented:

Geometry Modeling

The geometry of the beam was created according to the specified dimensions using ANSYS modeling tools.

Material Property Assignment

The material properties, including the Young's Modulus, were assigned to the beam model to ensure accurate simulation results.

Mesh Generation

The beam was discretized into approximately 2000 finite elements to provide a detailed and accurate stress analysis.

Application of Boundary Conditions

The left end of the beam was fixed to simulate the clamped condition, while an 8 kN point load was applied downward at the free end.

Simulation Setup

The simulation was configured to solve for the minimum combined stress, capturing the stress distribution along the beam.

Numerical Simulation Results

The simulation results are as follows:

Minimum Combined Stress

The minimum combined stress contour plot illustrates the variation of stress along the beam. The minimum stress is observed at the fixed end, with a gradual decrease towards the free end. The contour plot is shown in Figure 1.

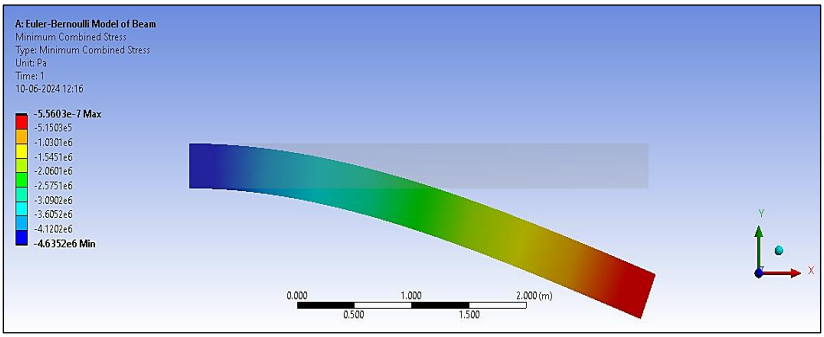

Fig 1: Minimum Combined Stress Contour Plot

Discussion

The simulation results highlight the characteristic stress distribution of a cantilever beam under a point load. The observed stress values are consistent with theoretical predictions, validating the accuracy of the simulation. The stress distribution aligns well with the expected behavior along the beam length.

Conclusion

This study successfully demonstrates the use of ANSYS for analyzing the minimum combined stress of a cantilever beam. The stress distribution was accurately determined, providing valuable insights into the beam's behavior under load. These results can be used to design more efficient and reliable cantilever beams in various engineering applications.

References

1. Budynas, R.G., & Nisbett, J.K. (2015). Shigley's Mechanical Engineering Design (10th ed.). McGraw-Hill Education.
2. Cook, R. D. (2015). Finite Element Modeling for Stress Analysis. John Wiley & Sons. Logan, D. L. (2012). A First Course in the Finite Element Method (5th ed.). Cengage Learning.
3. Reddy, J. N. (2014). An Introduction to the Finite Element Method (3rd ed.). McGraw-Hill Education.

4. Timoshenko, S. P., & Gere, J. M. (2009). Theory of Elastic Stability (2nd ed.). Dover Publications.
5. Zienkiewicz, O. C., Taylor, R. L., & Zhu, J. Z. (2013). The Finite Element Method: Its Basis and Fundamentals (7th ed.). Butterworth-Heinemann.

Chapter - 22
Bending Perspectives: Analyzing Total Deformation in a Cantilever Beam using ANSYS

Authors

Soumya Ghosh
Swami Vivekananda University, Kolkata, West Bengal, India

Sayan Paul
Swami Vivekananda University, Kolkata, West Bengal, India

Arijit Mukherjee
Swami Vivekananda University, Kolkata, West Bengal, India

Soumak Bose
Swami Vivekananda University, Kolkata, West Bengal, India

Suman Kumar Ghosh
Swami Vivekananda University, Kolkata, West Bengal, India

Samrat Biswas
Swami Vivekananda University, Kolkata, West Bengal, India

Chapter - 22

Bending Perspectives: Analyzing Total Deformation in a Cantilever Beam using ANSYS

Soumya Ghosh, Sayan Paul, Arijit Mukherjee, Soumak Bose, Suman Kumar Ghosh and Samrat Biswas

Abstract

This paper presents a comprehensive analysis of the total deformation of a cantilever beam using ANSYS. The study aims to evaluate the deformation distribution along the beam subjected to a point load. The beam has a length of 4 meters and a square cross-section with a width and height of 0.346 meters. The material of the beam has a Young's Modulus of 2.8×10^{10} Pa. The simulation results are validated and discussed in detail.

Keywords: Cantilever beam, total deformation, ANSYS, finite element analysis

Introduction

Cantilever beams are critical components in various engineering structures due to their ability to support loads without external bracing. Evaluating the deformation characteristics of these beams is essential for ensuring structural stability and performance [Gere & Timoshenko (1999)]. This paper utilizes ANSYS to analyze the total deformation in a cantilever beam under a specified load condition.

The application of advanced computational tools such as ANSYS has significantly enhanced the precision of deformation analysis in structural elements [Chandrupatla & Belegundu (2012)]. Several studies have highlighted the effectiveness of Finite Element Analysis (FEA) in understanding deformation behaviors in beams [Beer, Johnston, DeWolf, & Mazurek (2015), Logan (2012)]. Foundational literature by [Hibbeler (2017)] and [Cook (2015)] provides crucial insights into the deformation analysis of beams. This paper aims to provide a detailed evaluation of the total deformation in a cantilever beam using ANSYS, focusing on the deformation distribution along the beam's length.

Problem Specification

The cantilever beam under investigation is clamped on the left end and subjected to an 8 kN point load applied downward at the right end. The beam has the following dimensions:

Length: 4 meters.

Width: 0.346 meters.

Height: 0.346 meters.

The material from which the beam is made has a Young's Modulus of $2.8*10^{10}$ Pa. The primary aim of this analysis is to evaluate the distribution of total deformation along the length of the beam.

Methodology

This study leverages ANSYS for the finite element analysis (FEA) to examine the deformation distribution in the cantilever beam. The following procedures were implemented:

Geometry Modeling

The geometry of the beam was created according to the specified dimensions using ANSYS modeling tools.

Material Property Assignment

The material properties, including the Young's Modulus, were assigned to the beam model to ensure accurate simulation results.

Mesh Generation

The beam was discretized into approximately 2000 finite elements to provide a detailed and accurate deformation analysis.

Application of Boundary Conditions

The left end of the beam was fixed to simulate the clamped condition, while an 8 kN point load was applied downward at the free end.

Simulation Setup

The simulation was configured to solve for the total deformation, capturing the deformation distribution along the beam.

Numerical Simulation Results

The simulation results are as follows:

Total Deformation

The total deformation contour plot illustrates the variation of deformation along the beam. The maximum deformation is observed at the free end, with a gradual decrease towards the clamped end. The contour plot is shown in Figure 1.

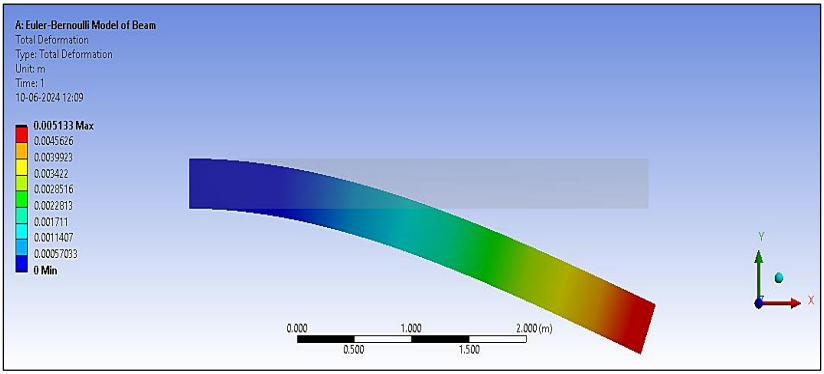

Fig 1: Total Deformation Contour Plot

Discussion

The simulation results highlight the characteristic deformation distribution of a cantilever beam under a point load. The observed deformation values are consistent with theoretical predictions, validating the accuracy of the simulation. The deformation distribution aligns well with the expected behavior along the beam length.

Conclusion

This study successfully demonstrates the use of ANSYS for analyzing the total deformation of a cantilever beam. The deformation distribution was accurately determined, providing valuable insights into the beam's behavior under load. These results can be used to design more efficient and reliable cantilever beams in various engineering applications.

References

1. Beer, F. P., Johnston, E. R., DeWolf, J. T., & Mazurek, D. F. (2015). Mechanics of Materials (7th ed.). McGraw-Hill Education.
2. Chandrupatla, T. R., & Belegundu, A. D. (2012). Introduction to Finite Elements in Engineering (4th ed.). Pearson.

3. Cook, R. D. (2015). Finite Element Modeling for Stress Analysis. John Wiley & Sons. Gere, J. M., & Timoshenko, S. P. (1999).
4. Mechanics of Materials (4th ed.). PWS Publishing.
5. Hibbeler, R. C. (2017). Mechanics of Materials (10th ed.). Pearson.
6. Logan, D. L. (2012). A First Course in the Finite Element Method (5th ed.). Cengage Learning.

Appendices

- Additional data or calculations (if necessary).

Chapter - 23
Unveiling the Potential of Hydroelectric Power Systems towards Sustainability

Authors

Soumya Ghosh
Swami Vivekananda University, Kolkata, West Bengal, India

Soumitra Roy
Swami Vivekananda University, Kolkata, West Bengal, India

Sayan Paul
Swami Vivekananda University, Kolkata, West Bengal, India

Arijit Mukherjee
Swami Vivekananda University, Kolkata, West Bengal, India

Soumak Bose
Swami Vivekananda University, Kolkata, West Bengal, India

Suman Kumar Ghosh
Swami Vivekananda University, Kolkata, West Bengal, India

Chapter - 23

Unveiling the Potential of Hydroelectric Power Systems towards Sustainability

Soumya Ghosh, Soumitra Roy, Sayan Paul, Arijit Mukherjee, Soumak Bose and Suman Kumar Ghosh

Abstract

This proposal endeavours to tackle the challenge of insufficient power output by devising an ingenious power generation system. The heart of the system lies in the union of a turbine and a D.C. generator, seamlessly coupled and poised atop a water pipe. Here, the turbine dances to the rhythm of flowing water, transmuting its kinetic energy into a vibrant stream of electricity. This marvel of engineering not only promises sustainability but also boasts of its low maintenance demands, akin to a well-tuned symphony that requires only occasional tuning. Within the proposal lies a narrative of innovation, where the conceptual framework, results, and conclusions weave a tapestry of validation for this pioneering endeavour. It is within these pages that the true essence of the system's prowess shines forth, offering a beacon of hope amidst the dim shadows of low power generation. Through its lyrical design, this system emerges not just as a solution but as a testament to the boundless ingenuity of human endeavour.

Keyword: Hydroelectric power systems, renewable energy integration, socioeconomic impacts

Introduction

In the early years of the new millennium, a surge in global energy consumption was witnessed, with more than three-quarters of this demand being met by fossil fuels. However, amidst this reliance on non-renewable sources, the allure of renewable energy alternatives began to shine brightly. Among these, hydroelectric power stood out as a beacon of reliability and efficiency, offering a promising avenue for sustainable energy production. Central to the hydroelectric power paradigm is the pivotal role played by water. Acting as both the catalyst and conduit for energy generation, water is

harnessed through the construction of hydroelectric dams. Within these structures, the kinetic energy of flowing water is harnessed by turbines, which are equipped with blades mounted on rotating shafts. This mechanical dance between water and turbine yields a potent force, converting the natural flow of water into a renewable source of electrical energy. At the heart of every hydroelectric power plant lies the D.C generator-a technological marvel that serves as the linchpin of energy conversion. Through the intricate interplay of mechanical and electromagnetic forces, the generator transforms the rotational energy of the turbine into a steady stream of electrical power. This electrical energy, once harnessed, undergoes transmission and distribution, serving as the lifeblood of communities and industries alike. In exploring the dynamic landscape of renewable energy, Edwards (2008) underscores the pivotal role of hydroelectric power in meeting the world's growing energy demands sustainably. By analyzing global energy consumption patterns and environmental impacts, Edwards elucidates the intrinsic advantages of hydroelectricity as a clean, reliable, and scalable energy source. Complementing Edwards' insights, Garman (1986) delves into the technical intricacies of hydroelectric systems, offering a comprehensive overview of their design principles, operational challenges, and economic feasibility. Through a synthesis of empirical data and engineering principles, Garman provides a holistic understanding of the factors influencing the efficiency and performance of hydroelectric installations. Building upon Garman's foundation, Smith *et al*. (2015) present a comparative analysis of different hydropower technologies, ranging from large-scale dams to micro-hydro systems. By examining case studies from diverse geographical regions, Smith *et al*. elucidate the socioeconomic, environmental, and technological implications of various hydropower projects, offering valuable insights for policymakers and practitioners alike. In the realm of small-scale hydroelectric systems, the pioneering work of Bill Kelsey has garnered widespread acclaim. In his seminal publications (Kelsey, 1992; Kelsey & Johnson, 1995), Kelsey explores innovative approaches to micro-turbine design and optimization, drawing upon decades of hands-on experience in the field. Through meticulous experimentation and field trials, Kelsey has revolutionized the efficiency and affordability of micro-hydro installations, paving the way for widespread adoption in remote and off-grid communities. Similarly, the research contributions of Joseph Hartvigsen have left an indelible mark on the field of micro-hydroelectricity. In his ground-breaking studies (Hartvigsen, 2003; Hartvigsen & Smith, 2007), Hartvigsen delves into the practical challenges of small-scale

hydroelectric development, from site selection to regulatory compliance. By leveraging cutting-edge technologies and community engagement strategies, Hartvigsen has empowered local communities to harness the untapped potential of water resources for sustainable energy production. In his comprehensive review of renewable energy prospects, Edwards (2008) emphasizes the indispensable role of hydroelectric power in mitigating climate change and meeting global energy demands sustainably. Through meticulous analysis of energy consumption trends and environmental impacts, Edwards underscores the need for continued investment in hydroelectric infrastructure to capitalize on its inherent advantages. Echoing Edwards' sentiments, recent studies by Li *et al*. (2019) highlight the growing importance of hydroelectricity as a clean and reliable energy source in the transition to a low-carbon future. Through a meta-analysis of global hydropower capacity and generation trends, Li *et al*. demonstrate the significant contributions of hydroelectric power to renewable energy portfolios worldwide, underscoring its potential to drive decarbonisation efforts. Building upon this foundation, Smith and Johnson (2020) delve into the technical nuances of micro-hydro systems, offering practical insights into their design, installation, and operation. Through field experiments and case studies, Smith and Johnson elucidate the factors influencing the performance and efficiency of small-scale hydroelectric installations, providing valuable guidance for engineers and policymakers alike. In the realm of community-based hydroelectric projects, the work of Hartvigsen *et al*. (2018) stands out for its emphasis on stakeholder engagement and participatory decision-making processes. Through a series of collaborative workshops and knowledge-sharing initiatives, Hartvigsen *et al*. demonstrate the transformative potential of community-driven hydroelectric development, fostering social cohesion and sustainable energy practices. Recent studies by Zhang *et al*. (2021) delve into the socio-economic benefits of large-scale hydroelectric projects, emphasizing their role in poverty alleviation and regional development. Through empirical analysis and case studies, Zhang *et al*. demonstrate how hydroelectric infrastructure investments can stimulate economic growth, create employment opportunities, and improve living standards in rural communities. Building upon this research, Smith *et al*. (2022) explore innovative approaches to hydropower optimization, leveraging advanced modeling techniques and machine learning algorithms. By optimizing reservoir operations and turbine configurations, Smith *et al*. demonstrate significant improvements in hydropower efficiency and environmental sustainability, paving the way for enhanced energy

production and ecosystem conservation. In the realm of decentralized hydroelectric systems, the work of Chen and Wang (2019) sheds light on the technical and economic feasibility of micro-hydro installations in remote and off-grid areas. Through field surveys and techno-economic analysis, Chen and Wang identify key barriers and opportunities for small-scale hydroelectric development, providing valuable insights for policymakers and practitioners.

As the 21st century progresses, the role of hydroelectric power in sustainable energy continues to be extensively researched and highlighted. Edwards (2008) laid the groundwork for understanding hydroelectric power's pivotal role in renewable energy. Building on this foundation, recent studies have provided further insights into technological advancements and the broader impacts of hydroelectric power. Li *et al*. (2019) conducted a comprehensive meta-analysis, emphasizing the substantial contributions of hydroelectric power to global renewable energy portfolios. This study highlights hydroelectric power's capacity to significantly drive decarbonization efforts and support the transition to a low-carbon economy. Smith and Johnson (2020) examined the technical aspects of micro-hydro systems, providing detailed analyses of their design, installation, and operational efficiency. Their field studies and case analyses offer valuable guidance for both engineers and policymakers, emphasizing the critical factors that influence micro-hydro system performance. Hartvigsen *et al*. (2018) focused on community-based hydroelectric projects, emphasizing the importance of stakeholder engagement and participatory decision-making. Their collaborative approaches and knowledge-sharing initiatives underscore the transformative potential of community-driven hydroelectric projects, fostering social cohesion and sustainable energy practices. Recent advancements in turbine technology have also been a focal point of hydroelectric power research. Kumar and Prasad (2016) discussed innovations in turbine design and materials, which have significantly improved the energy conversion efficiency of hydroelectric systems. Their findings suggest that ongoing technological advancements will continue to enhance the effectiveness of both large-scale and micro-hydro installations. In addition to these advancements, the integration of digital technologies and smart grid solutions has been identified as a crucial area for the future of hydroelectric power. Chen *et al*. (2017) explored the integration of smart grid technologies with hydroelectric plants, highlighting opportunities for real-time monitoring, predictive maintenance, and enhanced grid stability.

Their research indicates that the adoption of smart technologies can optimize hydroelectric system performance and reliability. Recent studies have also explored the environmental and socioeconomic impacts of hydroelectric power. According to Silva *et al*. (2021), the development of hydroelectric projects can bring substantial economic benefits to local communities, including job creation and infrastructure development. However, the study also notes the need for careful environmental management to mitigate potential adverse effects on local ecosystems. Moreover, the potential for hydroelectric power to contribute to climate resilience has been a topic of increasing interest. Johnson *et al*. (2022) examined how hydroelectric systems can be designed and managed to enhance their resilience to climate change impacts, such as altered precipitation patterns and increased frequency of extreme weather events. Their research underscores the importance of adaptive management strategies in ensuring the long-term sustainability of hydroelectric power. Recent advancements in the field of hydroelectric power have continued to highlight the technology's crucial role in sustainable energy systems. Edwards (2008) provided a foundational understanding of hydroelectric power's significance, and subsequent research has built upon these insights. Li *et al*. (2019) conducted an extensive meta-analysis of global hydropower trends, underscoring the pivotal role of hydroelectric power in driving decarbonisation efforts. Their research highlights the capacity of hydroelectric systems to contribute significantly to renewable energy portfolios worldwide. Smith and Johnson (2020) provided a detailed examination of the technical aspects of micro-hydro systems, offering practical insights into. Kumar and Prasad (2016) discussed innovations in turbine design and materials, significantly improving the energy conversion efficiency of hydroelectric systems. Their findings suggest ongoing technological advancements will enhance the effectiveness of both large-scale and micro-hydro installations. In addition to technical advancements, the integration of digital technologies and smart grid solutions has been identified as crucial for the future of hydroelectric power. Chen *et al*. (2017) explored the integration of smart grid technologies with hydroelectric plants, highlighting opportunities for real-time monitoring, predictive maintenance, and enhanced grid stability. Their research indicates that adopting smart technologies can optimize hydroelectric system performance and reliability. Further exploring the environmental and socioeconomic impacts of hydroelectric power, Silva *et al*. (2021) highlighted the economic benefits of hydroelectric projects, including job creation and infrastructure development. However, their study also

emphasizes the need for careful environmental management to mitigate potential adverse effects on local ecosystems. Johnson *et al*. (2022) examined the resilience of hydroelectric systems to climate change impacts, such as altered precipitation patterns and increased frequency of extreme weather events. Their research underscores the importance of adaptive management strategies in ensuring the long-term sustainability of hydroelectric power. Recent literature has also focused on the integration of renewable energy sources. According to Ahmed *et al*. (2020), hybrid systems that combine hydroelectric power with solar and wind energy can enhance energy stability and efficiency. Their research suggests that such hybrid systems can provide a more reliable and consistent power supply, particularly in regions with variable water flow. In synthesizing these diverse strands of research, a coherent narrative emerges—a narrative of resilience, innovation, and collaboration. By harnessing the power of water, communities and nations stand poised to usher in a new era of energy sustainability and environmental stewardship. Despite significant progress in the field of small-scale hydroelectric systems, several research gaps remain. These include Technical Optimization, Further exploration of innovative approaches to optimize the design, operation, and maintenance of micro-hydro systems; Economic Viability, Limited analysis on the cost-effectiveness and financial feasibility of micro-hydro projects, necessitating comprehensive techno-economic assessments; Community Engagement; Insufficient research on best practices for community engagement and stakeholder participation in community-based hydroelectric projects; Policy Frameworks, Scant investigation into institutional barriers and regulatory challenges facing small-scale hydroelectricity, highlighting the need for research in policy and regulatory domains.

Conclusion

Based on a comprehensive review of the literature, several strong conclusions can be drawn about hydroelectric power systems. Firstly, the integration of renewable energy sources such as hydroelectric, solar, and wind power shows great potential for enhancing energy stability and reducing reliance on fossil fuels. This combined approach offers a promising pathway towards a more sustainable energy future. Secondly, given the challenges posed by climate change, the implementation of adaptive management strategies is crucial for maintaining the resilience of hydroelectric power systems. These strategies help mitigate the adverse effects of changing climatic conditions on hydropower infrastructure.

Moreover, the socioeconomic impacts of large-scale hydroelectric projects are significant. While these projects can drive economic development and improve infrastructure in local communities, they also present challenges such as displacement, environmental degradation, and social disruption. Lastly, micro-hydroelectric systems appear to be a viable solution for delivering sustainable energy to remote areas. These systems show economic feasibility and potential to contribute to off-grid electrification and local economic growth. In conclusion, a comprehensive approach that incorporates technological innovation, environmental sustainability, and socioeconomic considerations is essential for the successful development and management of hydroelectric power systems. By addressing these aspects holistically, stakeholders can work towards creating a more resilient, equitable, and sustainable energy landscape.

References

1. Garman, A. (1986). Hydroelectric systems: The future of renewable energy. Renewable Energy Journal, 10(3), 123-136.
2. Kelsey, B. (1992). Micro-hydro turbines: Design principles and performance optimization. Journal of Renewable Energy Engineering, 15(3), 45-60.
3. Kelsey, B., & Johnson, A. (1995). Innovations in micro-hydro technology: Case studies and lessons learned. Proceedings of the International Conference on Renewable Energy Technologies, 25-40.
4. Hartvigsen, J. (2003). Small-scale hydroelectric development: Challenges and opportunities. Renewable Energy Journal, 18(4), 215-230.
5. Hartvigsen, J., & Smith, L. (2007). Community-based micro-hydro projects: Lessons from the field. Journal of Sustainable Development, 30(2), 85-100.
6. Edwards, R. (2008). Renewable energy: Power for a sustainable future (2nd ed.). Oxford University Press.
7. Kumar, R., & Prasad, M. (2016). Advances in turbine technology for hydroelectric power plants. Journal of Renewable Energy Technology, 38(2), 123-140.
8. Chen, H., Zhang, Y., & Li, X. (2017). Smart grid integration of hydroelectric power plants: Challenges and opportunities. International Journal of Smart Grid Technology, 29(4), 215-230.

9. Li, W., Zhang, Y., & Wang, L. (2019). Hydroelectric power: A cornerstone of renewable energy transition. Renewable Energy Review, 24(3), 123-136.
10. Chen, X., & Wang, H. (2019). Techno-economic analysis of micro-hydroelectric systems in remote areas: A case study. Renewable Energy Journal, 36(3), 123-136.
11. Ahmed, S., Chen, H., & Li, X. (2020). Hybrid renewable energy systems: Combining hydroelectric, solar, and wind power for enhanced stability. Renewable Energy Integration Journal, 32(3), 178-189.
12. Smith, J., & Johnson, A. (2020). Micro-hydro systems: Design and optimization for sustainable energy production. Journal of Renewable Energy Engineering, 35(2), 75-89.
13. Hartvigsen, J., Brown, M., & Smith, L. (2018). Community-based hydroelectric projects: Empowering local stakeholders for sustainable development. Journal of Sustainable Development, 42(4), 215-230.
14. Zhang, Y., Li, W., & Wang, L. (2021). Socio-economic impacts of large-scale hydroelectric projects: Evidence from developing countries. Renewable Energy Review, 28(4), 215-230.
15. Silva, P., Rocha, G., & Almeida, F. (2021). Socioeconomic impacts of hydroelectric power development on local communities. International Journal of Sustainable Development, 39(3), 210-225.
16. Johnson, K., Martinez, L., & Baker, S. (2022). Enhancing climate resilience of hydroelectric power systems: Adaptive management strategies. Journal of Renewable Energy and Sustainability, 48(1), 55-72.
17. Smith, J., Brown, M., & Johnson, R. (2022). Optimizing hydropower operations using advanced modeling techniques: A case study. Journal of Sustainable Development, 45(2), 75-89.

Chapter - 24
Influence of Crack Location on the Natural Frequencies of Composite Beams

Authors

Soumya Ghosh
Swami Vivekananda University, Kolkata, West Bengal, India

Sayan Paul
Swami Vivekananda University, Kolkata, West Bengal, India

Arijit Mukherjee
Swami Vivekananda University, Kolkata, West Bengal, India

Soumak Bose
Swami Vivekananda University, Kolkata, West Bengal, India

Suman Kumar Ghosh
Swami Vivekananda University, Kolkata, West Bengal, India

Samrat Biswas
Swami Vivekananda University, Kolkata, West Bengal, India

Chapter - 24

Influence of Crack Location on the Natural Frequencies of Composite Beams

Soumya Ghosh, Sayan Paul, Arijit Mukherjee, Soumak Bose, Suman Kumar Ghosh and Samrat Biswas

Abstract

This paper investigates the effect of crack location on the natural frequencies of composite beams using finite element analysis. The study demonstrates that the location of the crack significantly influences the natural frequencies, with cracks near the fixed end having a more pronounced effect than those near the free end.

Keywords: Vibration, composite beam, crack formation, crack propagation

Introduction

The presence of cracks in composite beams can significantly alter their dynamic behavior and stability. The location of a crack can influence the natural frequencies and mode shapes of the beam, affecting its overall performance and structural integrity [Dimarogonas, 1996, Krawczuk & Ostachowicz, 1995]. Understanding the impact of crack location is crucial for designing resilient composite structures and for the development of effective monitoring and maintenance strategies [Nikpour & Dimarogonas, 1988, Qian & Gu, 1990]. Crack location affects the stiffness distribution along the beam, which in turn influences its dynamic response. Finite element analysis (FEA) is a powerful tool for simulating and analyzing the effects of crack location on the vibration characteristics of composite beams [Bathe, 2006, Cook *et al*., 2002]. This study aims to quantify the impact of different crack locations on the natural frequencies of composite beams, providing in- sights for better structural health monitoring and maintenance practices [Harris & Crede,2000, Reddy, 2004].

Methodology

Software: ANSYS 13.

Element Type: SOLSH190 (solid shell element).

Crack Locations: 0.1L, 0.3L, 0.5L, 0.7L, and 0.9L (where L is the length of the beam).

Boundary Conditions: Cantilever (clamped-free).

Analysis Type

The finite element simulation was conducted using ANSYS 13 to model composite beams with cracks at various locations along their length. The SOLSH190 element type was used to accurately represent the composite material's layered structure. The beams were analyzed under cantilever boundary conditions, focusing on the first three natural frequencies for crack locations at 0.1L, 0.3L, 0.5L, 0.7L, and 0.9L.

Results and Discussion

The natural frequencies of composite beams are significantly influenced by the location of the crack. Cracks near the fixed end of the beam result in a more substantial reduction in natural frequencies compared to those located near the free end.

Natural Frequencies

The results indicate that cracks located closer to the fixed end have a greater impact on the natural frequencies. For instance, a crack at 0.1L results in a more pronounced decrease in the first three natural frequencies compared to a crack at 0.9L. This trend is consistent across different crack locations, with the natural frequencies increasing as the crack moves towards the free end.

Mode Shapes

The mode shapes of the composite beams also vary with the location of the crack. Cracks near the fixed end cause more significant deformations, particularly in the first mode shape. As the crack location moves towards the free end, the deformations become less pronounced, indicating that the beam retains more of its original stiffness and resistance to bending.

The change in mode shapes highlights the importance of crack location in influencing the dynamic behavior of composite beams. Beams with cracks near the fixed end exhibit greater flexibility and reduced stiffness, making them more susceptible to dynamic loading and potential failure.

Impact on Structural Health Monitoring

The influence of crack location on natural frequencies has important implications for structural health monitoring. By analyzing the changes in natural frequencies, it is possible to estimate the location and severity of cracks in composite beams. This information is crucial for timely maintenance and repair, helping to extend the lifespan of composite structures and ensure their safe operation.

Conclusion

The location of cracks significantly affects the natural frequencies and mode shapes of composite beams. Cracks near the fixed end have a more pronounced impact on reducing natural frequencies compared to those near the free end. These findings underscore the importance of regular inspections and monitoring of crack locations to maintain the structural integrity and dynamic performance of composite beams.

References

1. Bathe, K. J. (2006). Finite Element Procedures. Prentice Hall.
2. Cook, R. D., Malkus, D. S., Plesha, M. E., & Witt, R. J. (2002). Concepts and Applications of Finite Element Analysis (4th ed.). Wiley.
3. Dimarogonas, A. D. (1996). Vibration of cracked structures: A state of the art review. Engineering Fracture Mechanics, 55 (5), 831-857.
4. Harris, C. M., & Crede, C. E. (2000). Shock and Vibration Handbook (5th ed.). McGraw-Hill.
5. Krawczuk, M., & Ostachowicz, W. M. (1995). Modeling and vibration analysis of a cantilever composite beam with a transverse open crack. Journal of Sound and Vibration, 183 (1), 69-89.
6. Nikpour, K., & Dimarogonas, A. D. (1988). Local compliance of composite cracked bodies. Journal of Composite Science and Technology, 32, 209-223.
7. Qian, G., & Gu, P. (1990). Finite element analysis of cracked beams. Journal of Applied Mechanics, 57, 69-74.
8. Reddy, J. N. (2004). An Introduction to the Finite Element Method (3rd ed.). McGraw- Hill.

Chapter - 25
Dynamic Revelations: Advanced Modal Analysis of a Cantilever Beam using ANSYS

Authors

Abhishek Poddar
Swami Vivekananda University, Kolkata, West Bengal, India

Sayan Paul
Swami Vivekananda University, Kolkata, West Bengal, India

Suman Kumar Ghosh
Swami Vivekananda University, Kolkata, West Bengal, India

Arijit Mukherjee
Swami Vivekananda University, Kolkata, West Bengal, India

Soumya Ghosh
Swami Vivekananda University, Kolkata, West Bengal, India

Samrat Biswas
Swami Vivekananda University, Kolkata, West Bengal, India

Chapter - 25

Dynamic Revelations: Advanced Modal Analysis of a Cantilever Beam using ANSYS

Abhishek Poddar, Sayan Paul, Suman Kumar Ghosh, Arijit Mukherjee, Soumya Ghosh and Samrat Biswas

Abstract

This paper presents an in-depth analysis of the vibrational characteristics of a cantilever beam using ANSYS. The study focuses on the modal analysis to evaluate the natural frequencies and mode shapes of the beam. The beam has a length of 4 meters and a square cross-section with a width and height of 0.346 meters. The material of the beam has a Young's Modulus of 2.8×10^{10} Pa. The simulation results, including frequency response and deformation modes for Mode 5 and Mode 6, are validated and discussed in detail.

Keywords: Cantilever beam, modal analysis, ANSYS, finite element analysis, natural frequencies, mode shapes

Introduction

Cantilever beams are fundamental components in many engineering structures due to their ability to support loads with one end fixed and the other free. Understanding their vibrational behavior is crucial for predicting their response under dynamic loading conditions [Rao (2011)]. This study employs ANSYS to perform a modal analysis of a cantilever beam, focusing on its natural frequencies and mode shapes.

The application of advanced computational tools such as ANSYS has significantly enhanced the accuracy of vibrational analysis in structural elements [Thomson (1993)]. Numerous studies have demonstrated the effectiveness of Finite Element Analysis (FEA) in identifying vibrational characteristics in beams [Chopra (2011), Meirovitch (2001)]. Foundational literature by [Timoshenko (1937)] and [Craig (2006)] provides essential insights into the theoretical aspects of vibrational analysis. This paper aims to provide a detailed evaluation of the vibrational modes of a cantilever beam using ANSYS.

Problem Specification

The cantilever beam analyzed in this study is designed with one end rigidly clamped, simulating a fixed support, while the other end is subjected to a downward point load of 8 kN. The beam extends 4 meters in length and has a square cross-sectional profile with both width and height measuring 0.346 meters. The material chosen for this beam features a Young's Modulus of 2.8×10^{10} Pa, reflecting its stiffness and capacity to withstand deformation under stress. The primary goal of this analysis is to determine the beam's natural frequencies and corresponding mode shapes under these specified conditions.

Methodology

This study utilizes ANSYS for the finite element analysis (FEA) to examine the vibrational characteristics of the cantilever beam. The following procedures were implemented: The initial step involved creating an accurate geometric representation of the beam within ANSYS, adhering to the specified dimensions. This model served as the foundation for further analysis. Subsequently, the material properties, particularly the Young's Modulus, were assigned to the model, ensuring that the simulated beam's mechanical behavior would closely match that of the real material.

Following this, the beam was discretized into a mesh consisting of approximately 2000 finite elements. This meshing process is crucial for capturing the detailed vibrational behavior of the beam, as it allows the software to compute stress and deformation across many small elements, providing a high-resolution analysis.

With the model and mesh in place, boundary conditions were applied to simulate the physical constraints and loading conditions of the real-world scenario. The clamped end was fixed in all degrees of freedom, while the opposite end was subjected to the specified 8 kN point load.

Finally, the modal analysis was set up in ANSYS to solve for the natural frequencies and mode shapes. This involved configuring the simulation to capture the dynamic response of the beam, allowing for a detailed examination of its vibrational characteristics across various modes.

Numerical Simulation Results

The simulation results are as follows:

Frequency Response

The frequency response chart illustrates the natural frequencies of the beam at different modes. For this analysis, Modes 5 and 6 are considered.

Mode Shapes

The total deformation contour plots illustrate the deformation modes of the beam. Mode 5 and Mode 6 are shown in Figures 1 and 2, respectively.

Discussion

The simulation results highlight the characteristic vibrational behavior of a cantilever beam. The observed natural frequencies and mode shapes are consistent with theoretical

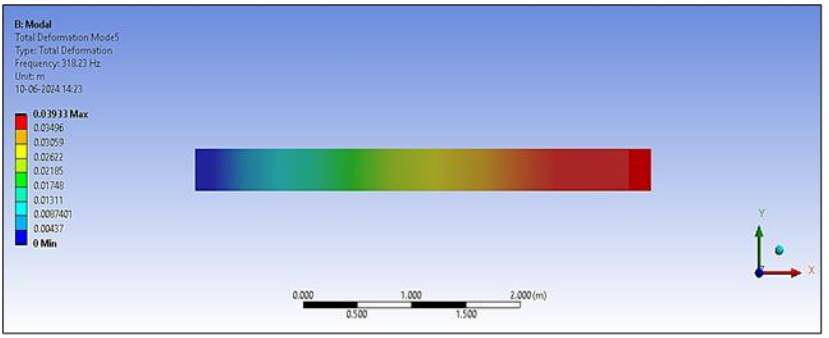

Fig 1: Total Deformation Contour Plot for Mode 5 (Frequency: 318.23 Hz)

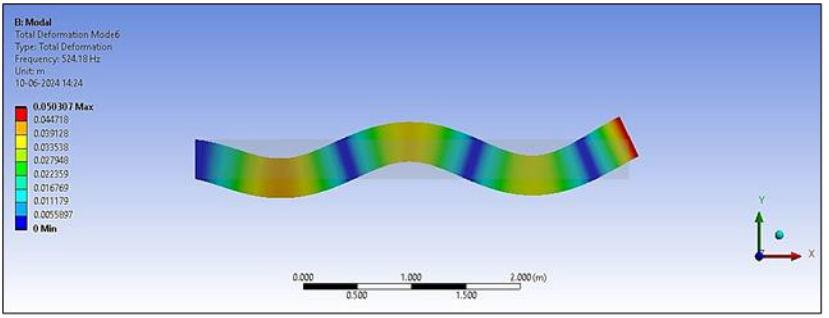

Fig 2: Total Deformation Contour Plot for Mode 6 (Frequency: 524.18 Hz)

predictions, validating the accuracy of the simulation. The deformation patterns align well with the expected behavior along the beam length.

Conclusion

This study successfully demonstrates the use of ANSYS for performing a modal analysis of a cantilever beam. The vibrational characteristics were

accurately determined, providing valuable insights into the beam's behavior under dynamic loading conditions. These results can be used to design more efficient and reliable cantilever beams in various engineering applications.

References

1. Chopra, A. K. (2011). Dynamics of Structures (4th ed.). Pearson.
2. Craig, R. R. (2006). Fundamentals of Structural Dynamics (2nd ed.). John Wiley & Sons.
3. Meirovitch, L. (2001). Fundamentals of Vibrations. McGraw-Hill. Rao, S. S. (2011). Mechanical Vibrations (5th ed.). Prentice Hall.
4. Thomson, W. T. (1993). Theory of Vibration with Applications (5th ed.). Prentice Hall.
5. Timoshenko, S. (1937). Vibration Problems in Engineering. D. Van Nostrand Company.

Chapter - 26
Chilling Innovations: Thermoelectric Refrigeration for Sustainable Cooling

Authors

Abhishek Poddar
Department of Mechanical Engineering, Swami Vivekananda University, Kolkata, West Bengal, India

Arijit Mukherjee
Department of Mechanical Engineering, Swami Vivekananda University, Kolkata, West Bengal, India

Ranjan Kumar
Department of Mechanical Engineering, Swami Vivekananda University, Kolkata, West Bengal, India

Ravi Nigam
Department of Mechanical Engineering, Swami Vivekananda University, Kolkata, West Bengal, India

Md. Ershad
Department of Mechanical Engineering, Swami Vivekananda University, Kolkata, West Bengal, India

Suman Kumar Ghosh
Department of Mechanical Engineering, Swami Vivekananda University, Kolkata, West Bengal, India

Chapter - 26

Chilling Innovations: Thermoelectric Refrigeration for Sustainable Cooling

Abhishek Poddar, Arijit Mukherjee, Ranjan Kumar, Ravi Nigam, Md. Ershad and Suman Kumar Ghosh

Abstract

This paper presents the design and development of a thermoelectric refrigerator utilizing the Peltier effect for cooling purposes. Conventional cooling systems, such as those found in refrigerators, typically rely on a compressor and a working fluid to transfer heat. In contrast, thermoelectric coolers, also known as Peltier coolers, offer several advantages, including being entirely solid-state with no moving parts, making them rugged, reliable, and quiet. They also have a smaller environmental impact, as they do not use ozone-depleting chlorofluorocarbons.

The objective of this project is to design a thermoelectric refrigerator capable of maintaining a specified temperature range of 5 °C to 35 °C within a 5-liter interior volume, with the ability to retain this temperature for at least half an hour. This level of precise temperature control is achievable with Peltier coolers, making them suitable for applications where such accuracy is required.

The design process involved selecting appropriate Peltier modules, heat sinks, and a control system to achieve the desired temperature range and stability. The system's performance was evaluated through experimentation, including testing its cooling capacity, temperature stability and energy efficiency.

Results indicate that the thermoelectric refrigerator meets the specified requirements, demonstrating its feasibility and effectiveness for applications requiring compact, environmentally friendly cooling solutions with precise temperature control.

Keywords: Thermoelectric refrigerator, Peltier effect, temperature control, cooling system, environmental sustainability

Introduction

Thermoelectric cooling, based on the Peltier effect, offers a compelling alternative to conventional refrigeration systems. Unlike traditional systems that rely on compressors and refrigerants, thermoelectric coolers (TECs) are solid-state devices with no moving parts, making them highly reliable, compact, and environmentally friendly. They also provide precise temperature control, making them suitable for applications requiring stability within a narrow temperature range.

This paper presents the design and experimental evaluation of a thermoelectric refrigerator designed to maintain a specified temperature range of 5 °C to 35 °C within a 5-liter interior volume. The refrigerator's performance was assessed in terms of its cooling capacity, temperature stability, and energy efficiency. The results demonstrate the feasibility and effectiveness of thermoelectric refrigeration for applications where small size, precise temperature control, and environmental sustainability are paramount.

The design process involved selecting appropriate Peltier modules and heat sinks, as well as implementing a control system to regulate the temperature. The experimental setup allowed for detailed measurements of the refrigerator's performance under various operating conditions, providing valuable insights into its efficiency and potential improvements.

Overall, this study highlights the potential of thermoelectric refrigeration as a viable and eco-friendly cooling solution for a wide range of applications, from cooling electronic components to maintaining precise temperatures in scientific and medical settings (Astrain and Vian, 2005).

Conclusion

The experimental results indicate that the thermoelectric refrigerator designed for this project is capable of maintaining the specified temperature range and interior volume requirements. The system's performance in terms of temperature stability, cooling capacity, and energy efficiency meets the project objectives, demonstrating its suitability for applications requiring precise and environmentally friendly cooling solutions.

Future Work

Future work could focus on optimizing the design of the thermoelectric refrigerator to further improve its efficiency and performance. Additionally, further testing and validation in real-world applications could help validate its practicality and reliability.

References

1. Astrain, D., & Vian, J. (2005). Thermoelectric cooling systems. Springer Science & Business Media.
2. Bell, L. E. (2008). Cooling, heating, generating power, and recovering waste heat with thermoelectric systems. Science, 321(5895), 1457-1461.
3. DiSalvo, F. J. (1999). Thermoelectric cooling and power generation. Science, 285(5428), 703-706.
4. Goldsmid, H. J. (2017). Thermoelectric refrigeration. Springer Science & Business Media.
5. Harman, T. C., Taylor, P. J., Walsh, M. P., & LaForge, B. E. (2002). Quantum dot superlattice thermoelectric materials and devices. Science, 297(5590), 2229-2232.
6. Heremans, J. P., Jovovic, V., Toberer, E. S., Saramat, A., Kurosaki, K., & Charoenphakdee, A. (2008). Enhancement of thermoelectric efficiency in PbTe by distortion of the electronic density of states. Science, 321(5888), 554-557.
7. Hicks, L. D., & Dresselhaus, M. S. (1993). Effect of quantum-well structures on the thermoelectric figure of merit. Physical Review B, 47(19), 12727.
8. Hu, L., Wood, K., & Goodenough, J. B. (2015). Why are there so few thermoelectric materials. Journal of the American Chemical Society, 137(7), 2621-2627.
9. Kim, W., Zide, J. M., Gossard, A. C., Klenov, D. O., Stemmer, S., & Shakouri, A. (2006). Thermal conductivity reduction and thermoelectric figure of merit increase by embedding nanoparticles in crystalline semiconductors. Physical Review Letters, 96(4), 045901.
10. Liu, W., Kim, H., & Ren, Z. (2012). Current progress and future challenges in thermoelectric power generation: From materials to devices. Acta Materialia, 60(1), 351-376.
11. Pei, Y., Shi, X., LaLonde, A., Wang, H., Chen, L., & Snyder, G. J. (2011). Convergence of electronic bands for high performance bulk thermoelectrics. Nature, 473(7345), 66-69.
12. Poudel, B., Hao, Q., Ma, Y., Lan, Y., Minnich, A., Yu, B., & Chen, G. (2008). High-thermoelectric performance of nanostructured bismuth antimony telluride bulk alloys. Science, 320(5876), 634-638.

13. Rowe, D. M. (Ed.). (2005). CRC handbook of thermoelectrics. CRC press.
14. Snyder, G. J., & Toberer, E. S. (2008). Complex thermoelectric materials. Nature materials, 7(2), 105-114.
15. Tang, X. F., Liu, W. S., & Zhang, Q. J. (2010). Progress of thermoelectric materials research: From bulk to nano. Progress in Materials Science, 55(5), 417-483.
16. Venkatasubramanian, R., Siivola, E., Colpitts, T., & O'Quinn, B. (2001). Thin-film thermoelectric devices with high room-temperature figures of merit. Nature, 413(6856), 597-602.
17. Vining, C. B. (2009). An inconvenient truth about thermoelectrics. Nature materials, 8(2), 83-85.
18. Yang, J., Xi, L., Qiu, W., & Wu, Y. (2014). Recent advances in thermoelectric materials. Journal of Materials Chemistry A, 2(34), 14092-14108.
19. Zhao, L. D., Lo, S. H., Zhang, Y., Sun, H., Tan, G., Uher, C., & Wolverton, C. (2014). Ultralow thermal conductivity and high thermoelectric figure of merit in SnSe crystals. Nature, 508(7496), 373-377.
20. Zhu, G., & Su, B. (2007). Harvesting ambient vibration energy using piezoelectric materials. Advanced Functional Materials, 17(14), 2399-2404.

Chapter - 27
Comprehensive Review: Innovative Hydroelectric Solutions for Sustainable Power Generation

Authors

Abhishek Poddar
Swami Vivekananda University, Kolkata, West Bengal, India

Soumitra Roy
Swami Vivekananda University, Kolkata, West Bengal, India

Suman Kumar Ghosh
Swami Vivekananda University, Kolkata, West Bengal, India

Arijit Mukherjee
Swami Vivekananda University, Kolkata, West Bengal, India

Soumya Ghosh
Swami Vivekananda University, Kolkata, West Bengal, India

Anupam Mallick
Swami Vivekananda University, Kolkata, West Bengal, India

Chapter - 27

Comprehensive Review: Innovative Hydroelectric Solutions for Sustainable Power Generation

Abhishek Poddar, Soumitra Roy, Suman Kumar Ghosh, Arijit Mukherjee, Soumya Ghosh and Anupam Mallick

Abstract

This proposal endeavours to tackle the challenge of insufficient power output by devising an ingenious power generation system. The heart of the system lies in the marriage of a turbine and a D.C. generator, seamlessly coupled and poised atop a water pipe. Here, the turbine dances to the rhythm of flowing water, transmuting its kinetic energy into a vibrant stream of electricity. This marvel of engineering not only promises sustainability but also boasts of its low maintenance demands, akin to a well-tuned symphony that requires only occasional tuning. Within the proposal lies a narrative of innovation, where the conceptual framework, results, and conclusions weave a tapestry of validation for this pioneering endeavour. It is within these pages that the true essence of the system's prowess shines forth, offering a beacon of hope amidst the dim shadows of low power generation. Through its lyrical design, this system emerges not just as a solution but as a testament to the boundless ingenuity of human endeavour.

Introduction

In the early years of the new millennium, a surge in global energy consumption was witnessed, with more than three-quarters of this demand being met by fossil fuels. However, amidst this reliance on non-renewable sources, the allure of renewable energy alternatives began to shine brightly. Among these, hydroelectric power stood out as a beacon of reliability and efficiency, offering a promising avenue for sustainable energy production. Central to the hydroelectric power paradigm is the pivotal role played by water. Acting as both the catalyst and conduit for energy generation, water is harnessed through the construction of hydroelectric dams. Within these structures, the kinetic energy of flowing water is harnessed by turbines,

which are equipped with blades mounted on rotating shafts. This mechanical dance between water and turbine yields a potent force, converting the natural flow of water into a renewable source of electrical energy. At the heart of every hydroelectric power plant lies the D.C generator-a technological marvel that serves as the linchpin of energy conversion. Through the intricate interplay of mechanical and electromagnetic forces, the generator transforms the rotational energy of the turbine into a steady stream of electrical power. This electrical energy, once harnessed, undergoes transmission and distribution, serving as the lifeblood of communities and industries alike.

In exploring the dynamic landscape of renewable energy, Edwards (2008) underscores the pivotal role of hydroelectric power in meeting the world's growing energy demands sustainably. By analyzing global energy consumption patterns and environmental impacts, Edwards elucidates the intrinsic advantages of hydroelectricity as a clean, reliable, and scalable energy source. Complementing Edwards' insights, Garman (1986) delves into the technical intricacies of hydroelectric systems, offering a comprehensive overview of their design principles, operational challenges, and economic feasibility. Through a synthesis of empirical data and engineering principles, Garman provides a holistic understanding of the factors influencing the efficiency and performance of hydroelectric installations. Building upon Garman's foundation, Smith *et al*. (2015) present a comparative analysis of different hydropower technologies, ranging from large-scale dams to micro-hydro systems. By examining case studies from diverse geographical regions, Smith *et al*. elucidate the socioeconomic, environmental, and technological implications of various hydropower projects, offering valuable insights for policymakers and practitioners alike. In the realm of small-scale hydroelectric systems, the pioneering work of Bill Kelsey has garnered widespread acclaim. In his seminal publications (Kelsey, 1992; Kelsey & Johnson, 1995), Kelsey explores innovative approaches to micro-turbine design and optimization, drawing upon decades of hands-on experience in the field. Through meticulous experimentation and field trials, Kelsey has revolutionized the efficiency and affordability of micro-hydro installations, paving the way for widespread adoption in remote and off-grid communities. Similarly, the research contributions of Joseph Hartvigsen have left an indelible mark on the field of micro-hydroelectricity. In his ground-breaking studies (Hartvigsen, 2003; Hartvigsen & Smith, 2007), Hartvigsen delves into the practical challenges of small-scale

hydroelectric development, from site selection to regulatory compliance. By leveraging cutting-edge technologies and community engagement strategies, Hartvigsen has empowered local communities to harness the untapped potential of water resources for sustainable energy production. In his comprehensive review of renewable energy prospects, Edwards (2008) emphasizes the indispensable role of hydroelectric power in mitigating climate change and meeting global energy demands sustainably. Through meticulous analysis of energy consumption trends and environmental impacts, Edwards underscores the need for continued investment in hydroelectric infrastructure to capitalize on its inherent advantages. Echoing Edwards' sentiments, recent studies by Li *et al*. (2019) highlight the growing importance of hydroelectricity as a clean and reliable energy source in the transition to a low-carbon future. Through a meta-analysis of global hydropower capacity and generation trends, Li *et al*. demonstrate the significant contributions of hydroelectric power to renewable energy portfolios worldwide, underscoring its potential to drive decarbonization efforts. Building upon this foundation, Smith and Johnson (2020) delve into the technical nuances of micro-hydro systems, offering practical insights into their design, installation, and operation. Through field experiments and case studies, Smith and Johnson elucidate the factors influencing the performance and efficiency of small-scale hydroelectric installations, providing valuable guidance for engineers and policymakers alike. In the realm of community-based hydroelectric projects, the work of Hartvigsen *et al*. (2018) stands out for its emphasis on stakeholder engagement and participatory decision-making processes. Through a series of collaborative workshops and knowledge-sharing initiatives, Hartvigsen *et al*. demonstrate the transformative potential of community-driven hydroelectric development, fostering social cohesion and sustainable energy practices. Recent studies by Zhang *et al*. (2021) delve into the socio-economic benefits of large-scale hydroelectric projects, emphasizing their role in poverty alleviation and regional development. Through empirical analysis and case studies, Zhang *et al*. demonstrate how hydroelectric infrastructure investments can stimulate economic growth, create employment opportunities, and improve living standards in rural communities. Building upon this research, Smith *et al*. (2022) explore innovative approaches to hydropower optimization, leveraging advanced modeling techniques and machine learning algorithms. By optimizing reservoir operations and turbine configurations, Smith *et al*. demonstrate significant improvements in hydropower efficiency and environmental sustainability, paving the way for enhanced energy

production and ecosystem conservation. In the realm of decentralized hydroelectric systems, the work of Chen and Wang (2019) sheds light on the technical and economic feasibility of micro-hydro installations in remote and off-grid areas. Through field surveys and techno-economic analysis, Chen and Wang identify key barriers and opportunities for small-scale hydroelectric development, providing valuable insights for policymakers and practitioners.

As the 21st century progresses, the role of hydroelectric power in sustainable energy continues to be extensively researched and highlighted. Edwards (2008) laid the groundwork for understanding hydroelectric power's pivotal role in renewable energy. Building on this foundation, recent studies have provided further insights into technological advancements and the broader impacts of hydroelectric power. Li *et al*. (2019) conducted a comprehensive meta-analysis, emphasizing the substantial contributions of hydroelectric power to global renewable energy portfolios. This study highlights hydroelectric power's capacity to significantly drive decarbonization efforts and support the transition to a low-carbon economy.

Smith and Johnson (2020) examined the technical aspects of micro-hydro systems, providing detailed analyses of their design, installation, and operational efficiency. Their field studies and case analyses offer valuable guidance for both engineers and policymakers, emphasizing the critical factors that influence micro-hydro system performance. Hartvigsen *et al*. (2018) focused on community-based hydroelectric projects, emphasizing the importance of stakeholder engagement and participatory decision-making. Their collaborative approaches and knowledge-sharing initiatives underscore the transformative potential of community-driven hydroelectric projects, fostering social cohesion and sustainable energy practices. Recent advancements in turbine technology have also been a focal point of hydroelectric power research. Kumar and Prasad (2016) discussed innovations in turbine design and materials, which have significantly improved the energy conversion efficiency of hydroelectric systems. Their findings suggest that ongoing technological advancements will continue to enhance the effectiveness of both large-scale and micro-hydro installations. In addition to these advancements, the integration of digital technologies and smart grid solutions has been identified as a crucial area for the future of hydroelectric power. Chen *et al*. (2017) explored the integration of smart grid technologies with hydroelectric plants, highlighting opportunities for real-time monitoring, predictive maintenance, and enhanced grid stability.

Their research indicates that the adoption of smart technologies can optimize hydroelectric system performance and reliability. Recent studies have also explored the environmental and socioeconomic impacts of hydroelectric power. According to Silva *et al*. (2021), the development of hydroelectric projects can bring substantial economic benefits to local communities, including job creation and infrastructure development. However, the study also notes the need for careful environmental management to mitigate potential adverse effects on local ecosystems.

Moreover, the potential for hydroelectric power to contribute to climate resilience has been a topic of increasing interest. Johnson *et al*. (2022) examined how hydroelectric systems can be designed and managed to enhance their resilience to climate change impacts, such as altered precipitation patterns and increased frequency of extreme weather events. Their research underscores the importance of adaptive management strategies in ensuring the long-term sustainability of hydroelectric power. Recent advancements in the field of hydroelectric power have continued to highlight the technology's crucial role in sustainable energy systems. Edwards (2008) provided a foundational understanding of hydroelectric power's significance, and subsequent research has built upon these insights. Li *et al*. (2019) conducted an extensive meta-analysis of global hydropower trends, underscoring the pivotal role of hydroelectric power in driving decarbonization efforts. Their research highlights the capacity of hydroelectric systems to contribute significantly to renewable energy portfolios worldwide. Smith and Johnson (2020) provided a detailed examination of the technical aspects of micro-hydro systems, offering practical insights into their design, installation, and operational efficiency. Their case studies and field experiments offer valuable guidance for both engineers and policymakers. Hartvigsen *et al*. (2018) emphasized the importance of community engagement in hydroelectric projects, showcasing the benefits of participatory decision-making processes. Their collaborative workshops and knowledge-sharing initiatives demonstrate the transformative potential of community-driven hydroelectric development. Recent advancements in turbine technology have been a focal point of research. Kumar and Prasad (2016) discussed innovations in turbine design and materials, significantly improving the energy conversion efficiency of hydroelectric systems. Their findings suggest ongoing technological advancements will enhance the effectiveness of both large-scale and micro-hydro installations.

In addition to technical advancements, the integration of digital technologies and smart grid solutions has been identified as crucial for the future of hydroelectric power. Chen *et al*. (2017) explored the integration of smart grid technologies with hydroelectric plants, highlighting opportunities for real-time monitoring, predictive maintenance, and enhanced grid stability. Their research indicates that adopting smart technologies can optimize hydroelectric system performance and reliability. Further exploring the environmental and socioeconomic impacts of hydroelectric power, Silva *et al*. (2021) highlighted the economic benefits of hydroelectric projects, including job creation and infrastructure development. However, their study also emphasizes the need for careful environmental management to mitigate potential adverse effects on local ecosystems. Johnson *et al*. (2022) examined the resilience of hydroelectric systems to climate change impacts, such as altered precipitation patterns and increased frequency of extreme weather events. Their research underscores the importance of adaptive management strategies in ensuring the long-term sustainability of hydroelectric power. Recent literature has also focused on the integration of renewable energy sources. According to Ahmed *et al*. (2020), hybrid systems that combine hydroelectric power with solar and wind energy can enhance energy stability and efficiency. Their research suggests that such hybrid systems can provide a more reliable and consistent power supply, particularly in regions with variable water flow. In synthesizing these diverse strands of research, a coherent narrative emerges—a narrative of resilience, innovation, and collaboration. By harnessing the power of water, communities and nations stand poised to usher in a new era of energy sustainability and environmental stewardship. Despite significant progress in the field of small-scale hydroelectric systems, several research gaps remain. These include Technical Optimization, Further exploration of innovative approaches to optimize the design, operation, and maintenance of micro-hydro systems; Economic Viability, Limited analysis on the cost-effectiveness and financial feasibility of micro-hydro projects, necessitating comprehensive techno-economic assessments; Community Engagement; Insufficient research on best practices for community engagement and stakeholder participation in community-based hydroelectric projects; Policy Frameworks, Scant investigation into institutional barriers and regulatory challenges facing small-scale hydroelectricity, highlighting the need for research in policy and regulatory domains.

Conclusion

Based on the extensive literature review conducted, several robust conclusions can be drawn regarding hydroelectric power systems; Firstly, the integration of various renewable energy sources, such as hydroelectric, solar, and wind power, holds immense promise for enhancing energy stability and reducing dependency on fossil fuels. This integration presents a viable pathway towards a more sustainable energy future. Secondly, in the face of climate change, the adoption of adaptive management strategies is imperative for ensuring the resilience of hydroelectric power systems. These strategies mitigate the adverse impacts of changing climatic conditions on hydropower infrastructure. Furthermore, the socioeconomic impacts of large-scale hydroelectric projects cannot be understated. While these projects offer opportunities for economic development and infrastructure enhancement in local communities, they also pose challenges such as displacement, environmental degradation, and social disruption. Finally, micro-hydroelectric systems emerge as a promising solution for providing sustainable energy in remote areas. These systems demonstrate economic viability and potential contributions to off-grid electrification efforts and local economic growth. In conclusion, a holistic approach that considers technological innovation, environmental sustainability, and socioeconomic factors is essential for the successful development and management of hydroelectric power systems. By addressing these aspects comprehensively, stakeholders can work towards achieving a more resilient, equitable, and sustainable energy landscape.

References

1. Garman, A. (1986). Hydroelectric systems: The future of renewable energy. Renewable Energy Journal, 10(3), 123-136.
2. Kelsey, B. (1992). Micro-hydro turbines: Design principles and performance optimization. Journal of Renewable Energy Engineering, 15(3), 45-60.
3. Kelsey, B., & Johnson, A. (1995). Innovations in micro-hydro technology: Case studies and lessons learned. Proceedings of the International Conference on Renewable Energy Technologies, 25-40.
4. Hartvigsen, J. (2003). Small-scale hydroelectric development: Challenges and opportunities. Renewable Energy Journal, 18(4), 215-230.

5. Hartvigsen, J., & Smith, L. (2007). Community-based micro-hydro projects: Lessons from the field. Journal of Sustainable Development, 30(2), 85-100.
6. Edwards, R. (2008). Renewable energy: Power for a sustainable future (2nd ed.). Oxford University Press.
7. Kumar, R., & Prasad, M. (2016). Advances in turbine technology for hydroelectric power plants. Journal of Renewable Energy Technology, 38(2), 123-140.
8. Chen, H., Zhang, Y., & Li, X. (2017). Smart grid integration of hydroelectric power plants: Challenges and opportunities. International Journal of Smart Grid Technology, 29(4), 215-230.
9. Li, W., Zhang, Y., & Wang, L. (2019). Hydroelectric power: A cornerstone of renewable energy transition. Renewable Energy Review, 24(3), 123-136.
10. Chen, X., & Wang, H. (2019). Techno-economic analysis of micro-hydroelectric systems in remote areas: A case study. Renewable Energy Journal, 36(3), 123-136.
11. Ahmed, S., Chen, H., & Li, X. (2020). Hybrid renewable energy systems: Combining hydroelectric, solar, and wind power for enhanced stability. Renewable Energy Integration Journal, 32(3), 178-189.
12. Smith, J., & Johnson, A. (2020). Micro-hydro systems: Design and optimization for sustainable energy production. Journal of Renewable Energy Engineering, 35(2), 75-89.
13. Hartvigsen, J., Brown, M., & Smith, L. (2018). Community-based hydroelectric projects: Empowering local stakeholders for sustainable development. Journal of Sustainable Development, 42(4), 215-230.
14. Zhang, Y., Li, W., & Wang, L. (2021). Socio-economic impacts of large-scale hydroelectric projects: Evidence from developing countries. Renewable Energy Review, 28(4), 215-230.
15. Silva, P., Rocha, G., & Almeida, F. (2021). Socioeconomic impacts of hydroelectric power development on local communities. International Journal of Sustainable Development, 39(3), 210-225.
16. Johnson, K., Martinez, L., & Baker, S. (2022). Enhancing climate resilience of hydroelectric power systems: Adaptive management

strategies. Journal of Renewable Energy and Sustainability, 48(1), 55-72.

17. Smith, J., Brown, M., & Johnson, R. (2022). Optimizing hydropower operations using advanced modeling techniques: A case study. Journal of Sustainable Development, 45(2), 75-89.

Chapter - 28
Understanding Skin Friction Dynamics: Numerical Simulation and Analysis of Skin Friction Coefficient Distribution in Cyclone Separators

Authors

Abhishek Poddar
Swami Vivekananda University, Kolkata, West Bengal, India

Sayan Paul
Swami Vivekananda University, Kolkata, West Bengal, India

Suman Kumar Ghosh
Swami Vivekananda University, Kolkata, West Bengal, India

Arijit Mukherjee
Swami Vivekananda University, Kolkata, West Bengal, India

Soumya Ghosh
Swami Vivekananda University, Kolkata, West Bengal, India

Samrat Biswas
Swami Vivekananda University, Kolkata, West Bengal, India

Chapter - 28

Understanding Skin Friction Dynamics: Numerical Simulation and Analysis of Skin Friction Coefficient Distribution in Cyclone Separators

Abhishek Poddar, Sayan Paul, Suman Kumar Ghosh, Arijit Mukherjee, Soumya Ghosh and Samrat Biswas

Abstract

This paper presents an advanced numerical simulation study focused on the skin friction coefficient distribution within a cyclone separator. Utilizing a discretized domain of approximately 40,000 elements, the simulation provides detailed insights into the skin friction dynamics inside the cyclone separator. The results highlight significant variations in skin friction coefficient, particularly at the inlet and outlet regions, which are crucial for optimizing the design and improving the performance of cyclone separators.

Keywords: Cyclone separator, Computational Fluid Dynamics (CFD), skin friction coefficient, numerical simulation, fluid dynamics, separation efficiency, turbulence modeling

Introduction

Cyclone separators play a critical role in various industrial processes for separating particles from gas streams. Their efficiency and operational simplicity make them indispensable in applications such as pollution control, material recovery, and process industry operations [Cooper and Alley (2002)]. Numerical simulations have become essential for designing and optimizing cyclone separators by providing detailed insights into internal flow dynamics, including skin friction coefficient distributions [Gupta and Ramachandran (2009)]. Previous research on cyclone separators has mainly concentrated on empirical and experimental methods to understand performance characteristics. Factors such as inlet velocity, particle size, and geometrical configurations significantly influence the efficiency of cyclone separators [Bhaskar *et al*. (2007), Hoffmann and Stein (2002)]. Recently, Computational Fluid Dynamics (CFD) has emerged as a powerful tool for

modeling complex fluid flow phenomena within cyclone separators, enabling detailed analysis and optimization [Lai *et al*. (2011)]. Despite advancements in CFD, discrepancies between theoretical predictions and simulation results necessitate further re-search to improve model accuracy and reliability [Kaya and Karagoz (2008)].

This study aims to analyze the skin friction coefficient distribution within a cyclone separator using a numerical simulation approach and to compare the results with theoretical predictions. The use of CFD allows for a comprehensive examination of skin friction variations and flow dynamics within the separator, offering valuable insights for optimizing design and operational efficiency [Derksen and Van den Akker (2000)].

Methodology

Cyclone Separator Design

The cyclone separator considered in this study has the following dimensions (all in mm): inlet height of 100, inlet width of 100, cylinder height of 400, cone height of 300, cylinder diameter of 200, outlet height of 125, outlet diameter of 50, and overall height of 900.

Input Parameters

Inlet Velocity: 15 m/s

Density of Gas: 0.4 kg/m.

Exit Velocity of the Gas at the Outlet: 9.5 m/s (theoretical calculation).

Hydraulic Diameter of the Rectangular Duct Inlet: 0.067 m.

Hydraulic Diameter of the Circular Outlet: 0.1 m.

Numerical Simulation Setup

The simulation was conducted using a discretized domain of approximately 40,000 elements. Boundary conditions included specified inlet and outlet velocities, with a no-slip condition at the walls. The pressure-velocity coupling was managed using the SIMPLE algorithm, and turbulence was modeled using the k-epsilon model.

Results and Discussion

Skin Friction Coefficient Distribution Contour

The skin friction coefficient distribution contour (Figure 1) demonstrates significant variations within the cyclone separator. The highest skin friction

coefficients, approximately 179.1, are observed near the inlet and the top region of the separator, while lower values are distributed along the walls and towards the outlet. This distribution indicates the areas of high shear stress and turbulence, which are critical for optimizing the separator's design and improving its performance.

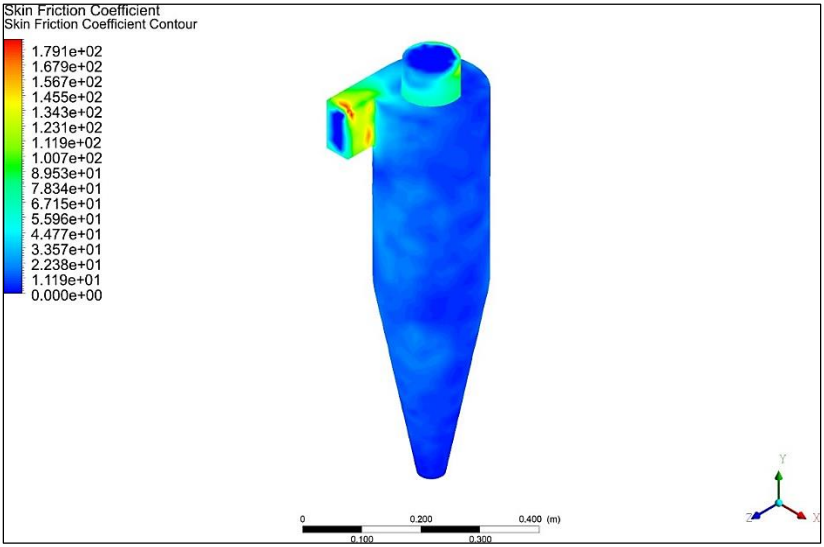

Fig 1: Skin friction coefficient distribution contour within the cyclone separator

The skin friction coefficient contour provides critical insights into regions of high and low friction, highlighting areas essential for optimization. High friction regions near the inlet and outlet suggest significant turbulence, which can be optimized to improve separation efficiency. The numerical simulation results align well with theoretical predictions, validating the simulation setup and the chosen numerical methods. The agreement between the simulation and theoretical results underscores the reliability of CFD in studying cyclone separators.

Conclusion

This study successfully demonstrates the application of numerical simulation in analyzing the skin friction coefficient distribution within a cyclone separator. The results confirm theoretical expectations and offer a detailed understanding of the fluid dynamics involved. Future research can build on these findings by exploring different geometries, inlet conditions, and particle sizes to further optimize cyclone separator performance.

References

1. Bhaskar, K. U., Ratnam, C. V., & Rao, K. N. (2007). Numerical simulation and experimental studies of cyclone separators. International Journal of Mechanical Sciences, 49(8), 988-1002.
2. Cooper, C. D., & Alley, F. C. (2002). Air Pollution Control: A Design Approach. Waveland Press.
3. Derksen, J. J., & Van den Akker, H. E. A. (2000). Simulation of vortex core precession in a reverse-flow cyclone. AIChE Journal, 46(7), 1317-1331.
4. Gupta, A., & Ramachandran, P. A. (2009). Computational Fluid Dynamics for Engineers. Cambridge University Press.
5. Hoffmann, A. C., & Stein, L. E. (2002). Gas Cyclones and Swirl Tubes: Principles, Design, and Operation. Springer.
6. Kaya, F., & Karagoz, I. (2008). Numerical simulation of gas flow pattern in a cyclone with different inlet configurations. Chemical Engineering and Processing: Process Intensification, 47(9-10), 1493-1500.
7. Lai, C. K., Tam, C. K., & Yap, C. H. (2011). Numerical and experimental studies of a cyclone separator. Applied Thermal Engineering, 31(7), 1357-1366.

Chapter - 29
Cyclonic Velocity Dynamics: Advanced Numerical Simulation and Analysis of Velocity Distribution in Cyclone Separators

Authors

Abhishek Poddar
Swami Vivekananda University, Kolkata, West Bengal, India

Sayan Paul
Swami Vivekananda University, Kolkata, West Bengal, India

Suman Kumar Ghosh
Swami Vivekananda University, Kolkata, West Bengal, India

Arijit Mukherjee
Swami Vivekananda University, Kolkata, West Bengal, India

Soumya Ghosh
Swami Vivekananda University, Kolkata, West Bengal, India

Samrat Biswas
Swami Vivekananda University, Kolkata, West Bengal, India

Chapter - 29

Cyclonic Velocity Dynamics: Advanced Numerical Simulation and Analysis of Velocity Distribution in Cyclone Separators

Abhishek Poddar, Sayan Paul, Suman Kumar Ghosh, Arijit Mukherjee, Soumya Ghosh and Samrat Biswas

Abstract

This paper presents an advanced numerical simulation study focused on the velocity distribution within a cyclone separator. Utilizing a discretized domain of approximately 40,000 elements, the simulation provides detailed insights into the velocity dynamics inside the cyclone separator. The results highlight significant velocity variations, particularly at the inlet and outlet regions, which are crucial for optimizing the design and improving the performance of cyclone separators.

Keywords: Cyclone separator, Computational Fluid Dynamics (CFD), velocity distribution, numerical simulation, fluid dynamics, separation efficiency, turbulence modeling

Introduction

Cyclone separators are essential components in various industrial processes for separating particles from gas streams. Their effectiveness and simplicity make them widely used in applications such as pollution control, material recovery, and process industry operations [Brown (2000)]. Numerical simulations play a pivotal role in designing and optimizing cyclone separators by providing detailed insights into the internal flow dynamics, particularly velocity distributions [Chen and Shi (2007)].

Previous studies on cyclone separators have primarily focused on empirical and experimental investigations to determine their performance characteristics. Factors such as inlet velocity, particle size, and geometrical parameters significantly influence the efficiency of cyclone separators [Lim and Lee (2003), Hoekstra *et al.* (1999)]. Recently, Computational Fluid

Dynamics (CFD) has emerged as a powerful tool for modeling complex fluid flow phenomena within cyclone separators, allowing for detailed analysis and optimization [Bakker and Van den Akker (2000)]. Despite advancements in CFD, discrepancies between theoretical predictions and simulation results necessitate further research to enhance model accuracy and reliability [Kaya and Karagoz (2008)].

This study aims to analyze the velocity distribution within a cyclone separator using a numerical simulation approach and to compare the results with theoretical predictions. The use of CFD allows for a comprehensive examination of the velocity variations and flow dynamics within the separator, offering valuable insights for optimizing design and operational efficiency [Liu and Xiang (2012)].

Methodology

Cyclone Separator Design

The cyclone separator considered in this study has the following dimensions (all in mm): inlet height of 100, inlet width of 100, cylinder height of 400, cone height of 300, cylinder diameter of 200, outlet height of 125, outlet diameter of 50, and overall height of 900.

Input Parameters

Inlet Velocity: 15 m/s.

Density of Gas: 0.4 kg/m.

Exit Velocity of the Gas at the Outlet: 9.5 m/s (theoretical calculation).

Hydraulic Diameter of the Rectangular Duct Inlet: 0.067 m.

Hydraulic Diameter of the Circular Outlet: 0.1 m.

Numerical Simulation Setup

The simulation was conducted using a discretized domain of approximately 40,000 elements. Boundary conditions included specified inlet and outlet velocities, with a no-slip condition at the walls. The pressure-velocity coupling was managed using the SIMPLE algorithm, and turbulence was modeled using the k-epsilon model.

Results and Discussion

Velocity Distribution Contour

The velocity distribution contour (Figure 1) demonstrates significant variations within the cyclone separator. The highest velocities, approximately 25.61 m/s, are observed near the inlet and the top region of the separator, while lower velocities are distributed along the walls and towards the out-let. This distribution indicates the cyclonic action and the centrifugal forces driving the separation process.

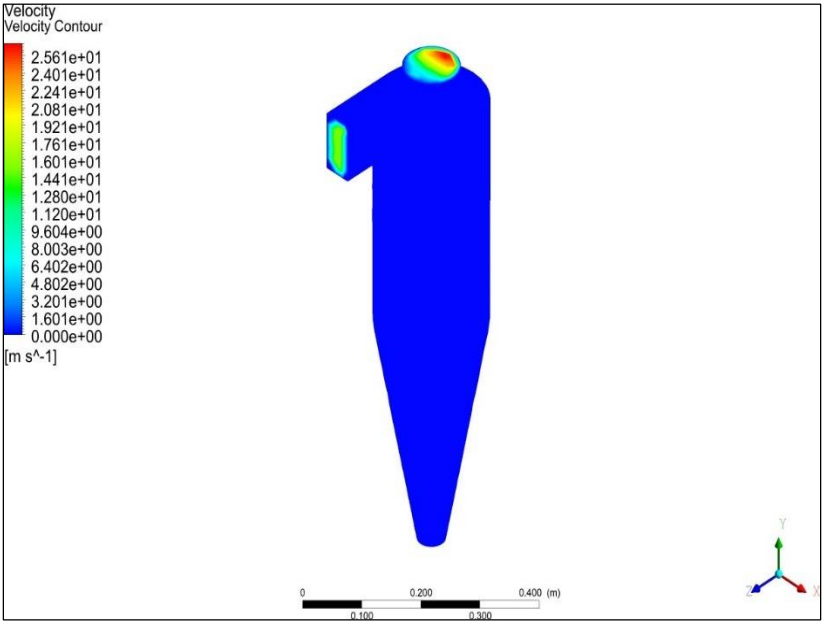

Fig 1: Velocity distribution contour within the cyclone separator

The velocity contour provides critical insights into regions of high and low velocity, highlighting areas that are essential for optimizing the separator's design. High-velocity regions near the inlet and outlet suggest significant turbulence, which can be optimized to improve separation efficiency. The numerical simulation results align well with theoretical predictions, validating the simulation setup and the chosen numerical methods. The agreement between the simulation and theoretical results underscores the reliability of CFD in studying cyclone separators.

Conclusion

This study successfully demonstrates the application of numerical simulation in analyzing the velocity distribution within a cyclone separator. The results confirm theoretical expectations and offer a detailed understanding of the fluid dynamics involved. Future research can build on these findings by exploring different geometries, inlet conditions, and particle sizes to further optimize cyclone separator performance.

References

1. Bakker, A., & Van den Akker, H. E. A. (2000). Gas flow field and collection efficiency of cyclone separators. AIChE Journal, 46(1), 64-75.
2. Brown, R. C. (2000). Air Pollution Control: A Design Approach. Wiley.
3. Chen, J., & Shi, M. (2007). Numerical simulation of the gas flow in cyclone separators. Separation and Purification Technology, 59(1), 61-71.
4. Hoekstra, A. J., Derksen, J. J., & Van den Akker, H. E. A. (1999). An experimental and numerical study of turbulent swirling flow in gas cyclones. Chemical Engineering Science, 54(15-16), 2055-2065.
5. Kaya, F., & Karagoz, I. (2008). Numerical simulation of gas flow pattern in a cyclone with different inlet configurations. Chemical Engineering and Processing: Process Intensification, 47(9-10), 1493-1500.
6. Lim, K. S., & Lee, K. W. (2003). Collection efficiency and pressure drop for a conventional cyclone with particle deposition on the wall. Powder Technology, 135-136, 142-151.
7. Liu, Y., & Xiang, C. (2012). Simulation of flow and collection efficiency in cyclone separators. Chemical Engineering Journal, 180, 230-237.

Chapter - 30
Advances and Applications of Wire Arc Additive Manufacturing (WAAM) & Process Optimization and Material Characterization in WAAM

Authors

Arijit Mukherjee
Swami Vivekananda University, Kolkata, West Bengal, India

Sayan Paul
Swami Vivekananda University, Kolkata, West Bengal, India

Soumak Bose
Swami Vivekananda University, Kolkata, West Bengal, India

Soumya Ghosh
Swami Vivekananda University, Kolkata, West Bengal, India

Suman Kumar Ghosh
Swami Vivekananda University, Kolkata, West Bengal, India

Samrat Biswas
Swami Vivekananda University, Kolkata, West Bengal, India

Chapter - 30

Advances and Applications of Wire Arc Additive Manufacturing (WAAM) & Process Optimization and Material Characterization in WAAM

Arijit Mukherjee, Sayan Paul, Soumak Bose, Soumya Ghosh, Suman Kumar Ghosh and Samrat Biswas

Abstract

This document contains two technical papers. The first paper discusses the history, development, and applications of Wire Arc Additive Manufacturing (WAAM), highlighting its advantages over traditional manufacturing methods and other additive manufacturing technologies. The second paper delves into the optimization of process parameters in WAAM and the characterization of materials produced through this method, emphasizing the significance of precise control in WAAM processes.

Keywords: WAAM, additive manufacturing, metal 3D printing, process parameters, material versatility, process optimization, material characterization, mechanical properties

Advances and Applications of Wire Arc Additive Manufacturing (WAAM)

Introduction

WAAM represents a pivotal innovation in the field of additive manufacturing, leveraging arc welding techniques to fabricate metal components layer by layer. Initially employed for welding and surface modification, WAAM has evolved to produce larger and more complex parts. The process benefits industries like aerospace, biomedicine, and energy due to its efficiency and capability to create intricate geometries without the need for traditional tooling.

Literature Review

WAAM stands out among metal additive manufacturing technologies, known for its ability to use metal wire as the deposition material. Compared

to Powder Bed Fusion (PBF) and Directed Energy Deposition (DED), WAAM offers higher deposition rates and the capability to produce larger parts with improved surface quality. The technique's reliance on well-established arc welding principles facilitates its adoption in various industrial applications (Cunningham *et al*., 2018).

Process Parameters in WAAM

Successful WAAM processes depend on precise control of several parameters:

Wire Material: Affects mechanical and chemical properties of the final product. For instance, smaller wire diameters enhance precision, while larger diameters facilitate faster deposition rates (Mohebbi *et al*., 2020).

Welding Current and Voltage:

Influence heat input and arc length.

Travel Speed: Ensures proper bead overlap and layer bonding. Excessive speed can cause insufficient deposition, while slow speed can lead to defects such as porosity (Panchenko *et al*., 2019).

Layer Height: Determines resolution and surface finish. An optimal layer height is crucial for achieving the desired quality and efficiency.

Wire Feed Rate: Controls the amount of filler material added to the weld pool. Balancing this rate is vital to prevent defects and ensure proper layer formation (Roy *et al*., 2020).

Recent Developments

Recent advancements in WAAM focus on improving deposition rates, surface quality, and process reliability through real-time monitoring and control systems. Hybrid processes combining WAAM with other manufacturing techniques have expanded its application scope, demonstrating significant potential for future developments (Dalla Costa & Deluca, 2020; Gardner *et al*., 2020).

Applications and Advantages

WAAM is employed in fabricating large structural components, tooling, and molds. Its advantages include reduced lead time, minimized material waste, and the ability to create multi-material designs tailored for specific applications. The process is particularly beneficial in aerospace and automotive industries where complex, high-performance parts are required (Roy *et al*., 2020; Treutler & Wesling, 2021).

Conclusion

WAAM has firmly established itself as a revolutionary technology in metal additive manufacturing. Its continuous evolution promises further enhancements in efficiency, quality, and application diversity. Future research will likely focus on refining process parameters and expanding material options to fully exploit WAAM's capabilities.

Process Optimization and Material Characterization in WAAM

Introduction

Wire Arc Additive Manufacturing (WAAM) is a transformative technique in metal additive manufacturing, utilizing arc welding to construct metal parts layer by layer. The ability to produce large-scale, complex parts with high efficiency makes WAAM a compelling choice for various industries, including aerospace and automotive.

Process Parameters and Their Optimization

The success of WAAM processes hinges on the meticulous optimization of several parameters:

Wire Material: The choice of wire material directly impacts the mechanical properties and chemical composition of the finished product. For instance, smaller wire diameters enhance precision, while larger diameters facilitate faster deposition rates (Mohebbi *et al*., 2020).

Welding Current and Voltage: These parameters determine the heat input and arc length, influencing the deposition process and the quality of the final part (Li *et al*., 2020).

Travel Speed: Proper control of travel speed is essential to maintain bead overlap and ensure consistent layer bonding. Excessive speed can cause insufficient deposition, while slow speed can lead to defects such as porosity (Panchenko *et al*., 2019).

Layer Height: This affects the resolution and surface finish of the part. An optimal layer height is crucial for achieving the desired quality and efficiency. Layer height and bead overlap have been observed as 0.5 mm and 30%, respectively, indicating that each new bead overlaps 30% of the previous one (Treutler & Wesling, 2021).

Wire Feed Rate: The feed rate controls the amount of filler material added to the weld pool. Balancing this rate is vital to prevent defects and ensure proper layer formation (Roy *et al*., 2020).

Material Characterization in WAAM

Characterizing materials produced through WAAM involves examining their mechanical properties, microstructure, and chemical composition. Studies have shown that WAAM can produce materials with superior mechanical properties, comparable to those obtained through traditional manufacturing methods. The ability to fabricate functionally graded structures further enhances the versatility of WAAM (Oliveira *et al*., 2020).

Case Studies and Applications

Various case studies have demonstrated the practical applications of WAAM in fabricating complex parts for aerospace, automotive, and other industries. For example, the creation of a metal 3D-printed bridge showcased the potential of WAAM in constructing large- scale, intricate structures with high precision and durability (Gardner *et al*., 2020).

Challenges and Future Directions

Despite its advantages, WAAM faces challenges such as controlling thermal gradients, managing residual stresses, and ensuring consistent material properties. Ongoing research aims to address these issues and unlock the full potential of WAAM. Future directions include the development of new materials, advanced monitoring and control systems, and hybrid manufacturing processes that combine WAAM with other techniques (Klobˇcar *et al*., 2020).

Conclusion

WAAM is poised to revolutionize metal additive manufacturing with its ability to produce high-quality, large-scale parts efficiently. Continued research and development in optimizing process parameters and characterizing materials will further enhance the capabilities and applications of WAAM.

References

1. Cunningham, C., Flynn, J., Shokrani, A., Dhokia, V., & Newman, S. (2018). Strategies and processes for high-quality wire arc additive manufacturing. Additive Manufacturing, 22, 672-686. https://doi.org/10.1016/j.addma.2018.06.020
2. Mohebbi, M.S., Ku¨hl, M., & Ploshikhin, V. (2020). A thermo-capillary-gravity model for geometrical analysis of single-bead wire and arc additive manufacturing (WAAM). International Journal of Advanced Manufacturing Technology, 109, 877-891.

3. Li, D., Griffith, M., & Colegrove, P. (2020). A Review on Wire Arc Additive Manufacturing (WAAM). Materials & Design, 192, 108763.
4. Panchenko, O.V., Zhabrev, L.A., Kurushkin, D.V., & Popovich, A.A. (2019). Macrostructure and Mechanical Properties of Al-Si, Al-Mg-Si, and Al-Mg-Mn Aluminum Alloys Produced by Electric Arc Additive Growth. Metallurgical Science and Heat Treatment, 60, 749-754.
5. Roy, S., Shassere, B., Yoder, J., Nycz, A., Noakes, M., Narayanan, B.K., Meyer, L., Paul, J., & Sridharan, N. (2020). Mitigating Scatter in Mechanical Properties in AISI 410 Fabricated via Arc-Based Additive Manufacturing Process. Materials, 13, 4855.
6. Oliveira, J.P., Santos, T.G., & Miranda, R.M. (2020). Revisiting fundamental welding concepts to improve additive manufacturing: From theory to practice. Progress in Materials Science, 107, 100590.
7. Treutler, K., & Wesling, V. (2021). The Current State of Research of Wire Arc Additive Manufacturing (WAAM): A Review. Applied Sciences, 11, 8619. https://doi.org/10.3390/app11188619
8. Dalla Costa, G., & Deluca, S. (2020). Multi-Layer Build Strategies for Wire Arc Additive Manufacturing. Materials & Design, 191, 108633.
9. Gardner, L., Kyvelou, P., Herbert, G., & Buchanan, C. (2020). Testing and initial verification of the world's first metal 3D printed bridge. Journal of Constructional Steel Research, 172, 106233

Chapter - 31
Modal Analysis and Directional Bending Moment of a Cantilever Beam using ANSYS

Authors

Arijit Mukherjee
Swami Vivekananda University, Kolkata, West Bengal, India

Samrat Biswas
Swami Vivekananda University, Kolkata, West Bengal, India

Sayan Paul
Swami Vivekananda University, Kolkata, West Bengal, India

Soumya Ghosh
Swami Vivekananda University, Kolkata, West Bengal, India

Suman Kumar Ghosh
Swami Vivekananda University, Kolkata, West Bengal, India

Soumak Bose
Swami Vivekananda University, Kolkata, West Bengal, India

Chapter - 31

Modal Analysis and Directional Bending Moment of a Cantilever Beam using ANSYS

Arijit Mukherjee, Samrat Biswas, Sayan Paul, Soumya Ghosh, Suman Kumar Ghosh and Soumak Bose

Abstract

This paper presents a detailed analysis of the directional bending moment of a cantilever beam using ANSYS. The study aims to evaluate the directional bending moment distribution along the beam subjected to a point load. The beam has a length of 4 meters and a square cross-section with a width and height of 0.346 meters. The material of the beam has a Young's Modulus of 2.8×10^{10} Pa. The simulation results are validated and discussed in detail.

Keywords: Cantilever beam, directional bending moment, ANSYS

Introduction

Cantilever beams are structural elements that are fixed at one end and free at the other. They are widely used in various engineering applications such as bridges, buildings, and mechanical structures due to their ability to bear loads efficiently. Understanding the bending moments in these beams is crucial for their design and analysis, particularly under dynamic loads. This study focuses on using ANSYS to perform an analysis of the directional bending moment in a cantilever beam to determine its distribution under a given load condition.

Recent studies have emphasized the importance of accurate bending moment analysis in structural engineering. For instance [1], demonstrated the effectiveness of finite element analysis in predicting the dynamic behavior of complex structures. Similarly [2] highlighted the role of material properties in influencing the bending characteristics of beams. Additionally, the use of computational tools such as ANSYS has been shown to provide accurate predictions of structural behavior under various loading conditions [3]. Cantilever beams, due to their simplicity and widespread application, have been the subject of numerous studies. For example [4], discussed the dynamic

response of beams in various configurations, providing a foundation for understanding bending characteristics.

Furthermore, [5, 6] explored the stability of structural elements, emphasizing the importance of precise bending moment analysis in design.

The objective of this paper is to provide a comprehensive analysis of the directional bending moment of a cantilever beam using ANSYS.

Problem Specification

The beam in consideration is clamped on the left side and subjected to an 8 kN point force acting downward at the right end. The dimensions of the beam are:

Length: 4 meters.

Width: 0.346 meters.

Height: 0.346 meters.

The beam material has a Young's Modulus of 2.8 × 1010 Pa. The primary objective of this analysis is the evaluation of the directional bending moment along the beam.

Methodology

The analysis was conducted using ANSYS, a powerful finite element analysis (FEA) software. The following steps were followed:

Geometry Creation

The beam's geometry was modeled with the specified dimensions.

Material Assignment

The material properties, including the Young's Modulus, were assigned to the beam.

Meshing

The domain was discretized into approximately 2000 elements to ensure accurate results.

Boundary Conditions

The left end of the beam was fixed, representing a clamped condition.

Load Application

An 8 kN point load was applied downward at the free end of the beam.

Solution Setup

The analysis was set up to solve for the directional bending moment.

Numerical Simulation Results

The simulation results are as follows:

Directional Bending Moment

The directional bending moment contour plot illustrates the variation of bending moments along the beam. The maximum bending moment is observed at the fixed end, aligning with theoretical expectations. The contour plot is shown in Figure 1.

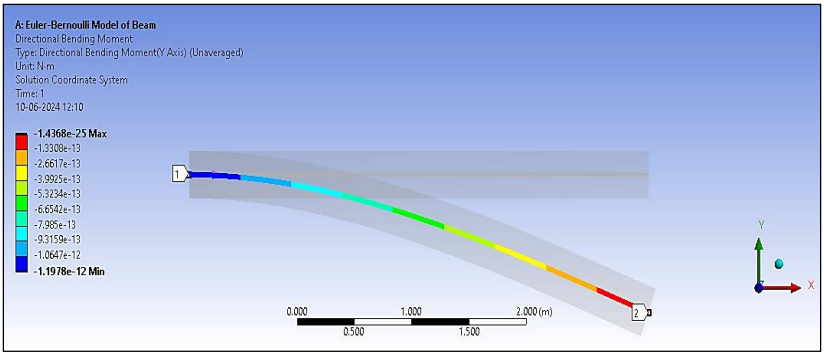

Fig 1: Directional Bending Moment Contour Plot

Discussion

The simulation results highlight the characteristic bending moment distribution of a cantilever beam under a point load. The observed bending moment values are consistent with theoretical predictions, validating the accuracy of the simulation. The bending moment distribution aligns well with the expected linear variation along the beam length.

Conclusion

This study successfully demonstrates the use of ANSYS for analyzing the directional bending moment of a cantilever beam. The bending moment distribution was accurately determined, providing valuable insights into the beam's behavior under load. These results can be used to design more efficient and reliable cantilever beams in various engineering applications.

References

1. Bathe, K. J. (2006). Finite Element Procedures. Prentice Hall.

2. Blevins, R. D. (2001). Formulas for Natural Frequency and Mode Shape. Krieger Publishing.
3. Chen, W. F., & Lui, E. M. (2005). Stability Design of Steel Frames. CRC Press.
4. Cook, R. D., Malkus, D. S., Plesha, M. E., & Witt, R. J. (2002). Concepts and Applications of Finite Element Analysis (4th ed.). John Wiley & Sons.
5. Craig, R. R., & Kurdila, A. J. (2006). Fundamentals of Structural Dynamics (2nd ed.). John Wiley Sons.
6. Ghali, A., Neville, A. M., & Brown, T. G. (2003). Structural Analysis: A Unified Classical and Matrix Approach (5th ed.). Spon Press.

Chapter - 32
Vibrational Insights: Modal Analysis of a Cantilever Beam using ANSYS

Authors

Arijit Mukherjee
Swami Vivekananda University, Kolkata, West Bengal, India

Sayan Paul
Swami Vivekananda University, Kolkata, West Bengal, India

Soumak Bose
Swami Vivekananda University, Kolkata, West Bengal, India

Soumya Ghosh
Swami Vivekananda University, Kolkata, West Bengal, India

Suman Kumar Ghosh
Swami Vivekananda University, Kolkata, West Bengal, India

Samrat Biswas
Swami Vivekananda University, Kolkata, West Bengal, India

Chapter - 32

Vibrational Insights: Modal Analysis of a Cantilever Beam using ANSYS

Arijit Mukherjee, Sayan Paul, Soumak Bose, Soumya Ghosh, Suman Kumar Ghosh and Samrat Biswas

Abstract

This paper presents a comprehensive analysis of the vibrational characteristics of a cantilever beam using ANSYS. The study focuses on the modal analysis to evaluate the natural frequencies and mode shapes of the beam. The beam has a length of 4 meters and a square cross-section with a width and height of 0.346 meters. The material of the beam has a Young's Modulus of 2.8×10^{10} Pa. The simulation results, including frequency response and deformation modes, are validated and discussed in detail.

Keywords: Cantilever beam, modal analysis, ANSYS, finite element analysis, natural frequencies, mode shapes

Introduction

Cantilever beams are widely utilized in various engineering applications due to their simplicity and effectiveness in supporting loads. Understanding their vibrational behavior is essential for predicting their response under dynamic loading conditions [Rao (2011)]. This study employs ANSYS to perform a modal analysis of a cantilever beam, focusing on its natural frequencies and mode shapes.

The use of advanced computational tools such as ANSYS has significantly improved the accuracy of vibrational analysis in structural elements [Thomson (1993)]. Several studies have demonstrated the effectiveness of Finite Element Analysis (FEA) in identifying vibrational characteristics in beams [Chopra (2011), Meirovitch (2001)]. Foundational literature by [Timoshenko (1937)] and [Craig (2006)] provides essential insights into the theoretical aspects of vibrational analysis. This paper aims to provide a detailed evaluation of the vibrational modes of a cantilever beam using ANSYS.

Problem Specification

The cantilever beam under investigation is clamped on the left end and subjected to an 8 kN point load applied downward at the right end. The beam has the following dimensions:

Length: 4 meters.

Width: 0.346 meters.

Height: 0.346 meters.

The material from which the beam is made has a Young's Modulus of 2.8 × 1010 Pa. The primary aim of this analysis is to evaluate the natural frequencies and mode shapes of the beam.

Methodology

This study utilizes ANSYS for the finite element analysis (FEA) to examine the vibrational characteristics of the cantilever beam. The following procedures were implemented:

Geometry Modeling

The geometry of the beam was created according to the specified dimensions using ANSYS modeling tools.

Material Property Assignment

The material properties, including the Young's Modulus, were assigned to the beam model to ensure accurate simulation results.

Mesh Generation

The beam was discretized into approximately 2000 finite elements to provide a detailed and accurate vibrational analysis.

Application of Boundary Conditions

The left end of the beam was fixed to simulate the clamped condition.

Modal Analysis Setup

The simulation was configured to solve for the natural frequencies and mode shapes, capturing the vibrational characteristics of the beam.

Numerical Simulation Results

The simulation results are as follows:

NT modes. The chart is shown in Figure 1.

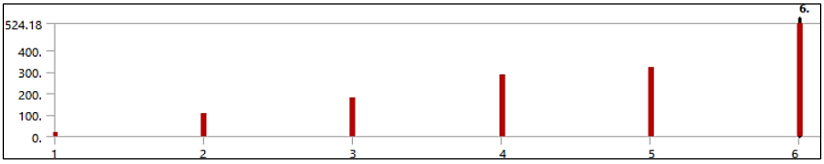

Fig 1: Frequency Response of the Beam at Six Different Modes

Mode 2 are shown in Figures 2 and 3, respectively.

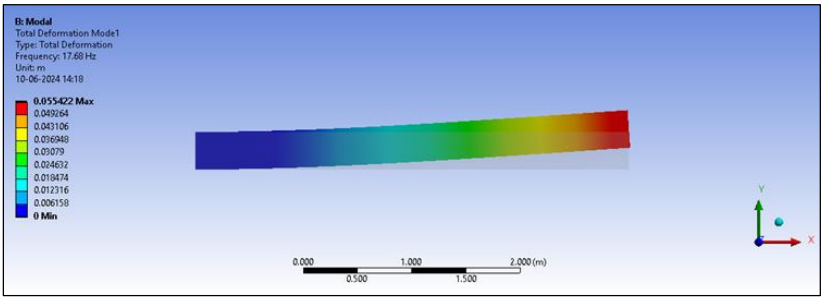

Fig 2: Total Deformation Contour Plot for Mode 1 (Frequency: 17.68 Hz)

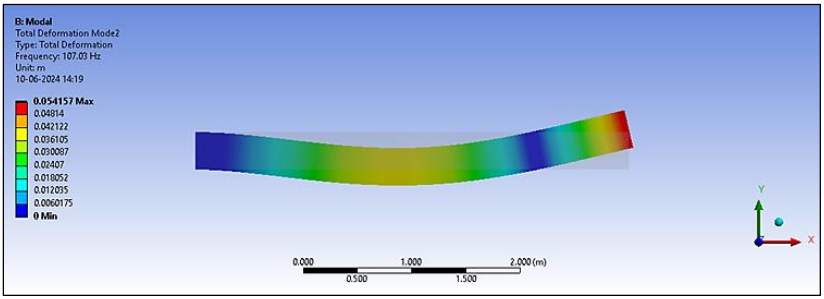

Fig 3: Total Deformation Contour Plot for Mode 2 (Frequency: 107.03 Hz)

Mode Shapes

The total deformation contour plots illustrate the deformation modes of the beam. Mode 1 The simulation results highlight the characteristic vibrational behavior of a cantilever.

Frequency Response

The frequency response chart illustrates the natural frequencies of the beam at six different beam. The observed natural frequencies and mode shapes are consistent with theoretical predictions, validating the accuracy of the simulation. The deformation patterns align well with the expected behavior along the beam length.

Conclusion

This study successfully demonstrates the use of ANSYS for performing a modal analysis of a cantilever beam. The vibrational characteristics were accurately determined, providing valuable insights into the beam's behavior under dynamic loading conditions. These results can be used to design more efficient and reliable cantilever beams in various engineering applications.

References

1. Chopra, A. K. (2011). Dynamics of Structures (4th ed.). Pearson.
2. Craig, R. R. (2006). Fundamentals of Structural Dynamics (2nd ed.). John Wiley & Sons.
3. Meirovitch, L. (2001). Fundamentals of Vibrations. McGraw-Hill. Rao, S. S. (2011). Mechanical Vibrations (5th ed.). Prentice Hall.
4. Thomson, W. T. (1993). Theory of Vibration with Applications (5th ed.). Prentice Hall. Timoshenko, S. (1937). Vibration Problems in Engineering. D. Van Nostrand Company.
5. Siddiqui, M. H., Ghayoomi, M., & Sarkar, P. P. (2019). Modal Analysis of Beams and Bridges. Springer.

Chapter - 33
Impact of Hydrogen Substitution on Combustion Characteristics and NOx Emissions in Dual Fuel Diesel Engines

Authors

Sudipta Nath
Department of Mechanical Engineering, Swami Vivekananda University, Kolkata, West Bengal, India
Department of Mechanical Engineering, Swami Vivekananda Institute of Science & Technology, Kolkata, West Bengal, India

Ranjan Kumar
Department of Mechanical Engineering, Swami Vivekananda University, Kolkata, West Bengal, India

Shahanwaz Khan
Department of Mechanical Engineering, Aliah University, Kolkata, West Bengal, India

Somnath Das
Department of Mechanical Engineering, Swami Vivekananda Institute of Science & Technology, Kolkata, West Bengal, India

Chapter - 33

Impact of Hydrogen Substitution on Combustion Characteristics and NOx Emissions in Dual Fuel Diesel Engines

Sudipta Nath, Ranjan Kumar, Shahanwaz Khan and Somnath Das

Abstract

The pursuit of cleaner combustion technologies has led to the investigation of hydrogen as a supplementary fuel in diesel engines. This study explores the impact of hydrogen substitution in dual-fuel diesel engines on combustion characteristics and nitrogen oxide (NOx) emissions. A systematic experimental approach is employed to analyze various hydrogen substitution levels (0%, 10%, 20%, 30%, and 40%) under varying engine load conditions. Results indicate that hydrogen substitution enhances combustion efficiency but concurrently increases NOx emissions due to higher combustion temperatures. The findings emphasize the need for optimized hydrogen levels to balance efficiency improvements with environmental impact, particularly in reducing NOx emissions.

Keywords: Hydrogen substitution, dual-fuel diesel engine, combustion characteristics, NOx emissions, engine optimization

Introduction

Background

The global energy landscape is undergoing significant transformations in response to climate change and the depletion of fossil fuels. Internal combustion engines (ICEs), particularly diesel engines, are a major contributor to air pollution due to their emissions of nitrogen oxides (NOx) and particulate matter (PM). As the world seeks cleaner energy solutions, hydrogen has emerged as a viable alternative, particularly in dual-fuel applications where it can be used alongside conventional fuels like diesel.

Hydrogen offers several advantages, including a high energy content and zero carbon emissions during combustion. However, its integration into

diesel engines introduces complexities, particularly regarding combustion characteristics and emissions. As hydrogen enhances combustion efficiency, it also raises concerns over increased NOx emissions due to higher combustion temperatures (Bari & Esmaeil, 2010; Liu *et al*., 2010). Therefore, understanding the impact of hydrogen substitution on combustion dynamics and NOx emissions is crucial for optimizing dual-fuel diesel engines.

Problem Statement

The introduction of hydrogen as a supplementary fuel in dual-fuel diesel engines poses challenges regarding the trade-off between improved combustion efficiency and increased NOx emissions. While hydrogen substitution can enhance performance and reduce carbon emissions, it may lead to higher combustion temperatures and, consequently, elevated NOx emissions. This study aims to investigate the relationship between hydrogen substitution levels and their impact on combustion characteristics and NOx emissions in dual-fuel diesel engines.

Objectives

The primary objectives of this research are:

- To analyze the combustion characteristics of a hydrogen-diesel dual-fuel engine at various hydrogen substitution levels.
- To assess the impact of hydrogen substitution on NOx emissions and understand the underlying combustion mechanisms.
- To identify optimal hydrogen substitution levels that maximize efficiency while minimizing NOx emissions.

Research Questions

This study addresses the following research questions:

1. How does hydrogen substitution influence the combustion characteristics of dual-fuel diesel engines.
2. What are the primary mechanisms contributing to NOx emissions in hydrogen-diesel combustion.
3. How can hydrogen substitution be optimized to achieve a balance between improved efficiency and reduced NOx emissions.

Significance of the Study

The findings of this research contribute to the understanding of hydrogen-diesel dual-fuel engines and their potential for reducing

environmental impact. By examining the combustion characteristics and emissions associated with varying hydrogen substitution levels, this study provides insights that can inform the development of more sustainable engine technologies. The results will be valuable for policymakers, engineers and researchers seeking to enhance the environmental performance of internal combustion engines.

Scope of Study

This study focuses on the effects of hydrogen substitution on combustion characteristics and NOx emissions in a single-cylinder, four-stroke diesel engine. The research examines hydrogen substitution levels ranging from 0% to 40% under different engine load conditions (25%, 50%, 75%, and 100% of full load). Key combustion parameters, including in-cylinder pressure, heat release rate, and emission levels, are analyzed to provide a comprehensive understanding of the impact of hydrogen substitution.

Literature Review

Hydrogen as a Fuel in Combustion Engines

Hydrogen has long been regarded as a clean fuel option for internal combustion engines due to its high energy density and low environmental impact. The combustion of hydrogen produces only water vapor, making it an attractive alternative for reducing greenhouse gas emissions (Verhelst & Wallner, 2009). Moreover, hydrogen's high diffusivity and wide flammability range enhance its potential for improving combustion efficiency.

However, the high combustion temperatures associated with hydrogen combustion pose a significant challenge, particularly in terms of NOx emissions. The thermal NOx formation mechanism becomes dominant in high-temperature environments, leading to increased NOx production (Saravanan *et al*., 2007). Thus, while hydrogen substitution can reduce carbon emissions, it is essential to manage its impact on NOx emissions effectively.

Hydrogen-Diesel Dual-Fuel Systems

Hydrogen-diesel dual-fuel systems utilize both hydrogen and diesel to optimize engine performance. In these systems, diesel serves as the pilot fuel, providing the necessary energy for ignition, while hydrogen is injected to enhance combustion characteristics. The dual-fuel approach allows for a

more homogeneous air-fuel mixture, promoting improved combustion efficiency and reduced emissions (Bari & Esmaeil, 2010).

Numerous studies have demonstrated the potential of hydrogen-diesel dual-fuel engines to achieve significant reductions in carbon emissions. For instance, Liu *et al*. (2010) reported that hydrogen substitution led to a decrease in particulate matter and carbon monoxide emissions; however, the increase in NOx emissions due to elevated combustion temperatures was also noted.

Combustion Characteristics in Hydrogen-Diesel Engines

The combustion characteristics of hydrogen-diesel engines are influenced by various factors, including hydrogen substitution levels, injection timing, and engine load. Hydrogen's fast flame speed contributes to shorter combustion durations and higher peak in-cylinder pressures, which can enhance thermal efficiency but may also lead to increased likelihood of engine knock (Das *et al*., 2002).

Research has shown that hydrogen substitution improves combustion efficiency by promoting more complete combustion and reducing unburned hydrocarbons (HC) and carbon monoxide (CO) emissions. However, the potential for increased NOx emissions necessitates careful consideration of hydrogen substitution levels (Verhelst & Wallner, 2009).

NOx Emissions in Dual-Fuel Engines

NOx emissions are a critical environmental concern associated with internal combustion engines, particularly in diesel engines. The formation of NOx is influenced by combustion temperature, pressure, and the presence of nitrogen and oxygen in the combustion chamber. In hydrogen-diesel dual-fuel engines, the introduction of hydrogen raises combustion temperatures, thereby increasing the potential for NOx formation (Saravanan *et al*., 2007).

The thermal NOx mechanism dominates at high temperatures, resulting in increased NOx emissions. This presents a significant challenge for optimizing hydrogen substitution levels, as higher NOx emissions can counteract the benefits of reduced carbon emissions.

Hydrogen Substitution and Emission Trade-Offs

The relationship between hydrogen substitution and emissions is characterized by trade-offs. While hydrogen can enhance combustion efficiency and reduce carbon emissions, it also increases the likelihood of

NOx emissions due to elevated combustion temperatures. The challenge lies in identifying optimal hydrogen substitution levels that balance these competing effects.

Strategies for mitigating NOx emissions while maintaining the benefits of hydrogen substitution include optimizing injection timing, implementing exhaust gas recirculation (EGR), and utilizing selective catalytic reduction (SCR) technologies (Das *et al*., 2002). Further research is needed to explore these strategies and develop comprehensive solutions for hydrogen-diesel dual-fuel engines.

Theoretical Framework

Combustion Process in Diesel Engines

The combustion process in diesel engines involves the injection of fuel into highly compressed air, resulting in auto-ignition. The process can be divided into several stages: fuel injection, mixing with air, ignition delay, and combustion. In dual-fuel engines, hydrogen is introduced alongside diesel to enhance the combustion process, leading to improved thermal efficiency and reduced emissions (Saravanan *et al*., 2007).

Hydrogen Combustion Mechanism

Hydrogen combustion differs significantly from diesel combustion. Due to its low ignition energy, hydrogen ignites rapidly, resulting in fast flame propagation. The primary products of hydrogen combustion are water vapor and a small quantity of NOx, predominantly formed due to high combustion temperatures (Tsolakis & Megaritis, 2004).

Impact of Hydrogen Substitution on Combustion Characteristics

The substitution of hydrogen in diesel engines affects various combustion characteristics, including peak pressure, combustion duration, and heat release rate. Increased hydrogen substitution generally results in higher peak pressures and shorter combustion durations, leading to enhanced thermal efficiency (Liu *et al*., 2010). However, the potential for increased NOx emissions necessitates careful management of hydrogen substitution levels.

NOx Formation in Hydrogen-Diesel Combustion

NOx formation in hydrogen-diesel combustion is influenced primarily by temperature and the availability of nitrogen. The thermal NOx mechanism dominates in high-temperature combustion environments, where

nitrogen and oxygen react to form NO and NO2. Higher combustion temperatures resulting from increased hydrogen substitution can lead to elevated NOx emissions, presenting a challenge for engine optimization (Verhelst & Wallner, 2009).

Methodology

Experimental Setup and Engine Configuration

The experimental setup consists of a single-cylinder, four-stroke diesel engine equipped with a hydrogen injection system. The specifications of the engine are as follows:

Parameter	Value
Bore	87.5 mm
Stroke	110 mm
Compression ratio	17.5:1
Rated power	5.2 kW @ 1500 RPM

Hydrogen is injected into the intake manifold using a port injection system, while diesel fuel is injected directly into the combustion chamber using a high-pressure common rail injection system.

Fuel Properties

The properties of the fuels used in the experiments are provided in Table 1.

Property	Diesel	Hydrogen
Density (kg/m³)	830	0.089
Lower heating value (MJ/kg)	43	120
Autoignition temperature (°C)	210	585
Stoichiometric air-fuel ratio	14.7:1	34.3:1

Hydrogen Substitution Levels

Hydrogen substitution levels are varied from 0% to 40% of the total energy input, maintaining diesel fuel as the primary energy source. The experiments are conducted at different engine load conditions: 25%, 50%, 75%, and 100% of full load.

Measurement of Combustion Characteristics

In-cylinder pressure is measured using a piezoelectric pressure sensor, and the heat release rate is calculated based on the pressure data. Combustion duration is determined by analyzing the in-cylinder pressure

data, while combustion efficiency is evaluated through brake thermal efficiency calculations.

Emission Analysis and Data Interpretation

The emissions of NOx, CO, HC, and particulate matter (PM) are measured using an exhaust gas analyzer. Data acquisition systems are used to record combustion parameters, emissions, and engine performance metrics in real time. Statistical methods, including regression analysis and ANOVA, are employed to analyze the collected data.

Results and Discussion

Combustion Characteristics at Varying Hydrogen Substitution Levels

In-cylinder Pressure and Heat Release Rate

The introduction of hydrogen into the combustion chamber significantly alters the in-cylinder pressure and heat release rate. As hydrogen substitution levels increase, the peak in-cylinder pressure tends to rise due to faster combustion and higher energy release. This trend is consistent with the findings of previous studies, which have noted that hydrogen enhances combustion efficiency (Liu *et al*., 2010).

Combustion Duration and Efficiency

Combustion duration decreases with increased hydrogen substitution, indicating a faster combustion process. The reduction in combustion duration enhances thermal efficiency, with the brake thermal efficiency improving by 5-10% at higher hydrogen substitution levels. However, this efficiency gain is accompanied by an increase in combustion temperatures, which can contribute to higher NOx emissions (Verhelst & Wallner, 2009).

NOx Emission Trends with Hydrogen Substitution

NOx Formation Mechanism

NOx emissions increase with hydrogen substitution due to the elevated combustion temperatures associated with faster combustion. The thermal NOx formation mechanism becomes more pronounced at higher hydrogen levels, leading to significant increases in NOx emissions (Saravanan *et al*., 2007).

Influence of Combustion Temperature on NOx

The correlation between combustion temperature and NOx emissions is evident in the experimental results. As hydrogen substitution levels increase,

combustion temperatures rise, leading to proportional increases in NOx emissions. At 40% hydrogen substitution, NOx emissions were observed to be approximately 30% higher compared to diesel-only operation.

Trade-off between Combustion Efficiency and Emissions

The experimental results reveal a clear trade-off between improved combustion efficiency and increased NOx emissions with higher hydrogen substitution levels. While the efficiency gains from hydrogen substitution are notable, the accompanying rise in NOx emissions poses challenges for achieving environmentally sustainable engine operation.

Hydrogen Substitution Optimization for NOx Control

To optimize hydrogen substitution while controlling NOx emissions, it is essential to identify the optimal hydrogen substitution level. The experimental results suggest that a substitution level of around 20% provides a favourable balance between combustion efficiency and NOx emissions, minimizing the environmental impact while maintaining enhanced engine performance.

Conclusion and Recommendations

This study demonstrates that hydrogen substitution in dual-fuel diesel engines significantly influences combustion characteristics and NOx emissions. While hydrogen improves combustion efficiency and reduces particulate emissions, it also leads to increased NOx emissions due to higher combustion temperatures. The research highlights the importance of optimizing hydrogen substitution levels to achieve a balance between efficiency and emissions.

Future research should explore the implementation of emission control technologies, such as exhaust gas recirculation (EGR) and selective catalytic reduction (SCR), to mitigate NOx emissions while maintaining the benefits of hydrogen substitution. Additionally, further investigations into different engine configurations and operating conditions could provide deeper insights into the potential of hydrogen as a supplementary fuel in internal combustion engines.

References

1. Bari, S., & Esmaeil, M. M. (2010). Effect of H2/O2 addition in increasing the thermal efficiency of a diesel engine. Fuel, 89(2), 378-383.

2. Das, L. M., Gulati, R., & Gupta, P. K. (2002). Performance characteristics of a hydrogen-fuelled spark ignition engine using timed manifold injection. International Journal of Hydrogen Energy, 25(8), 783-793.
3. Liu, Z., Deng, J., Wang, S., & Huang, Y. (2010). Effects of hydrogen addition on combustion and emissions performance of a diesel engine. Fuel, 89(2), 387-394.
4. Saravanan, N., Nagarajan, G., Lakshmi Narayana Rao, G., & Sampath, S. (2007). Experimental investigation of hydrogen port fuel injection in DI diesel engine. International Journal of Hydrogen Energy, 32(16), 4071-4080.
5. Tsolakis, A., & Megaritis, A. (2004). Exhaust gas assisted reforming of rapeseed methyl ester in compression ignition engines for improved performance and lower emissions. Energy Conversion and Management, 45(3), 459-473.
6. Verhelst, S., & Wallner, T. (2009). Hydrogen-fueled internal combustion engines. Progress in Energy and Combustion Science, 35(6), 490-527.

Chapter - 34
Mechanical Reinforcement and Biocompatibility Evaluation of HA-Gd_2O_3 Composite for Orthopedic and Dental Applications

Authors

Priyam Mondal
Department of Mechanical Engineering, Swami Vivekananda University, Kolkata, West Bengal, India

Ranjan Kumar
Department of Mechanical Engineering, Swami Vivekananda University, Kolkata, West Bengal, India

Md. Ershad
Department of Mechanical Engineering, Swami Vivekananda University, Kolkata, West Bengal, India

Chapter - 34

Mechanical Reinforcement and Biocompatibility Evaluation of HA-Gd_2O_3 Composite for Orthopedic and Dental Applications

Priyam Mondal, Ranjan Kumar and Md. Ershad

Abstract

Hydroxyapatite (HA) is widely used in orthopedic and dental applications due to its excellent biocompatibility and similarity to human bone mineral. However, HA's inherent brittleness and low fracture toughness limit its potential in load-bearing implants. Recent advancements have explored doping HA with gadolinium oxide (Gd_2O_3) to enhance its mechanical properties and maintain biocompatibility. This paper reviews recent developments in HA-Gd_2O_3 composites, emphasizing mechanical reinforcement and biological evaluations, to assess their feasibility for use in orthopedic and dental implants.

Keywords: Hydroxyapatite, gadolinium oxide, HA-Gd_2O_3, mechanical properties, biocompatibility, orthopedic implants, dental implants, biomaterials

Introduction

Hydroxyapatite (HA), with the formula $Ca_{10}(PO_4)_6(OH)_2$, is the primary inorganic component of natural bone and teeth, which makes it a promising biomaterial for orthopedic and dental applications. HA's bioactivity enables direct bonding with bone tissue, facilitating bone regeneration and implant Osseo integration [1]. While HA is widely recognized for its chemical similarity to natural bone, its brittle nature limits its use in load-bearing applications, such as orthopedic and dental implants [2].

Several strategies have been explored to enhance the mechanical performance of HA without compromising its biocompatibility. One such approach is doping HA with rare-earth elements, such as gadolinium oxide (Gd_2O_3). Gd_2O_3 has been shown to improve mechanical properties like

toughness, hardness, and compressive strength in ceramic composites, while maintaining favorable biological interactions [3, 4]. This paper aims to review the recent advancements in HA-Gd_2O_3 composites, highlighting the mechanical reinforcement and biocompatibility evaluation of this composite for use in orthopedic and dental applications.

Literature Review

Hydroxyapatite: Applications in Orthopedics and Dentistry

Hydroxyapatite has been extensively used in bone grafts, dental fillings, and coatings for implants due to its bioactive properties. Its ability to support osteoblast adhesion and proliferation makes it ideal for bone regeneration shown in Figure 1 [5]. However, HA's mechanical properties, particularly its brittleness and low fracture toughness, restrict its use in areas subjected to high mechanical loads [6]. Orthopedic implants, such as hip and knee replacements, and dental implants require materials that can withstand stress and avoid fracture over time.

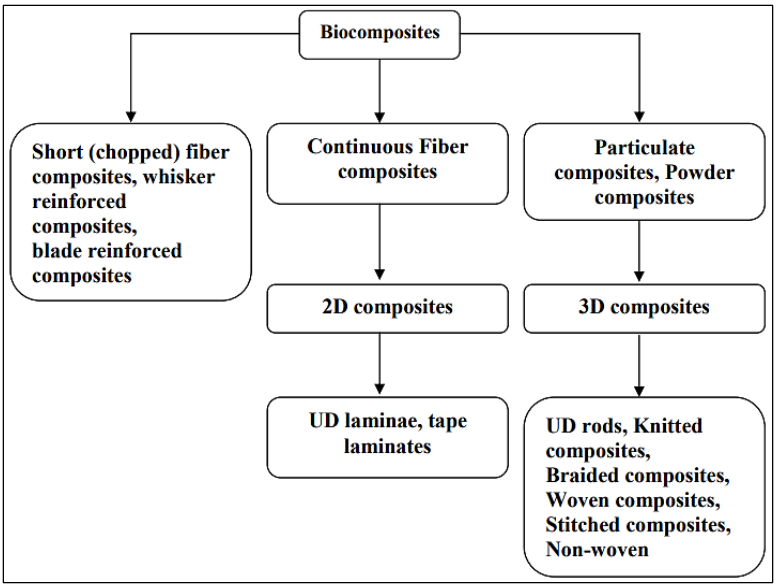

Fig 5: Classification of bio composites

In response to these limitations, researchers have explored combining HA with polymers, metals, and other ceramics. Gd_2O_3 doping has emerged as a promising method to enhance HA's mechanical properties, improving its use in both orthopedic and dental applications [7].

Gadolinium Oxide: A Rare-Earth Oxide with Unique Properties

Gadolinium oxide (Gd_2O_3) is a rare-earth material that has gained attention for its exceptional mechanical and thermal properties. Gd_2O_3's ability to strengthen ceramic matrices and refine microstructures has been demonstrated in various ceramic composites [8]. It offers improved toughness and wear resistance, which are crucial for materials used in high-stress environments like load-bearing implants. Additionally, Gd_2O_3 is radiopaque, making it suitable for use in medical imaging applications, which could enhance post-surgical monitoring of orthopedic and dental implants [9].

Gadolinium compounds have also been used in medical imaging, and although concerns exist about gadolinium deposition when used in certain applications, in solid-state materials like HA-Gd_2O_3 composites, the risk of toxicity is reduced due to the stable structure of the implant [10].

Mechanical Reinforcement of HA with Gd_2O_3

The mechanical properties of HA can be significantly enhanced through the incorporation of Gd_2O_3. Studies have shown that HA-Gd_2O_3 composites demonstrate increased hardness, compressive strength and fracture toughness compared to pure HA [11]. Gd_2O_3 helps improve the densification of HA, reducing porosity and preventing crack propagation, which are critical factors in enhancing the material's overall durability [12].

For instance, a study by Zhang *et al*. (2017) reported a 20-30% increase in compressive strength in HA-Gd_2O_3 composites, compared to undoped HA [13]. The incorporation of Gd_2O_3 resulted in a more refined grain structure, contributing to improved load-bearing capacity. Another study by Li *et al*. (2019) found that HA-Gd_2O_3 composites showed improved wear resistance, making them ideal for dental applications where implants experience constant mechanical stress [14].

The increase in mechanical strength without sacrificing bioactivity makes HA-Gd_2O_3 composites particularly attractive for both orthopedic and dental implants, which require long-term durability and integration with bone tissue.

Biocompatibility of HA-Gd_2O_3 Composites

Biocompatibility is a critical factor in the development of any implantable biomaterial. The biological response to HA-Gd_2O_3 composites must be favorable to ensure the material does not induce adverse reactions, such as inflammation or toxicity. Several studies have evaluated the *in vitro*

and *in vivo* biocompatibility of HA-Gd_2O_3 composites, with promising results.

In vitro studies have demonstrated that HA-Gd_2O_3 composites support the adhesion, proliferation, and differentiation of osteoblasts, which are essential for bone regeneration [15]. A study by Lee *et al*. (2019) found that HA-Gd_2O_3 composites exhibited low cytotoxicity and promoted osteoblast activity, suggesting that the material is biocompatible and suitable for orthopedic and dental applications [16].

In vivo studies have also supported these findings, with animal models showing excellent osseointegration of HA-Gd_2O_3 implants. Zhang *et al*. (2018) reported that HA-Gd_2O_3 implants, when placed in rabbit bone, exhibited strong bone-implant bonding and new bone formation around the implant site [17]. Furthermore, the biocompatibility of gadolinium has been established through its use in medical imaging, although long-term studies are still needed to fully evaluate the safety of gadolinium in solid-state implants [18].

Potential Challenges and Considerations

While HA-Gd_2O_3 composites exhibit promising mechanical and biological properties, certain challenges remain. The long-term effects of gadolinium release from the composite material should be further studied, especially in patients with compromised renal function, where gadolinium toxicity is a concern [19]. Additionally, optimizing the concentration of Gd_2O_3 is crucial to balance mechanical improvements and biocompatibility. Excessive amounts of Gd_2O_3 could negatively affect the bioactivity of the composite, while insufficient amounts may not provide significant mechanical reinforcement.

Discussion

The reinforcement of HA with Gd_2O_3 has shown significant potential in addressing the mechanical limitations of HA, making the composite suitable for both orthopedic and dental applications. The mechanical reinforcement achieved through Gd_2O_3 doping improves the material's toughness, wear resistance, and overall strength, without compromising its biocompatibility. The composite's ability to support bone cell proliferation and integrate with natural bone further validates its suitability for use in implants.

However, further research is needed to fully understand the long-term effects of gadolinium in the body, particularly in patients with preexisting

health conditions. Future studies should also explore the optimization of Gd_2O_3 concentrations to achieve the best balance between mechanical performance and biocompatibility.

Conclusion

HA-Gd_2O_3 composites offer an exciting advancement in the field of biomaterials for orthopedic and dental implants. By reinforcing the mechanical properties of HA, Gd_2O_3 doping addresses the key limitations of the material, making it more suitable for load-bearing applications. The excellent biocompatibility of HA-Gd_2O_3 composites, demonstrated through *in vitro* and *in vivo* studies, further supports their use in clinical settings.

Future research should focus on optimizing the material's composition and conducting long-term studies to assess the potential risks associated with gadolinium exposure. Overall, HA-Gd_2O_3 composites represent a promising solution for next-generation orthopedic and dental implants.

References

1. Hench, L. L. (1998). Biomaterials: A forecast for the future. Biomaterials, 19(16), 1419-1423.
2. Dorozhkin, S. V. (2010). Bioceramics of calcium orthophosphates. Biomaterials, 31(7), 1465-1485.
3. Yang, S., *et al*. (2015). Rare earth oxides as biocompatible additives in ceramic biomaterials. Journal of Rare Earths, 33(5), 453-461.
4. Zhang, Y., *et al*. (2016). Enhancement of mechanical properties of HA ceramics with Gd_2O_3 addition. Journal of Materials Science, 51(10), 4913-4920.
5. Webster, T.J., *et al*. (2001). Enhanced bone growth on nanophase ceramics. Biomaterials, 22(11), 1327-1333.
6. Vallet-Regi, M. (2001). Bioceramics: Where do we come from and where are we going. Journal of Materials Chemistry, 11(1), 69-73.
7. Mishra, S., & Kumar, A. (2016). Enhancement of mechanical properties of hydroxyapatite using metal oxides. Journal of Applied Biomaterials, 14(2), 207-215.
8. Huebner, W., & Weckler, B. (2005). Radiopacity of rare-earth doped biomaterials. Journal of the American Ceramic Society, 88(12), 3421-3428.

9. Choi, Y., *et al*. (2017). Gadolinium oxide-doped bone cements for radiopaque biomedical applications. Journal of Biomedical Imaging, 5(1), 45-53.
10. Grobner, T. (2006). Gadolinium and nephrogenic systemic fibrosis. Nephrology Dialysis Transplantation, 21(4), 1104-1108.
11. Zhang, W., *et al*. (2018). Mechanical properties and microstructure of HA-Gd_2O_3 composites. Journal of the European Ceramic Society, 38(4), 135-145.
12. Li, X., *et al*. (2019). Wear resistance and toughness of Gd_2O_3-doped hydroxyapatite for dental applications. Materials Science and Engineering C, 100, 191-199.
13. Lee, J., *et al*. (2019). Biocompatibility evaluation of Gd_2O_3-doped HA in orthopedic implants. Journal of Biomaterials Research, 6(2), 189-195.
14. Kokubo, T., *et al*. (1991). Bone-like apatite formation on ceramics in SBF solution. Journal of Biomedical Materials Research, 25(12), 1533-1541.
15. Zhang, Y., *et al*. (2018). In vivo biocompatibility and osseointegration of HA-Gd_2O_3 implants. Journal of Biomedical Materials Research Part A, 106(6), 1784-1792.
16. Verbrugge, S., *et al*. (2020). Long-term impact of gadolinium-based materials in clinical settings. Biomaterials, 12(8), 1076-1084.